

**DEVELOPMENTAL REGULATION OF THE DRUG-PROCESSING GENOME
IN MOUSE LIVER**

By

Julia Yue Cui

B.S., Chukeychen Honors College, Zhejiang University, 2005

Submitted to the Graduate Degree Program in Pharmacology, Toxicology, and
Therapeutics and the Graduate Faculty of the University of Kansas in partial
fulfillment of the requirements for the degree of Doctor of Philosophy

Dissertation Committee

Curtis Klaassen, Ph.D. (Chair) _____

Yu-Jui Yvonne Wan, Ph.D. _____

Bruno Hagenbuch, Ph.D. _____

Grace Guo, Ph.D. _____

Lane Christenson, PhD. _____

Date defended: _____

The Dissertation Committee for Julia Yue Cui certifies that this is the approved
version of the following dissertation:

**DEVELOPMENTAL REGULATION OF THE DRUG-PROCESSING GENOME
IN MOUSE LIVER**

Dissertation Committee

Curtis Klaassen, Ph.D. (Chair) _____

Yvonne Wan, Ph.D. _____

Bruno Hagenbuch, Ph.D. _____

Grace Guo, Ph.D. _____

Lane Christenson, PhD. _____

Date approved: _____

ACKNOWLEDGEMENTS

I would like to acknowledge my dissertation committee, Drs. Curtis Klaassen, Yu-Jui Yvonne Wan, Bruno Hagenbuch, Grace Guo, and Lane Christenson for their insightful suggestions and constructive criticisms to improve my dissertation.

I am very grateful to my academic father, Dr. Curtis Klaassen, for introducing me to the world of toxicology, for his guidance and enthusiasm in my research, and endless support of my PhD studies. He always encourages me to do the most and best I can for my career. From him, not only have I learnt how to do good science, but also how to be a good scientist and educator. He is the person I trust the most in my career, the person I find confidence from always, and the person I will be eternally grateful for the rest of my life.

I would like to acknowledge all the faculty members of the Department of Pharmacology, Toxicology, and Therapeutics for their help and advice. I would like to especially thank Dr. Thomas Pazdernik for his help with my course work.

I would like to thank all the present and past members in Dr. Curtis Klaassen's laboratory for their help and contribution to my research, especially Drs. Lauren Aleksunes, Yuji Tanaka, Xingguo Cheng, and Cheryl Rockwell. I would also like to acknowledge Dr. Sumedha Gunewardena from the Kansas Intellectual and Developmental Disabilities Research Center, who has collaborated with me on one of my research projects.

I would like to acknowledge all the department staff and my fellow graduate students for their generous assistance during the past five years.

TABLE OF CONTENTS

Chapter I. General introduction and background.....	1
Chapter II. Statement of purpose.....	40
Chapter III. Experimental materials and methods.....	43
Chapter IV. Global picture of the ontogeny of critical drug-processing genes and regulatory factors in liver development.....	67
Chapter V. The ontogeny of novel cytochrome P450 gene isoforms during postnatal liver maturation in mice.....	87
Chapter VI. Genetic and epigenetic regulation and expression signatures of glutathione S-transferases in developing mouse liver	127
Chapter VII. Developmental regulation of liver transporters in mice Part I. Bile acids via FXR initiate the expression of major transporters involved in the enterohepatic circulation of bile acids in newborn mice	157
Part II. Regulation of xenobiotic transporters by PXR.....	198
Chapter VIII. Ontogenic regulation of transcription factors Ahr, PPAR α and PGC-1 α in mouse liver.....	212
Chapter IX. General summary and conclusions.....	259
Chapter X. References.....	263
Appendices	297

LIST OF ABBREVIATIONS

Abbreviation	Full name
Abcg5	ATP binding cassette g5
Abcg8	ATP binding cassette g8
AhR	Aryl hydrocarbon receptor
Aldh	Aldehyde dehydrogenase
ARNT	AhR nuclear translocator
Asbt	Apical sodium-dependent bile acid transporter
Bcrp	Breast cancer resistance protein
bDNA	Branched DNA
Bsep	Bile-salt export pump
CA	Cholic acid
CAR	Constitutive androstane receptor
ChIP	Chromatin immunoprecipitation
Chr	Chromosome
Cnt	Concentrative nucleoside transporter
Cyp	Cytochrome P450 enzymes
DCA	Deoxycholic acid
EHC	Enterohepatic circulation
Ent	Equilibrative nucleoside transporter
Fgf15	Fibroblast growth factor 15
Fgfr4	Fibroblast growth factor receptor 4
FXR	Farnesoid X receptor
GADD45	Growth arrest and DNA damage
Gapdh	Glyceraldehyde-3-phosphate dehydrogenase
Gst	Glutathione S-transferase
H3K27Me3	Trimethylation of H3 at lysine-27
H3K4Me2	Dimethylation of histone H3 at lysine-4
IGB	Integrated genome browser
HSP90	Heat shock protein 90
LC-MS	Liquid chromatography-mass spectrometry
LCA	Lithocholic acid
lit/lit mice	Mice with a spontaneous mutation in the growth-hormone releasing-hormone receptor
Mate	Multidrug and toxin extrusion protein
MCA	Muricholic acid
Mdr	Multidrug resistance protein
Mrp	Multidrug resistance-associated protein
NcoR1	Nuclear receptor co-repressor 1
Nrf2	Nuclear factor erythroid 2-related factor 2
Ntcp	Na ⁺ -taurocholate cotransporting polypeptide
Oat	Organic anion transporter
Oatp	Organic anion transporting polypeptide
Oct	Organic cation transporter
Ost	Organic solute transporter
RT-qPCR	Reverse transcription-quantitative polymerase chain reaction
PGC-1 α	Peroxisome proliferator-activated- γ coactivator 1 α
PPAR α	Peroxisome proliferator-activated receptor α
PXR	Pregnane X receptor
RLU	Relative light units
RXR	Retinoid-X-receptor
SHP	Small heterodimer partner
SRC-1	Steroid receptor coactivator-1
Sult	Sulfotransferase
TAS	Affymetrix Tiling Analysis Software
T-BA	Taurine-conjugated bile acid
TR	Thyroid hormone receptor

Abbreviation	Full name (Cont'd)
TSS	Transcriptional start site
UDCA	Ursodeoxycholic acid
Ugt	UDP-glucuronosyltransferase
UTR	Untranslated region
VDR	Vitamin D receptor

LIST OF TABLES

Table 1.1. List of critical drug-processing genes and transcription factors in liver.....	11
Table 1.2. List of subfamily members of nuclear receptors.....	17
Table 1.3. Some transcriptional activating and repressing histone modifications.....	31
Table 3.1. The human homologs for the mouse Cyps (if present), as well as their DNA and protein identities.....	45
Table 3.2. The Cyp gene names, accession numbers, and the panel information for the multiplex branched amplification technology.....	48
Table 3.3. Cyp gene names, accession numbers, and the forward and reverse primer sequences for RT-PCR.....	50
Table 3.4. Oligonucleotide probes generated for analysis of mouse FXR and SHP mRNA by bDNA.....	54
Table 6.1. Consensus PXR-DNA binding motifs within the ChIP-DNA sequences for PXR.....	143

LIST OF FIGURES

Figure 1.1. Illustration of phase-I and -II drug metabolism as well as transporters in liver.....	2
Figure 1.2. The hierarchy of organization from chromosome to nucleosome.....	27
Figure 4.1. Developmental expression of drug-processing genes in mouse liver.....	69
Figure 4.2. The ontogeny of transcription factors in mouse liver during development...	71
Figure 4.3. Relative enrichment of epigenetic marks (H3K4Me2, H3K27Me3, and DNAMe) on representative chromosomes (chr5, 12, and 15) during mouse liver development.....	73
Figure 4.4. Western blot of tissue distribution of H3K4Me2 (A) as well as immunofluorescence staining of H3K4Me2 during mouse liver development (B).....	74
Figure 4.5. A roadmap of enrichment in hepatic PXR-DNA binding in the entire mouse genome.....	76
Figure 4.6. Motif analysis of PXR-DNA binding profiles in mouse liver.....	78
Figure 4.7. A diagram of the helical turns of DNA and the formation of DR-(5n+4) like DNA motifs.....	80
Figure 4.8. Quantification of PXR binding to DR-(5n+4)-like DNA sequences by ELISA-based transcription factor binding assays.....	83
Figure 4.9. An overlay between PXR-DNA binding and presence of three epigenetic marks (H3K4Me2, H3K27Me3, and DNAMe) on representative chromosomes (chr5, 12, and 15) in mouse liver.....	85
Figure 5.1. Genomic locations of Cyp gene cluster within the first 4 families.....	95
Figure 5.2. The mRNA ontogenic expression of the Cyp1 family (Cyp1a1, 1a2, and 1b1), and most of the Cyp2 family (Cyp2a4, 2a5, 2a22, 2b9, 2b10, 2b13, 2b19, 2b23, 2c29, 2c37, 2c38, 2c39, 2c40, 2c44, 2c50, 2c54, and 2c55)	

in male and female livers from day -2 to day 45 of age.....	97
Figure 5.3. The mRNA ontogenic expression of most of the Cyp2 family (Cyp2c66, 2c67, 2c68, 2c69, 2c70, 2d9, 2d10, 2d11, 2d12, 2d22, 2d26, 2d34, 2d40, 2e1, 2f2, 2g1, 2j5, 2j6, 2j7, and 2j8) in male and female livers from day -2 to day 45 of age.....	100
Figure 5.4. The mRNA ontogenic expression of most of the Cyp2 family (Cyp2j9, 2j11, 2j13, 2j13, 2t4, 2u1, and 2w1), the Cyp3 family (Cyp3a11, 2a13, 2a16, 3a25, 3a59, 3a41a, 3a41b, 3a44), and part of the Cyp4 family (Cyp4a10, 4a12a/b, 4a14, 4a29, and 4a30b) in male and female livers from day -2 to day 45 of age.....	103
Figure 5.5. The mRNA ontogenic expression of most of the Cyp4 family (Cyp4a31, 4a32, 4b1, 4f13, 4f14, 4f15, 4f16, 4f17, 4f18, 4f39, 4f40, 4v3, 4x1) in male and female livers from day -2 to day 45 of age.....	109
Figure 5.6. A two-way hierachical clustering of expression profiles for Cyp1-4 genes in livers of male (left panel) and female mice.....	112
Figure 5.7. Location and fold-enrichment of three epigenetic marks (DNAMe, H3K4Me2, and H3K27Me3) to the Cyp3a gene locus during liver development.....	115
Figure 5.8. Location and fold-enrichment of PXR-DNA binding to the Cyp3a gene locus (A), as well as mRNA expression of Cyp3a11 and Cyp3a25 in WT and PXR-null mouse livers.....	117
Figure 6.1. The ontogenic expression of the mRNAs of 19 Gst isoforms in mouse liver.....	135
Figure 6.2. Heatmaps of the mRNA ontogeny of all the Gst isoforms as well as five xenobiotic-sensing transcription factors (AhR, CAR, PXR, PPAR α , and Nrf2) in developing mouse liver.....	138

Figure 6.3. Location and fold enrichment of PXR-binding sites to various <i>Gst</i> polycistron clusters in mouse liver.....	140
Figure 6.4. Location and fold enrichment of PXR binding to <i>MGst1</i> , <i>Mgst2</i> , <i>Mgst3</i> , and <i>Gsta3</i> in mouse liver.....	142
Figure 6.5. Dimethylation of histone H3 at lysine-4 (H3K4me2) at the <i>Gstz1</i> gene locus during mouse liver development.....	145
Figure 6.6. DNAMe and H3K27Me3 signatures around the <i>Gstz1</i> gene locus during mouse liver development.....	146
Figure 6.7. Human <i>GSTA</i> polycistron cluster and their homologous mouse <i>Gsta</i> cluster family.....	152
Figure 6.8. Human <i>GSTM</i> polycistron cluster and their homologous mouse <i>Gstm</i> cluster family.....	153
Figure 6.9. Human <i>GSTT</i> and <i>GSTP</i> polycistron clusters and their homologous mouse <i>Gstt</i> and <i>Gstp</i> cluster families.....	154
Figure 7.1.1. Ontogeny of liver transporters: <i>Ntcp</i> (basolateral uptake), <i>Ostα</i> , <i>Ostβ</i> , and <i>Mrp4</i> (basolateral efflux), <i>Bsep</i> and <i>Mdr2</i> (canalicular efflux) in wild-type mice from day -2 to day 45 of age.....	165
Figure 7.1.2. Ontogeny of ileal transporters: <i>Ostα</i> and <i>Ostβ</i> (basolateral efflux), and <i>Asbt</i> (apical uptake) in wild-type mice from day -2 to day 45 of age.....	167
Figure 7.1.3. Immunofluorescence of <i>Ntcp</i> and <i>Bsep</i> protein in livers from day -2, day 1, and day 45 of age.	169
Figure 7.1.4. Messenger RNA expression of bile-acid synthesizing enzymes (<i>Cyp7a1</i> , <i>8b1</i> , <i>27a1</i> , and <i>7b1</i>) in livers, as well as the ileal <i>Fgf15</i> in wild-type mice during development.....	171
Figure 7.1.5. Serum and liver bile acid concentrations (total BA, total CA, and total	

MCA) during development in mice.....	174
Figure 7.1.6. Serum individual bile acid concentrations during development in mice..	177
Figure 7.1.7. Liver individual bile acid concentrations during development in mice....	178
Figure 7.1.8. Percentage of various components of bile acids in serum and liver at day 1 and 45 days of age.....	180
Figure 7.1.9. Up-regulation of the mRNA expression of FXR, SHP (prototypical target gene of FXR), PXR, and Cyp3a11 (prototypical target gene of PXR) in neonatal wild-type mouse liver.....	182
Figure 7.1.10. Messenger RNA expression of FXR, SHP (prototypical target gene of FXR), PXR, and Cyp3a11 (prototypical target gene of PXR) in neonatal wild-type mouse ileum.....	183
Figure 7.1.11. A. The mRNA expression of liver transporters Ntcp, Bsep, Mdr2, Mrp4, and Ost β in wild-type, PXR-null (upper panel), and FXR-null mice (lower panel) at day 1 of age. B. The mRNA expression of ileal transporters Asbt, Ost α , and Ost β in wild-type, PXR-null (upper panel), and FXR-null mice (lower panel) at 1 day of age. C. Immunofluorescence of Ntcp and Bsep protein in livers from wild-type and FXR-null mice at day 1 of age.....	185
Figure 7.1.12. Messenger RNA expression of human transporters (NTCP, BSEP, and MDR3), as well as bile-acid biosynthetic enzymes (CYP7A1 and 8B1) in human livers during development.....	187
Figure 7.1.13. A schematic of the working hypothesis for the molecular mechanisms underlying the neonatal induction of hepatic transporters involved in the EHC of bile acids.....	190
Figure 7.2.1. Messenger RNA expression of basolateral uptake transporters for	

xenobiotics in livers of wild-type mice during development.....	200
Figure 7.2.2. Messenger RNA expression of basolateral efflux transporters for xenobiotics in livers of wild-type mice during development.....	201
Figure 7.2.3. Messenger RNA expression of canalicular efflux transporters for xenobiotics in livers of wild-type mice during development.....	202
Figure 7.2.4. Heatmap of the mRNA ontogeny of xenobiotic transporters and PXR in liver during development.....	204
Figure 7.2.5. PXR-DNA binding signatures to the <i>Oatp1a4</i> gene locus.....	206
Figure 7.2.6. PXR-DNA binding signatures to the <i>Mrp3</i> gene locus.....	208
Figure 7.2.7. Location and fold enrichment of H3K4Me2 (A), H3K27Me3 (B), and DNAMe (C) to the <i>Mdr</i> gene loci (<i>Mdr1a</i> , <i>Mdr1b</i> , and <i>Mdr2</i>) at 45 days of age	210
Figure 8.1. Ontogenic mRNA and protein expression of <i>Ahr</i> in mouse liver.....	224
Figure 8.2. DNA methylation status of the <i>Ahr</i> gene in mouse liver development.....	225
Figure 8.3. Di-methylation of histone H3 at lysine-4 (H3K4Me2) at the <i>Ahr</i> gene locus during mouse liver development.....	227
Figure 8.4. Tri-methylation of histone H3 at lysine-27 (H3K27Me3) at the <i>Ahr</i> gene locus during mouse liver development.....	229
Figure 8.5. Regression analysis between <i>Ahr</i> mRNA and the fold changes of the three epigenetic marks (DNA and histone di- and tri-methylations) at day -2, 1, 5, and 45 of age during liver development in mice.....	231
Figure 8.6. Ontogenic expression of <i>PPARα</i> and <i>PGC-1α</i> mRNA in mouse liver.....	233
Figure 8.7. DNA methylation status of the <i>PPARα</i> gene during mouse liver development.....	235
Figure 8.8. Di-methylation of histone H3 at lysine-4 (H3K4Me2) of the <i>PPARα</i> gene	

	locus during mouse liver development.....	237
Figure 8.9.	Tri-methylation of histone H3 at lysine-27 (H3K27Me3) of the <i>PPARα</i> gene locus during mouse liver development.....	239
Figure 8.10.	DNA methylation status of the <i>PGC-1α</i> gene during mouse liver development.....	241
Figure 8.11.	Di-methylation of histone H3 at lysine-4 (H3K4Me2) of the <i>PGC-1α</i> gene locus during mouse liver development.....	243
Figure 8.12.	Tri-methylation of histone H3 at lysine-27 (H3K27Me3) of <i>PGC-1α</i> gene locus during mouse liver development.....	244
Figure 8.13.	Serum triglyceride and glucose levels during mouse development.....	246

ABSTRACT

The liver is an essential organ for drug metabolism and nutrient homeostasis. Various xenobiotics and endogenous compounds enter hepatocytes by basolateral uptake transporters and are then converted into more hydrophilic metabolites by phase-I and –II drug-metabolizing enzymes. These metabolites are subsequently eliminated from the hepatocytes by basolateral and/or canalicular efflux transporters.

Despite the recent progress in understanding the expression patterns and regulatory mechanisms of drug-processing genes, namely phase-I and –II drug metabolizing enzymes and transporters in adults, very little is known of the alterations of these genes during liver development. Therefore, newborns and children are potentially at a higher risk of adverse drug reactions. The purpose of my dissertation is to use multidisciplinary approaches to characterize the expression and regulatory mechanisms of the drug-processing genes during postnatal liver maturation. The present study integrated various research models and technologies, including genetically engineered mice, messenger RNA and protein assays, microarray, ChIP-on-chip, ChIP-Seq, transcription-factor binding assays, LC-MS/MS, and bioinformatics analysis. The ontogenic expression and the regulatory mechanisms have been examined for various drug metabolizing enzymes and transporters in the liver. By characterizing the ontogeny of the drug-processing genome in the liver, the present study has provided novel

insights into identifying and further understanding the molecular targets for effective and safe drug treatments for children.

First, cluster analysis demonstrated that the ontogenic expression of drug-processing genes separate into 4 distinct patterns: perinatal enriched, early adolescent enriched, late-adolescent enriched, and adult enriched. In addition, the mRNA ontogeny of over 70 transcription factors was examined. These mRNAs also separate into 4 patterns. Critical nuclear receptors, including the xenobiotic sensor pregnane X receptor (PXR, *N112*), as well as the bile-acid sensor farnesoid X receptor (FXR, *NR1H4*), are crucial in regulating the expression of drug-processing genes during liver development. Initiation of bile acid signaling, mediated largely via FXR, is a hallmark of the neonatal induction of major liver transporters involved in the enterohepatic circulation (EHC), whereas PXR is more important for the induction of xenobiotic-processing genes in adolescent and adult period, when the organism is exposed to more xenobiotics.

The accessibility of transcription factors to the target genes was determined by the methylation status of histones and gene promoters. The present studies have illustrated that various drug-processing genes and transcription factors are expressed in distinct dynamic patterns in developing mouse livers, and their expressions correlated with the chromatin architecture. Among various types of epigenetic signatures, histone H3 lysine 4 di-methylation (H3K4Me₂) appeared to

be the choice of nature to induce numerous drug-processing genes during postnatal liver development. These drug-processing genes include some cytochrome P450s (Cyps), some UDP glucuronosyl transferases (Ugts), some glutathione S-transferases (Gsts), and some transporters, such as the sodium-taurocholate cotransporting polypeptide (Ntcp, *Slc10a1*). In addition, the ontogeny of several transcription factors also appeared to be associated with altered occupancy of H3K4Me2, including the xenobiotic sensor aryl hydrocarbon receptor (AhR), the lipid sensor peroxisome proliferator-activated receptor α PGC-1 α (PPAR α , *NR1C1*), as well as the master endobiotic metabolism regulator and transcription co-activator, peroxisome proliferator-activated receptor- γ coactivator 1 α (PGC1 α , *PPargc1*).

Under a permissive chromatin environment, FXR triggered the “day-1” surge pattern of liver transporters involved in the EHC. Both the mRNA and protein expression of these transporters were decreased in livers of the FXR-null mice at 1 day of age. The bile-acid bio-synthetic enzymes from the classic pathway, including cytochrome P450 7a1 and 8b1, were more activated than enzymes from the alternative pathway during the neonatal period. Using LC-MS/MS analysis, I have detected 11 bile acids in serum and 17 in the liver. Cholic acid, which can only be synthesized from the classic pathway, was the predominant bile acid in newborns, and appeared to be responsible for the FXR-mediated neonatal upregulation of transporters. The mRNAs of human transporters and bile-acid bio-synthesizing enzymes were also quantified in the present study.

The transporters NTCP, bile salt export pump (BSEP, *ABCB11*), and multidrug resistance protein 3 (MDR3, *ABCB4*, human homolog of the mouse *Mdr2* [*Abcb4*]), as well as the bile-acid bio-synthesizing enzymes in the classic pathway, namely CYP7A1 and 8B1, were also increased in neonatal livers. This suggests that the “day-1” surge pattern of bile acid transporters also occurs in humans.

Whereas FXR mediates the induction of bile-acid and lipid transporters in neonatal ages, PXR, which is enriched from adolescent to the adult period during liver development, appears to regulate the induction of many xenobiotic-processing genes in early adulthood. These genes include numerous cytochrome P450s, the Gsts, and a few xenobiotic transporters, such as the organic anion co-transporting polypeptide 1a4 (*Oatp1a4*, *Slco1a4*), and the multi-drug resistance-associated protein 4 (*Mrp4*, *Abcc4*). However, the induction of drug-processing genes could be due to direct PXR binding to DNA, or due to a secondary effect. Very little is known about the PXR DNA-binding signatures *in vivo*, or how PXR regulates novel direct targets on a genome-wide scale. Therefore, to further consolidate critical roles of PXR in regulating drug-processing genes during the early adult period, a roadmap of hepatic PXR bindings in the entire mouse genome was generated by ChIP-Seq. The most frequent PXR DNA-binding motif was two AGTTCA-like direct repeats with a 4bp spacer (DR-4). Surprisingly, there were also high frequencies of motifs with spacers of a periodicity of 5bp, forming a novel DR-(5n+4) pattern for PXR

binding. For the PXR-target gene *Oatp1a4*, DR-9 (n=1) was the only motif within the ChIP DNA sequences bound by the PXR protein. ELISA-based transcription factor binding assay validated that PXR binds to DR-(5n+4) like sequences, including DR-4, DR-9, DR-14, and DR-19. This novel finding challenges the existing paradigm for the current understanding of nuclear receptor consensus sequences. PXR-binding overlaps with the epigenetic mark for gene activation (histone-H3K4-di-methylation), but not with the epigenetic marks for gene suppression (DNA methylation or histone-H3K27-tri-methylation) (ChIP-on-chip). The PXR agonist PCN was administered to mice to determine whether there would be increased PXR binding at the original binding sites, and whether there would be new binding sites for PXR. Indeed, pharmacological activation of PXR further increased the total binding sites and enrichment at the original sites of many drug-processing genes. In addition, increased PXR binding triggered the trans-activation of critical drug-metabolizing enzymes and transporters. The induction of these mRNAs was absent in PXR-null mice.

In conclusion, for the present dissertation, I have performed a systemic characterization of critical drug-processing genes and transcription factors during postnatal liver maturation. In addition, I have demonstrated that the developmental regulation of drug metabolism and transport is a sequential event associated with changes of chromatin epigenetic signatures, which set a permissive environment for ligand-activated nuclear receptors to gain access to the target genes prior to transcription initiation. Through multidisciplinary

approaches, the current work has generated basic knowledge that will serve as a foundation for further understanding of pediatric pharmacology and toxicology in humans.

CHAPTER ONE. GENERAL INTRODUCTION AND BACKGROUND

Liver in drug metabolism and transport.

Liver is an essential organ for drug metabolism and nutrient homeostasis. Foreign compounds, including therapeutic drugs, environmental toxicants, and dietary factors, are commonly referred to as xenobiotics. The endogenous compounds produced *in vivo* are termed endobiotics, including bile acids, lipids, etc. Many xeno- and endo-biotic compounds are lipophilic, and must be biotransformed to increase their hydrophilicity, and the increased hydrophilicity of substrates allows for excretion into urine or bile. In addition, various prodrugs require biotransformation to form metabolites that activate their therapeutic targets, a process termed “bioactivation”. Therefore, biotransformation is critical in both protecting the organism against chemical toxicity, and mediating pharmacological responses. Liver is the primary organ where xenobiotics and other compounds are biotransformed. Various chemicals are taken up into hepatocytes by basolateral uptake transporters. These chemicals are then converted into more hydrophilic metabolites by phase-I and –II drug-metabolizing enzymes. These compounds are then eliminated from the hepatocytes by basolateral and canalicular efflux transporters (Figure 1.1).

Phase-I metabolism. Phase-I metabolism includes three major reactions: oxidation, reduction, and hydrolysis. Phase-I metabolism usually precedes phase-II, though not necessarily. During phase-I reactions, hydrophilic functional

Figure 1.1

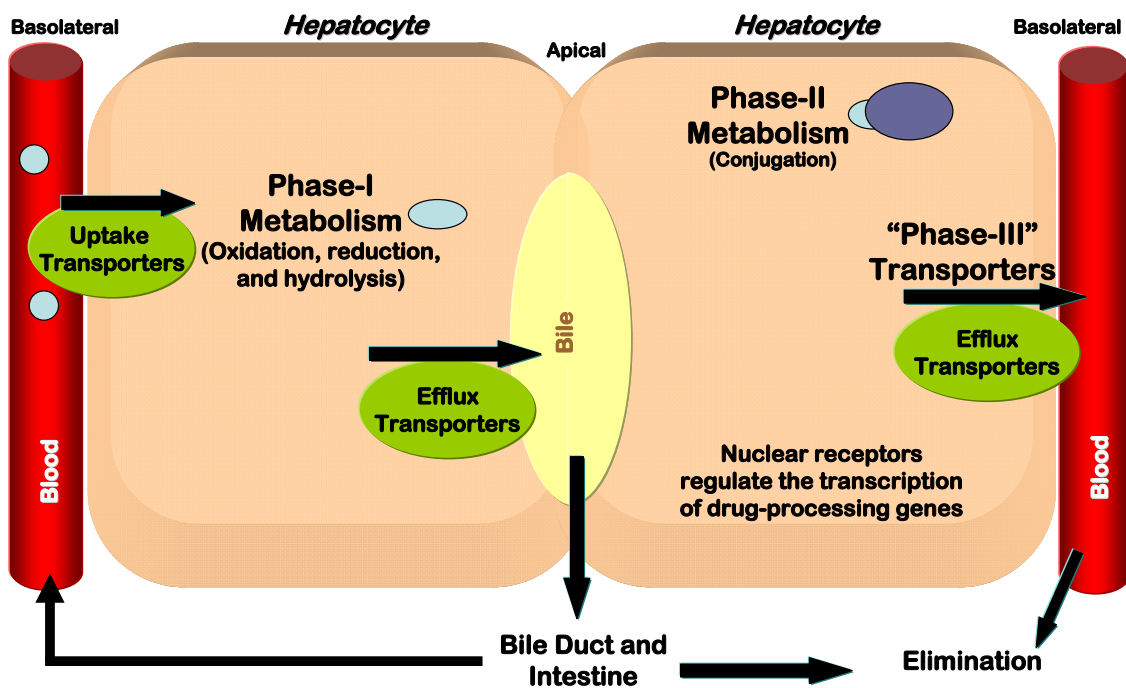


Figure 1.1. Illustration of phase-I and -II drug metabolism as well as transporters in liver. Various compounds are taken up from the portal blood into hepatocytes via uptake transporters on the basolateral membrane, and then converted to more water soluble compounds by phase-I metabolism (oxidation, reduction, or hydrolysis). Phase-II metabolism conjugates the substrates with large, bulky molecules (cosubstrates). Various metabolites are eliminated from hepatocytes via canalicular efflux transporters into bile, and basolateral efflux transporters into blood (excreted into urine). Nuclear receptors mediate the transcriptional regulation of many genes in drug metabolism and transport.

groups are either introduced or unmasked, resulting in increased polarity of metabolites. For numerous pharmaceutical drugs, phase-I reactions lead to either bioactivation or inactivation of the drug. Phase-I enzymes are usually found in the smooth endoplasmic reticulum of hepatocytes, whereas a few are found in mitochondria. The enzymes involved in oxidation include the cytochrome P450 monooxygenase system, the flavin-containing monooxygenase system, alcohol dehydrogenases and aldehyde dehydrogenases, monoamine oxidases, and peroxidases. The enzymes important for reduction include NADPH-cytochrome P450 reductase and cytochrome P450s, whereas enzymes for hydrolysis include esterases and amidases, as well as epoxide hydrolases.

Among all these phase-I enzymes, it is well known that approximately three-quarters of drugs that are primarily cleared via metabolism are biotransformed by members of the cytochrome P450 family (Cyps). The Cyps are essential membrane-bound enzymes with widespread and diverse functions in mammals. The name “cytochrome P450” derives from the fact that these enzymes all have a heme group, with an unusual absorption spectrum at 450nm, in contrast to other heme-containing proteins, which do not absorb at this wavelength. According to the genomic data base, there are 57 functional CYPs identified in humans, and 102 Cyps in mice (Nelson et al., 2004). It is generally considered that CYPs in families 1-4 are critical and inducible components of the phase-I biotransformation systems in various species (Wei et al., 2000; Estabrook, 2003; Kang et al., 2007; Li et al., 2007), and many of them are also

important for metabolizing lipids, including steroids (CYP2), bile acids (CYP3A), fatty acids (CYP4), and many other endogenous compounds (Nebert and Russell, 2002). Whereas genetic mutations in Cyps are responsible for various types of inborn errors of metabolism and human diseases (Nebert and Russell, 2002; Caldwell, 2004), induction of some Cyps is a risk factor for adverse drug interactions and cancer. Previous studies have demonstrated that the mRNAs of Cyp1-4 are inducible by ligands of four classes of xeno-receptors, namely the aryl hydrocarbon receptor (AhR), the constitutive androstane receptor (CAR, *Nr1i3*), the pregnane X receptor (PXR), and the peroxisome proliferator-activated receptor alpha (PPAR α) (Petrick and Klaassen, 2007). Although these receptors have overlapping targets, it is generally considered that AhR is responsible for the mRNA induction of Cyp1, CAR for Cyp2, PXR for Cyp3, and PPAR α for the mRNA induction of Cyp4.

Other Cyp families besides Cyp1-4 are more specialized in endobiotic synthesis and metabolism. To note, the major enzymes involved in the classic pathway of bile-acid synthesis include Cyp7a1, which is the rate-limiting enzyme for bile-acid synthesis, as well as Cyp8b1, and these two enzymes catalyze the formation of cholic acid (CA). In the absence of Cyp8b1, chenodeoxycholic acid (CDCA) is the main bile-acid (Chiang, 2004). The Cyp enzymes in the alternative bile-acid biosynthesis pathway include Cyp27a1, 7b1, as well as Cyp39a1 (relatively lowly expressed in liver), with CDCA as the primary product (Russell, 2003).

Phase-II metabolism. Phase-II metabolism is also referred to as conjugation reactions, and it usually leads to detoxification of the chemical. Taking advantage of electrophilic functional groups present on the molecule, including carboxyl (-COOH), hydroxyl (-OH), amino (NH₂), and sulfhydryl (-SH) groups, the phase-II drug-metabolizing enzymes are characterized by their ability to conjugate xenobiotics with small molecular weight, organic donor molecules (often termed “co-substrates”), such as glutathione, UDP-glucuronic acid, PAPS, amino acids (glycine and taurine), acetyl coenzyme A, etc.

The Gsts are thought to play important roles in protecting macromolecules against electrophiles and products of oxidative stress, thus providing an efficient detoxification mechanism. There is a broad spectrum of Gst substrates in the environment, including halogenonitrobenzenes, arene oxides, quinones, as well as unsaturated carbonyls (Keen and Jakoby, 1978; Hayes and Pulford, 1995; Armstrong, 1997; McDonagh et al., 1999; Sheehan et al., 2001). The ability of Gst(s) to metabolize cancer chemotherapeutic drugs, insecticides, herbicides, and carcinogens suggests that their expression can influence the efficacy of drugs and capacity for detoxification, as well as an individual’s susceptibility to cancer (Hayes and Pulford, 1995; Board et al., 1997).

Gsts catalyze nucleophilic attack by GSH on nonpolar compounds that contain an electrophilic carbon, nitrogen, or sulfur atom, resulting in the formation of (usually) less reactive, more hydrophilic GSH conjugates. There are three

major families of proteins that exhibit glutathione transferase activity, namely cytosolic, mitochondrial, and microsomal. The cytosolic Gsts include alpha, mu, omega, pi, sigma, theta, and zeta family members. Cytosolic Gst enzymes represent the largest family, and they were highly conserved during evolution. In rodents and humans, cytosolic Gsts typically share more than 40% identity within a class. The mitochondrial Gst enzyme is the Gst kappa isoform. Gstk has only one isoform in mice, rats, and humans (Hayes and Pulford, 1995; Hayes et al., 2005), suggesting it is highly important for survival. The third family is microsomal Gst enzymes, which are now referred to as membrane-associated proteins in eicosanoid and glutathione (MAPEG) metabolism.

The UDP-glucuronosyl transferases (Ugts) are critical enzymes for phase-II glucuronidation reactions. These Ugts conjugate lipophilic substrates with UDP-glucuronic acid, by increasing the hydrophilicity of the substrates and enhancing the excretion into bile and urine. The endogenous substrates for Ugts include numerous steroids and metabolic products, including testosterone, estradiol, thyroxine, bilirubin, bile acids, etc. In addition, numerous xenobiotics are also substrates for Ugts, including therapeutic drugs such as chloramphenicol, acetaminophen, morphine, propofol, and nonsteroidal anti-inflammatory drugs (NSAIDs), as well as environmental toxicants, such as plant-derived dietary flavonoids, carcinogens, etc. (Radominska-Pandya et al., 1999; Tukey and Strassburg, 2000). There are 16 different UGT enzymes in humans, nine of these are encoded from the Ugt1 gene locus, which consists of different

functional promoters and first exons, and these UGT1 isoforms are produced by alternative splicing within common exons 2-5. UGT1A1 is the primary enzyme for bilirubin conjugation. In mice, the Ugt1a subfamily contains 14 first exons, coding nine enzymes and five pseudogenes. The Ugt2 and 3 families are much less studied compared to the first Ugt family. UGT2B has been suggested to be involved in chloramphenicol metabolism and Grey Baby Syndrome (McCarver and Hines, 2002). UGT3 was the last gene family to be identified, and very recent findings suggested that UGT3 has a unique function termed *N*-acetylglucosaminidation (Meech and Mackenzie, 2010).

Sulfotransferases (Sults) encode at least 11 distinct enzymes that catalyze the sulfate conjugation of a variety of endogenous and exogenous chemicals using 3'-phosphoadenosine-5'-phosphosulfate (PAPS) as a donor to target endo- and xenobiotics (Glatt, 2000). PAPS is formed from inorganic sulfate by the action of the enzyme PAPS synthase (PAPSs). The sulfotransferases can be classified into two major classes based on their subcellular location, including cytosolic Sults, which are located in cytosol, as well as membrane-associated Sults that are bound to the Golgi apparatus. It has been determined that membrane-associated Sults are involved in post-translational modifications of large molecules, including glycosaminoglycans, glycoproteins, sphingolipids, and tyrosine residues of proteins, whereas cytosolic Sults are important for the sulfation of small endo- and xenobiotics (Niehrs et al., 1994).

It is generally considered that glucuronidation, glutathione conjugation, and sulfation are the most important phase-II conjugation reactions for various therapeutic drugs, environmental toxicants, and endogenous chemicals. Therefore these three classes of reactions have been most extensively studied. Other phase-II conjugation reactions are also important in the detoxification of chemicals. To note, glycine and taurine conjugations are essential for bile-acid conjugation (Falany et al., 1994). In humans, glycine and taurine conjugates of bile acids are found in similar amounts, whereas in mice, bile acids are mainly conjugated with taurine (Alnouti et al., 2008a).

Transporters. Transporters are membrane proteins that are critical in the disposition of chemicals in an organism. In liver, basolateral uptake transporters are important in hepatic uptake of xenobiotics and other compounds absorbed from the intestine. Canalicular transporters are responsible for biliary excretion of various chemicals, whereas basolateral efflux transporters eliminate substrates from hepatocytes into blood, and these chemicals are eventually excreted via urine. The present laboratory has characterized numerous xenobiotic and endobiotic transporters enriched in liver (Klaassen and Aleksunes, 2010; Klaassen and Lu, 2008). The basolateral uptake transporters that are highly expressed in liver include the sodium taurocholate cotransporting polypeptide (Ntcp, *Slc10a1*), the organic anion transporting polypeptide 1b2 (*Oatp1b2*, *Slco1b2*), *Oatp1a1* and *1a4*, organic cation transporter 1 (*Oct1*, *Slc22a1*), organic anion transporter 2 (*Oat2*, *Slc22a7*), and equilibrative

nucleoside transporter 1 (*Ent1*, *Slc29a1*). The canalicular transporters enriched in liver include multidrug resistance protein 2 (*Mdr2*, *Abcb4*), bile salt export pump (*Bsep*, *Abcb11*), *Abcg5*, *Abcg8*, multidrug resistance-associated protein 2 (*Mrp2*, *Abcc2*), breast cancer resistance protein (*Bcrp*, *Agcg2*), multidrug and toxin extrusion 1 (*Mate1*, *Slc47a1*), and *ATP7b1*. The basolateral efflux transporters in liver include *Mrp3* (*Abcc3*), *Mrp6* (*Abcc6*), and *Abca1*. The organic solute transporters α and β (*Ost α* and *Ost β*), as well as *Mrp4* (*Abcc4*), are lowly expressed in liver, but they play important roles in bile-acid transport during cholestasis (Ballatori et al., 2005; Mennone et al., 2006).

Numerous liver transporters are important for xenobiotic disposition, including many *Oatps*, *Mrps*, etc, whereas other transporters play essential roles in maintaining the EHC of the endogenous bile acids. *Ntcp* is the major basolateral bile-acid uptake transporter in liver (Hagenbuch et al., 1996), whereas *Bsep* is the canalicular transporter for bile-acid excretion into bile (Wang et al., 2003; Lam et al., 2005). Whereas most bile acids are sequestered in the EHC under physiological conditions, during cholestasis, bile acids are also excreted back into blood from liver via basolateral transport systems, which include *Mrp4* (Mennone et al., 2006), as well as *Ost α* and *Ost β* that function as a heterodimer (Ballatori et al., 2005). In addition to bile-acid transporters, *Mdr2* in liver flips phospholipids from the inner to the outer leaflet of the canalicular membrane. Phospholipids enter bile to form micelles with bile acids, thereby protecting the biliary tree from injury (Smit et al., 1993), as well as facilitating nutrient absorption.

Table 1.1 lists the mRNAs of many critical drug-processing genes in phase-I and –II metabolism, transporters for processing xeno- and endobiotic chemicals, as well as critical transcription factors in liver. Although considerable amount of research has been reported on the expression and regulation of these genes in adults, very little is known about the ontogeny of the drug-processing genes during postnatal liver development.

Neonatal diseases associated with impaired drug metabolism and transport.

For phase-I metabolism, many well characterized Cyps have been found to be enriched in adult liver (Nebert and Russell, 2002). Interestingly, before birth, liver is mainly a hematopoietic organ with very limited capacity for drug metabolism. However, right after birth, liver becomes the major organ for processing drugs and other chemicals. The physiological changes in liver during development are undoubtedly responsible for age-related differences in drug disposition. Very little is known about how and when the drug-metabolizing P450s become activated or suppressed during postnatal liver development, resulting in higher risks for adverse drug reactions in pediatric patients. In 1959, it was found that a number of drugs that are metabolized by Cyps in liver microsomes from adult rabbit are not metabolized in livers of newborn rabbits (Fouts and Adamson, 1959). However, at that time, only two Cyp enzymes were thought to exist. At the end of the 20th century and the beginning of the 21st century, as several cytochrome P450 genes were cloned, the ontogeny of a few Cyps have been

Table 1.1. List of the mRNAs of critical drug processing genes and transcriptional factors in liver

Function	Classification	mRNAs
Phase I	Cytochrome P450s (Cyps)	Cyp1 Cyp1a1 Cyp1a2 Cyp1b1
		Cyp2 Cyp2a4 Cyp2b10 Cyp2c29 Cyp2c39 Cyp2c66 Cyp2d9 Cyp2d22 Cyp2e1 Cyp2f2 Cyp2j6
		Cyp3 Cyp3a11 Cyp3a12 Cyp3a16 Cyp3a25 Cyp3a41 Cyp3a44
		Cyp4 Cyp4a14 Cyp4f18
	Bile-acid synthesis	Cyp7a1 Cyp7b1 Cyp8b1 Cyp27a1
	Aldehyde Dehydrogenases (Aldhs) 15	Aldh1a1* Aldh1a2 Aldh1a3 Aldh1a7* Aldh1b1* Aldh2* Aldh3a1 Aldh3a2* Aldh3b1 Aldh4a1* Aldh6a1* Aldh7a1* Aldh8a1 Aldh9a1 Aldh18a1
	Carboxyesterases (Cess) 12	Ces1B2 Ces1B4 Ces1D1 Ces1E1 Ces1G2 Ces1H1 Ces2A4 Ces2A6 Ces2A12 Ces3A2 Ces4B2 Ces5B1
Paroxonases (Pons)	Pon1 Pon2 Pon3	
Phase II	UDP-glucuronyl transferases (Ugts)	Ugt1a1 Ugt1a2 Ugt1a5 Ugt1a6 Ugt1a7 Ugt1a8 Ugt1a9 Ugt1a10 Ugt2a3 Ugt2b1 Ugt2b5 Ugt2b34 Ugt2b35 Ugt2b36 Ugt2b37 Ugt2b38 Ugt3a1 Ugt3a2 uridine diphosphoglucose dehydrogenase (Udpgh)
	Glutathione-S-transferases (Gsts)	GSTa1 GSTa3 GSTk1 GSTo1 GSTp1/2 GSTz1 GSTm1 GSTm2 GSTm3 GSTm4 GSTm5 GSTm6 GSTt1 GSTt2 GSTmicrosomal1 GSTmicrosomal2 GSTmicrosomal3
	Sulfotransferases (Sults)	Sult1a1* Sult1b1# Sult1c1* Sult1c2* Sult1d1* Sult2a1/2* Sult2b1# Sult3a1* Sult4a1 Sult5a1 PAPSs1 PAPSs2#
	Methyltransferase	Comt
Transporters	Uptake transporters	Oatp1a1* [∇] Oatp1a4* [∇] Oatp1a5* Oatp1a6 [∇] Oatp1b2* Oatp2a1* [∇] Oatp2b1* [∇] Oatp3a1 [∇] Oatp4a1 Oatp4c1 Cnt1 Cnt2 Cnt3 Pept1 Pept2 Npt1 Npt2a Npt2b Oat1 [∇] Oat2 [∇] Oat3 [∇] Oat5 Urat1 Oct1* [∇] Oct2 [∇] Oct3 OctN1 OctN2 [∇] Npc1L1 Ntcp* Atp8b1 Ibat
	Efflux transporters	Mrp1 [∇] Mrp2* [∇] Mrp3* [∇] Mrp4* [∇] Mrp5 [∇] Mrp6* [∇] Mdr1a Mdr1b Mdr2 Mate1 Mate2 Ent1 Ent2 Ent3 Bsep* AbcG5 AbcG8 Abca1 Ostα Ostβ
Transcription Factors/regulators	AhR CAR FXR PXR RXRα RXRβ RXRγ LXRα LXRβ LRH-1 PPARα PPARδ PPARγ COUP-TFII AR ERα GR PR TRα TRβ VDR Prlr GHR IGF-1 Stat5a Stat5b HNF1α HNF1β HNF3α HNF3β HNF3γ HNF4α HNF4γ HNF6 C/EBPα C/EBPβ C/EBPδ DBP CREB Srebp-1 Srebp-2 Nrf1 Nrf2 Nrf3 Egr-1 Gadd45α Gadd45β c-jun p53 CHOP PBP PGC-1α SRC-1 SRC-2 Smrt Ncor1 SHP	

* Ontogenic expression in liver has been reported: 25 genes in total

Ontogenic expression in duodenum has been reported: 3 genes in total

[∇] Ontogenic expression in kidney has been reported: 19 genes in total

characterized in human livers (de Wildt et al., 1999; Blake et al., 2005; Leeder et al., 2005; Gaedigk et al., 2006; Hines, 2007), but at most 10 Cyp isoforms were included in these studies, and nobody has aimed at characterizing all the drug-metabolizing Cyps systematically. Clinically, it has been demonstrated that the clearance of various therapeutic drugs is altered in infants due to the different expression of Cyps than in adults. For example, the clearance of intravenously administered midazolam, which is primarily metabolized by CYP3A4 and 3A5, is low in newborns, and markedly increases in the first three months of life (de Wildt et al., 2001; Kearns et al., 2003). Conversely, the clearance of carbamazepine, another CYP3A substrate, is higher in children than in adults (Kearns et al., 2003). Phenytoin, which is an anti-convulsant metabolized by CYP2C9 and CYP2C19, has a prolonged half-life in preterm infants, but it decreases markedly in term infants during the first week of life. The CYP1A2 substrates, caffeine and theophylline, are commonly prescribed for neonates and young infants, and their plasma clearance in infants primarily reflects enzyme activity (Kearns et al., 2003). It is crucial to understand the molecular mechanisms underlying the ontogeny of these CYPs involved in xenobiotic metabolism, so as to achieve safe and effective pharmacological treatments.

Several Cyps are important for normal endobiotic metabolism during liver development, and genetic inborn errors of these genes often lead to neonatal diseases. For example, genetic mutations in CYP7A1 and CYP27A1 can both cause defects in bile-acid synthesis, leading to neonatal cholestasis, and fat-

soluble-vitamin deficiencies. These diseases are characterized by a failure to produce normal bile acids in liver, and an accumulation of unusual bile acids and other oxysterol intermediates (Stellaard and Wolthers, 1993; Bjorkhem, 1994; Heubi et al., 2007). Failure to diagnose these inborn errors of bile-acid synthesis in newborns can result in progressive chronic liver diseases.

In phase-II metabolism, UGT1A1, the primary enzyme for bilirubin conjugation, is lowly expressed from fetal liver, but its expression is induced by processes associated with birth and the activity markedly increases within the first 6 month of birth in humans (McCarver and Hines, 2002). Genetic mutations in UGT1A1 lead to neonatal jaundice and kernicterus due to hyperbilirubinemia. Excessive 2-bp insertions (TA) in the promoter region of UGT1A1 is called Gilbert syndrome, resulting in decreased enzyme production. Crigler-Najjar syndrome type I is associated with mutations resulting in a complete absence of Ugts, whereas type II is associated with mutations leading to decreased activity of the Ugts (Hirschfield and Alexander, 2006). UGT1A6, which is important in the glucuronidation of acetaminophen, is absent in fetuses, only slightly increases in newborns, and does not reach adult levels until approximately 10 years of age (McCarver and Hines, 2002). The delayed onset of the UGT2B subfamily has been found to be responsible for the adverse reactions to chloramphenicol therapy observed in neonates, commonly referred to as “Grey Baby Syndrome”, characterized by high serum and tissue drug levels (McCarver and Hines, 2002).

For Gsts, lower Gst expression was observed in mouse livers at birth and the early postnatal period, whereas the expression of many Gst isoforms was higher in adults (Cui et al., 2010; Tee et al., 1992). Maturation of these GSTs is essential during postnatal liver development, to protect the children from electrophiles and oxidative stress. It has been demonstrated that polymorphisms in several GST genes are associated with increased susceptibility to childhood malignant diseases (Zielinska et al., 2004), and GSTP1 gene polymorphism is a risk factor for childhood asthma (Lee et al., 2004b).

For sulfotransferases, a comparative ontogeny study between SULT1A2 and 1A3 was the first to demonstrate the expression of substantial SULT in fetal tissue (Cappiello et al., 1991). The activity of SULT1A3 is higher in fetal liver, whereas SULT1A1 activity is higher in adult tissue. SULT2A1 is lowly expressed in liver before 25 weeks of gestation, but markedly increases during the later half of gestation to approach adult levels in neonates. SULT1C3 mRNA was also shown to be expressed in fetal liver (Barker et al., 1994; McCarver and Hines, 2002).

For transporters, genetic inborn errors have been found in genes encoding certain transporters, leading to intrahepatic cholestasis in newborns. For example, inborn error in human ATP8B1 results in progressive familial intrahepatic cholestasis (PFIC type I) (Davit-Spraul et al., 2010), an inborn error in human BSEP results in severe progressive familial intrahepatic cholestasis

(PFIC type II) (Wang et al., 2002), as well as hepatocellular carcinoma in young children (Knisely et al., 2006). In addition, although the phospholipid transporter MDR3 (the human homolog of the mouse Mdr2) in liver does not transport bile acids, the defect in MDR3 also results in progressive familial intrahepatic cholestasis (PFIC type III) (de Vree et al., 1998). Mdr2-null mice develop hepatocyte degeneration and focal necrosis, as well as abnormalities in bile composition (Smit et al., 1993). Together these data have highlighted the importance of Mdr2/MDR3 in maintaining bile-acid circulation and liver protection.

Data from my previous work and other colleagues in the present laboratory have characterized the ontogeny of many drug-processing genes in the C57BL/6 mouse model. These genes include a few Cyps (Hart et al., 2009), and Aldhs (Alnouti and Klaassen, 2008) in phase-I metabolism; Ugts (Choudhuri et al., 2010), Gsts (Cui et al., 2010), and Sults (Alnouti and Klaassen, 2006) in phase-II metabolism; as well as various transporters including Oatps (Cheng et al., 2005a), Mdrs (Cui et al., 2009a), and Mrps (Maher et al., 2005b). However, very little is known about the mechanisms underlying the regulation of these drug-processing genes. In this dissertation, the transcription factor-mediated genetic regulation, as well as epigenetic regulation of these genes will be discussed.

Nuclear receptors and other transcription factors in regulating drug metabolism and transport.

Nuclear receptors and other transcription factors/co-factors for xenobiotics and endogenous compounds are important in regulating the metabolism and disposition of chemicals. Nuclear receptors are ligand-activated transcription factors that have a typical modular structure. They contain a highly conserved DNA-binding domain in the N-terminal region, and a moderately conserved ligand-binding domain in the C-terminal region. The classifications, distribution, and functions of nuclear receptors have been integrated in the Nuclear Receptor Signaling Atlas (NURSA, <http://www.nursa.org/>). In humans, there are 48 nuclear receptors identified according to their sequence homology, falling into 7 subfamilies, including thyroid hormone-receptor like, retinoid X receptor-like, estrogen-receptor-like, nerve growth factor IB-like, steroidogenic factor-like, germ cell nuclear factor, and miscellaneous members (Table 1.2).

PXR. Among various types of nuclear receptors, the pregnane X receptor (PXR; *NR1I2*) is a key regulator in mediating xeno- and endobiotic metabolism and disposition in liver, serving as a critical component of the liver's defense against toxic substances (Kliewer et al., 2002). As a member of the nuclear receptor family, PXR is a ligand-activated transcription factor that functions with its binding partner, the retinoid X receptor (RXR). Once activated, the PXR/RXR complex binds to DNA in the nucleus and regulates gene transcription (Kliewer et al., 1998). PXR is highly expressed in mammalian liver, and its DNA-binding domain is highly conserved across species (Kliewer et al., 2002). However, the ligand binding domain displays more variability among species, allowing PXR to be

Table 1.2

Subfamily of NRs	Type of NRs	Members of NRs in the Subfamily
Subfamily 1	Thyroid-hormone receptor like	thyroid hormone receptors (TR α and β), retinoic acid receptor (RXR α , β , and γ), peroxisome proliferator-activated receptor (PPAR α , β/σ , and γ), Rev-ErbA α and β , RAR-related orphan receptors (ROR α , β , and γ), liver X receptor-like (LXR α , β , and γ), farnesoid X receptor (FXR), and vitamin D-receptor like including vitamin D receptor (VDR), pregnane X receptor (PXR), constitutive androstane receptor (CAR)
Subfamily 2	Retinoid X receptor-like	hepatocyte nuclear receptor factor-4 (HNF4 α and γ), retinoid X receptors (RXR α , β , and γ), testicular receptors (TR2 and 4), TLX/PNR (human homologue of the <i>Drosophila</i> tailless gene, and photoreceptor cell-specific nuclear receptor), COUP/EAR (Chicken ovalbumin upstream promoter-transcription factors (COUP-TFI and II), V-erbA-related gene (EAR-2)
Subfamily 3	Estrogen receptor-like members	estrogen receptors (ER α and β), estrogen-related receptors (ERR α , β , and γ), glucocorticoid receptor (GR), mineralocorticoid receptor (MR), progesterone receptor (PR), androgen receptor (AR)
Subfamily 4	nerve growth factor IB-like	nerve growth factor IB (NGF1B), nuclear receptor related 1 (NURR1), neuron-derived orphan receptor 1(NOR1)
Subfamily 5	steroidogenic factor like	steroidogenic factor (SF1), liver receptor homolog-1 (LRH-1)
Subfamily 6	germ cell nuclear factor	germ cell nuclear factor (GCNF)
Subfamily 0	miscellaneous	DAX/SHP (dosage-sensitive sex reversal, and renal hypoplasia critical region, on chromosome X, gene 1, small heterodimer partner), nuclear receptors with two DNA binding domains (1DBD-NR)

activated by a wide spectrum of chemicals, including various drugs like the antibiotic rifampicin, the anti-inflammatory drug dexamethasone, and the anticonvulsant phenobarbital (Kliewer et al., 2002), environmental polybrominated diphenyl ethers (PBDE) (Pacyniak et al., 2007), and endogenous chemicals, such as bile acids (Staudinger et al., 2001; Xie et al., 2001). Although PXR ligands can be species specific, the target gene profiles share marked similarities between rodents and humans, including genes encoding drug metabolizing enzymes and transporters (together termed “drug-processing genes” in this study). The synthetic compound PCN, is a potent activator of mouse PXR, and is widely used by researchers to recapitulate human PXR activation in rodents (Kliewer et al., 1998).

Data from this and other laboratories have shown that numerous drug-processing genes in mouse liver are up-regulated following PCN administration (Cheng et al., 2005b; Maher et al., 2005a; Alnouti et al., 2008b; Alnouti and Klaassen, 2008; Knight et al., 2008). For example, our laboratory has shown that 18 drug-processing genes are induced by PXR in mouse liver, but only a few genes have been shown to be direct PXR targets (Kliewer et al., 2002; Zhou et al., 2006; Zhou et al., 2008). It remains to be determined whether the induction of critical drug-processing genes is due to direct trans-activation by PXR or due to secondary effects. More importantly, as it is becoming increasingly evident that PXR has novel physiological functions, such as trans-activating genes involved in lipid metabolism (Zhou et al., 2006; Zhou et al., 2008) and cell

proliferation (Guzelian et al., 2006), novel PXR-target genes need to be characterized, and this will fill a critical knowledge gap in predicting and further understanding the multifaceted roles of PXR in liver.

Numerous studies have characterized PXR response elements. It has been shown that PXR binds to AGGTCA-like direct repeats separated by 3 or 4 base pairs (DR-3 and DR-4) and everted repeats separated by 6 or 8 base pairs (ER-6 and ER-8) (Kliwer et al., 2002). Unfortunately, most of these findings are based on naked DNAs (such as in gel-shift assays), or cell cultures of non-hepatic origin with certain proteins artificially over-expressed, or cryopreserved hepatocytes that may have lost many features of *in vivo* cells. In addition, most studies have limited the detection range for PXR binding only to the gene promoter regions. Such designs are inherently biased, in that they do not seek to detect novel genomic PXR binding sites that may be equally important for gene regulation. It is therefore necessary to determine the most preferred DNA-binding signatures for PXR *in vivo*. Recent technological advancements, including CHIP-on-chip and CHIP-sequencing (CHIP-Seq), have made such unbiased genome-wide investigations possible (Margolin et al., 2009; Schmidt et al., 2009).

FXR. Whereas PXR is generally considered as a xenobiotic sensor, the Farnesoid X Receptor (FXR, *NR1H4*) is the major bile-acid sensor in liver. Once activated by bile acids, FXR down-regulates the major bile-acid uptake transporter Ntcp (Zollner et al., 2005), up-regulates the main bile-acid efflux

transporter Bsep (Plass et al., 2002), and up-regulates the basolateral bile-acid efflux transporters Ost α and β (Zollner et al., 2006). In addition, intestinal FXR down-regulates the major liver enzyme for bile-acid synthesis, Cyp7a1, through a mechanism that involves the stimulation of the intestinal signal fibroblast growth factor 15 (Fgf15), which travels to the liver and eventually represses Cyp7a1 mRNA expression (Inagaki et al., 2005). In various liver disease models, FXR serves as a negative feedback mechanism to reduce hepatic bile-acid concentrations. FXR-null mice have elevated serum bile-acid concentrations in adults (Sinal et al., 2000), indicating the important role of FXR in bile-acid synthesis and/or disposition. In addition to regulation of bile-acid synthesis and metabolism, a large body of evidence indicates that FXR is important in regulating lipid and glucose metabolism (Chiang, 2004). Less is known of the role of FXR during liver development. However, clinically, decreased FXR expression in ileum was observed in children with progressive familial intrahepatic cholestasis type I (Chen et al., 2004), and functional variants of FXR in liver have been identified in intrahepatic cholestasis of pregnancy (Van Mil et al., 2007), indicating FXR is important for both perinatal and maternal bile-acid homeostasis.

PPAR α and PGC-1 α . The peroxisome proliferator-activated receptor α (PPAR α , *NR1C1*) and peroxisome proliferators-activated receptor γ coactivator 1 (PGC-1 α , *Ppargc1a*) are two important metabolic regulators in liver for nutrient homeostasis. PPAR α is an essential nuclear receptor that regulates fatty acid

metabolism, and is therefore termed the “lipid sensor”. In contrast, PGC-1 α is a transcription co-activator important for the metabolism of glucose. PPAR α was first identified by Issemann and Green in 1990, and was named “PPAR” because its activation increases hepatic peroxisome volume and density, or peroxisome proliferation. PPAR α -null mice are resistant to peroxisome proliferation in response to administration of PPAR α ligands (Lee et al., 1995). PPAR α is expressed abundantly in liver where it regulates fatty-acid catabolism, as well as a few other organs including heart, muscle, and kidney. The endogenous ligands for PPAR α are fatty acids that bind PPAR α with relatively low affinities, and exogenous PPAR α ligands including fibrates are used to treat hypertriglyceridemia in patients. In addition, a few potent agonists have been used in the laboratory for non-human studies (GW7647, Wy-14643). Upon ligand activation, PPAR α hetero-dimerizes with the retinoid X receptor (RXR), and binds to the response element of a large battery of target genes involved in lipid homeostasis. For example, PPAR α stimulates peroxisomal β -oxidation of fatty acids to produce energy. The β -oxidation of fatty acids shortens long-chain fatty acids, and thus prevents lipid accumulation and toxicity. It also up-regulates fatty acid transport protein and long-chain acyl-CoA synthetase genes in liver, induces the expression of mitochondrial HMG-CoA synthetase to form ketone bodies, increases apolipoproteins apoA-I and apoA-II, and decreases apoC-III (Li and Glass, 2004). Consequently, PPAR α activators increase HDL and decrease triglyceride levels. PPAR α also regulates cholesterol homeostasis in macrophages. For example, PPAR α activation can lead to the induction of LXRA

expression, and LXR α then stimulates the expression of the cholesterol efflux transporter ABCA1, and promotes efflux of cholesterol to apoA-I (Chinetti et al., 2001). PPAR α can also inhibit esterification and increase the efflux of free cholesterol in human macrophages (Chinetti et al., 2000; Chinetti et al., 2003).

PGC-1 α is a critical transcriptional coactivator in liver to promote gluconeogenesis (Yoon et al., 2001). PGC-1 α was first identified in brown adipose tissue as a key regulator of adipocyte differentiation (Puigserver et al., 1998), and it was later found that PGC-1 α is a versatile metabolic regulator for adaptive thermogenesis, mitochondrial biogenesis, and fuel homeostasis (Puigserver and Spiegelman, 2003) in various organs. Although the basal expression of PGC-1 α is low in liver, which is the major producer of glucose, the hepatic expression of PGC-1 α is increased markedly by fasting (Yoon et al., 2001) and in type I diabetes (Puigserver and Spiegelman, 2003). It has been shown that PGC-1 α activates glucose biosynthesis by inducing all three key genes of gluconeogenesis in primary hepatocytes, namely phosphoenol-pyruvate carboxykinase (PEPCK), fructose 1,6-bisphosphatase, and glucose 6-phosphatase (Yoon et al., 2001). PGC-1 α stimulates a 3-fold increase in glucose secretion by hepatocytes when provided with gluconeogenic precursors such as lactate, pyruvate, glycerol, and alanine (Puigserver and Spiegelman, 2003). In addition to promoting glucose biosynthesis, PGC-1 α also cooperates with PPAR α in the transcriptional control of genes encoding mitochondrial fatty acid oxidation enzymes (Vega et al., 2000). As a coactivator of transcription, PGC-1 α

exerts its function by direct interaction with transcription factors after being recruited to particular sequences in gene promoters, and it has been shown that PGC-1 α can recruit proteins that contain histone acetyl-transferase activities that consequently unwind the chromatin to promote gene transcription (Puigserver et al., 1999).

Recent evidence suggests that PPAR α and PGC-1 α may be important during development, as they may mediate adaptations to changes in nutrient supply. It has been shown that PPAR α -null mice have severe fatty infiltration and elevated triglycerides in liver under fasting conditions (Lee et al., 2004a). In humans, a genetic defect in PGC-1 α signaling results in a defect in hepatic energy metabolism, and death usually occurs between 6 months and 12 years of age (Cooper et al., 2006).

Ahr. The aryl hydrocarbon receptor (Ahr) is well recognized as a ligand-activated transcription factor for aromatic hydrocarbons, including TCDD (2,3,7,8-tetrachlorodibenzo-*p*-dioxin) and polycyclic aromatic hydrocarbons. In mice, Ahr is most enriched in lung, and is expressed at intermediate levels in liver and the gastrointestinal tract (Petrick and Klaassen, 2007). In the absence of a ligand, Ahr is sequestered in the cytosol by two molecules of heat-shock protein 90 (HSP90). Upon ligand binding, Ahr is released from HSP90, translocates into the nucleus, and dimerizes with the Ahr nuclear translocator (ARNT). (ARNT is constitutively localized in the nucleus.) The Ahr-ARNT heterodimer then binds to

the xenobiotic response element of target genes, and usually increases gene transcription (Li et al., 1994; Ma et al., 1995).

Ahr regulates the expression of a large battery of drug-metabolizing genes, including the prototypical target genes CYP1A1, 1A2, and 1B1 (Rowlands and Gustafsson, 1997), several liver aldehyde dehydrogenases in mice (Alnouti and Klaassen, 2008), some liver UDP glucuronosyltransferases in rats (Shelby and Klaassen, 2006) and mice (Buckley and Klaassen, 2009), the organic anion transporting polypeptides 2b1 and 3a1 in mice (Cheng et al., 2005), and some multidrug resistance-associated protein efflux transporters in mice (Cheng et al., 2005b; Maher et al., 2005a).

In addition to its role in drug metabolism, Ahr is also important for normal liver development. Ahr-null mice have been engineered, either by deleting exon 1 (Fernandez-Salguero et al., 1995; Gonzalez and Fernandez-Salguero, 1998) or exon 2 (Schmidt et al., 1996; Harstad et al., 2006). Common phenotypes of the two lines of Ahr-null mice include a marked decrease in liver size per gram of body weight, moderate hepatic portal fibrosis, and decreased constitutive expression of certain xenobiotic-metabolizing enzymes, such as Cyp1a2 (Lahvis and Bradfield, 1998). In addition to the common liver phenotypes, Ahr-null mice with exon 1 deletion also have increased mortality within the first 2 weeks of age, hyper-proliferative blood vessels in the portal areas of the liver, glycogen depletion in liver, inflammation of bile ducts, and adenocarcinomas with aging

(Gonzalez and Fernandez-Salguero, 1998). In contrast, Ahr-null mice with exon 2 deletion are viable and fertile, but exhibit a spectrum of hepatic defects including transient microvesicular fatty metamorphosis, prolonged extramedullary hematopoiesis, and portal hypercellularity with thickening and fibrosis (Schmidt et al., 1996).

Very little is known about the ontogenic expression patterns, regulatory mechanisms, as well as the roles of these nuclear receptors and co-factors in liver development. Therefore, the expression signatures and functions of these factors will be examined in the present dissertation, in parallel with the characterization of drug-processing genes in postnatal liver maturation. The highly expressed xenobiotic sensor PXR, bile-acid sensor FXR, lipid sensor PPAR α , glucose sensor PGC-1 α , as well as the aryl-hydrocarbon receptor for detoxifying environmental aromatic hydrocarbons, will be emphasized in these studies.

Molecular targets of epigenetic regulation.

Besides nuclear receptor-mediated gene transcription, it has become increasingly evident that gene regulation during development is under stringent epigenetic control (Kiefer, 2007). As reviewed by Choudhuri et al. (2010), the term “epigenetics” was defined by Conrad Waddington in 1942 to describe developmental events leading from fertilization to the mature organism. In the context of genetics and molecular biology, epigenetics is defined as the “study of

mitotically or meiotically heritable changes in gene function that cannot be explained by changes in DNA sequence” (Riggs, 1996). Current studies on epigenetic modifications focus on DNA methylation and histone modifications. In general, alterations in DNA methylation status and chromatin environment are the ultimate regulatory mechanisms of gene transcription, as they determine whether the transcription machinery will be recruited to the gene promoters. The understanding of epigenetics has evolved over time as the knowledge increased on DNA methylation and chromatin modifications and their effects on gene expression (Felsenfeld, 2007; Reinberg, 2007). The current explosion of research on DNA methylation and chromatin modification has expanded the scope of research on drug metabolism and transport during liver development. Epigenetic inheritance involves the information transfer (epigenetic mark) not encoded in the DNA sequence, from parent cell to daughter cells, and from generation to generation. Epigenetic mark is like a bookmark that flags the chromatin state, “on” or “off”, “open” or “closed”, so it may be identified and maintained in the daughter cells (Choudhuri, 2009a). In the spirit of the term genomics, the term epigenomics has come into existence, and is a new frontier that studies epigenetic changes at the level of the entire genome (Callinan and Feinberg, 2006).

Chromatin (the DNA–histone complex in the nucleus) can be envisioned as a repeat of structural units called “nucleosomes” (Figure 1.2). The nucleosome core particle is composed of a histone octamer and the DNA that wraps around it.

Figure 1.2

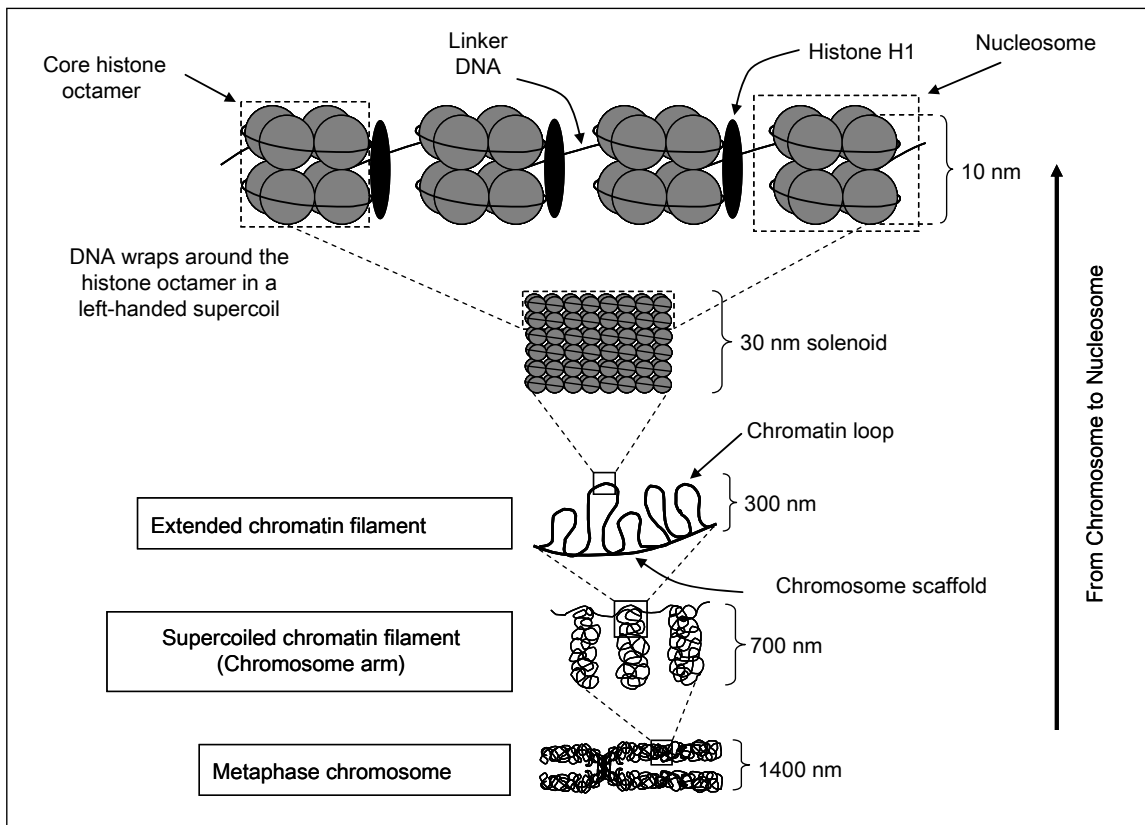


Figure 1.2. The hierarchy of organization from chromosome to nucleosome. (Chouhuri et al., 2010)

Histones are globular basic proteins with a flexible N-terminus (the so-called 'tail') that protrudes from the nucleosome. Histones are subject to various covalent modifications, and histone modifications occur primarily on the tail. The histone octamer contains two molecules each of histones H2A, H2B, H3, and H4. DNA wraps around the octamer in a left-handed supercoil of about 1.70 turns that contains approximately 150bp. Histone H1 is the "linker histone" that, along with "linker DNA" (the DNA in between two nucleosome core particles), physically connects the adjacent nucleosome core particles. The length of linker DNA varies with species and cell types. Although the DNA associated with the histone octamer is approximately 150bp, the entire nucleosome also includes part of the DNA on both sides of the core particle; hence the full nucleosome encompasses approximately 180- and 200-bp of DNA. Chromatin can undergo changes in its conformation in response to various cellular metabolic demands. Altered chromatin conformation, in turn, can limit or enhance the accessibility and binding of the transcription machinery, thereby precipitating an epigenetic effect on transcription.

Transcriptional silencing is the result of a condensed state of chromatin brought about by DNA methylation. It is thought to be achieved by two mechanisms; both are supported by experimental evidence: 1) recruitment of methyl CpG-binding transcriptional repressors, and 2) interference with the DNA binding of transcriptional activators. DNA methylation involves covalent modification of cytosine (C) bases at the carbon-5 position of CG dinucleotides

(5-MeC), referred to as CpG dinucleotides. The enzyme involved is DNA methyltransferase, known as DNMT, and the methyl donor is S-adenosylmethionine (SAM). The C of CpG is methylated in both strands of DNA. In the genome, CpGs may or may not occur in clusters. CpG clusters, i.e., CpG-rich sequences of the genome, are known as CpG islands. By definition, CpG islands are genomic regions that are at least 200-bp long with 50% or higher G+C content and 60% or higher observed/expected CpG ratio (Fazzari and Greally, 2004). In mammalian cells, the majority of CpG sites that do not exist as CpG clusters are methylated, such as satellite DNA, repetitive elements (e.g., transposons), non-repetitive intergenic DNA, and exons of genes. Exceptions to this general CpG methylation paradigm are the CpG islands, which are unmethylated CpG clusters (Illingworth and Bird, 2009). In other words, isolated CpG sites are methylated but CpG clusters (CpG islands) are not methylated. Although CpG islands generally remain methylation-free, the methylated state of CpG islands with low levels of DNA methylation has also been reported (Wise and Pravtcheva, 1999; Straussman et al., 2009). A number of factors may dictate these undermethylated states of CpG islands, such as local sequence features, Sp1 binding sites, specific *cis*-acting enhancer elements, as well as specific histone methylation marks, which prevent the binding of the *de novo* methylation complex (Straussman et al., 2009). Methylation of the C of CpG is associated with transcriptional silencing, and the absence of methylation is associated with active transcription. Thus, unmethylated CpG islands are associated with the promoters of transcriptionally active genes, such as

housekeeping genes and many regulated genes, such as genes showing tissue-specific expression. How CpG islands remain unmethylated remains unclear (Li and Bird, 2007).

Histone modification is a covalent modification that precisely regulates DNA repair, chromatin assembly/disassembly, and gene transcription. Histones are subject to many different types of reversible covalent post-translational modifications, such as acetylation, methylation, phosphorylation, ADP-ribosylation, ubiquitination, and sumoylation. The roles of these histone modifications in gene transcription are listed in Table 1.3.

Of these types of histone modifications discussed in Table 1.3, histone acetylation (ac) is a transcription-activating modification that is achieved by the addition of an acetyl group ($-\text{CH}_3\text{CO}$) from acetyl Coenzyme A, to one or more lysine residues at the ϵ -amino group by histone acetyltransferases (HATs). Acetylation reduces the overall positive charge of histones by neutralizing the positive charge of the target lysine; therefore, it decreases the affinity of the histone for the negatively charged DNA. A reduced DNA–histone interaction results in a decondensed, relaxed (i.e., open) chromatin conformation, which allows the transcriptional activators to gain access to their cognate recognition elements and initiate/enhance transcription. Many transcriptional coactivators have HAT activity. Histone acetylation and its stimulatory effects on transcription have been known for long time. Some other histone modifications are

Table 1.3: Some transcriptional activating and repressing histone modifications (Chouhuri et al., 2010)

Activating modifications	Repressing modifications
Acetylation: H2A: K5, K9, K13 H2B: K5, K12, K15, K20 H3: K9, K14, K18, K23, K56 H4: K5, K8, K13, K16	
Methylation: H3: K4, K36, K79 H3: R17, R23 H4: R3	Methylation: H3: K9, K27 H4: K20
Phosphorylation: H3: T3 H3: S10, S28 H3: Y41 H2AX: S139 (for DNA repair)	
Ubiquitination: H2B: K120, H2B: K123 (yeast)	Ubiquitination: H2A: K119
	Sumoylation: H2A: K126 (yeast) H2B: K6, K7 (yeast) H4: K5, K8, K12, K16, K20

transcription activating but some are transcription repressing, yet others may have transcription activating or repressing effects depending on which amino acid residue of histone is modified.

Histone methylation (me) is catalyzed by histone methyltransferases (HMTs) at lysine and arginine residues, primarily of histone H3 and H4. The methyl group donor is S-adenosylmethionine (SAM). Methylation increases the bulk but does not interfere with the charge. Methylation can be mono- (me), di- (me₂), or trimethylation (me₃). Histone phosphorylation (ph) is a transcription-activating modification. It is achieved by kinase-catalyzed addition of the negatively charged γ -phosphate, usually from ATP or GTP, to one or more serine and/or threonine residues of histone H3; serine 10 being a frequent target (H3S10ph). The addition of a negatively charged phosphate to the N-terminal of histone tails presumably disrupts the electrostatic interactions between histones and DNA, thereby destabilizing local chromatin conformation, and triggering transcriptional activation.

For histone ubiquitination (ub), it has been shown *in vivo* that histone H1, H2A, H2B, and H3 can all be ubiquitinated at lysine residues, but H2A and H2B ubiquitinations are the most common. H2BK123ub in yeast is required for histone H3K4 and H3K79 methylation. H3K4 and H3K79 methylation in turn activate gene transcription. Ubiquitination of histone H1 results in its release from the DNA; this helps reduce chromatin condensation and facilitates

transcriptional activation. Histone de-ubiquitination is carried out by ubiquitin proteases.

Histone ADP-ribosylation is catalyzed by ADP-ribosyltransferase and involves the transfer of ADP-ribose moiety of NAD^+ to a specific amino acid of the acceptor protein with the simultaneous release of nicotinamide. Arginine, glutamate and lysine residues in the histone are frequently subject to ADP-ribosylation. Histones are ADP-ribosylated in response to DNA damage. DNA strand breaks are recognized by poly (ADP-ribose) polymerase-1 (PARP-1), which catalyzes histone ADP-ribosylation at the lysine residues. The resulting negative charge to the histone causes electrostatic repulsion between the histone and the negatively charged DNA. This leads to the pulling of the DNA away from the histones, hence loosening the chromatin structure and making it more accessible to repair enzymes (Edwards and Myers, 2007).

Histone sumoylation occurs at the lysine residues, and was first reported in 2003 in human cell lines (Shiio and Eisenman, 2003). Small ubiquitin-related modifier (SUMO) is a member of a growing family of ubiquitin-like proteins involved in posttranslational modifications of proteins implicated in crucial cellular processes, such as cell-cycle regulation, transcription, nucleocytoplasmic transport, DNA replication and repair, chromosome dynamics, apoptosis, and ribosome biogenesis (Vertegaal et al., 2006).

Among various types of histone modifications described above, histone H3 lysine-4 di-methylation (H3K4Me₂) is a more specific epigenetic mark related to initiation of gene transcription, evidenced by the presence of H3K4Me₂ in promoters and transcribed regions of many active genes; whereas H3 lysine-27 tri-methylation (H3K27Me₃) is associated with suppression of gene transcription. Compared to other types of histone modifications, namely, acetylation, ubiquitination, phosphorylation, poly-ADP-ribosylation and sumoylation, histone methylations are more stable and the enzymes that catalyze the histone methylation are implicated in playing essential roles during development (Barski et al., 2007). Therefore, methylations of histone were selected in the present study over other types of histone modifications.

Although the genetic regulation of various drug-metabolizing enzymes and transporters has been studied for many years, studies on their epigenetic regulation is relatively recent. A number of publications have demonstrated various aspects of the epigenetic regulation of drug and xenobiotic enzymes and transporters. Various CYP isoforms in humans that have been shown to have an epigenetic component in their regulation include CYP1A1, 1A2, 1B1, 2E1, 2W1, and 2A13 (Rodriguez-Antona et al., 2010). The epigenetic aspect of regulation of CYP enzymes may explain, at least in part, the observed inter-individual variability in their expression, and further modulate an individual's genetic ability to cope with environmental chemicals, including drugs. For example, DNA methylation is an important epigenetic mechanism regulating CYP1A1 mRNA

expression. In a prostate cancer cell line LNCaP, promoter methylation of the *CYP1A1* gene prevents the binding of the AhR complex to the dioxin response element (DRE), resulting in repression of *CYP1A1* mRNA expression (Okino et al. 2006). In contrast, hypomethylation of the promoter in noncancerous cell lines, PWR-1E and RWPE-1, facilitates binding of the nuclear receptors to the direct repeat elements (DRE). For *CYP1A2*, a single CpG in the sequence CCGG at position –2759 and next to the AP-1 binding site in the 5'-flanking region can reduce *CYP1A2* gene expression (Hammons et al., 2001). The epigenetic regulation of *CYP1A2* expression may explain the great degree of inter-individual variability observed in *CYP1A2* expression, and the ability to metabolize *CYP1A2* substrates. Similar promoter/enhancer methylation-driven alterations in expression has been reported for *CYP1B1*, *CYP2E1*, *CYP2W1*, and *CYP2A13* genes, whereas hypermethylation is associated with decreased expression, and hypomethylation is associated with increased expression (reviewed by Rodriguez-Antona et al., 2010). In addition to DNA methylation, it has been shown in the mouse Hepa-1 cell line that chromatin structure also plays an essential role in *Cyp1a1* gene transcription. Specifically, induction of *Cyp1a1* gene transcription is strongly associated with hyperacetylation of histone H3K14 and H4K16, as well as other modifications, such as H3K4me3 and H3S10ph (Schnekenburger et al., 2007).

In an effort to understand whether the developmental switch between *Cyp3a16* (neonatal isoform) and *Cyp3a11* (adult isoform) expression in mouse

has an epigenetic basis, Li et al (2009) studied DNA methylation, and histone modifications (H3K4me2, H3K27me3) around the *Cyp3a* locus at various developmental stages, from prenatal through neonatal to young adults. No DNA hypermethylation was observed at the *Cyp3a* locus at any age. However, the expression of *Cyp3a16* in neonatal livers and *Cyp3a11* in adult livers was strongly correlated with increases in H3K4me2, which is a gene expression-promoting histone modification. Likewise, the suppression of *Cyp3a16* expression in adult livers correlated with decreases in H3K4me2 and increases in H3K27me3, the latter being a gene expression-repressing histone modification. Thus, the developmental switch between *Cyp3a11* and *Cyp3a16* gene expression is controlled by dynamic epigenetic regulation of these loci through histone modifications. An earlier study (Jin et al., 2004) showed that mouse *Cyp1a2* gene expression coincides well with the methylation status of DNA during liver development. For phase-II drug and xenobiotic metabolizing enzymes, we have demonstrated that the adult-enriched permissive signal H3K4me2, in the absence of suppressive signals like DNA methylation or H3K27me3 at any age, marks the adult-specific expression of *Ugt2* and *Ugt3* (UDP-glucuronosyltransferase 2 and 3) gene polycistron clusters in mouse liver (Choudhuri et al., 2010). Taken together, the “time-clock” for the ontogeny of drug-metabolizing enzymes appears to be at least in part determined by distinct epigenetic signatures.

Just like the drug- and xenobiotic-metabolizing enzymes, the regulation of various drug and xenobiotic transporters also show an epigenetic component. Recently, Imai et al. (2009) reported the analysis of DNA methylation and histone modification profiles of various mouse liver-specific transporter genes, such as *Oatp1b2* (*Slco1b2*), *Ntcp* (*Slc10a1*), *Bsep* (*Abcb11*), as well as *Abcg5* and *Abcg8*. Methylation analysis around the transcription start site (TSS) of these genes in liver, kidney and cerebrum showed that the CpG dinucleotides around the TSS of *Oatp1b2*, *Ntcp*, *Bsep*, and *Abcg5/8* are hypomethylated in the liver but hypermethylated in the kidney and cerebrum. The opposite pattern was observed for *Pept2*, which is expressed in the kidney and cerebrum but not in the liver. Thus, the CpG methylation pattern correlates directly with the expression pattern of these transporters. Promoter histone modification status also correlates well with the expression of these transporters. Chromatin immunoprecipitation experiments demonstrated histone H3 hyperacetylation in the promoters of hepatic *Oatp1b2*, *Ntcp*, *Bsep* and *Abcg5/8*, but little acetylation in the kidney and cerebrum. In contrast, the upstream region of *Pept2* is hyperacetylated only in the kidney and cerebrum where it is expressed. In mouse liver, the efflux transporters *Mdr1a* and *1b* mRNAs are expressed at a low level, but *Mdr2* mRNA is expressed at a high level and is induced right after birth (Cui et al., 2009). Distinct epigenetic signatures were also identified around the *Mdr* gene cluster. The permissive signal H3K4me2 was only observed in the *Mdr2* gene locus, and the *Mdr2* mRNA is highly expressed in liver, whereas the non-permissive signal H3K27me3 was not observed at any regions within this

gene cluster. In addition, DNA hypermethylation was observed within the 3'-UTR regions of *Mdr1a* and *1b*, corresponding to low mRNA expression of *Mdr1a* and *1b* at all ages. In contrast, DNA methylation was observed in the intragenic region of *Mdr2* with relatively less enrichment. Thus, differential epigenetic signatures appear to correlate, at least in part, with the expression of *Mdr* genes in liver. Therefore, the data from the above studies demonstrate the existence of distinct epigenetic components in the regulation of tissue-specific expression of many transporters. Conceivably, the same principle may also apply for transporters of other species including humans. A similar promoter methylation-driven regulation of expression was reported earlier for the mouse *Abcc6* (*Mrp6*) gene (Douet et al., 2007), and human *OAT3* gene (Kikuchi et al., 2006). In mice, high and moderate levels of methylation of the *Abcc6* promoter correlate with low levels of *Abcc6* expression. *Abcc6* expression in kidney, tail extremity, and skin was determined to be ~5%, 1%, and 0.1% of that in liver where it is expressed at the highest level. The mechanism of repression of *Abcc6* gene expression was found to be CpG methylation-driven interference of the binding of the transcription factor Sp1, thereby inhibiting Sp1-dependent transcription.

Although some work has been done in characterizing the roles of epigenetic marks in regulating drug-processing genes in adults, very little is known about their roles during liver development. The epigenetic aspect of regulation of various drug and xenobiotic metabolizing enzymes and transporters may provide

an explanation of different ontogenic expression patterns of the drug-processing genes.

CHAPTER TWO. STATEMENT OF PURPOSE

Very little is known of the ontogenic expression of phase-I and –II drug metabolizing enzymes and transporters during postnatal liver maturation, nor the genetic and epigenetic mechanisms underlying the regulation of these drug processing genes. Therefore, the present dissertation is poised to fill this critical knowledge gap, using multidisciplinary approaches. Four aims have been included in this dissertation, based on the categories of drug processing genes and transcription factors. The central hypothesis is that the developmental regulation of drug-processing genes is a sequential event regulated by distinct chromatin epigenetic signatures, which set a permissive environment for transcription factor recruitment, and trans-activation of target genes during postnatal liver maturation, forming age-specific expression patterns of the drug-metabolizing enzymes and transporters.

Aim 1 was designed to characterize the expression of known and novel cytochrome P450 genes in liver during development. For this study, I have focused on the ontogeny of the first four families of cytochrome P450s (Cyp1-4), and these Cyps are important for drug metabolism. Last year, we and our collaborator's laboratory characterized the ontogeny of 19 Cyps in mouse liver, and addressed the epigenetic mechanisms underlying the molecular switch of the Cyp3a genes during liver development (Hart et al., 2009; Li et al., 2009). As genome-scale investigations have identified many novel Cyp isoforms recently, it is critical to perform a systematic characterization of these Cyps during liver

development. In this study, livers were collected from C57BL/6 mice at 2 days before birth and various postnatal ages. The mRNAs of 75 Cyp isoforms (Cyp1-4) were quantified by the bDNA assay and RT-qPCR, and analyzed by hierarchical clustering. The conservation of these CyPs for humans and their genomic locations were examined. The PXR-mediated genetic mechanisms were determined by ChIP-Seq, and as we reported previously, the epigenetic mechanisms for the regulation of these CyPs were determined by ChIP-on-chip.

Aim 2 was designed to characterize the ontogeny and regulatory mechanisms for phase-II metabolism, mainly focusing on the Gsts, which are critical phase-II enzymes in protecting cellular macromolecules against electrophiles and oxidative stress. The ontogeny of 19 known Gst isoforms were investigated in mouse liver during development, and various ontogenic patterns were defined by a two-way hierarchical clustering dendrograph. The PXR-binding signatures and epigenetic marks were also examined.

Aim 3 was designed to determine the ontogeny of liver transporters for the disposition of xeno- and endobiotics. The ontogeny of the major liver transporters for the enterohepatic circulation (EHC) of bile acids, as well as the ontogeny of other xenobiotic transporters was determined in this study. The molecular mechanisms underlying the neonatal induction of bile-acid transporters were characterized using nuclear-receptor gene null mice (FXR-null and PXR-null). The ontogenic expression of bile-acid biosynthetic enzymes was

determined by bDNA assays, and the concentrations of various bile acids were quantified in liver and serum by LC-MS/MS to identify novel biomarkers in mediating the increase of these EHC transporters. For xenobiotic transporters, the PXR-DNA binding signatures of these genes were characterized. A novel PXR-DNA binding motif was identified in the xenobiotic uptake transporter *Oatp1a4*, and confirmed *in vitro* by an ELISA-based transcription factor binding assay. The epigenetic mechanisms underlying the regulation of some of these transporters were also discussed.

Aim 4 was designed to characterize the ontogeny of transcription factor genes. The ontogenic expression of over seventy transcription factors was determined by messenger RNA assays. The epigenetic mechanisms underlying the developmental regulation of AhR, PPAR α , as well as PGC-1 α (co-activator) have been determined.

In summary, by integrating various research models and high-throughput technologies, the present studies have examined the expression patterns and the mechanisms for the ontogeny of drug-processing genes and regulatory factors during liver development. The present study has provided novel insights into identifying and further understanding the molecular targets for efficacious and safe drug treatments in children.

CHAPTER THREE. EXPERIMENTAL MATERIALS AND METHODS

Reagents: Anti-PXR antibody (sc-25381, rabbit polyclonal) was obtained from Santa Cruz (Santa Cruz, CA). Rabbit polyclonal antibody against 5-methylcytosine (ab51552) was purchased from Abcam (Cambridge, MA). Rabbit polyclonal antibody against methylated H3K4 and H3K27 were purchased from Millipore Upstate (Billerica, MA). Anti-AhR antibody (SA-210, rabbit polyclonal) was purchased from Enzo Life Sciences (Plymouth Meeting, PA). Anti- β -actin antibody (ab8227, rabbit polyclonal) was purchased from Abcam (Cambridge, MA). Rabbit polyclonal antibodies against Bsep (K44) and Ntcp (K4) were generous gifts from Dr. Bruno Steiger (University Hospital, Zurich, Switzerland).

Animals. Eight-week old C57BL/6 breeding pairs were purchased from Charles River Laboratories (Wilmington, MA). Mice were housed according to the American Animal Association Laboratory Animal Care guidelines, and were bred under standard conditions at the University of Kansas Medical Center. Breeding pairs were established at 4:00pm, and separated the following day at 8:00am. The body weight of females was recorded each day to monitor pregnancy status. Livers from offspring were collected at the following ages: day -2, 0 (right after birth and before the start of lactation), 1, 3, 5, 10, 15, 20, 30, and day 45. Due to small size of liver in young mice (from day -2 to day 5), samples from male and female offspring (same litter) were pooled at each age to achieve the minimum amount of liver for subsequent experiments. After 10 days of age, males and females were separated. Livers were frozen immediately in liquid nitrogen, and

stored at -80°C. All animal procedures were reviewed and approved by the Institutional Animal Care and Use Committee at the University of Kansas Medical Center.

RNA Isolation. Total RNA was isolated using RNAzol Bee reagent (Tel-Test Inc., Friendswood, TX) per the manufacturer's protocol. RNA concentrations were quantified using a NanoDrop Spectrophotometer (NanoDrop Technologies, Wilmington, DE) at a wavelength of 260 nm. The integrity of the total RNA samples was evaluated by formaldehyde-agarose gel electrophoresis, and confirmed by visualization of 18S and 28S rRNA bands.

Selection of Cyp genes. Because the first four cytochrome P450 gene families (Cyp1, 2, 3, and 4) are known to be important in drug metabolism, 75 known and novel Cyp isoforms in these gene families are included in the present study. These Cyp genes are selected based on a literature search of PubMed (<http://www.ncbi.nlm.nih.gov/pubmed/>), the cytochrome P450 database by Dr. David Nelson (<http://drnelson.utmem.edu/CytochromeP450.html>), HighWire (<http://highwire.stanford.edu/>), and BioGPS (<http://biogps.gnf.org>). Pseudogenes were excluded from the present study. The human homologs for the mouse Cyps (if present), as well as their DNA and protein identities are shown in Table 3.1.

Table 3.1. The human homologs for the mouse Cyps (if present), as well as their DNA and protein identities

Mouse Cyps	Human Cyps	Mouse GeneID	Mouse mRNA ID	Mouse Protein ID	DNA Identity(%)	Protein Identity(%)	Chromosome Loc.
Cyp1a1	CYP1A1	13076	NM_009992	NP_034122	82.7	80.6	9
Cyp1a2	CYP1A2	13077	NM_009993	NP_034123	79.9	73	9
Cyp1b1	CYP1B1	13078	NM_009994	NP_034124	81.8	81	17
Cyp2a4	CYP2A6/7/13	13086	NM_009997	NP_034127	83.4/83.2/84.3	83.6/82/86.6	7
Cyp2a5	CYP2A6/7/13	13087	NM_007812	NP_031838	84.6/84.3/85.5	85.2/83/6/88/5	7
Cyp2a22	N/A	233005	NM_001101467	NP_001094937	N/A	N/A	7
Cyp2b9	N/A	13094	NM_010000	NP_034130	N/A	N/A	7
Cyp2b10	CYP2B6	13088	NM_009999	NP_034128	78.1	75.8	7
Cyp2b13	N/A	13089	NM_007813	NP_031839	N/A	N/A	7
Cyp2b19	N/A	13090	NM_007814	NP_031840	N/A	N/A	7
Cyp2b23	N/A	243881	NM_001081148	NP_001074617	N/A	N/A	7
Cyp2c29	N/A	13095	NM_007815.3	NP_031841.3	N/A	N/A	19
Cyp2c37	CYP2C19	13096	NM_010001	NP_034131	78.5	72.4	19
Cyp2c38	N/A	13097	NM_010002	NP_034132	N/A	N/A	19
Cyp2c39	N/A	13098	NM_010003	NP_034133	N/A	N/A	19
Cyp2c40	N/A	13099	NM_010004	NP_034134	N/A	N/A	19
Cyp2c44	N/A	226143	NM_001001446	NP_001001446	N/A	N/A	19
Cyp2c50	CYP2C19	107141	NM_134144	NP_598905	78.5	72.6	19
Cyp2c54	CYP2C19	404195	NM_206537	NP_996260	77.9	70.8	19
Cyp2c55	CYP2C18	72082	NM_028089	NP_082365	81.9	76.3	19
Cyp2c66	CYP2C8	69888	NM_001011707	NP_001011707	78.4	72.4	19
Cyp2c67	N/A	545288	NM_001024719	NP_001019890	N/A	N/A	19
Cyp2c68	N/A	433247	NM_001039555	NP_001034644	N/A	N/A	19
Cyp2c69	N/A	100043108	XM_001479745	XP_001479795	N/A	N/A	19
Cyp2c70	N/A	226105	NM_145499	NP_663474	N/A	N/A	19
Cyp2d9	N/A	13105	NM_010006	NP_034136	N/A	N/A	15
Cyp2d10	N/A	13101	NM_010005	NP_034135	N/A	N/A	15
Cyp2d11	N/A	545123	NM_001104531	NP_001098001	N/A	N/A	15
Cyp2d12	N/A	380997	NM_201360	NP_958748	N/A	N/A	15
Cyp2d22	CYP2D6	56448	NM_019823	NP_062797	79.9	75.8	15
Cyp2d26	N/A	76279	NM_029562	NP_083838	N/A	N/A	15
Cyp2d34	N/A	223706	NM_145474	NP_663449	N/A	N/A	15
Cyp2d40	N/A	71754	NM_023623	NP_076112	N/A	N/A	15
Cyp2e1	CYP2E1	13106	NM_021282	NP_067257	79.4	78.1	7
Cyp2g1	N/A	13108	NM_013809	NP_038837	N/A	N/A	7
Cyp2f2	CYP2F1	13107	NM_007817	NP_031843	82.6	81.9	7
Cyp2j5	N/A	13109	NM_010007	NP_034137	N/A	N/A	4
Cyp2j6	CYP2J2	13110	NM_010008	NP_034138	78.3	76.2	4

Table 3.1 cont'd. The human homologs for the mouse Cyps (if present), as well as their DNA and protein identities

Mouse Cyps	Human Cyps	Mouse GeneID	Mouse mRNA ID	Mouse Protein ID	DNA Identity(%)	Protein Identity(%)	Chromosome Loc.
Cyp2j7	N/A	546837	NM_001104926	NP_001098396	N/A	N/A	4
Cyp2j8	N/A	665095	NM_001104927	NP_001098397	N/A	N/A	4
Cyp2j9	N/A	74519	NM_028979	NP_083255	N/A	N/A	4
Cyp2j11	N/A	100066	NM_001004141	NP_001004141	N/A	N/A	4
Cyp2j12	N/A	242546	NM_001100182	NP_001093652	N/A	N/A	4
Cyp2j13	N/A	230459	NM_145548	NP_663523	N/A	N/A	4
Cyp2t4	N/A	384724	NM_001100184	NP_001093654	N/A	N/A	7
Cyp2u1	CYP2U1	71519	NM_027816	NP_082092	78.3	79.5	3
Cyp2w1	CYP2W1	545817	NM_001160265	NP_001153737	78.5	77.9	5
Cyp3a11	CYP3A4	13112	NM_007818	NP_031844	78.1	72.8	5
Cyp3a13	CYP3A7	13113	NM_007819	NP_031845	79.6	72.5	5
Cyp3a16	CYP3A4	13114	NM_007820	NP_031846	77.6	70.6	5
Cyp3a25	CYP3A43	56388	NM_019792	NP_062766	74.4	66.5	5
Cyp3a41a	CYP3A4	53973	NM_017396	NP_059092	77.2	71.6	5
Cyp3a41b	CYP3A4	100041375	NM_001105159	NP_001098629	77.3	71.4	5
Cyp3a44	CYP3A4	337924	NM_177380	NP_796354	76.7	69.6	5
Cyp3a57	CYP3A43	622127	NM_001100180	NP_001093650	74.8	65.6	5
Cyp3a59	CYP3A43	100041449	NM_001105160	NP_001098630	74.4	65.2	5
Cyp4a10	CYP4A11	13117	NM_010011	NP_034141	79.3	77.4	4
Cyp4a12a	CYP4A22	277753	NM_177406	NP_803125	79.2	75	4
Cyp4a12b	CYP4A22	13118	NM_172306	NP_758510	79.6	75.5	4
Cyp4a14	N/A	435802	NM_001100185	NP_001093655	N/A	N/A	4
Cyp4a29	N/A	230639	NM_001100183	NP_001093653	N/A	N/A	4
Cyp4a30b	N/A	435802	NM_001100185	NP_001093655	N/A	N/A	4
Cyp4a31	N/A	666168	NM_201640	NP_964002	N/A	N/A	4
Cyp4a32	CYP4A11	100040843	NM_001100181	NP_001093651	78.9	76.2	4
Cyp4b1	CYP4B1	13120	NM_007823	NP_031849	85.7	85.1	4
Cyp4f13	N/A	170716	NM_130882	NP_570952	N/A	N/A	17
Cyp4f14	CYP4F12	64385	NM_022434	NP_071879	79.1	75.3	17
Cyp4f15	CYP4F2	106648	NM_134127	NP_598888	81.6	80.4	17
Cyp4f16	N/A	70101	NM_024442	NP_077762	N/A	N/A	17
Cyp4f17	CYP4F8	208285	NM_001101445	NP_001094915	76.1	71.1	17
Cyp4f18	CYP4F3	72054	NM_024444	NP_077764	82.2	81.5	8
Cyp4f39	CYP4F22	320997	NM_177307	NP_796281	83	86.8	17
Cyp4f40	CYP4F11	631304	NM_001101588	NP_001095058	78.8	78.4	17
Cyp4v3	CYP4V2	285440	NM_133969	NP_598730	82.1	82.1	8
Cyp4x1	CYP4X1	81906	NM_001003947	NP_001003947	81.1	71.2	4

Messenger-RNA quantification for Cyps. The mRNAs of cytochrome P450s from Cyp1, 2, 3, and 4 gene families were determined from total RNA samples (n=4~5 per group). The majority of these Cyp mRNAs (55) were quantified by the Multiplex branched DNA amplification technology (bDNA assay). Briefly, individual bead-based oligonucleotide probe sets specific for each gene examined were developed by Affymetrix/Panomics Inc (Fremont, CA) (panel ID: 21211, 21212, 21213). The probe sequences are available at <http://www.panomics.com>. Samples (400 ng of total RNA per sample) were analyzed using a Bio-Plex 200 System Array reader with Luminex 100 X-MAP technology, and data were acquired using a Bio-Plex Data Manager Software Version 5.0 (Bio-Rad, Hercules, CA). Assays were performed according to the manufacturer's protocol. Data are expressed as the ratio of relative light units (RLU) specific to the mRNA expression, and normalized to the internal control Gapdh. The gene names, accession numbers, and the panel information are shown in Table 3.2.

Due to high sequence homology, the other 19 Cyp mRNAs were quantified by RT-qPCR to avoid cross-reaction. Reverse transcription of total RNA to cDNA was performed using Applied Biosystems High Capacity Reverse Transcriptase kits (Applied Biosystems, Foster City, CA). Briefly, equal volumes of 50 ng/ μ l RNA and 2X reverse-transcriptase reaction mix were combined and placed in an Eppendorf mastercycler under the following conditions: 25°C for 10 min; 37°C for 120 min; 85°C for 5 min. Subsequently, qPCR was performed on the resulting

Table 3.2. The Cyp gene names, accession numbers, and the panel information for the multiplex branched DNA amplification technology

<u>Gene Name</u>	<u>Accession Number</u>	<u>Panel ID</u>
Cyp1a1	NM_001136059	21211
Cyp1a2	NM_009993	21211
Cyp1b1	NM_009994	21211
Cyp2a4	NM_009997	21211
Cyp2a22	NM_001101467	21211
Cyp2b9	NM_010000	21211
Cyp2b10	NM_009999	21211
Cyp2b13	NM_007813	21211
Cyp2b19	NM_007814	21211
Cyp2b23	NM_001081148	21211
Cyp2c29	NM_007815	21211
Cyp2c38	NM_010002	21211
Cyp2c39	NM_010003	21211
Cyp2c44	NM_001001446	21211
Cyp2c55	NM_028089	21211
Cyp2c66	NM_001011707	21211
Cyp2c70	NM_145499	21211
Cyp2d22	NM_019823	21211
Cyp2d26	NM_029562	21212
Cyp2d34	NM_145474	21212
Cyp2d40	NM_023623	21212
Cyp2e1	NM_021282	21212
Cyp2g1	NM_013809	21212
Cyp2f2	NM_007817	21212
Cyp2j5	NM_010007	21212
Cyp2j6	NM_010008	21212
Cyp2j7	NM_001104926	21212
Cyp2j8	NM_001104927	21212
Cyp2j9	NM_028979	21212
Cyp2j11	NM_001004141	21212
Cyp2j13	NM_145548	21212
Cyp2t4	NM_001100184	21212
Cyp2u1	NM_027816	21212
Cyp2w1	NM_001160265	21212
Cyp3a11	NM_007818	21212
Cyp3a13	NM_007819	21212
Cyp3a16	NM_007820	21213
Cyp3a25	NM_019792	21213
Cyp3a41a	NM_017396	21213
Cyp3a44	NM_177380	21213
Cyp4a10	NM_010011	21213
Cyp4a14	NM_007822	21213
Cyp4a29	NM_001100183	21213
Cyp4a30b	NM_001100185	21213
Cyp4b1	NM_007823	21213
Cyp4f13	NM_130882	21213
Cyp4f14	NM_022434	21213
Cyp4f15	NM_134127	21213
Cyp4f16	NM_024442	21213
Cyp4f17	NM_001101445	21213
Cyp4f18	NM_024444	21213
Cyp4f39	NM_177307	21213
Cyp4f40	NM_001101588	21213
Cyp4v3	NM_133969	21213
Cyp4x1	NM_001003947	21213

cDNA. Primers for qPCR were designed using Primer-BLAST (www.ncbi.nlm.nih.gov/tools/primer-blast) and the bit scores and e-values were determined by a BLAST search (www.blast.ncbi.nlm.nih.gov/Blast.cgi) of the mouse genomic and transcript database. Primer target specificity was determined if off-target sequence matches had a bit score difference of > 6 bits, compared to the target sequence. In this regard, it should be noted that the primers for CYP3A59 (bit score = 40.1; e-value = 0.013) matched the off-target sequence of CYP3A25 with a bit score = 36.1 and e-value = 0.21. All primers were synthesized by Integrated DNA Technologies (Coralville, IA). Briefly, per reaction, the PCR reaction mix contained: 12.5 µl of Applied Biosystems SYBR® green PCR master mix, 2.5 µl of 3 µM forward and reverse primer mix, 5 µl RNase-free H₂O, and 5 µl of 2 ng/µl cDNA. Reactions were seeded in a 96-well optical reaction plate (Applied Biosystems) and fluorescence was quantified in real time using Applied Biosystems 7300 Real Time PCR System under the following conditions: 50°C for 2 min; 95°C for 10 min; 40 cycles of amplification (95°C for 15 sec; 60°C for 1 min); dissociation stage: 95°C for 15 sec; 60°C for 30 sec; and 95°C for 15 sec. Standard curves were generated for each target to determine the relative amount of transcript present in the sample. Relative amounts of the Cyp transcript were then normalized to the housekeeping transcript, Gapdh. The gene names, accession numbers, and the forward and reverse primer sequences are listed in Table 3.3. If the mRNA of a Cyp isoform was higher than 1% of Gapdh mRNA at one or multiple ages examined during

Table 3.3. Cyp gene names, accession numbers, and the forward and reverse primer sequences for RT-qPCR.

gene Name	accession Number	Forward Primer	Reverse Primer
Cyp2a5	NM_007812	agtgcatgggaaggggaagagagt	acccaaggccaaagcacacaga
Cyp2c37	NM_010001	tctgggctgtgctccttgc	tgcaaatctgcaaccaagggtg
Cyp2c40	NM_010004	tctacaggaaggcattgg	gacccttggttccata
Cyp2c50	NM_134144	ctcattggattggcctcagt	aggaatgaagcagagctgga
Cyp2c54	NM_206537	ttgaccatgggatgtctt	atccaatgccattccatta
Cyp2c67	NM_001024719	acaccgcagcccctgtatgc	tgaccaaactaattggccaaggt
Cyp2c68	NM_001039555	tggagtgcctgatcatacca	ccacagtgcaggagaagca
Cyp2c69	XM_001479745	gtgcttcatccctgtggaat	tgggactgggttaatgagg
Cyp2d9	NM_010006	aaggctggctgacaaggccc	tcggggtgcttgacagggt
Cyp2d10	NM_010005	ttccggtgccccctacccc	tcagcctgcctcctacca
Cyp2d11	NM_001104531	tctcagtgcctgatggacag	cacagagctggtagggaag
Cyp2d12	NM_201360	acactgctgaccgccctcca	tgctctgccactcaggcca
Cyp2j12	NM_001100182	ctgatagcacactggctgga	ggccctgtgaagagctgtc
Cyp3a41a/b	NM_017396 / NM_001105159	agcagaagcaccgagttgat	gactgggctgtgatcccat
Cyp3a59/25	NM_001105160	agtactggccagagcctcaa	tcgttctctgtctgaacct
Cyp4a12a/b	NM_177406 / NM_172306	ctcattctgcccttctcag	gggatgggattgggactct
Cyp4a31	NM_201640	tgcaggcagcctctctggct	gggcggtgatgggaactgct
Cyp4a32	NM_001100181	tctgctctaagcccagccga	gcagcaggagcagaccgagc

liver development, that Cyp gene is designated as Cyp expressed in liver at that age.

Branched DNA (bDNA) Signal Amplification Assay for the ontogeny of Gst mRNAs and five xeno-sensors in liver. The mRNA expression of all the Gst isoforms was determined by the single-plex bDNA technology. Mouse Gst gene sequences were obtained from GenBank. Oligonucleotide probe sets were designed using Probe Designer software, version 1.0 (Bayer Diagnostics, East Walpole, MA). Due to >90% similarity, one probe set was designed to recognize both Gsta1 and Gsta2 isoforms; for the same reason, one probe set was designed to recognize both Gstp1 and Gstp2 isoforms. The sequences of various capture extender and label extender probes were presented previously (Knight et al., 2007). Each probe was designed with a T_m of approximately 63°C to ensure optimal hybridization conditions. Probe sets were submitted to the National Center for Biotechnology Information (NCBI) for nucleotide comparison by the basic logarithmic alignment search tool (BLAST_n) to ensure minimal cross-reactivity with mouse genomic sequences and expressed sequence tags (ESTs).

The lyophilized oligonucleotide probe sets for Gsts were reconstituted in Tris-EDTA buffer, pH 8.0, per the manufacturer's instructions (Quantigene® bDNA Signal Amplification Kit, Panomics/Affymetrix, Fremont, CA). Total RNA (1 µg/µl; 10 µl = 10 µg) was added to each well of a 96-well plate containing 50 µl capture hybridization buffer and 50 µl of each diluted probe set. Total RNA was allowed

to hybridize overnight at 53°C in a hybridization oven. Hybridization and subsequent wash steps were carried out according to the manufacturer's protocol. Luminescence was quantified using Quantiplex® 320 bDNA luminometer, interfaced with Quantiplex® Data Management Software Version 5.02.

The ontogenic expression of mRNAs of the five xenobiotic-sensing transcription factors (AhR, CAR, PXR, PPAR α , and Nrf2) was determined by the multiplex suspension bDNA technology (Panomics/Affymetrix, Fremont, CA). Individual bead-based oligonucleotide probe sets specific for each gene examined were developed by Panomics/Affymetrix Inc (panel ID: 2051, www.panomics.com). Samples were analyzed using a Bio-Plex 200 System Array reader with Luminex 100 X-MAP technology; the data were acquired using a Bio-Plex Data Manager Software Version 5.0 (Bio-Rad, Hercules, CA). Assays were performed according to the manufacturer's protocol. Data are expressed as the ratio of relative light units (RLU) specific to the mRNA expression, and normalized to 10 μ g of total RNA.

Messenger RNA quantification for the ontogeny of the mRNAs of transporters and bile acid bio-synthesizing enzymes. Mouse liver mRNA expression was determined from total RNA. The mRNA expression of Ntcp, Bsep, Mdr2, Mrp4, Ost α , Ost β , FXR, PXR, SHP, Cyp3a11, Cyp7a1, Cyp8b1, Cyp7b1, Cyp27a1, and Fgf15 was determined by bDNA assay (QuantiGene 1.0

bDNA signal amplification kit, Affymetrix/Panomics, Fremont, CA) (Hartley and Klaassen, 2000). Probe sets for Ntcp, Mrp4, Mdr2, Bsep, PXR, Cyp3a11, Ost α , and Ost β have been described previously (Aleksunes et al., 2005; Cheng et al., 2005a; Cheng et al., 2005b; Maher et al., 2005b; Cheng and Klaassen, 2006; Mennone et al., 2006; Beilke et al., 2009). Multiple oligonucleotide probe sets for SHP, FXR and Fgf15 (including capture, label, and blocker probes) were designed using ProbeDesigner Software v1.0 as described previously (Cheng et al., 2005b). The probe sets for SHP, FXR, and Fgf15 are shown in Table 3.4. Data are reported as relative light units (RLU) per 10 μ g total RNA. The mRNA expression of human NTCP, BSEP, MDR3 (ortholog of the mouse Mdr2), CYP7A1, and CYP8B1 was determined by the multiplex suspension bead technology. The human liver samples at various developmental ages were kindly provided by Dr. Steven Leeder (Clinical Pharmacology, Children's Mercy Hospitals & Clinics, Kansas City, KS). Individual bead-based oligonucleotide probe sets specific for each gene examined were developed by Affymetrix/Panomics Inc (Fremont, CA) (panel ID: 11103 and 11104). The probe sequences are available at www.panomics.com. One μ g of total RNA was loaded per sample. Data were analyzed using a Bio-Plex 200 System Array reader with Luminex 100 X-MAP technology, and data were acquired using a Bio-Plex Data Manager Software Version 5.0 (Bio-Rad, Hercules, CA). Assays were performed according to the manufacturer's protocol. Data are expressed as the ratio of relative light units (RLU) specific to the mRNA expression, and normalized to the internal control Gapdh.

Table 3.4. Oligonucleotide probes generated for analysis of mouse FXR and SHP mRNA by bDNA

Gene	Function	Sequence
FXR	CE	CtctctgcactccttagccgTTTTTctcttgaaagaaagt
	CE	TggctgccgtgagttccgTTTTTctcttgaaagaaagt
	CE	AgatttattgtgattcctgaggTTTTTctcttgaaagaaagt
	CE	CtgaagccttttgaattctaTTTTTctcttgaaagaaagt
	LE	GtgcccccgttcttacctTTTTTtagcataggaccgtgtct
	LE	GcatgtacctgcatcacgcaTTTTTtagcataggaccgtgtct
	LE	CattcagcaacaatccccatTTTTTtagcataggaccgtgtct
	LE	gatttacctggattcagttaacaaaTTTTTtagcataggaccgtgtct
	LE	TcacattttccttagccgtttaTTTTTtagcataggaccgtgtct
	LE	TgtctgatcagcgtgctgtTTTTTtagcataggaccgtgtct
	LE	TtcgctgtcgtcctcattcacTTTTTtagcataggaccgtgtct
	LE	TtgtcgcaagtcacgcccTTTTTtagcataggaccgtgtct
	LE	CattctctgtttgtgtacgaatccTTTTTtagcataggaccgtgtct
	LE	CgagaatctgtacatggctggtTTTTTtagcataggaccgtgtct
	BL	Gcactcctggcacttctctgc
	BL	Caaaacttggtgtggagggtcac
	BL	Ataataataccaggagggtctgc
	BL	Tttctctgcactaaattctcttta
	BL	Tgccatttctgtaatatgagaaaat
	SHP	CE
CE		GccccagcagcactctagcaTTTTTctcttgaaagaaagt
CE		GctgtggcttcccttagcagTTTTTctcttgaaagaaagt
CE		TgaactgcagccagtgaggTTTTTctcttgaaagaaagt
LE		CcaaggcctccctgcaggTTTTTtagcataggaccgtgtct
LE		GccgccgctgatcctcatTTTTTtagcataggaccgtgtct
LE		AggtcacagcatcctggcTTTTTtagcataggaccgtgtct
LE		GgagcctcagccacctgaTTTTTtagcataggaccgtgtct
LE		CtgggcaccctgggtaccTTTTTtagcataggaccgtgtct
LE		TtgtggccggtctgatggTTTTTtagcataggaccgtgtct
LE		GgcagcgtgcagccacTTTTTtagcataggaccgtgtct
BL		Ggctactgtcttgctaggacat
BL		Ggggcagggtggcagaagg
BL		Caaccaagcaggaagagagg
BL		Gatcttctaagtatactgggcacc
BL	Gatcttctaagtatactgggcacc	
Fgf15	CE	CttggcctggatgaagatgataQTTTQctcttgaaagaaagt

Gene (cont'd)	Function	Sequence
Fgf15	CE	AaggagcggtgaaacacggQTTTQctctggaagaaagt
	CE	GgctccgatggcagccaQTTTQctctggaagaaagt
	LE	ctgtactggttagcctaacaacagtcQTTTQaggcataggaccgtgtct
	LE	CtggccccggttcaaagQTTTQaggcataggaccgtgtct
	LE	cagggagaacatttagacctcagQTTTQaggcataggaccgtgtct
	LE	tgatcaagtctagccactaacacaaQTTTQaggcataggaccgtgtct
	LE	GgcaggtgtcaacttaagtcaQTTTQaggcataggaccgtgtct
	LE	aactggagtaacttaggcacatacaQTTTQaggcataggaccgtgtct
	BL	Tggagatggtcctcatggat
	BL	Tcctggagctgtctctggg
	BL	Ggataaagttgagggttctgg
	BL	Atgtgtcactcaccagggg
	BL	Ccaccatcctgaacggatcc
	BL	Actctcactaggtggtctacatct
	BL	Ctgtcattctggaagctggg
	BL	Ttttccatcctgtcggaatc
	BL	Gttcacgggaccttgggg
	BL	Tgtacagcttctaagggggaa
	BL	Caggtccatgtgagactagaata
	BL	Gcagcctccaagtcaagtg

Branched DNA Amplification (bDNA) Technology for the ontogeny of Ahr

mRNA. The mRNA expression of Ahr was determined by bDNA assays (QuantiGene bDNA signal amplification kit, Affymetrix/Panomics, Fremont, CA). Multiple oligonucleotide probe sets for Ahr (including capture, label, and blocker probes) were designed using ProbeDesigner Software v1.0 (Bayer Corp., Diagnostics Div.) as previously described (Petrick and Klaassen, 2007). Ten μg of total RNA was added to each well of a 96-well plate (n=5 per age). The mRNA was captured by specific probe sets and attached to a branched DNA amplifier. Enzymatic reactions occur upon substrate addition and the luminescence for each well is reported as Relative Light Units (RLU). Statistical significance compared to day-45 expression levels were considered at $p < 0.05$ (one way ANOVA followed by Duncan's multiple range post hoc test (SPSS program, Chicago, IL).

Multiplex suspension array for the ontogeny of PPAR α and PGC-1 α mRNAs.

Mouse liver mRNA expression was determined from total RNA. Equal amounts of total RNA from five livers (n=5) were pooled as one sample at each age. Individual bead-based oligonucleotide probe sets specific for each gene examined were developed by Affymetrix/Panomics Inc (Fremont, CA). The probe sequences for PPAR α and PGC-1 α mRNAs are available at www.panomics.com (panel ID: 21073). Samples were analyzed using a Bio-Plex 200 System Array reader with Luminex 100 X-MAP technology, and data were acquired using a Bio-Plex Data Manager Software Version 5.0 (Bio-Rad,

Hercules, CA). Assays were performed according to the manufacturer's protocol. All data were standardized to the internal control Gapdh. Data are expressed as the ratio of each specific mRNA to Gapdh mRNA.

ChIP-on-chip assay of DNA methylation and histone methylation.

Genpathway's ChIP-on-chip assays (San Diego, CA) using Affymetrix GeneChip Mouse Tiling 2.0R E array were used to determine the following epigenetic profiles: DNAm, H3K4me2, and H3K27me3 as described previously (Cui et al., 2009b). These experiments were performed in livers at day -2, 1, 5, and 45 of age (male only). The detection threshold value was set at 3.0-fold above the background input for DNAm, and 4.0-fold for H3K4me2 and H3K27me3, based on the calculation of false discovery rate estimated by the "negative peaks" approach as previously described (Johnson et al., 2006). The raw and processed data are stored in the Gene Expression Omnibus (GEO) data base with the accession number GSE14620.

Briefly, for DNA methylation, genomic DNA from mouse livers was isolated and sonicated to an average length of 300-500bp. An antibody against 5-methylcytosine was used for immunoprecipitation (ab51552, Abcam, Cambridge, MA). DNA without immunoprecipitation was used as a control for background hybridization. The specificity of the immunoprecipitation was validated by quantitative PCR reactions with positive and negative control primers. Both the immunoprecipitated and control DNA were amplified by random priming. The

amplified DNA was purified, quantified, and tested by quantitative PCR at the same genomic regions as the original immunoprecipitated DNA to assess quality of the amplification reactions. Amplified DNAs were fragmented and labeled using the DNA Terminal Labeling Kit (Affymetrix, Santa Clara, CA), and then hybridized to Affymetrix GeneChip Mouse Tiling 2.0R E Array at 45°C overnight. Arrays were washed and scanned by a GeneChip HT Array Plate Scanner.

For histone modifications, liver homogenates were fixed with 1% formaldehyde and quenched with glycine. Chromatin containing DNA cross-linked by formaldehyde was isolated and sonicated to an average length of 300-500bp. Methylated histone H3 proteins at lysine 4 and 27 were immunoprecipitated with polyclonal antibodies (Millipore 07-030 for H3K4Me₂, and Millipore 07-449 for H3K27Me₃) (Millipore, Billerica, MA). Complexes were washed, eluted from the beads with SDS buffer, and subjected to RNase and proteinase K treatment. Crosslinking was reversed by incubation overnight at 65°C, and DNA fragments were purified by phenol-chloroform extraction, precipitated by ethanol, labeled, and then hybridized to the Affymetrix GeneChip Mouse Tiling 2.0R E arrays. Arrays were scanned with a GeneChip HT Array Plate Scanner.

Data from the arrays were analyzed using the Affymetrix Tiling Analysis Software (TAS), which generated BAR files that contain the intensities for all probes on the arrays. The intensities are expressed as signals (estimating the

fold enrichment). The data image was viewed by the Integrated Genome Browser (IGB) (Affymetrix, Santa Clara, CA). The boundaries of detection were set from 10kb upstream of the transcription start site, to 10kb downstream from the end of the entire gene locus. Based upon recommendations by Affymetrix and known positive and negative genomic regions, thresholds were set as >3-fold enrichment of the probe intensities for DNA methylation, and >4-fold enrichment for histone methylations. Enrichments above the recommended thresholds reflect a false discovery rate below 2%. Intervals were defined as regions with signals higher than the threshold values, and active regions are genomic regions that contain one or more intervals in close proximity to each other (with intervals overlapping by at least 1bp to be added to the same active region).

ChIP-Seq Analysis. Livers of 8-week old C57BL/6 male mice were used for ChIP-Seq experiments. Fragments of DNA were tagged by 35-nucleotide identifiers and subjected to sequencing by the Illumina Genome Analyzer Sequencer, based on Solexa Technology (Illumina, San Diego, CA). Preprocessing of the ChIP-Seq data was performed by Genpathway (San Diego, CA). Briefly, the tags identified were mapped to the genome using Eland Software, which resulted in a list of their chromosome coordinates. Only tags that mapped uniquely and that have no more than 1 mismatch were retained. Because the 5'-end of the sequence tags represented the end of ChIP-fragments, the tags were extended *in silico* using Genpathway software at their 3'-ends to a

length of 110-bp, which was the average fragment length in the size-selected library. To identify the density of fragments (extended tags) along the mouse genome, the genome was divided into 32-nucleotide bins, and the number of fragments in each bin was determined and stored together in a Binary Analysis Results (BAR) file. The BAR files were then viewed in the Affymetrix Integrated Genome Browser (IGB) for PXR binding in the mouse genome. The locations of fragment-density peaks, defined by chromosome number and a start and end coordinate were termed as “intervals”. For each BAR file, intervals were calculated using the Affymetrix Tiling Analysis Software (TAS) and compiled into Browser Extensible Data (BED) file. Three parameters of intervals were identified: threshold, MaxGap, and MinRun. The threshold was set at 20-fold over background signal, and this threshold was adjusted depending on the number of tags sequenced, information on positive and negative test sites, and estimation of false discovery rate per the company’s recommendation (Genpathway, San Diego, CA). The exact locations of intervals along with their proximities to gene annotations and other genomic features were then determined. In addition, average and peak fragment densities within intervals were compiled.

Global Motif Analysis for PXR-DNA binding patterns. In order to refine the targets of PXR binding, the top 500 ChIP-DNA sequences with highest enrichment peak values in both control and PCN-treated conditions were retrieved from the UCSC genome browser. ChIP-Seq data, which localizes PXR-

binding regions to around 500bp, were further analyzed *in silico* to identify the exact PXR-binding targets. PXR-binding profiles were generated using a novel k-mer based approach designed by our collaborator Dr. Sumedha Gunewardena, for analyzing high throughput sequence data. PXR-binding profiles were generated using a novel k-mer based approach designed for analyzing high throughput sequence data. In discussion that follows I will describe the algorithm as it applies to response elements with two complementary half sites separated by a variable spacer distance.

The algorithm begins by generating a set of initial seed sequences for a half site. The seed sequences comprise the first n_0 most significant k-mers, where k is the length of a half site. The significance of a k-mer is given by the weighted sum of the site and sequence significance scores of the k-mer. The significance score (Z_i) of k-mer i is given by

$$Z_i = \frac{X_i - Np_i}{\sqrt{Np_i(1 - p_i)}}$$

where for the site significance score, X_i is the frequency of k-mer i in the input sequences, N, the total number of k-mers and, p_i , the background probability of k-mer i. For the sequence significance score, X_i is the number of input sequences with k-mer i, N, the total number of input sequences with each k-mer, and, p_i , the probability of k-mer i appearing in a background sequence. For a given k, there are 4^k k-mers. The background sequences are composed of all

non-overlapping 500bp upstream (from the 5'end) and 500bp downstream (from the 3'end) sequence segments of the input sequences.

Statistical analysis for the ontogeny of Cyp mRNAs. Statistical differences in Cyp mRNA expression between male and female mice were determined using two-tailed Student's t-test, with significance set at $p < 0.05$. The mRNA ontogeny of the 73 detected Cyp isoforms was analyzed by a two-way hierarchical clustering method (JMP v. 8.0) using Ward's minimum variance and visualized by a dendrograph. Distances between genes reflect significance of associations. Red color represents higher and blue color represents lower expression levels, respectively.

Statistical Analysis for the ontogeny of Gst mRNAs. Statistical differences in Gst mRNA expression between male and female were determined using Student's t-test with significance set at $p \leq 0.05$. The mRNA ontogeny of all the Gst isoforms, as well as AhR, CAR, PXR, PPAR α , and Nrf2, was analyzed by a two-way hierarchical clustering method (JMP v. 7.0) using Ward's minimum variance and visualized by a dendrograph. Distances between genes reflect significance of associations. Red color represents higher and blue color represents lower expression levels, respectively.

Motif Analysis for PXR Binding to Gst gene loci. All chromosome coordinates of the positive PXR-binding sites within ± 10 kb of the Gst gene loci were retrieved

from the ChIP-Seq data base, and submitted to the UCSC Genome Browser, which returned a series of DNA sequences. These ChIP-DNA sequences were then analyzed by NHR-scan software for putative nuclear receptor binding sites (DR-3, DR-4, ER-6, ER-8, and IR-0) as described previously (Kliwer et al., 2002; Sonoda et al., 2002). The combined probability of entering match states was set at 0.05.

***In silico* analysis of CpG island localization around the *Ahr*, *PPAR α* and *PGC-1 α* gene loci.** CpG islands are defined as DNA sequences at least 200bp in length and with a GC percentage greater than 50%. An *in silico* analysis of CpG islands within 10kb upstream plus 1kb downstream of the gene promoter region was performed using the Methyl Primer Express Software v1.0 (Applied Biosystems, Foster City, CA).

Regression analysis of *Ahr* mRNA expression with DNA and histone methylations. The mRNA expression of *Ahr* during liver development and the patterns of the three epigenetic marks (DNA methylation, histone H3K4Me2 and H3K27Me3) were analyzed using Sigma Plot 10.0 (Systat Software Inc., San Jose, CA).

Sample preparation for bile-acid analysis. To determine the concentration and composition of bile acids during development, serum and liver samples were collected from pups at each age (n=3 per age). From 2 days before birth to 5

days of age, samples from the same litter were pooled (n= 3 litters) to achieve the desired amount of liver and serum for bile-acid isolation. Internal standards (IS: 40µg/ml d4-G-CDCA and 20µg/ml d4-CDCA in MeOH), as well as serum and liver samples were prepared for bile-acid analysis with methods reported by Alnouti et al (2008a) with some modifications. Briefly, for serum samples, simple protein precipitation by adding methanol (MeOH) was used. One ml of MeOH was added to 50 µl serum-spiked with 5 µl IS, vortexed, and centrifuged at 12,000g for 10 min. The supernatant was aspirated, evaporated under vacuum, and reconstituted in 50 µl of 50% MeOH. Liver samples were extracted by protein precipitation using ice-cold acetonitrile (ACN). Approximately 110 mg of liver was homogenized in 5 volumes of H₂O. Liver homogenate (600 µl) was spiked with 10 µl IS, 3 ml of ice-cold ACN (5% NH₄OH in ACN) was added, vortexed, shaken continuously for 1 hr, and centrifuged at 12,000g for 10 min. The supernatant was aspirated and precipitant was extracted with 1 ml of MeOH. Supernants from the 2 extraction steps were pooled, evaporated, and reconstituted in 100 µl of 50% MeOH.

Liquid chromatographic and mass spectrometric conditions of bile-acid analysis. A Waters ACQUITY ultra performance LC system (Waters, Milford, MA) and a Waters Quanttro Premier XE triple quadrupole instrument with an ESI source (Waters, Milford, MA) were used. The entire LS-MS system was controlled by MassLynx 4.1 software. All chromatographic separations were performed with an ACQUITY UPLC C₁₈ column (1.7µm, 100X 2.1 I.D.) equipped

with an ACQUITY UPLC C₁₈ guard column (Waters, Milford, MA). Based on peak areas of BAs and internal standards, various conjugated and unconjugated BAs were quantified, namely the taurine-conjugated bile acids including T-CA, T- α MCA, T- β MCA, T- ω MCA, T-MDCA, T-UDCA, T-HDCA, T-CDCA, T-DCA, and T-LCA; as well as the unconjugated bile acids including CA, α MCA, β MCA, ω MCA, MDCA, UDCA, HDCA, CDCA, DCA, and LCA.

Serum triglyceride and glucose quantification. Serum triglyceride and glucose concentrations of mice at different ages were determined by enzymatic-colorimetric assays per the manufacturer's protocol (Pointe Scientific, Canton, MI). Due to limited amount of samples, equal volume of serum from the same litter at each age were pooled as one sample, and three litters (three pooled samples) were used at each age. Data are expressed as mg of triglyceride or glucose per deciliter of serum.

Western blotting. Proteins were electrophoretically resolved without boiling by use of polyacrylamide gels and transblotted overnight at 4°C onto Polyvinylidene-Fluoride-Plus membranes (Micron Separations, Westboro, MA). Membranes were blocked for 1 h in 3% nonfat dry milk with 0.5% Tween-20 in phosphate buffered saline (PBS). All primary and secondary antibodies were diluted in 1% nonfat dry milk with 0.5% Tween-20 in PBS. Primary antibody dilutions were as follows: AhR (SA-210, 1:1000), H3K4Me2 (07-030, 1:2000), and β -actin (ab8227, 1:1000). Blots were subsequently incubated with a species-appropriate

horseradish peroxidase-conjugated secondary antibody for 1 h (rabbit anti mouse). Protein-antibody complexes were detected by use of an enhanced chemiluminescent kit (Thermo Scientific, Rockford, IL) and exposed to X-ray film (Denville Scientific, Metuchen, NJ). Intensities of protein bands were determined by use of the Discovery Series Quantity One 1-D Analysis software (Bio-Rad Laboratories, Hercules, CA).

Immunofluorescence Analysis. Livers were embedded in optimal cutting temperature compound, and rapidly frozen at -80 °C. Six μm sections were generated with a Leica CM3050 Cryostat (Meyer Instruments Inc., Pittsburg, PA) and fixed with 4% paraformaldehyde in PBS. Briefly, slides were blocked with 5% goat serum in 0.1% Triton X in PBS, and incubated with primary antibody diluted 1:100 for Ntcp (K4 rabbit anti-rat) and Bsep (K44 rabbit anti-rat). There are no specific antibodies available for staining Mdr2. Staining of Mrp4 and Ost β were not applicable due to low protein expression levels in liver. For H3K4Me₂, primary antibody was diluted 1:50. After washing, sections were incubated with a species-appropriate Alexa 488 IgG secondary antibody (1:200). Sections were mounted in Prolong Gold[®] (Invitrogen, Carlsbad, CA). Fluorescent staining was visualized on an Olympus B \times 41 microscope (Olympus Optical, Tokyo, Japan). Images were captured using an Olympus DP70 camera (40 \times) and DP Controller software.

CHAPTER FOUR. GLOBAL PICTURE OF THE ONTOGENY OF CRITICAL DRUG-PROCESSING GENES AND REGULATORY FACTORS IN LIVER DEVELOPMENT

Before examining the ontogeny and regulatory mechanisms of drug-processing genes and other factors in each category, it is logical to first provide a global picture of all the expression patterns of these genes, and characterize a roadmap of the genomic binding locations of critical regulatory factors in mouse liver. Detailed methods have been listed in each chapter of the dissertation at appropriate sections.

Drug-processing genes. Our laboratory has long been interested in the developmental regulation of drug processing and detoxifying genes, and data from my previous work and many other colleague's research have characterized the ontogeny of numerous drug-processing genes in liver (Cui et al., ; Klaassen, 1972; Klaassen, 1973a; Klaassen, 1973b; Klaassen, 1974; Hunter and Klaassen, 1975; Klaassen, 1975b; Klaassen, 1975a; Waalkes and Klaassen, 1984; Lehman-McKeeman et al., 1988; Klaassen and Lehman-McKeeman, 1989; Kershaw et al., 1990; Liu and Klaassen, 1996a; Liu and Klaassen, 1996b; Dunn et al., 1999; Choudhuri et al., 2001; Johnson et al., 2002; Li et al., 2002; Cui et al., 2009a; Hart et al., 2009; Li et al., 2009; Choudhuri et al., 2010). The mRNA expression of 82 hepatic drug-processing genes was summarized in a heatmap (JMP v. 7.0) at the following ages: day -2, day 0, day 5, day 10, day 15, day 20, day 30, and day 45 of age. Based on our previous publications and our

preliminary data, the mRNAs of these 82 hepatic drug-processing genes (in pooled male mouse liver samples) were expressed as percentage of highest expression levels during development, clustered by a two-way hierarchical clustering method, and visualized by a dendrograph (Figure 4.1A). As shown in the dendrograph, the developmental pattern of the mRNA expression of the selected hepatic drug-processing genes partition into 4 distinct clusters, namely, pattern 1, 2, 3, and 4. For each pattern, the average expression of the clustered genes is shown in Figure 4.1B. Pattern 1 represents the mRNAs of the adult-predominant genes, which include the mRNAs of the following drug-processing genes: Mrp3 (*Abcc3*), Ugt2a3, Ugt2b1, Gsta1, Gsto1, Cyp7b1, Gstp1/2, Cyp8b1, Ugt1a9, Gstmicrosomal 1, Ugt2b35, Ugt2b36, Ugt2b5, Ugt3a1/2, Oatp (*Slco*)1a1, Cyp4a10, and Cyp3a41. Pattern 2 represents low expression before birth, followed by a gradual increase after birth with a plateau around 20 days of age, including Oatp2b1, Cyp2a4, Gstm6, Gstm1, Cyp1a2, Gsta3, Cyp2e1, Cyp3a11, Cyp2c29, Cyp27a1, Ugt1a6, Cyp2d22, Ugt2b34, Udpgh, Mate1 (*Slc47a1*), Oatp1b2, Gstm2, Bsep, Cyp2j6, Mrp2 (*Abcc2*), Mdr2 (*Abcb4*), Gstt1, Ntcp, Gstm3, Gstm4, Ugt1a5, Oatp (*Slco*)1a4, Ent1 (*Slc29a1*), Sult1a1, Por, Cyp7a1, Cyp3a25, Gstt3, Sult1d1, Oct1 (*Slc22a1*), Gstk1, Gsta4, Atp8b1, and Gstz1. Pattern 3 starts off before birth with low expression, followed by a relatively rapid increase that peaks at 15 days of age, then decreases to neonatal levels, and these mRNAs include Ost β , fibroblast growth factor receptor 4 (FgfR4), Mrp6 (*Abcc6*), Oat2 (*Slc22a7*), Abca1, Cyp3a16, Abcg8, Agcg5, Sult2a1/2, PAPSS2, Gst microsomal 3, Ugt1a1, Sult1c2, and Cyp3a44. Pattern 4 represents

Figure 4.1

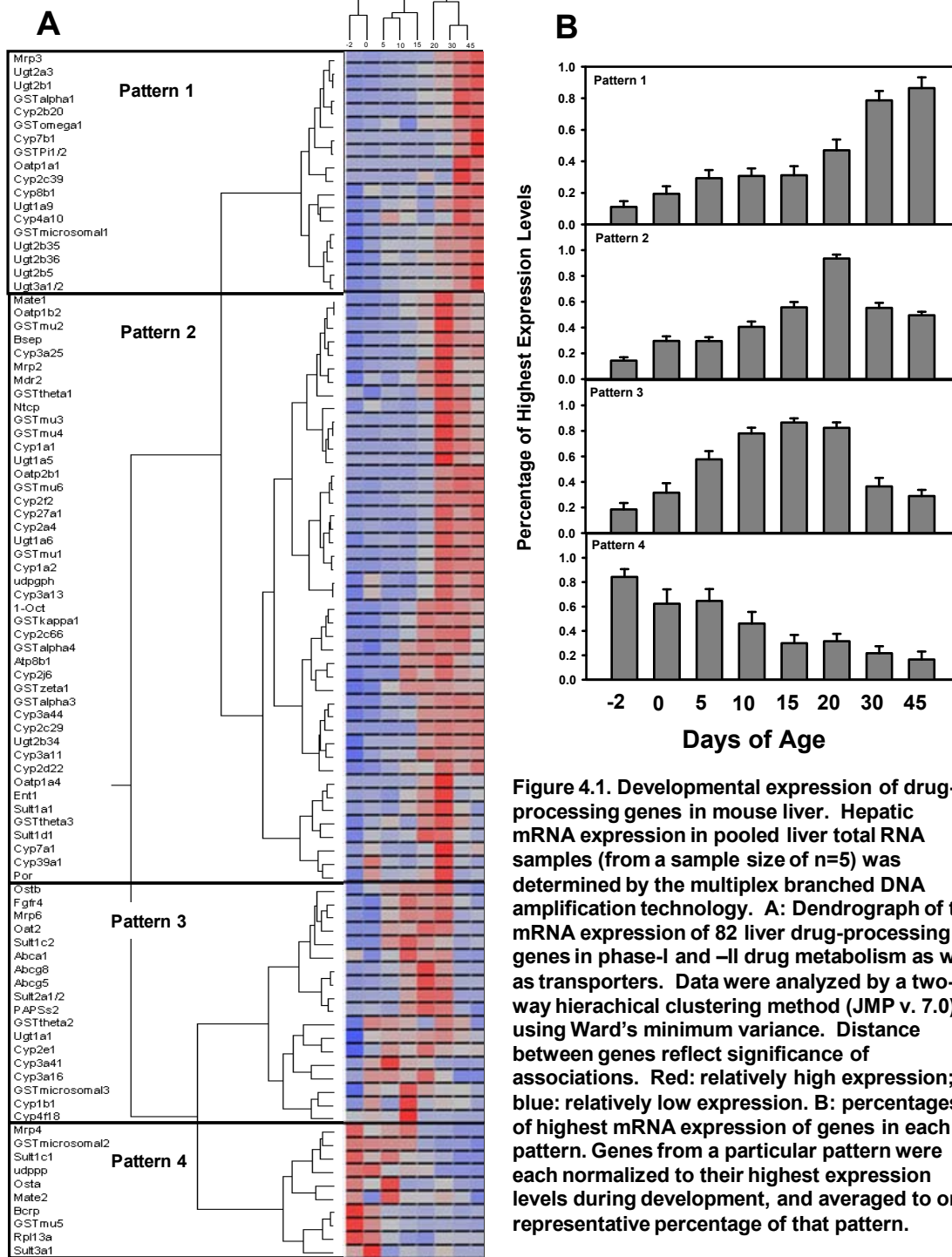


Figure 4.1. Developmental expression of drug-processing genes in mouse liver. Hepatic mRNA expression in pooled liver total RNA samples (from a sample size of $n=5$) was determined by the multiplex branched DNA amplification technology. **A:** Dendrogram of the mRNA expression of 82 liver drug-processing genes in phase-I and -II drug metabolism as well as transporters. Data were analyzed by a two-way hierarchical clustering method (JMP v. 7.0) using Ward's minimum variance. Distance between genes reflect significance of associations. Red: relatively high expression; blue: relatively low expression. **B:** percentages of highest mRNA expression of genes in each pattern. Genes from a particular pattern were each normalized to their highest expression levels during development, and averaged to one representative percentage of that pattern.

fetal/perinatal-specific genes, including Mrp4 (*Abcc4*), microsomal Gstm2, Sult1c1, Bcrp (*Abcg2*), Gstm5, Ost α , Mate2 (*Slc47a1*), Cyp39a1, Gstm2, Sult3a1, and Cyp3a13. These four patterns indicate multiple mechanisms may be involved in the regulation of drug-processing genes during development.

Transcription factors. In order to identify possible regulatory factors for the ontogeny of drug-processing genes, the mRNA expression of 71 critical transcription factors for liver development was determined by the multiplex suspension bDNA assay. The mRNA expression of these hepatic liver transporters was summarized in a heatmap from before birth to 45 days of age. As shown in the dendrograph (Figure 4.2), the developmental pattern of the mRNAs of the selected transcription factors forms 4 clusters. Transcription factor genes in the first pattern were induced right after birth, followed by a further induction at adolescent to adult ages. Genes in the second pattern were most highly expressed in the adult period. Genes in the third pattern were enriched in adolescent ages (from day 10 to day 20), and mRNAs in the last pattern were increased in newborns but peaked during adolescent ages. The ontogenic expression between transcription factors and drug-processing genes are different for each pattern respectively, indicating the presence of a second player in regulating the ontogeny of drug-processing genes.

Enrichment of epigenetic marks. The ontogenic epigenetic signatures of three marks, namely histone H3 lysine-4 di-methylation (H3K4Me2) for gene trans-

Figure 4.2.

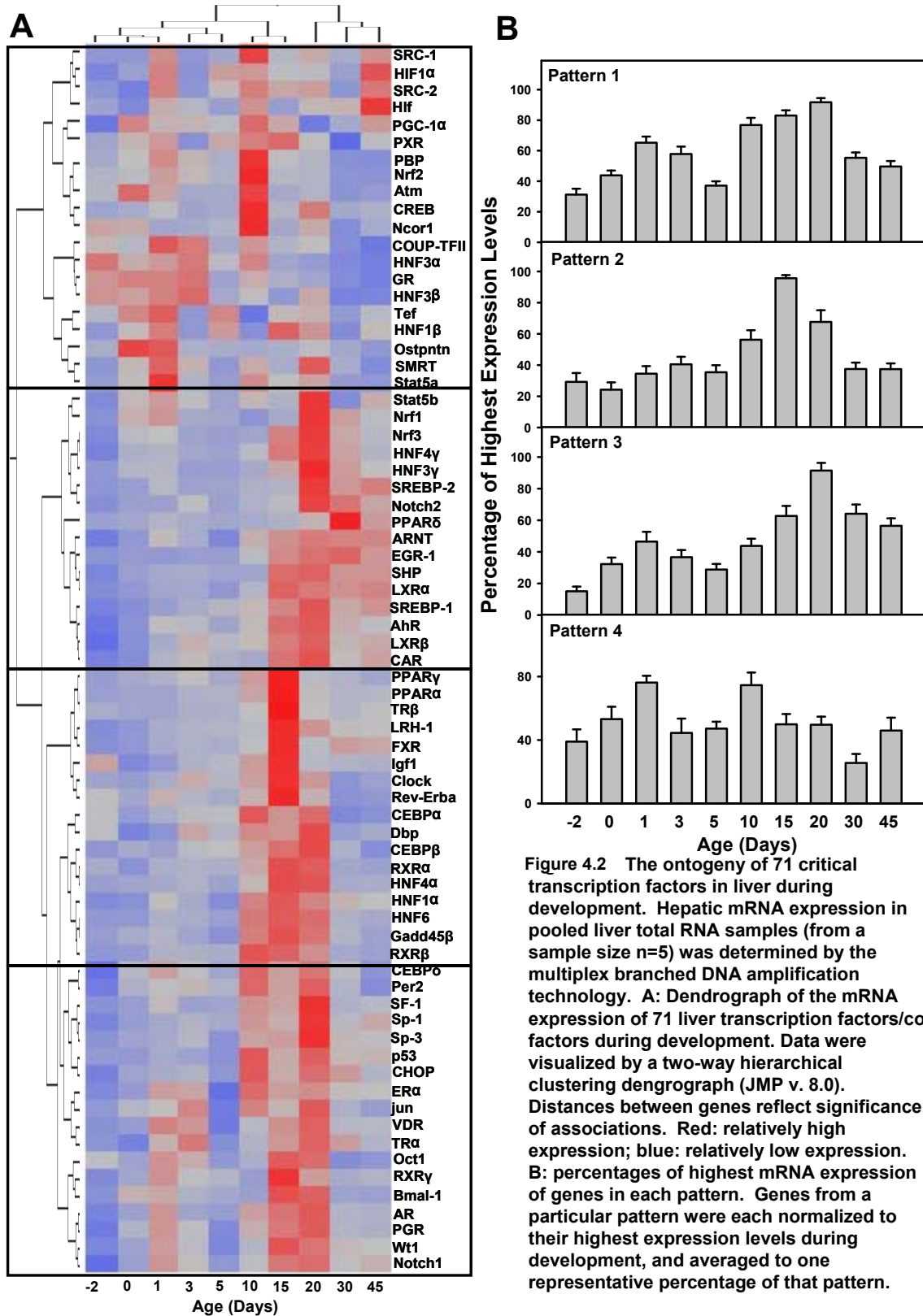


Figure 4.2 The ontogeny of 71 critical transcription factors in liver during development. Hepatic mRNA expression in pooled liver total RNA samples (from a sample size n=5) was determined by the multiplex branched DNA amplification technology. A: Dendrograph of the mRNA expression of 71 liver transcription factors/co-factors during development. Data were visualized by a two-way hierarchical clustering dendrograph (JMP v. 8.0). Distances between genes reflect significance of associations. Red: relatively high expression; blue: relatively low expression. B: percentages of highest mRNA expression of genes in each pattern. Genes from a particular pattern were each normalized to their highest expression levels during development, and averaged to one representative percentage of that pattern.

activation, and histone H3K lysine-27 tri-methylation (H3K27Me3) as well as DNA methylation for gene suppression, were determined on three representative chromosomes (chr 5, 12, and 15, which are enriched with drug-processing genes), at 4 ages during liver development (Figure 4.3). An overlay between patterns of epigenetic marks and alterations in gene expression during liver development will be described in detail in the following parts of the dissertation. Briefly, the chromosome-wide enrichment of H3K4Me2 was relatively high and stable on the three chromosomes, except for a moderate decrease at birth. Conversely, there was a marked and continuous decrease of H3K27Me3 during liver development, indicating there was a more permissive environment for gene transcription as the liver matures. DNA methylation was relatively lower at the first three neonatal ages, followed by a moderate increase at 45 days of age.

For proof of concept, the H3K4Me2 was selected as an example to characterize its tissue distribution in adult tissues, as well as ontogenic expression and subcellular localization using western blot and immunofluorescence staining (Figure 4.4). Interestingly, H3K4Me2 protein was ubiquitously expressed in many tissues with comparable amounts, and was present in all ages of liver development. Apparently, H3K4Me2 was exclusively localized in the nucleus, with a moderate increase in the staining intensity right after birth, and remained until 45 days of age. However, it remains to be determined whether the local expression of H3K4Me2 around a particular drug-processing gene locus will be altered as a function of age.

Figure 4.3.

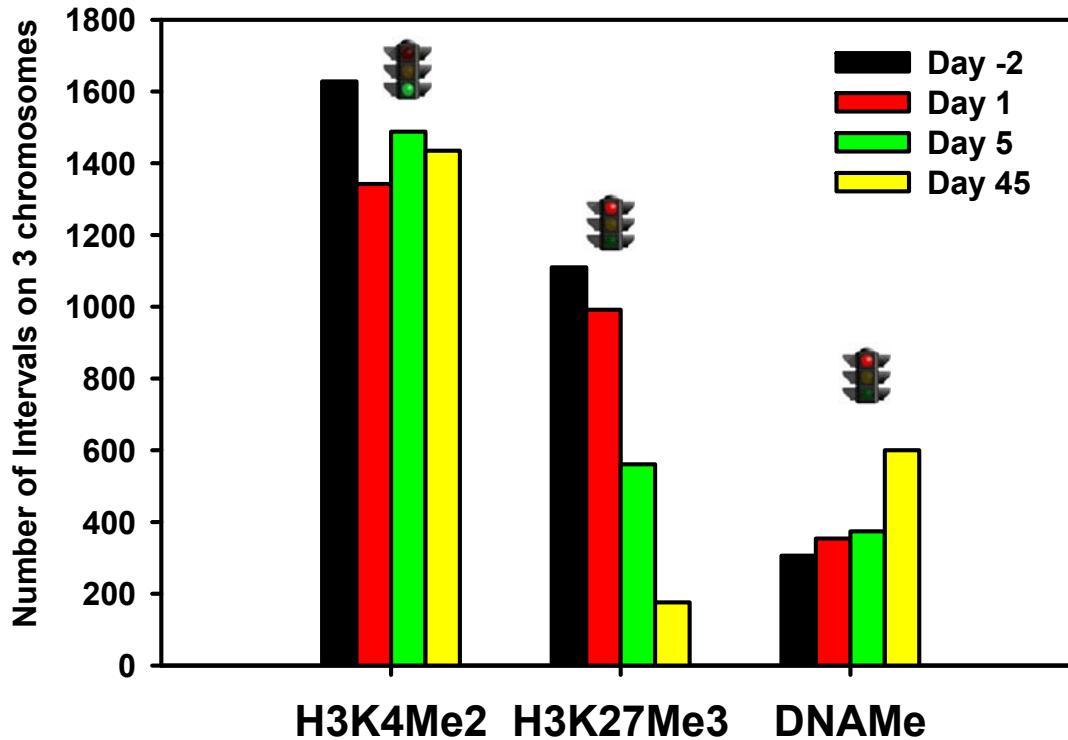


Figure 4.3. Relative enrichment of three distinct epigenetic marks, namely histone H3 lysine-4 di-methylation (H3K4Me2) for gene trans-activation, and histone H3K lysine-27 tri-methylation (H3K27Me3) as well as DNA methylation for gene suppression, on three representative chromosomes (chr 5, 12, and 15, which are enriched with drug-processing genes), at 4 ages during liver development. Data were obtained by ChIP-on-chip using specific antibodies against each epigenetic mark. Number of intervals represents numbers of sites with significant enrichment of a particular mark.

Figure 4.4

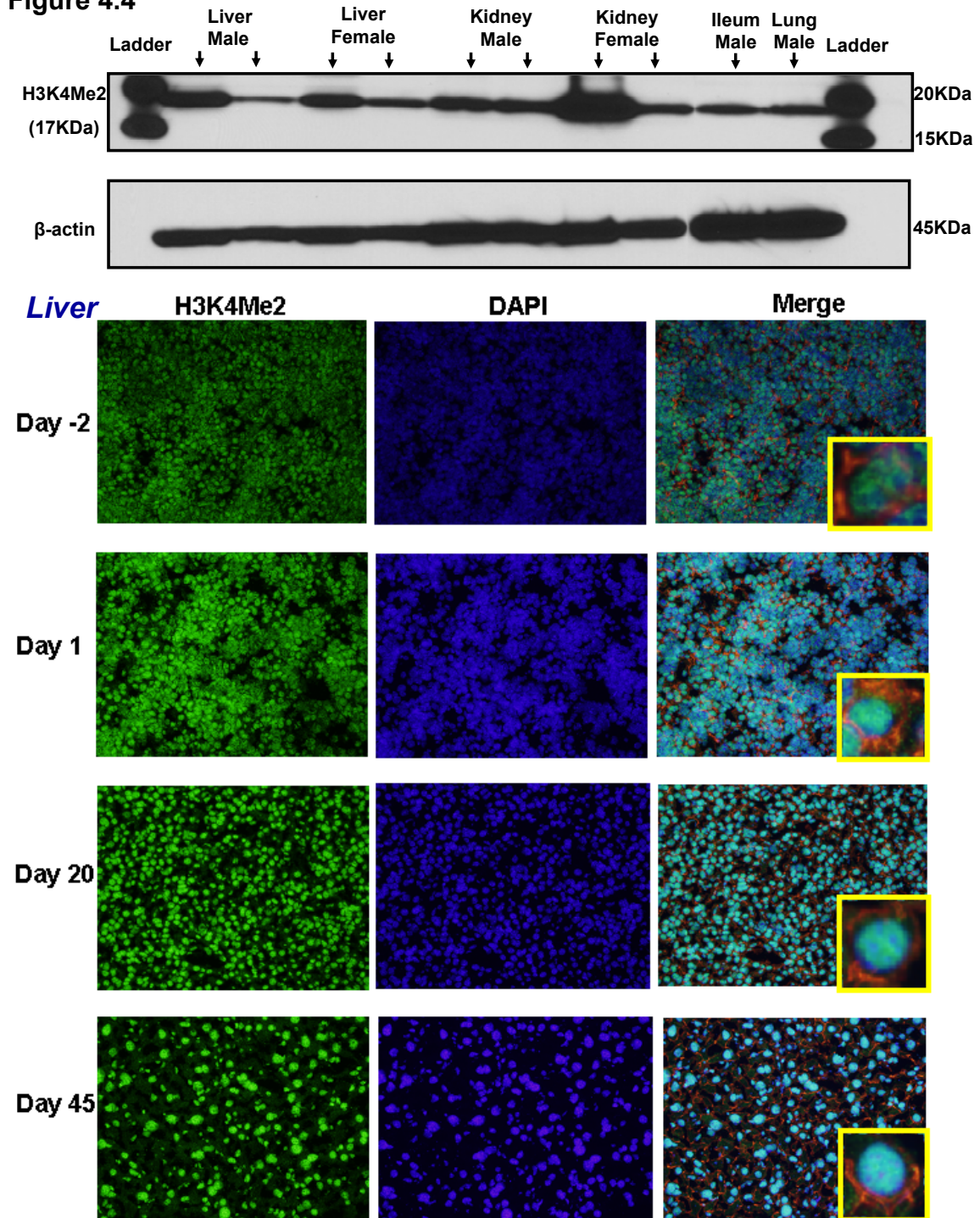


Figure 4.4. Upper panel: a western blot of H3K4Me2 in adult liver, kidney, ileum, and lung. Bottom panel: immunofluorescence staining of H3K4Me2 at four ages during liver development. Green: staining of H3K4Me2. Blue: DAPI staining for nuclei. Red: rhodamine phalloidin staining of actin adjacent to plasma membrane. Jade color: a merge between H3K4Me2 and DAPI staining.

A roadmap of PXR-DNA binding signatures. Because PXR is a well established transcription factor for numerous drug-metabolizing enzymes and transporters, it was selected in the present study to characterize the direct target gene profiles in liver. To further validate the significance of these binding sites, a pharmacological approach was used to further activate PXR by the synthetic ligand PCN, to determine whether there would be a further increase in PXR binding to DNA. CHIP-seq identified 3812 active regions for positive PXR-binding in control mice, indicating a need for PXR binding for basal functions. PCN treatment increased the total number of active regions to 6446 (Figure 4.5A). Interestingly, whereas there were 3026 common intervals between control and PCN-treated groups, there were 786 unique PXR-binding sites in control only, and 3420 in PCN-treatment only (Figure 4.5B). There were 2591 genes targeted by PXR within ± 10 kb of the gene loci in control, and increased to 3509 genes after PCN treatment (Figure 4.5C). Although more than 70% of the PXR-bindings were located within ± 10 kb of the NCBI-annotated genes, positive PXR-binding was observed in the intergenic regions (approximately 30%) (Figure 4.5D), suggesting that PXR might have novel functions in regulating non-protein-coding transcripts.

PXR-DNA binding profiles were generated from the top 500 CHIP-DNA sequences, with highest enrichment peak values, of both control and PCN-treated assays. The current work offers new insights into the binding patterns of PXR, suggesting a distinct correlation in the spacer distance between the two

Figure 4.5.

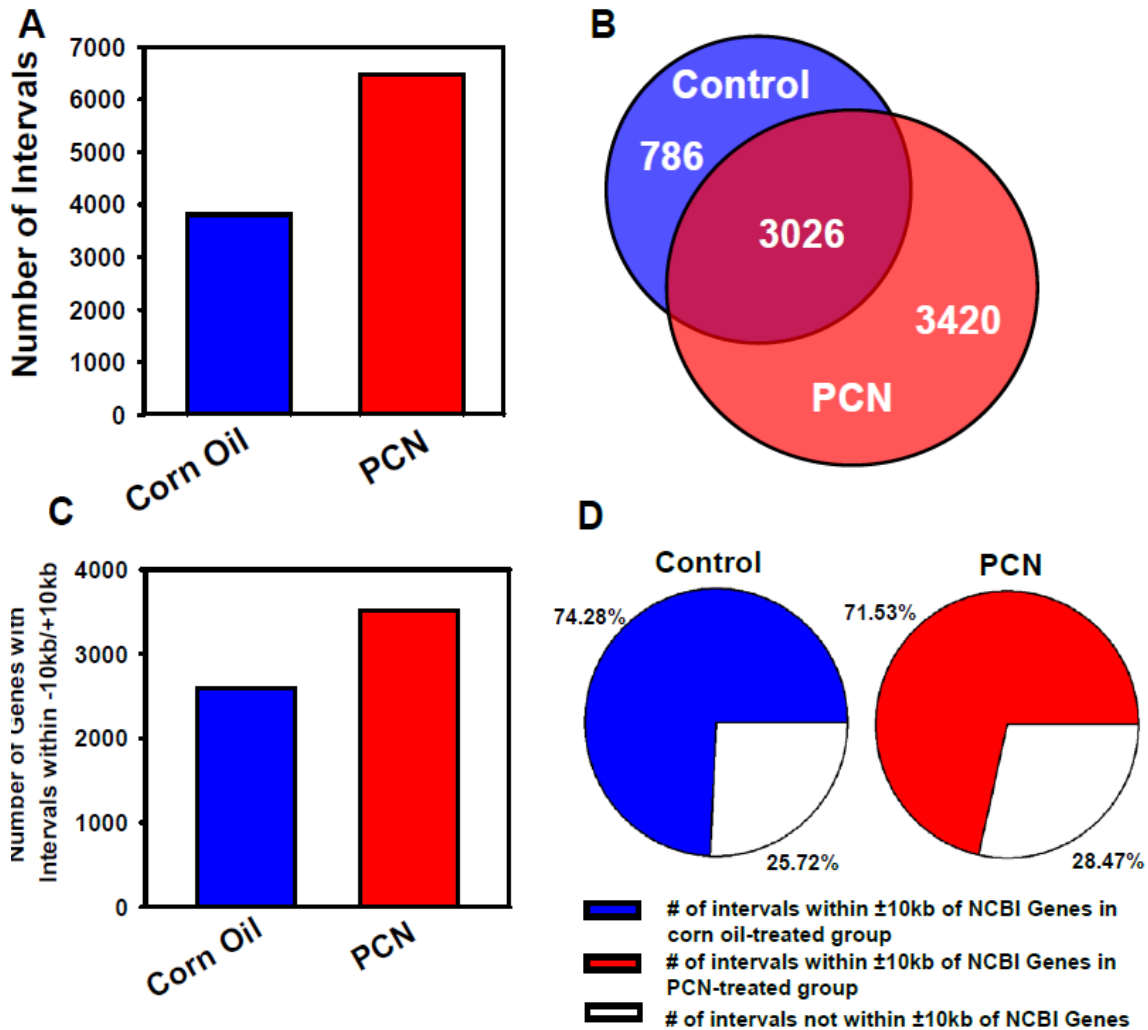


Figure 4.5. A roadmap of enrichment in PXR binding (intervals) in the entire mouse genome by ChIP-Seq analysis. (A) Total number of active regions for PXR binding in livers from control and PCN-treated mice. (B) An overlay of PXR-binding active regions between control and PCN-treated groups for common and distinct binding sites. (C) Total number of genes with PXR bindings (intervals) within $\pm 10\text{kb}$ of the gene loci in control and PCN-treated groups. (D) Classification of PXR-binding intervals based on their genomic locations (within $\pm 10\text{kb}$ of NCBI genes or in intergenic regions) in control and PCN-treated groups.

nuclear receptor half sites of high-affinity binding sites that span a distance much further than the furthest spacer (8-bp) reported in the literature. Whereas the direct repeats, DR-3 and DR-4, of the well established consensus motif AGTTCA featured prominently in our analysis, the everted repeats, ER-6 and ER-8, cited in the literature as PXR-binding motifs (Kliwer et al., 2002), were less evident. The current analysis suggests that by far the most favored spacer configuration for PXR binding in both control and PCN-treated mouse livers is DR-4 (Figure 4.6 A-C). Interestingly, the spacer distance distribution of half sites of the consensus direct repeat AGTTCA shows clear peaks at isochronal intervals of 5bp, corresponding to spacer distances of 4, 9, 14, 19, and so on (i.e. spacer distances of the form $5n+4$, $n=0,1,2,\dots$), extending to over a hundred base pairs. Sample partial autocorrelations have demonstrated that the periodicity of 5bp is indeed preferred by PXR binding to DNA (Figure 4.6D). Together these data have revealed a new structural configuration of half sites that favors a spacer distance that is periodically correlated with a period of 5bp. It also indicates that the binding of PXR to the consensus direct repeat AGTTCA is partial to response elements with a spacer distance of $5n+4$ between half sites over the proximity of the half sites to each other. The observed tapering of peak densities of these sites can be, as expected, explained by the increasing motif length (a regression fit on spacer distance explains 80% of the variation between peak densities, [Figure 4.6C: regression line]), however the significantly high density of DR-4 suggests that proximity between half sites is desired by PXR on a secondary level.

Figure 4.6.

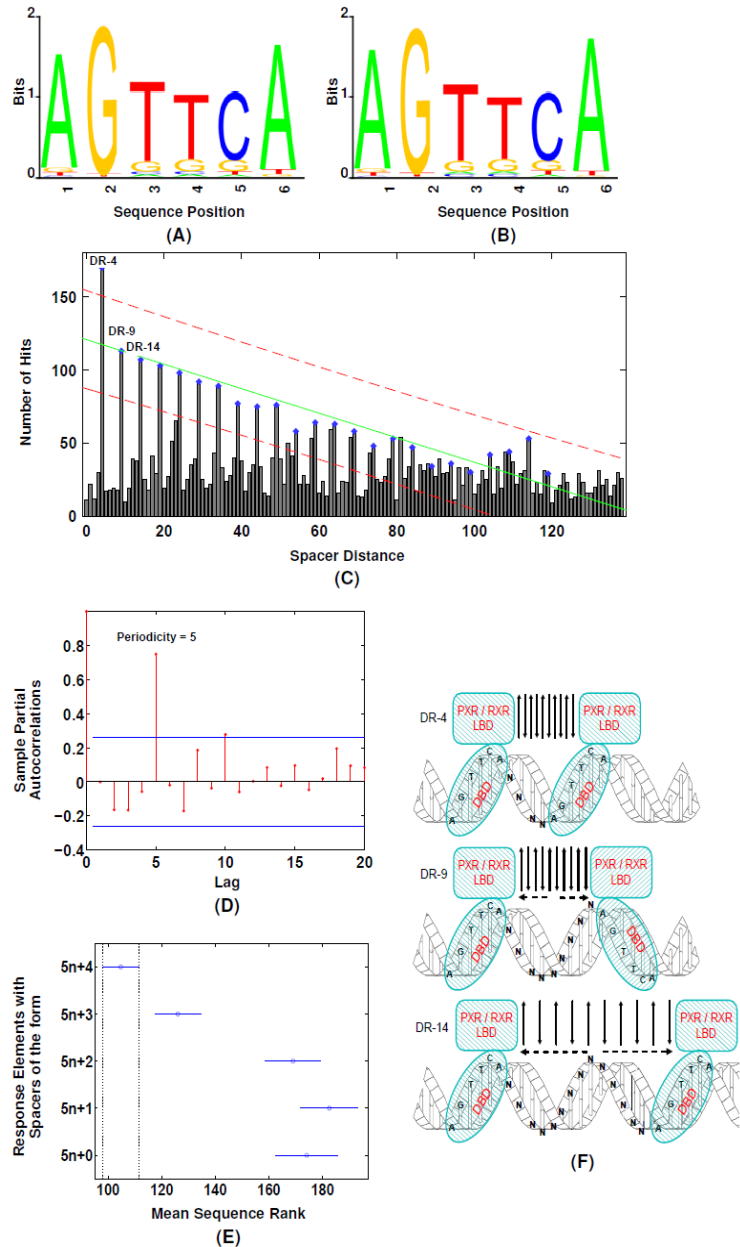


Figure 4.6. PXR-DNA binding profiles of the highest scoring motif (MAP score 6345.15, # hits=4744, #seq. hit =370) obtained from *in silico* analysis of ChIP-Seq data of PXR binding after PCN treatment. (A) Sequence logo representing the sequence conservation of the 3' half site. (B) Sequence logo representing the sequence conservation of the 5' half site. (C) Spacer distance distribution between the two half sites. Diamonds mark densities at spacer distances of $5n+4$. The linear regression line ($\beta_0=-0.83$, $\beta_1=120.75$, norm of residuals=70.14) of these points is shown with 95% confidence bounds (dash lines). (D) Sample partial autocorrelation function of the spacer distance distribution in Fig. 3C, with 95% confidence bounds. The lag corresponds to distance in base pairs. A significantly high lag of 5 base-pairs in the PACF suggests the presence of a recurring pattern of high site density occurring at 5 base-pair intervals. (E) Multiple comparison plot of mean sequence rank on binding affinity of the AGTTCA-like direct repeat with spacer distances of the form $5n+0$, $5n+1$, $5n+2$, $5n+3$, and $5n+4$, with comparison intervals around the mean estimates. Means with comparison intervals that do not overlap are significantly different at a significance level of $\alpha < 0.02$. (F) Illustration of the accordion model to explain the binding density of the PXR homodimer to AGTTCA like direct repeats with a $5n+4$ bp spacer distance. The PXR homodimer interface has a 10 β -strand structure that stretches to accommodate the spacer distances between the two DNA binding domains of the PXR/RXR complex as n increases.

To confirm that DR-(5n+4) is indeed the most preferred PXR-binding motifs, we analyzed the distribution of binding affinities of sequences with response elements of the form DR-(5n+0), (5n+1), (5n+2), (5n+3), and (5n+4) by comparing their mean sequence ranks, ranked on binding affinity. The enrichment peak values from ChIP-Seq data were used as a surrogate for binding affinity. Indeed, DR-(5n+4) ranks highest compared to the other patterns (Figure 4.6E).

The interesting observation for PXR-DNA binding motifs raises the question of whether there are any intrinsic features in the DNA or the PXR protein complex enforcing such a periodic pattern. As demonstrated by Watson and Crick in 1953, the double helical structure of DNA has a 3.4Å interval between the two adjacent bases, with 10 such intervals per turn (34 Å) (Watson and Crick, 1953). If one assumes that at the very beginning of PXR binding, the double helical structure of DNA is still preserved with only partial destruction of hydrogen bonds, then the length of one AGTTCA-like half site exactly matches the length of half a helical turn from trough to peak [$3.4\text{Å} \times (6-1) = 17\text{Å}$] (Figure 4.7). Therefore, DR-4, which is most preferred by the PXR-protein complex will form a structure of three half turns in tandem, with the 4bp spacers occupying the middle half turn. Similarly, DR-9 incorporates one more half turn between the two half sites, as 5 new intervals are introduced into the spacer region. Following this rule, as n half turns are incorporated between the two half sites, a DR (5n+4) pattern emerges

Figure 4.7.

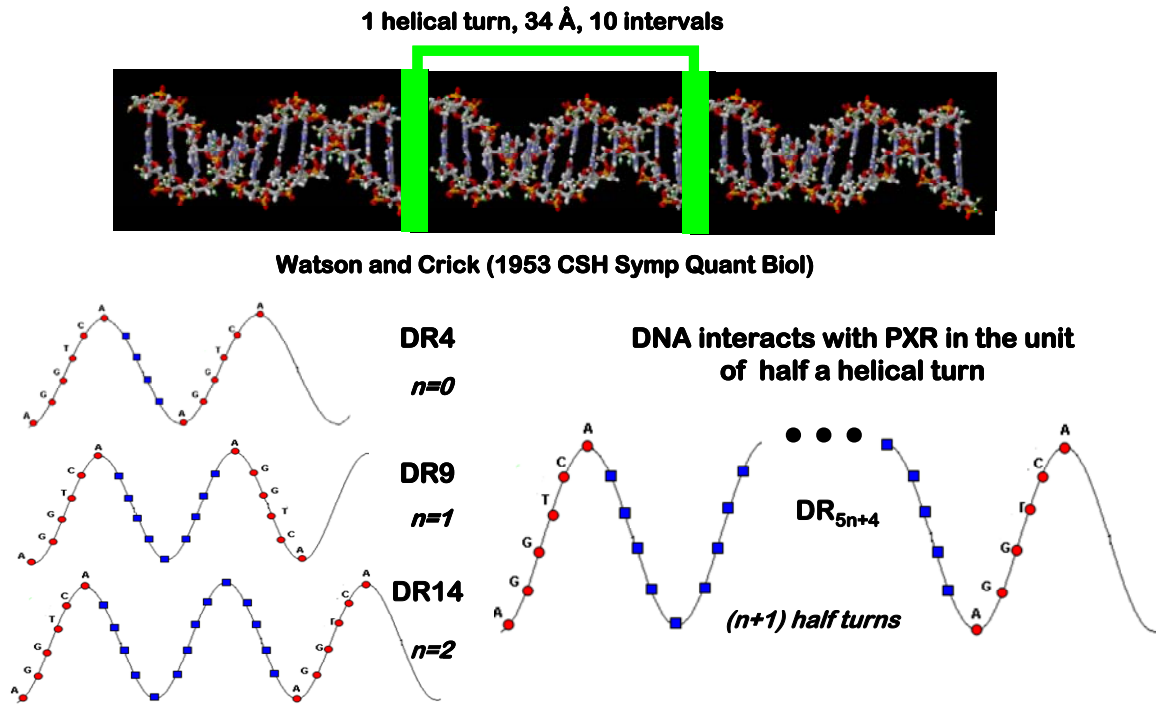


Figure 4.7. A diagram of the helical turns of DNA and the formation of DR-(5n+4) like DNA motifs.

($n=0,1,2,\dots$), which has a tandem structure of two half sites on the outermost half turns, and ($n+1$) half turns in between, forming the spacer region. Based on the observations in the present study, it seems that DNA interacts with PXR protein in a functional unit of half a helical turn. This means that DNA may be more likely targeted by PXR if there are two AGTTCA-like half sites still preserved in the helical structure, separated by at least one half turn in between.

If the proposed structure of DR-($5n+4$) is really the preferred DNA configuration for PXR binding, it suggests that some symmetry exists in the PXR-protein complex. Based on amino acid sequence homology (NCBI BLAST) and the available crystal structure of proteins in the current protein data bank, I predicted the 3D structure of the mouse PXR protein. The mouse PXR-ligand binding domain shows highest similarity to the tethered human PXR-LBDSRC-1p apoprotein (Wang et al., 2008) (PDB ID: 3CTB; E value: $8e-139$), and the human PXR forms a PXR-PXR homodimer interfaced with 10- β strands. Very recently, computational biologists have demonstrated that PXR functions as a heterotetramer with the unique β -stranded interface of the PXR homodimer in the middle, and two RXR proteins on the outside (Teotico et al., 2008). In addition, the key amino acids forming the homodimer interface are highly conserved across species, and disruption of these amino acids results in decreased transcriptional activity of PXR (Noble et al., 2006).

Based on the above evidence, I propose an “accordion model” to explain the interesting phenomenon of the DR-(5n+4) periodic PXR-DNA binding patterns (Figure 4.6F). The basic assumption of this model is that the PXR homodimer interface, which has a β -sheet structure with 10 β -strands, is stretchable like the bellows of an accordion that fine-tunes the distances between the two DNA binding domains of the PXR/RXR complex. The lowest energy configuration of the PXR/RXR complex corresponds to the binding to DR-4, and as the bellows of the accordion stretch out with less favorable configuration, the PXR/RXR-protein complex allows the incorporation of an integral number of half helical turns between the two DNA-binding domains. As more half turns of DNA are incorporated in the spacer region, the interface is further stretched out, which still allows the interactions between the PXR-protein complex and its response element, but with decreased predilection.

To obtain further information that PXR indeed binds to the novel DR-(5n+4)-like DNA sequences, I developed a quantitative ELISA-based transcription-factor binding assay for mouse PXR protein. The assay was developed from an existing commercially-available kit for the detection of other transcription factors (Active Motif, Carlsbad, CA), and modified accordingly for the detection of PXR. As shown in Figure 4.8, this assay can detect basal binding (CON) and PCN-induced binding (PCN) of PXR to the following binding sites: DR-3, DR-4, DR-9, DR-14, and DR-19. For each binding site, nuclear protein from PCN-treated mouse liver resulted in increased PXR binding to the DNA sequence. In addition,

Figure 4.8.

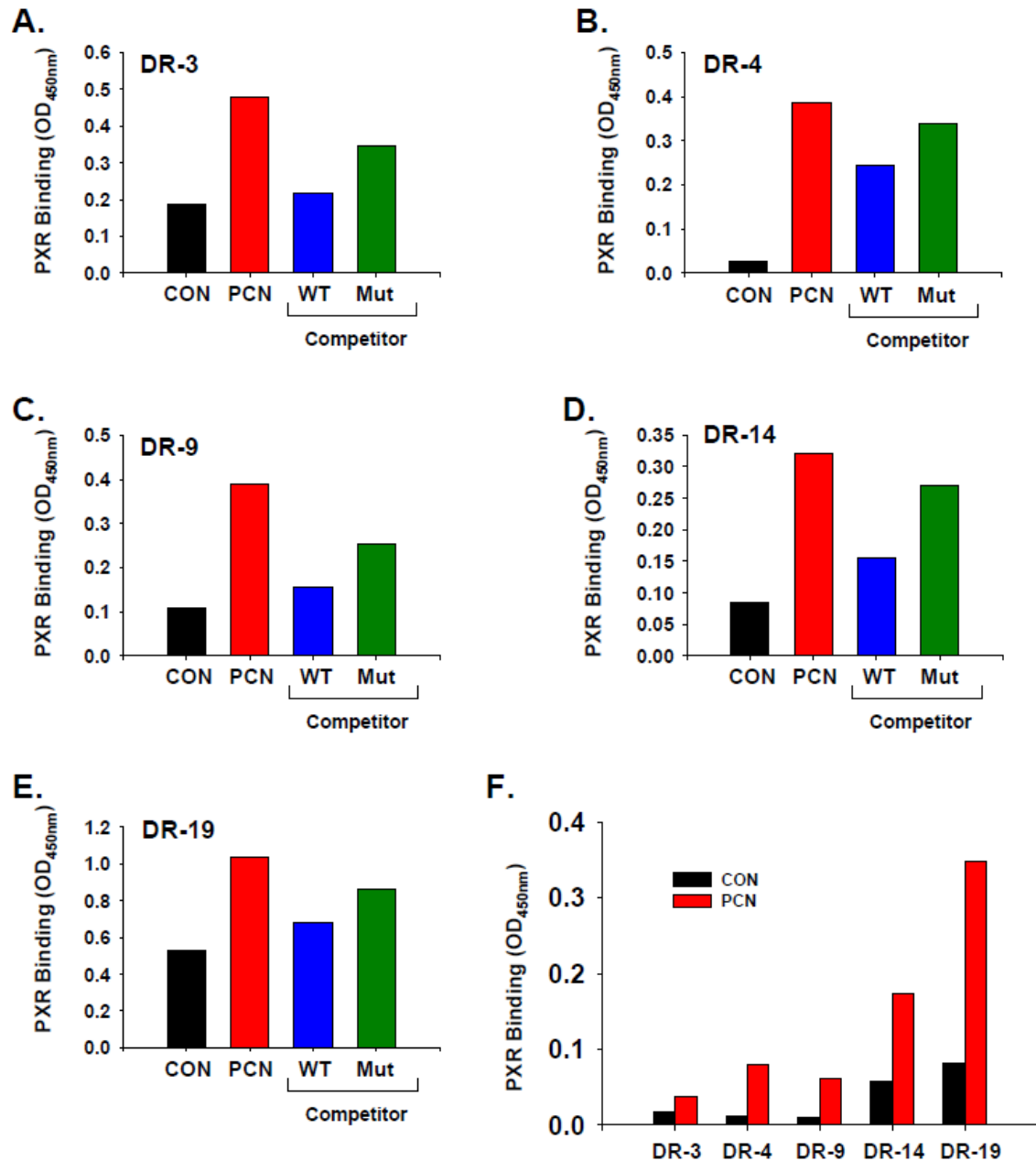


Figure 4.8. Quantification of PXR binding to the DR-3, DR-4, DR-9, DR-14, and DR-19 DNA-binding motifs. Nuclear protein extracts from the livers of mice treated with corn oil vehicle control (CON) or the PXR agonist, PCN, were incubated with oligonucleotides corresponding to various DNA binding motifs. The binding of PXR to the various DNA-binding motifs was quantified using an ELISA-based transcription-factor binding assay, as detailed in the Methods section. Binding of PXR to A) DR-3, B) DR-4, C) DR-9, D) DR-14, and E) DR-19. An unlabeled oligonucleotide competitor was included for each DR DNA binding motif to confirm the specificity of the assay (WT Comp) as well as a mutated oligonucleotide competitor, which should not compete effectively with the positive control (PCN treatment). F.) PXR binding to all the DNA-binding motifs was analyzed simultaneously in order to directly compare the intensity of binding among the different DR sequences.

binding of PXR to each DNA binding site was effectively competed off with an unlabeled competitor oligonucleotide, whereas mutated unlabeled oligonucleotides were either ineffective or less effective in competing with the labeled DNA sequences. Interestingly, under these binding conditions, PXR binding was strongest to DR-19, followed by DR-14, whereas DR-9, DR-4 and DR-3 were relatively similar (Figure 4.8F). Collectively, these data demonstrate that PXR binds to the DR-(5n+4) binding motif in mouse liver.

Overlay between PXR binding and epigenetic marks. The PXR-nuclear-binding signatures have raised the question of whether a permissive chromatin environment pre-exists at PXR-binding sites favoring the interaction between PXR protein and DNA. To explore the pre-existence of chromatin epigenetic signatures in predefining the binding signatures of PXR, three epigenetic marks, namely DNAMe, H3K4Me2, and H3K27Me3, were examined by ChIP-on-chip. Therefore, as a first attempt to discover the roles of epigenetic signatures in regulating PXR binding to drug-processing genes, we selected chromosomes 5, 12, and 15, because these chromosomes are enriched with drug-processing genes (for example, these chromosomes contain the Cyp3a gene subfamily, Ugt2 and Ugt3 gene clusters, and the Mdr gene cluster). An overlay was performed between these epigenetic signatures and PXR binding (ChIP-Seq) in both control and PCN-treated conditions. As expected, there were more nucleotides covered by PXR after PCN treatment (Figure 4.9). Minimal overlapping was observed between PXR binding and the non-permissive

Figure 4.9.

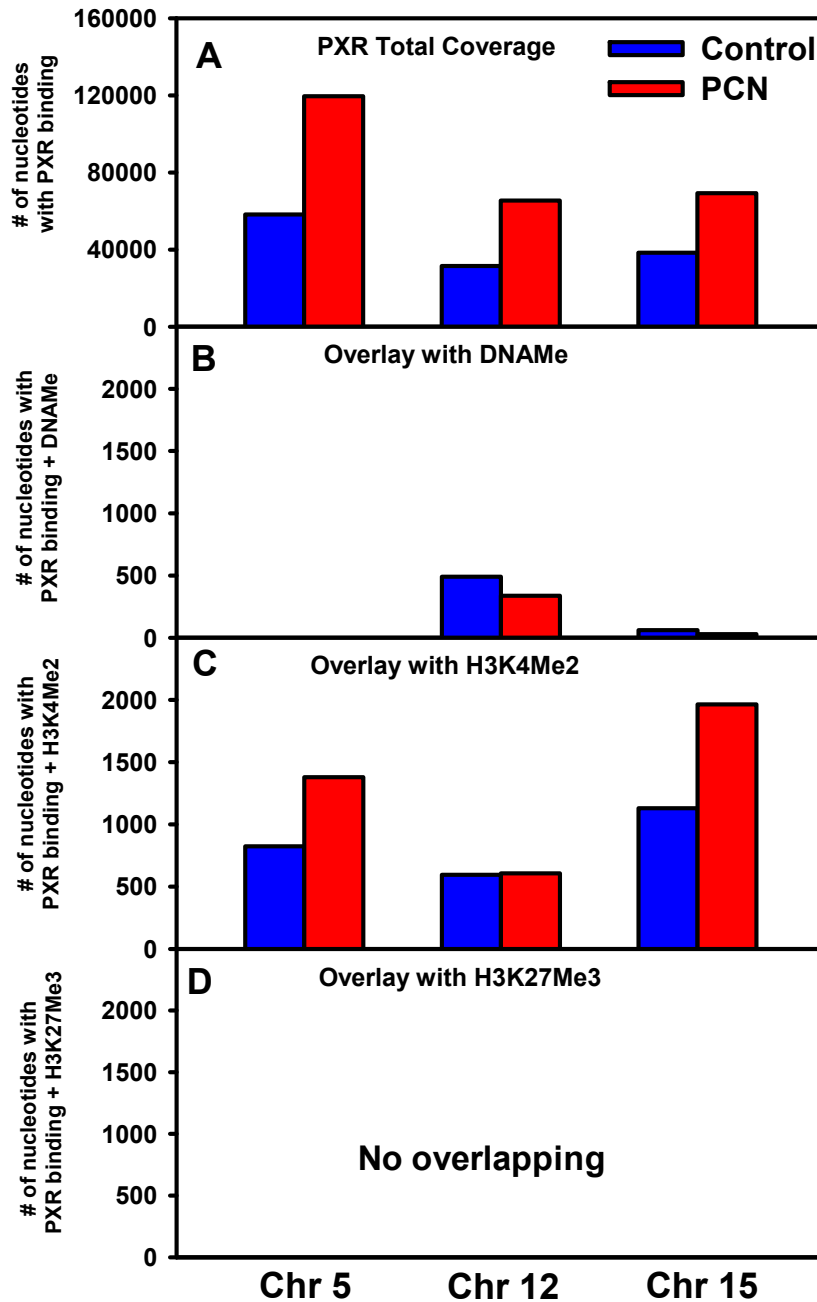


Figure 4.9. An overlay between PXR binding and presence of three epigenetic marks: DNAMe, H3K4Me2, and H3K27Me3 on mouse chromosome 5, 12, and 15. Presence of the three epigenetic marks was determined by ChIP-on-chip as described in EXPERIMENTAL PROCEDURES. (A) Total number of nucleotides bound by PXR in control and PCN-treated groups on mouse chromosome 5, 12, and 15, based on ChIP-Seq analysis. (B) An overlay between PXR binding and presence of DNAMe. (C) An overlay between PXR binding and presence of H3K4Me2. (D) An overlay between PXR binding and presence of H3K27Me3.

epigenetic mark DNAMe in control mice (0bp, 491bp, and 62bp on chr 5, 12, and 15, respectively), and even less in PCN-treated mice (0bp, 337bp, and 30bp on chr 5, 12, and chr15, respectively) (Figure 4.9B). In contrast, prominent portions of PXR-bound nucleotides overlapped with the permissive mark H3K4Me2 in control (824bp, 596bp, and 1130bp on chr 5, 12, and 15, respectively), and even more after PCN treatment (1379bp, 607bp, and 1964bp on chr 5, 12, and 15, respectively) (Figure 4.9C). There was no overlapping between PXR binding and the non-permissive mark H3K27Me3 in either control or PCN-treated conditions (0bp overlap) (Figure 4.9D).

In summary, the ontogeny of numerous drug-processing genes and transcription factors form distinct expression patterns during liver maturation. Dynamic changes in three epigenetic marks, namely DNAMe, H3K4Me2, and H3K27Me3, were observed on three representative chromosomes (chr5, 12, and 15) during liver development. In addition, a roadmap of the genome-wide DNA binding signatures for the xenobiotic sensor PXR has been generated, and shows a novel response element *in vivo* in liver, and some PXR-DNA binding sites overlap with the presence of H3K4Me2, an epigenetic mark for gene activation. The genetic and epigenetic mechanisms underlying the regulation of drug-processing genes during development will be described in the following four chapters of the dissertation.

CHAPTER FIVE

THE ONTOGENY OF NOVEL CYTOCHROME P450 GENE ISOFORMS

DURING POSTNATAL LIVER MATURATION IN MICE

ABSTRACT

The ontogeny of the first four families of cytochrome P450s (Cyp1-4) can markedly affect the biotransformation of drugs and environmental chemicals in liver, resulting in unique pharmacological and toxicological responses in children. As genome-scale investigations have identified many novel Cyp isoforms recently, it is critical to perform a systematic characterization of these Cyps during liver development. In this study, livers were collected from C57BL/6 mice at 2 days before birth and various postnatal ages. The mRNAs of 75 Cyp isoforms (Cyp1-4) were quantified by multiplex suspension bDNA assay and RT-qPCR. Over half of the mouse Cyps are conserved for humans, but there are more isoforms in mice. The mRNA of all these Cyp isoforms increased in mouse liver after birth, forming four distinct ontogeny patterns. Cyp1 mRNAs showed various ontogeny patterns, in that Cyp1a1 mRNA was highest right after birth, Cyp1a2 mRNA is highest between 20 and 45 days of age, whereas Cyp1b1 mRNA increased right after birth, followed by a decrease from day 3 and 5, but increased again after 10 days of age. For the Cyp2 genes, Cyp2b and 2c subfamilies tended to be female predominant, whereas Cyp2d and 2j mRNAs tended to be male predominant. Most Cyp3 and Cyp4 genes were most highly expressed in adults, whereas a few were enriched in neonatal liver. The majority of Cyps form a total of 8 genomic clusters, namely, Cyp1a1 and 1a2 on chr 9 (cluster 1), Cyp2a-2b-2f-g-2t genes on chr 7 (cluster 2), Cyp2c genes on chr 19 (cluster 3), Cyp2d genes on chr 15 (cluster 4), Cyp2j genes on chr 4 (cluster 5), Cyp3a genes on chr 5 (cluster 6), Cyp4a-4b-4x genes on chr 4 (cluster 7), and

Cyp4f genes on chr 17 (cluster 8). A number of the Cyp isoforms within the same chromosomal cluster showed similar ontogeny patterns. Both epigenetic mechanisms as well as nuclear receptor binding to the Cyp gene loci may contribute to the developmental regulation of the Cyp isoforms. ChIP-on-chip identified that the ontogenic expression of the Cyp3a genes associates with distinct histone methylation signatures. ChIP-Seq identified that under a permissive chromatin environment, PXR binds to some of the Cyp3a genes within the cluster marked with histone H3K4 dimethylation. In conclusion, the present study has revealed 4 patterns of ontogeny of novel Cyps in liver, and showed that some Cyps within a genomic cluster share similar ontogeny patterns, suggesting that some Cyps within a cluster are likely regulated by a common pathway during liver development, including chromatin epigenetic marks and PXR-DNA binding.

INTRODUCTION

It is generally considered that CYPs in families 1-4 are critical and inducible components of the phase-I biotransformation system in various species (Wei et al., 2000; Estabrook, 2003; Kang et al., 2007; Li et al., 2007), and many of them are also important for metabolizing lipids, including steroids (CYP2), bile acids (CYP3A), fatty acids (CYP4), and many other endogenous compounds (Nebert and Russell, 2002). In contrast, other CYP families specialize in endobiotic metabolism (Nebert and Russell, 2002). Whereas genetic mutations in CYPs are responsible for various types of inborn errors of metabolism and human diseases (Nebert and Russell, 2002; Caldwell, 2004), induction of some CYPs is a risk factor for adverse drug interactions. Previous studies have determined that the mRNAs of Cyp1-4 are inducible by ligands for four classes of xeno-receptors, namely the aryl hydrocarbon receptor (AhR), the constitutive androstane receptor (CAR), the pregnane X receptor (PXR), and the peroxisome proliferator-activated receptor alpha (PPAR α) (Petrick and Klaassen, 2007). Although these receptors have overlapping targets, it is generally considered that AhR is responsible for the mRNA induction of CYP1, CAR for CYP2, PXR for CYP3, and PPAR α for CYP4.

Liver is an essential organ for drug metabolism and nutrient homeostasis. Many well characterized CYPs have been found to be enriched in adult liver (Nebert and Russell, 2002). Interestingly, before birth, liver is mainly a hematopoietic organ with very limited capacity for drug metabolism in both

humans and mice. However after birth, the liver becomes the major organ for processing drugs and other chemicals. Very little is known about how and when the drug-metabolizing CYPs become activated or suppressed during postnatal liver development, resulting in higher risks for adverse drug reactions in pediatric patients. In 1959, it was found that a number of drugs that are metabolized by Cyps in liver microsomes from adult rabbits are not metabolized in livers of newborn rabbits (Fouts and Adamson, 1959). However, at that time, only two Cyp enzymes were thought to exist. After more CYP genes were cloned, the ontogeny of a few CYPs were characterized in human livers (de Wildt et al., 1999; Blake et al., 2005; Leeder et al., 2005; Gaedigk et al., 2006; Hines, 2007). However, these data are rather fragmentary in that at most 10 CYP isoforms were studied in each manuscript, and no one aimed to characterize all the drug-metabolizing Cyps systematically. At the beginning of the 21st century, two exciting findings were reported: first, in 2003, the Human Genome Project was declared complete, which indicated there were 57 human Cyps, and second, the NCBI data base was released, which indicated there were 102 mouse Cyps (Nelson et al., 2004). Many of these newly identified Cyps are still considered “orphans”, that is they have no known function. In addition, very little is known about the ontogeny of novel Cyps during postnatal liver development.

Mice have been a popular research tool to study the functions and ontogeny of Cyps (Choudhary et al., 2003; Choudhary et al., 2005; Hart et al., 2009), due to their homogenous genetic background, and the availability of genetically-

modified mouse models, including the Cyp gene-knockout mice and the Cyp gene-humanized transgenic mice (van Herwaarden et al., 2007; Lofgren et al., 2009; Zhou et al., 2010). Last year, we identified three patterns of Cyp gene expression during postnatal liver maturation in mice (Hart et al., 2009). However, only 19 Cyps were included. It remains to be determined whether the novel Cyp genes within the first four families are expressed in liver, and what their ontogeny patterns are during postnatal liver maturation.

Therefore, the purpose of the present study was to systematically determine the ontogeny of 75 known and novel Cyps in the Cyp1-4 families in mouse liver. In addition, we also compared their sequence homologies with humans, and determined the correlation between their chromosomal location and coordinate gene expression. The successful completion of the blueprint for the ontogeny of novel Cyps will generate many hypotheses in predicting functions of the “orphan” Cyps during liver development.

RESULTS

Sequence homology of Cyps between mice and human. Previously, we have characterized the ontogeny of 19 Cyps important for drug metabolism during mouse liver maturation, and compared the sequence homology of these genes with the human homologs (Hart et al., 2009). In the present study, as a first approach to determine which of the newly identified novel Cyps are conserved in humans, and which are mouse specific isoforms, the National Center for Biotechnology Information (NCBI) HomoloGene Database (<http://www.ncbi.nlm.nih.gov/>) was used to determine the homologous Cyp genes in mice that are conserved for human Cyps, as well as Cyp isoforms that are unique in mice, among the 75 mouse Cyp genes from Cyp1-4 families. Table 3.1 lists the mouse Cyp gene names, their human homologs (if present), mouse gene ID, mouse mRNA and protein accession numbers, identities of DNA and protein sequences between mice and humans, as well as the chromosomal locations of the mouse Cyp genes. Among these 75 Cyps in mice, 39 genes are conserved in humans, whereas 36 genes are mouse Cyp isoforms with no apparent human homologs. For the conserved Cyps, some mouse genes display more variations in their isoforms than human genes, as many human Cyps have multiple mouse homologs. For example, the human CYP2C19 is homologous to three mouse Cyp isoforms, namely Cyp2c37, 2c50, and 2c54; the human CYP3A4 is homologous to five mouse Cyp isoforms, namely Cyp3a11, 3a16, 3a41a, 3a41b, and 3a44; the human CYP3A43 is homologous to mouse Cyp3a57 and 3a59; and the human CYP4A22 is homologous to mouse

Cyp4a12a and 4a12b (Table 3.1). The other human CYPs only have one unique homologous gene in mice.

Interestingly, the majority of CyPs form a total of 8 genomic clusters on certain mouse chromosomes (Figure 5.1). The only Cyp genes in isolation (i.e. they do not form clusters with other CyPs) include Cyp1b1, 2c44, 2e1, 2u1, 2w1, 3a13, 4f18, and 4v3. Cyp1a and 3a gene families have human homologs for all the genes within these two genomic clusters (chr9 for Cyp1a, and chr5 for Cyp3a) (Figure 5.1 cluster 1 and 6), highlighting their functional significance during evolution. In contrast, only 4 out of 11 mouse Cyp2a-f genes within cluster 2, and 5 out of 14 mouse Cyp2c genes within cluster 3, have human homologs. Cyp2d22 is the only gene within cluster 4 that has a human homolog (CYP2D6), and Cyp2j6 is the only gene within cluster 5 that has a human homolog. In addition, 6 out of 10 Cyp4 genes within cluster 7, and 5 out of 7 Cyp4 genes within cluster 8, have human homologs (Table 3.1 and Figure 5.1).

In summary, among the 75 isoforms, over half of the CyPs within the first 4 gene families are conserved between mice and humans, but the mouse Cyp genes seem to have more sequence redundancy and display more variations in isoforms. In addition, the majority of Cyp isoforms form distinct genomic clusters on mouse chromosomes.

Figure 5.1

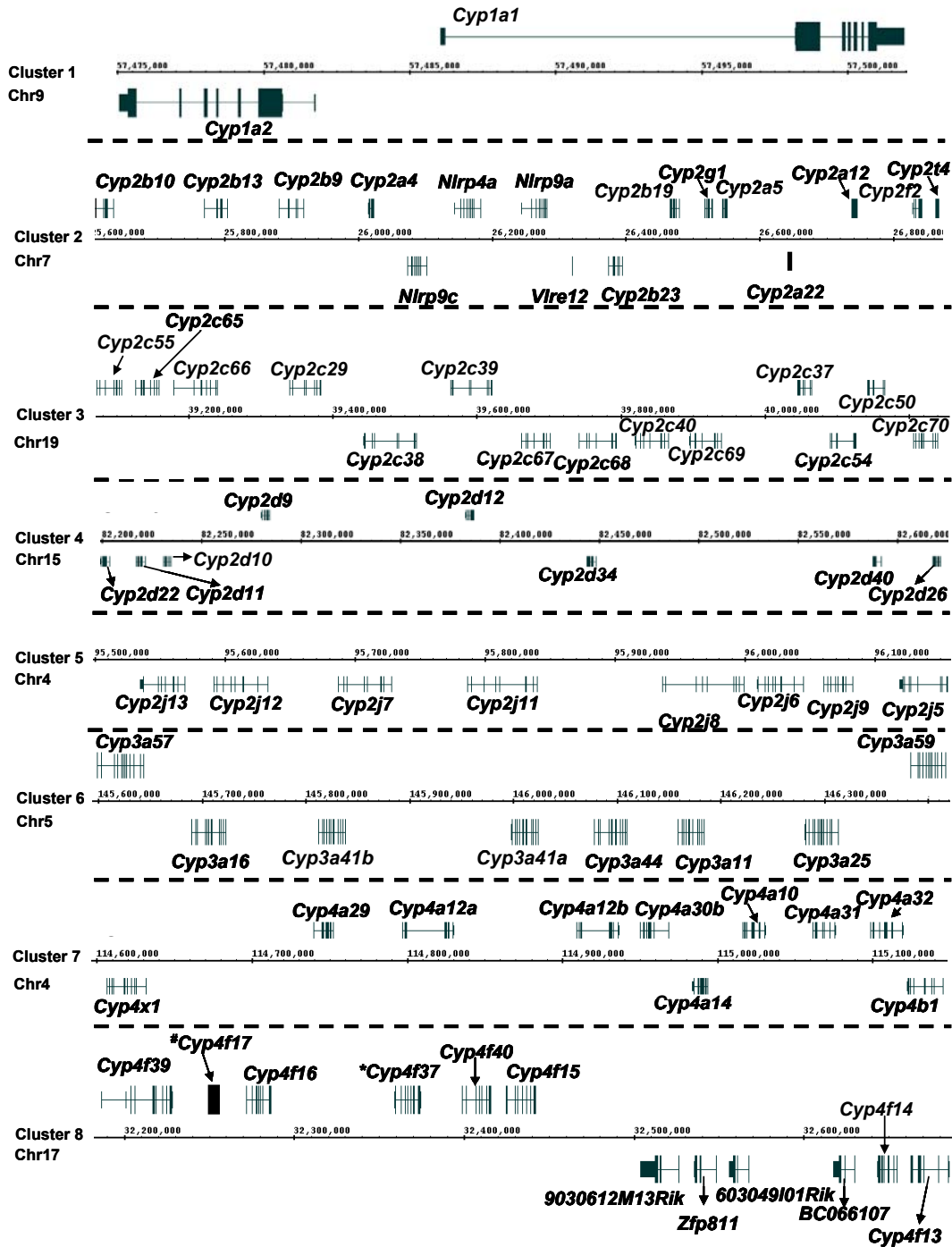


Figure 5.1. Genomic locations of Cyp gene clusters from Cyp1 (cluster 1), Cyp2 (clusters 2-5), Cyp3 (cluster 6), and Cyp4 (clusters 7-8) gene families. This map was generated from the Affymetrix Integrated Genome Browser (IGB). Genes above the chromatin coordinates are transcribed from the plus strand, and genes below are transcribed from the minus strand. Asterisks (*) represents a pseudogene. Pound (#) represents a gene annotated in NCBI database but not in IGB. Arrows point the gene names to the loci. Dashed lines separate panels from each other.

Ontogeny of the mRNA of the Cyp1 gene family. Within the Cyp1 gene family, *Cyp1a1* and *1a2* form a cluster on mouse chromosome (Chr) 7 but transcribe from opposite strands (*Cyp1a1*: plus strand; *Cyp1a2*: minus strand)(Figure 5.1 panel 1), whereas *Cyp1b1* is in isolation (data not shown). More specifically, *Cyp1a2* is embedded in the 5-UTR region of the *Cyp1a1* gene locus. The mRNAs of *Cyp1a1*, *1a2*, and *1b1* were quantified during liver development in mice (Figure 5.2). *Cyp1a1* mRNA was lowest before birth, but increased markedly after birth (1.7-fold of day -2 levels) and peaked at 1 day of age (255-fold of day -2 levels). After day 1, *Cyp1a1* mRNA decreased and gradually reached adult levels after 30 days of age (approximately 35-fold of day -2 levels) (Figure 5.2, left panel 1).

Compared to *Cyp1a1* and *1b1*, apparently more *Cyp1a2* mRNA was detected than the other two isoforms throughout postnatal liver maturation. *Cyp1a2* mRNA expression was lowest before birth, but increased 17 fold right after birth, and continued to increase until about 20-days of age.

Cyp1b1 mRNA was also lowest before birth, and increased 3-fold right after birth. The *Cyp1b1* mRNA remained relatively constant thereafter (Figure 5.2, left panel 3).

In summary, the ontogeny of the Cyp1 gene family displayed divergent patterns: *Cyp1a2* appeared to be the most abundant Cyp1 isoform, and it

Figure 5.2.

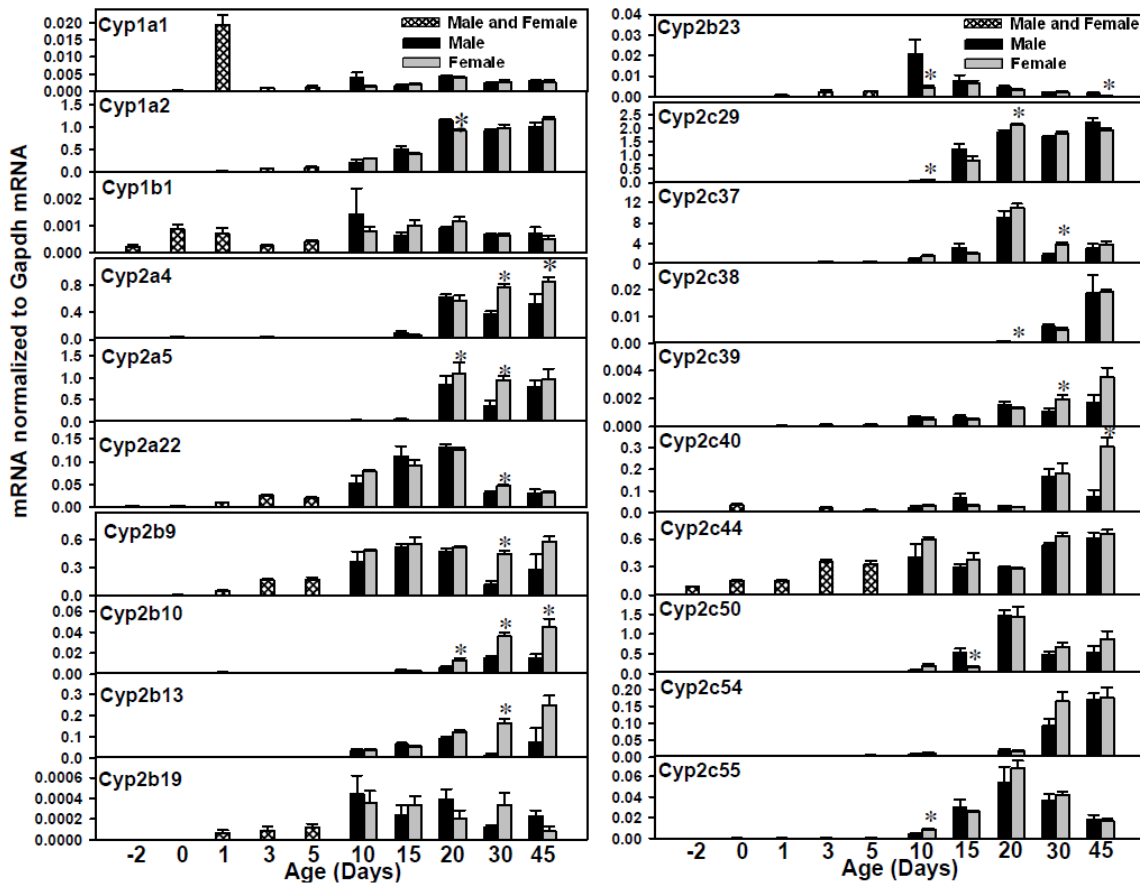


Figure 5.2. The mRNA ontogenic expression of the Cyp1 family (Cyp1a1, 1a2, and 1b1), and part of the Cyp2 family (Cyp2a4, 2a5, 2a22, 2b9, 2b10, 2b13, 2b19, 2b23, 2c29, 2c37, 2c38, 2c39, 2c40, 2c44, 2c50, 2c54, and 2c55) in male and female livers from day -2 to day 45 of age. Total RNA was isolated from liver at each age (n=5 per gender at each age). Genders were not differentiated from day -2 to day 5 of age (n=5 at each age). The mRNA expression of Cyp2a5, 2c37, 2c40, 2c50, and 2c54 was determined by RT-qPCR, whereas the mRNAs of other Cyps were quantified by the multiplex bDNA assay as described in MATERIALS AND METHODS. Data are presented as mean fluorescence intensity of mRNA \pm S.E.M normalized to Gapdh. Asterisks represent statistical significances between male and female mice ($p < 0.05$).

showed an adult enriched pattern in both males and females; whereas Cyp1a1 and 1b1 mRNAs were induced right after birth, but the levels reached adult expression at about 20 days of age, but the levels were relatively low. Although Cyp1a1 and 1a3 are located in the same genomic cluster, they showed different ontogeny patterns.

Ontogeny of the mRNA of the Cyp2 gene family. Compared to other Cyp gene families, the Cyp2 family has the largest number of subfamilies and gene isoforms, including the Cyp2a subfamily, Cyp2b, Cyp2c, and Cyp2d subfamily, as well as Cyp2e, Cyp2f, Cyp2g, Cyp2j, Cyp2s, Cyp2t, Cyp2u, and Cyp2w. The mRNAs of these Cyp2 genes were quantified during liver development in mice (Figure 5.2 left panel 4 to Figure 5.4 left panel 7), except for Cyp2a12, 2s1, 2c65, 2d13, and 2r1, due to potential cross-reaction among primers.

For the Cyp2a subfamily (Figure 5.2 left panel 4-6), both Cyp2a4 and 2a5 mRNAs were expressed at a very low level before birth, and gradually increased to adult levels at 20 days of age, and remained relatively stable thereafter. Cyp2a22 mRNA was also lowest before birth, followed by a gradual increase after birth until 20 days of age when the peak mRNA expression was observed. After day 20, Cyp2a22 mRNA decreased approximately 60% at both 30 and 45 days of age. Female-predominant expression of Cyp2a5 was observed at 20 and 30 days of age.

For the Cyp2b subfamily (Figure 5.2 left panel 7-10, and right panel 1), the expression of Cyp2b9, 2b10, and 2b13 mRNAs appeared to be more than that of Cyp2b19 and 2b23 during liver development. The mRNAs of Cyp2b9, 2b10, and 2b13 were all lowly expressed before birth, followed by a gradual increase after birth. Peak levels of Cyp2b9 mRNA were observed at 15 days of age, Cyp2b10 at 45 days of age, and Cyp2b13 mRNA at 45 days of age. Female-predominant expression was observed for Cyp2b9, Cyp2b10, and Cyp2b13. For Cyp2b19 and 2b23, minimal mRNA expression was observed before birth, followed by a gradual increase from 0 to 5 days of age, and peaked at around 10 days of age, and gradually decreased afterwards, and the mRNAs of Cyp2b19 and 2b23 were relatively lowly expressed in liver throughout development.

For the Cyp2c subfamily (Figure 5.2 right panel 2-10, and Figure 5.3 left panel 1-5), Cyp2c29 mRNA gradually increased to adult levels by 20 days of age. Cyp2c37 mRNA was also lowest before birth, increased after birth, and peaked at 20 days of age. After day 20, the Cyp2c37 mRNA decreased markedly to adult expression at 45 days of age. The mRNAs of Cyp2c38, 2c39, 2c40, 2c54, 2c67, 2c68, and 2c69 were all low before birth, but gradually increased to adult levels between 30 and 45 days of age. The mRNAs of 2c50, 2c55, 2c66, and 2c70 were all lowly expressed before birth, but increased after birth, reaching peak values between 10 and 20 days of age. Cyp2c44 mRNA was low before birth, and appeared to reach adult levels by 10 days of age. Most of the Cyp2b genes showed female-predominant expression pattern. Female-predominant

Figure 5.3.

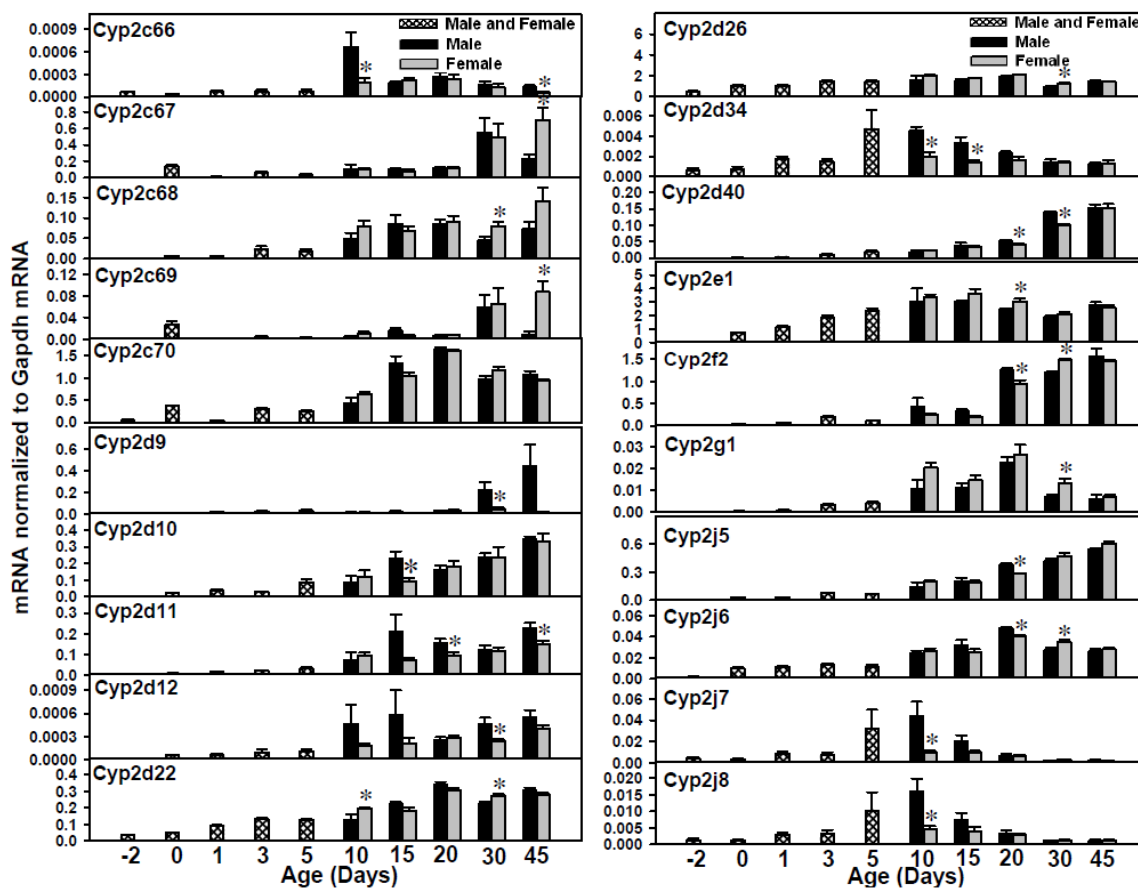


Figure 5.3. The mRNA ontogenic expression of part of the Cyp2 family (Cyp2c66, 2c67, 2c68, 2c69, 2c70, 2d9, 2d10, 2d11, 2d12, 2d22, 2d26, 2d34, 2d40, 2e1, 2f2, 2g1, 2j5, 2j6, 2j7, and 2j8) in male and female livers from day -2 to day 45 of age. Total RNA was isolated from liver at each age (n=5 per gender at each age). Genders were not differentiated from day -2 to day 5 of age (n=5 at each age). The mRNA expression of Cyp2c67, 2c68, 2c69, 2d9, 2d10, 2d11, and 2d12 was determined by RT-qPCR, whereas the mRNAs of other Cyps were quantified by the multiplex bDNA assay as described in MATERIALS AND METHODS. Data are presented as mean fluorescence intensity of mRNA \pm S.E.M normalized to Gapdh. Asterisks represent statistical significances between male and female mice ($p < 0.05$).

mRNA expression was observed for Cyp2c39, 40, 67, 68, and 69. Male-predominant mRNA expression was observed at 20 days of age for Cyp2c38 (although the gene expression in both genders was very low at this age), and at 10 and 45 days of age for Cyp2c66. Cyp2c65 mRNA was not determined in the present study due to high sequence homology.

For the Cyp2d subfamily (Figure 5.3 left panel 6-10, and right panel 1-3), Cyp2d9 is an adult-enriched male-predominant Cyp isoform, in that low Cyp2d9 mRNA expression was observed before 20 days of age, but after day 20, the male Cyp2d9 mRNA increased markedly, whereas Cyp2d9 was expressed lowly in females at all ages. The mRNAs of Cyp2d10, 2d11, 2d12, 2d22, 2d26, and 2d40 were lowly expressed before birth, and gradually increased to adult levels in both genders during development. For Cyp2d22 and 2d26, peak levels were observed at 20 days of age. Cyp2d34 mRNA was low before birth and in neonatal ages (day 0 to day 3), but increased and peaked at 5 days of age, and gradually decreased to prenatal levels.

Cyp2e1 mRNA was also low before birth, followed by a marked increase right after birth, and continued to increase and reached adult levels at 5 days of age. Cyp2f2 mRNA was low before birth, followed by a gradual increase after birth, and reached adult levels at about 20 days of age. Cyp2g1 mRNA was low before birth, followed by a gradual increase after birth until 20 days of age, when peak levels were observed, and its expression decreased thereafter.

The mRNAs of Cyp2j5, 2j6, and 2j9 were all low before birth, followed by an increase after birth, and peak levels were observed between 20 and 45 days of age (Figure 5.3 and 5.4). In contrast, the mRNAs of Cyp2j7, 2j8, 2j11, 2j12, and 2j13 gradually increased after birth, but peaked at about 10 days of age. The mRNA expression of Cyp2j11-13 mRNAs appeared to be lower than the other Cyp2j isoforms throughout liver development.

Cyp2t4 mRNA was low before birth, increased and appeared to reach a peak at 10 days of age, and attained adult levels at about 30 to 45 days of age. Cyp2u1 mRNA was low from before birth to 20 days of age, followed by a marked increase at 30 days of age, when peak levels were observed. The Cyp2u1 appeared to be a male-predominant Cyp because the Cyp2u1 mRNA tended to be lower in female mice after 30-days of age. Cyp2w1 mRNA was low before birth, followed by a gradual increase after birth, and peaked at 10 days of age in males, whereas the female Cyp2w1 remained stable from day 10 to day 30, and increased to peak expression at 45 days of age. In general, the Cyp2w1 mRNA signals were very low throughout liver development (<0.08% of Gapdh mRNA).

Most of the Cyp2 genes are contained within four genomic clusters, including the *Cyp2a-f* cluster on chr7 (Figure 5.1 cluster 2) (plus strand: *Cyp2b10*, *2b13*, *2b9*, *2a4*, *2b19*, *2g1*, *2a5*, *2a12*, *2f2*, and *2t4*; minus strand: *Cyp2a22* and *2b23*),

Figure 5.4.

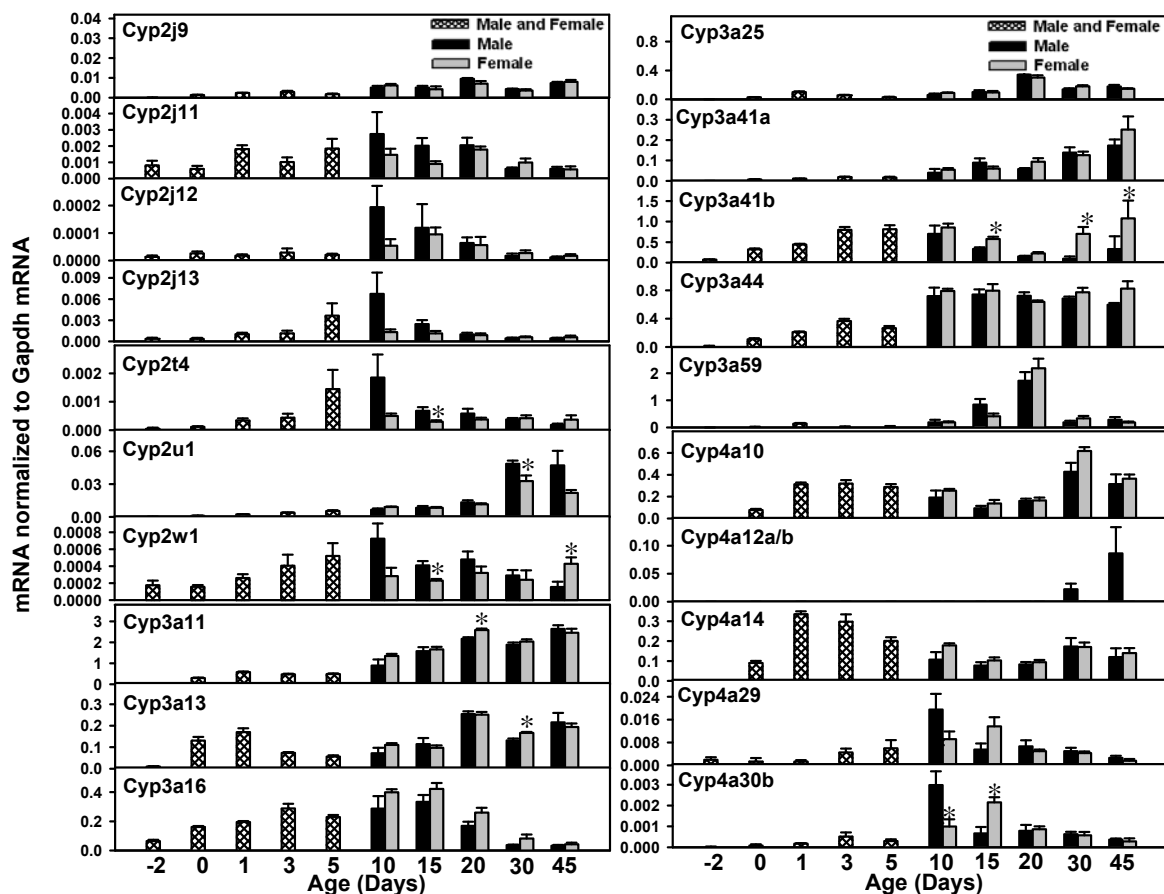


Figure 5.4. The mRNA ontogenic expression of part of the Cyp2 family (Cyp2j9, 2j11, 2j13, 2j13, 2t4, 2u1, and 2w1), Cyp3 family (Cyp3a11, 2a13, 2a16, 3a25, 3a59, 3a41a, 3a41b, 3a44), and part of the Cyp4 family (Cyp4a10, 4a12a/b, 4a14, 4a29, and 4a30b) in male and female livers from day -2 to day 45 of age. Total RNA was isolated from livers at each age (n=5 per gender at each age). Genders were not differentiated from day -2 to day 5 of age (n=5 at each age). The mRNA expression of Cyp2j12, 3a59, 3a41a, 4a12a/b was determined by RT-qPCR, whereas the mRNAs of other Cyps were quantified by the multiplex bDNA assay as described in MATERIALS AND METHODS. It should be noted that due to high sequence homology, primers for Cyp3a41a and 41b have cross-reactivity. Data are presented as mean fluorescence intensity of mRNA \pm S.E.M normalized to Gapdh. Asterisks represent statistical significances between male and female ($p < 0.05$).

the *Cyp2c* cluster on chr19 (Figure 5.1 cluster 3) (plus strand: *Cyp2c55*, *2c65*, *2c66*, *2c29*, *2c39*, *2c37*, and *2c50*; minus strand: *Cyp2c70*, *2c54*, *2c69*, *2c40*, *2c68*, *2c67*, and *2c38*), the *Cyp2d* cluster on chr15 (Figure 5.1 cluster 4) (plus strand: *Cyp2d9* and *2d12*; minus strand: *Cyp2d26*, *2d40*, *2d34*, *2d10*, *2d11*, and *2d22*), as well as the *Cyp2j* cluster on chr4 (Figure 5.1 cluster 5) (*Cyp2j5*, *2j9*, *2j6*, *2j8*, *2j11*, *2j7*, *2j12*, and *2j13*, all transcribed from the minus strand). The only *Cyp2* genes that are not clustered with other *Cyps* in the mouse genome include *Cyp2c44*, *2e1*, *2u1*, and *2w1*. Interestingly, within the *Cyp2a-f* cluster on chr7 (Figure 5.1 cluster 2), *Cyp2b10*, *2b13*, *2b9*, and *2a4*, which are clustered together on the left side (upstream), all displayed a female-predominant mRNA expression pattern with highest expression observed between 20 and 45 days of age (Figure 5.2, left panel 3, 6-8). Downstream of *Cyp2a4* gene, *Cyp2b19*, *2g1*, *2a5*, *2a12*, *2f2*, and *2t4* form another cluster, and are separated by the *Cyp2b10-2a4* cluster by four non-*Cyp* genes (*Nlrp9c*, *4a*, *9a*, and *Vlre12*) (Figure 5.1, cluster 2). Within this cluster, the mRNAs of *Cyp2b19*, *2g1*, and *2t4* were highest in adolescent ages (10-20 days of age) (Figure 5.2 left panel 10, Figure 5.3 right panel 6, and Figure 5.4 left panel 5), whereas *Cyp2a5* and *2f2* are in the middle of the cluster were both enriched between 30 and 45 days of age (Figure 5.2 left panel 5, and Figure 5.3 right panel 5). *Cyp2a12* mRNA was not determined in the present study due to high sequence homology.

Within the *Cyp2c* cluster on chr19 (Figure 5.1 cluster 3), on the left side of the cluster, the mRNAs of *Cyp2c55* and *2c66* were both high around 10-20 days of

age (Figure 5.2 right panel 10, and Figure 5.3 left panel 1) (*Cyp2c65* mRNA was not determined due to high sequence homology). Downstream of *Cyp2c66*, the mRNAs of *Cyp2c29*, *2c39*, *2c69*, *2c40*, *2c68*, *2c67*, and *2c38*, all displayed an adult enriched pattern, and many of them tended to be higher in females, such as *Cyp2c39*, *2c40*, *2c67*, *2c68*, and *2c69* (Figure 5.2 right panel 2, 4-6, and Figure 5.3 left panel 2-4). On the right side of the *Cyp2c* cluster, the mRNAs of *Cyp2c37*, *2c50*, and *2c70* were all high around 20 days of age (Figure 5.2 right panel 3 and 8, Figure 5.3 left panel 5). The only exception in this region was *Cyp2c54*, which was highly expressed around 45 days of age (Figure 5.2 right panel 9).

Within the *Cyp2d* cluster on chr15 (Figure 5.1 cluster 4), the mRNAs of most genes (*Cyp2d9*, *2d12*, *2d40*, *2d10*, *2d11*, and *2d22*) were most highly expressed at around 20 to 45 days of age, except for *Cyp2d26* and *2d34*, which were enriched around 10 days of age (Figure 5.3 left panel 6-10, right panel 1-3). In addition, many of these *Cyp2d* genes tended to be male-predominant between adolescent and adult ages (from day 10 to 45), such as *Cyp2d9* after 30 days of age, *2d11* at 20 and 45 days of age, *2d12* at 30 days of age, *2d34* at 10 and 15 days of age, and *2d40* at 20 and 30 days of age. In contrast, *Cyp2d22* and *2d26*, which are localized on the boundary region of the cluster, did not show a male-predominant pattern.

Within the *Cyp2j* cluster on chr4 (Figure 5.1 cluster 5), interestingly, on the left side of the cluster, the mRNAs of *Cyp2j13*, *2j12*, *2j7*, and *2j11*, and *2j8* genes were all high at around day 10 and tended to be male-predominant at this age. In the middle of the cluster, the mRNAs of *Cyp2j6* and *2j9* were both high at 20 days of age, whereas on the right side of the cluster, *Cyp2j5* mRNA was high at 45 days of age.

In summary, all of the 44 *Cyp2* genes were high after birth. Gender differences were observed for many *Cyp2* mRNAs from adolescent to adult ages. In addition, some of the *Cyp* isoforms within a genomic cluster tended to show similar ontogeny patterns.

Ontogeny of the mRNA of the *Cyp3* gene family. The *Cyp3a* subfamily includes 8 members, forming a cluster on chr5 (Figure 5.1 cluster 6), and this cluster includes *Cyp3a57* and *3a59* that are transcribed from the plus strand, as well as *Cyp3a25*, *3a11*, *3a44*, *3a41a*, *3a41b*, and *3a16* from the minus strand. *Cyp3a13* is the only *Cyp3a* that is in isolation (data not shown). The ontogeny of the *Cyp3a* mRNAs is most thoroughly characterized in the literature. Consistent with previous findings (Hart et al., 2009; Li et al., 2009), the mRNAs of *Cyp3a11*, *3a13*, and *Cyp3a25* increased postnatally and peaked between 20 and 45 days of age (Figure 5.4 left panel 8 and 9, right panel 1 and 4). *Cyp3a16* mRNA was low before birth, followed by a marked increase in neonatal ages, and decreased thereafter. Whereas *Cyp3a41b* mRNA increased in neonatal ages, it decreased

in male liver thereafter. However, in female livers, Cyp3a41b mRNA increased again after 30 days of age, and peaked at 45 days of age. In addition, the present study added three new Cyp3a genes, namely Cyp3a41a, and 3a44, and 3a59 (Figure 5.4 right panel 2-4). Cyp3a41a mRNA was low before birth, and gradually increased to peak levels at 45 days of age. Cyp3a44 mRNA was also low before birth, but increased to adult levels by 10 days of age, and the levels remained relatively constant thereafter. Interestingly, the Cyp3a59 mRNA was highest at 20 days of age in both genders, but decreased markedly thereafter.

Within the entire *Cyp3a* gene cluster on chr5 (Figure 5.1 cluster 6), only *Cyp3a16* and *3a59*, which are located at the boundary regions of the cluster, displayed an adolescent-enriched pattern (i.e. high around day 10 to 20) with low mRNA expression in adults. In contrast, the Cyp3a genes in the middle of the cluster, namely Cyp3a25, 3a11, 3a44, 3a41a, and 3a41b, all showed highest expression in adult ages. The Cyp3a57 mRNA was not determined in the present study due to high sequence homology.

Ontogeny of the mRNA of the Cyp4 gene family. The Cyp4 gene family includes 19 members: Cyp4a subfamily, Cyp4b1, Cyp4f subfamily, Cyp4v3, and Cyp4x1. Cyp4a10 mRNA was low before birth, but almost reached adult levels by one day of age.

Due to high sequence homology, Cyp4a12a and 4a12b were quantified together as Cyp4a12a/b (Figure 5.4 right panel 7). Interestingly, the Cyp4a12a/b mRNA was only expressed in male mice, and the expression was relatively low before day 30. Cyp4a14 mRNA was low before birth, with a strong induction in neonatal ages. After day 5, Cyp4a14 mRNA moderately decreased and returned to adult levels after 30 days of age (approximately 1500-fold of day -2 levels) (Figure 5.5 right panel 8). The mRNAs of Cyp4a29 and 4a30b were both low before birth, followed by a postnatal increase after birth, with peak levels observed at 10 days of age (10-fold of day -2 levels in males and 4.7-fold in females for Cyp4a29, as well as 213-fold in males and 71-fold in females for Cyp4a30b). After day 10, the mRNAs of Cyp4a29 and 4a30b in mice decreased to prenatal levels, whereas the female mRNAs continued to increase and reached a peak at 15 days of age, and decreased thereafter. The mRNAs of Cyp4a31 and 4a32 were expressed right after birth, with the first peak of expression observed at 5 days of age, and then the mRNAs gradually decreased, but returned to high levels at 30 days of age (Figure 5.5 left panel 1 and 2).

Cyp4b1 mRNA was low before birth, with a marked postnatal induction after birth. Both the male and female Cyp4b1 mRNAs remained relatively stable thereafter, except that the male Cyp4b1 mRNA showed further increase at 10 days of age (12.8-fold of day -2 levels) (Figure 5.5 left panel 3).

Figure 5.5.

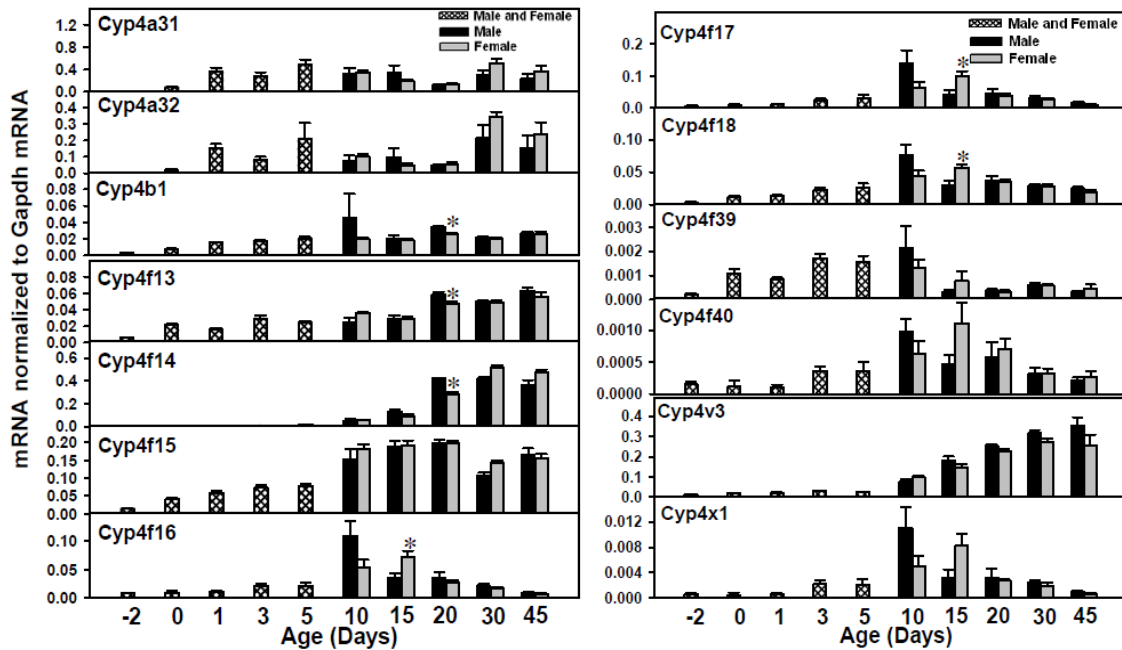


Figure 5.5. The mRNA ontogenic expression of part of the Cyp4 family (Cyp4a31, 4a32, 4b1, 4f13, 4f14, 4f15, 4f16, 4f17, 4f18, 4f39, 4f40, 4v3, 4x1) in male and female livers from day -2 to day 45 of age. Total RNA was isolated from liver at each age (n=5 per gender at each age). Gender was not differentiated from day -2 to day 5 of age (n=5 at each age). The mRNA expression Cyp4a31 and 4a32 was determined by RT-qPCR, whereas the mRNAs of other CyPs were quantified by the multiplex bDNA assay as described in MATERIALS AND METHODS. Data are presented as mean fluorescence intensity of mRNA \pm S.E.M normalized to Gapdh. Asterisks represent statistical significances between male and female mice ($p < 0.05$).

Within the *Cyp4f* subfamily, the mRNAs of *Cyp4f13-15* were expressed lowly before birth, followed by a gradual increase after birth, with adult expression reached between 20 to 45 days of age in both genders (Figure 5.5 left panel 4-6). In contrast, the mRNAs of *Cyp4a16-18*, as well as *Cyp4f39* and *4f40* (Figure 5.5 left panel 7, and right panel 1-4), were all high around 10 to 15 days of age. Female-predominant expression was observed at 15 days of age for *Cyp4f16*, *4f17*, and *4f18*.

Cyp4v3 mRNA was low before birth, and gradually increased to adult levels around 45 days of age. Whereas the *Cyp4x1* mRNA was high around 10 to 15 days of age (approximately 15-fold of day -2 levels), it decreased to prenatal levels thereafter.

The *Cyp4* gene family forms two genomic clusters (Figure 5.1 cluster 7 and 8). Cluster 7 contains *Cyp4a29*, *4a12a*, *4a12b*, *4a30b*, *4a10*, *4a31*, and *4a32* from the plus strand, as well as *Cyp4b1*, *4a14*, and *4x1* from the minus strand. Cluster 8 is the *Cyp4f* cluster, which includes *Cyp4f39*, *4f17*, *4f16*, *4f37*, *4f40*, and *4f15* from the plus strand, as well as *Cyp4f13* and *4f14* from the minus strand, with four non-*Cyp* genes between *Cyp4f15* and *4f13* (*BC066107*, *603049I01Rik*, *Zfp811*, and *9030612M13Rik*). *Cyp4f18* and *4v3* are the only *Cyp4* genes in isolation. Within cluster 7, *Cyp4x1* and *4a29*, and *4a30b* showed an adolescent-enriched mRNA expression pattern, whereas *Cyp431* and *4a32*

mRNAs were high in neonatal and adult ages. *Cyp4a12a/b* mRNA was high only in males at adult ages.

Interestingly, the *Cyp4f* cluster (Figure 5.1 cluster 8), *Cyp4f39*, *4f17*, *4f16*, and *4f40*, all displayed an adolescent-enriched mRNA expression pattern, with highest expression observed around 10 days of age. The mRNAs of these genes decreased markedly thereafter. In contrast, *Cyp4f15*, *4f14*, and *4f13* gradually increased after birth and reached adult levels after 20 days of age, and remained stable thereafter.

In summary, the *Cyp4* gene family was expressed after birth, with divergent expression patterns, in that some were enriched neonatally (from day 0 to 5) and adolescent ages (from day 10 to 20), and some were enriched in adult ages (day 30 to 45). Like the other genomic clusters of *Cyps*, distinct segments of the *Cyp4* isoforms within a certain region of the cluster tended to show similar ontogeny patterns.

Hierarchical clustering of the *Cyps* during liver development. In order to perform an unbiased classification of the expression patterns of the mouse *Cyp* isoforms, the mRNA ontogenic expression of these *Cyps* were analyzed in developing mouse liver (separated by gender) by a two-way hierarchical clustering method (JMP v. 8.0) and visualized as heatmaps described in MATERIALS AND METHODS. Four distinct classes of ontogenic expression

Figure 5.6.

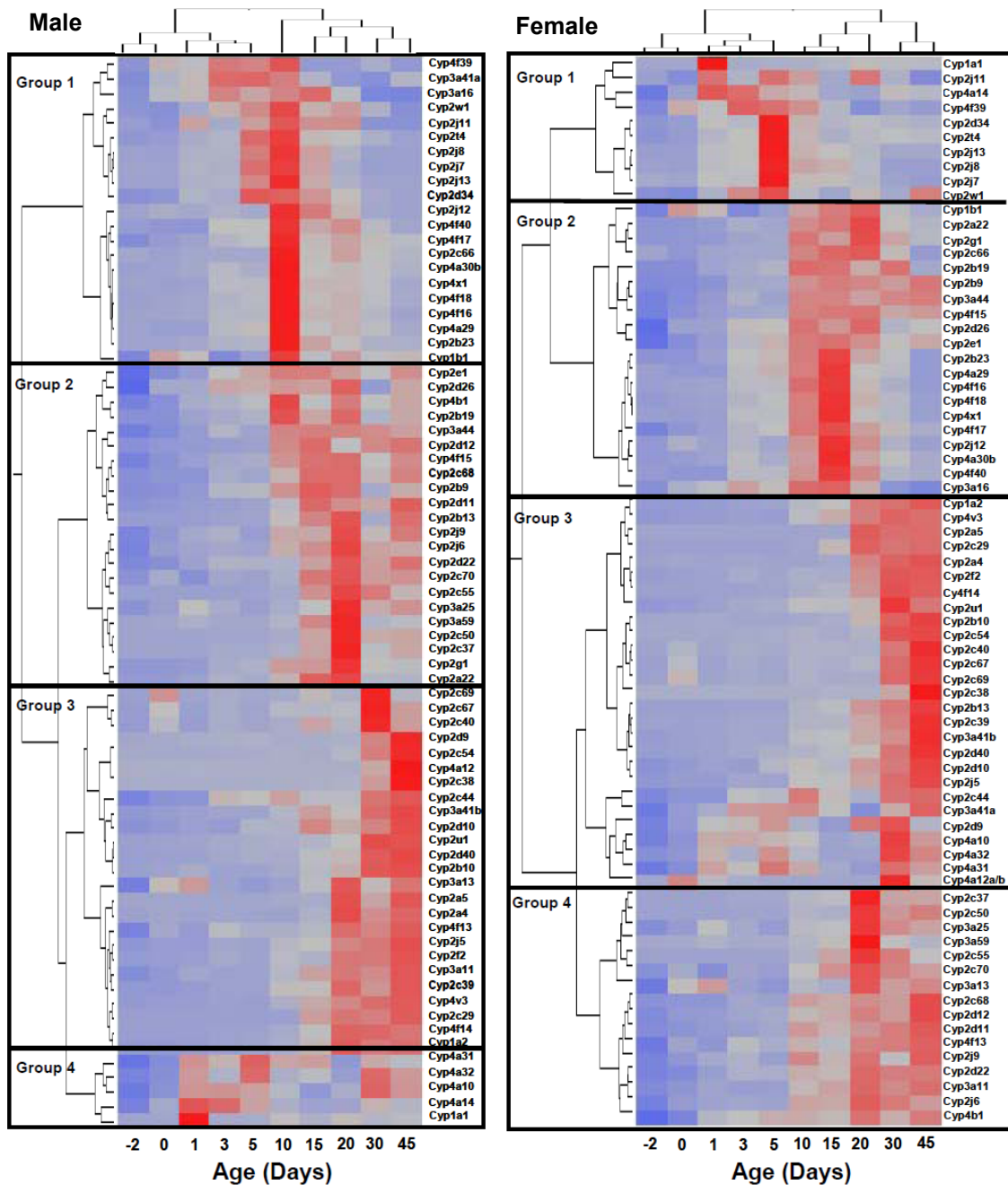


Figure 5.6. A two-way hierarchical clustering of expression profiles for Cyp1-4 genes in livers of male (left panel) and female mice (Ward's minimum variance, JMP v. 8.0). Two trees describe the relationship between different gene expression profiles (tree on the left of each panel) and different ages (tree on top of each panel). Distances between genes reflect significance of associations. Average expression from five animals per gender at each age is given by shaded squares. Red color represents relative high expression and blue color represents relative low expression.

patterns were identified, and were defined as groups 1, 2, 3, and 4 in the present study.

In males (Figure 5.6 left panel), group 1 showed low prenatal and neonatal expression, but highest expression at around 10 days of age. Group 2 had prominent mRNA increase after 10 days of age, with highest expression observed around 15 to 20 days of age. The mRNAs in group 3 were most enriched between 30 and 45 days of age. The mRNAs in group 4 increased markedly at neonatal ages (especially from day 1 to 5), followed by a decrease in adolescent period (from day 10 to 20), and a moderate increase in adult age (from day 30 to 45).

Female Cyps also fall into four distinct groups: group 1 mRNAs were all highly expressed in neonatal ages (0 to 5 days of age); group 2 had highest mRNA expression around 10 to 20 days of age; group 3 had highest mRNA expression observed in adults (45 days of age); and mRNAs in group 4 were highly expressed from 10 to 45 days of age. In general, these genes in group 4 achieved high expression after 20 days of age, and remained relatively high thereafter.

Epigenetic regulation of the ontogeny of the Cyp3a gene locus. In 2009, Dr. Xiao-bo Zhong's research group collaborated with this laboratory to characterize the existence of three epigenetic marks around the *Cyp3a* gene locus, namely DNAMe, H3K4Me2, and H3K27Me3 (Li et al., 2009). In that manuscript, four out of eight *Cyp3a* genes in the cluster were analyzed in detail, namely, *Cyp3a16*, *3a41b*, *3a11*, and *3a25*. For this dissertation, as our knowledge for the *Cyp* gene annotations and ontogenic expression patterns has increased, the complete epigenetic signatures around all eight genes in the *Cyp3a* gene cluster have been characterized as an addition to our previous work (Figure 5.7). DNA was consistently hypomethylated around the *Cyp3a* gene locus at all four ages during liver development (Figure 5.7A). Interestingly, presence of the epigenetic mark H3K4Me2 for gene activation occurred specifically at the right half of the *Cyp3a* gene cluster only at 45 days of age, with five positive peaks observed in total (Figure 5.7B). Conversely, presence of H3K27Me3, a hallmark for transcriptional repression of genes, was observed at the left side of the *Cyp3a* gene cluster, specifically at 45 days of age (Figure 5.7C). Presence of the suppressive mark H3K27Me3 in adults strongly associates with the down-regulation of *Cyp3a16* and *3a41b* in male adult liver during development. Whereas the presence of the permissive mark, H3K4Me2, only at the adult age, in the absence of any suppressive marks, (H3K27Me3 or DNAMe), seems to trigger the adult-enriched mRNA ontogeny pattern of *Cyp3a41a*, *3a44*, *3a11*, and *3a25* on the right side of the cluster. Interestingly, *Cyp3a59* gene, which is at the right end of the cluster, was actually highest expressed at 20 days of age,

Figure 5.7.

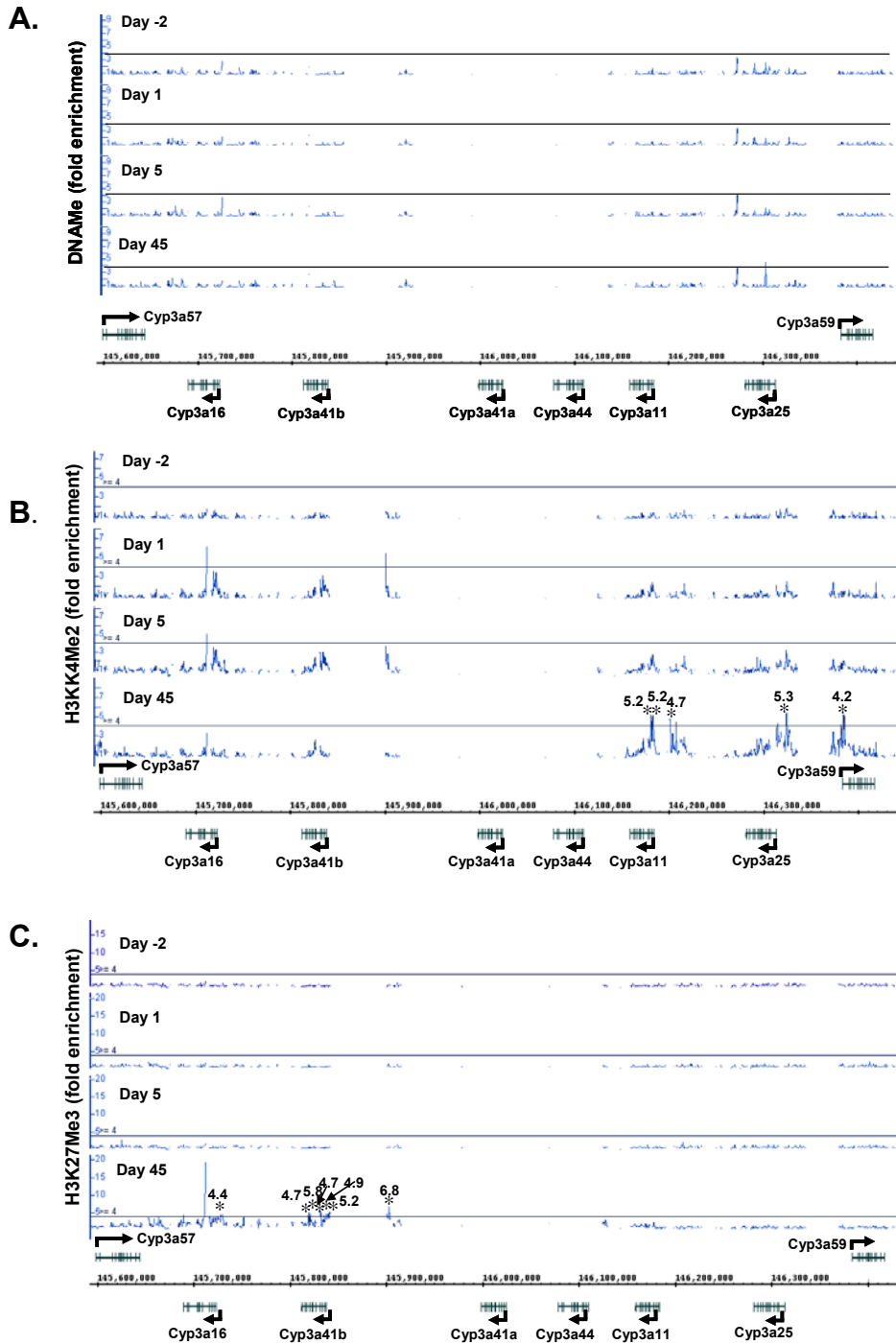


Figure 5.7. Location and fold enrichment of DNAMe (A), H3K4Me2 (B), and H3K27Me3 (C) to the Cyp3a gene locus during liver development. The gene map was generated by the Affymetrix Integrated Genome Browser (IGB). Line: threshold values (3.0-fold of input levels for DNAMe, and 4.0-fold for H3K4Me2 and H3K27Me3) based on calculations of false discovery rate. Asterisks (*) represent positive enrichment of epigenetic marks at a certain genomic location. Numbers represent fold-enrichment of an epigenetic mark compared to input background levels.

followed by a down-regulation at 30 and 45 days of age. This probably indicates that the transcription of Cyp3a59, which is the only gene on the opposite strand of the other Cyp3a genes, is likely interfered by the transcription of Cyps on the other strand.

PXR-DNA binding to the Cyp3a gene cluster. To determine the roles of PXR in regulating the trans-activation of all the genes in the Cyp3a gene cluster, ChIP-Seq was performed on mouse liver, and the PXR-DNA binding signatures to the Cyp3a gene cluster were analyzed in detail. Because 5 out of 8 Cyp3a genes were highly expressed in adults (from day 30 to 45), adult mouse liver was selected to characterized the direct target gene profiles. Most PXR-binding studies in the literature have only examined the promoter regions of a few genes. To determine whether novel PXR-binding sites exist in other regions of a particular gene, PXR binding within ± 10 kb of an entire gene locus was examined in the Integrated Genome Browser (IGB). Interestingly, corresponding to strong enrichment of the permissive mark, H3K4Me2, in adult mice, the PXR-DNA bindings to the right half of the Cyp3a cluster were markedly higher than the bindings to the left half, where the suppressive mark, H3K27Me3, was present (Figure 5.8). For proof of concept, the synthetic potent PXR ligand PCN was administered to mice, and livers were subjected to ChIP-Seq to identify the inducible PXR-binding profiles. Interestingly, there was a marked increase in both numbers of binding sites and binding fold-enrichment at original sites. Together, these data have identified novel PXR-DNA binding sites within the

Figure 5.8.

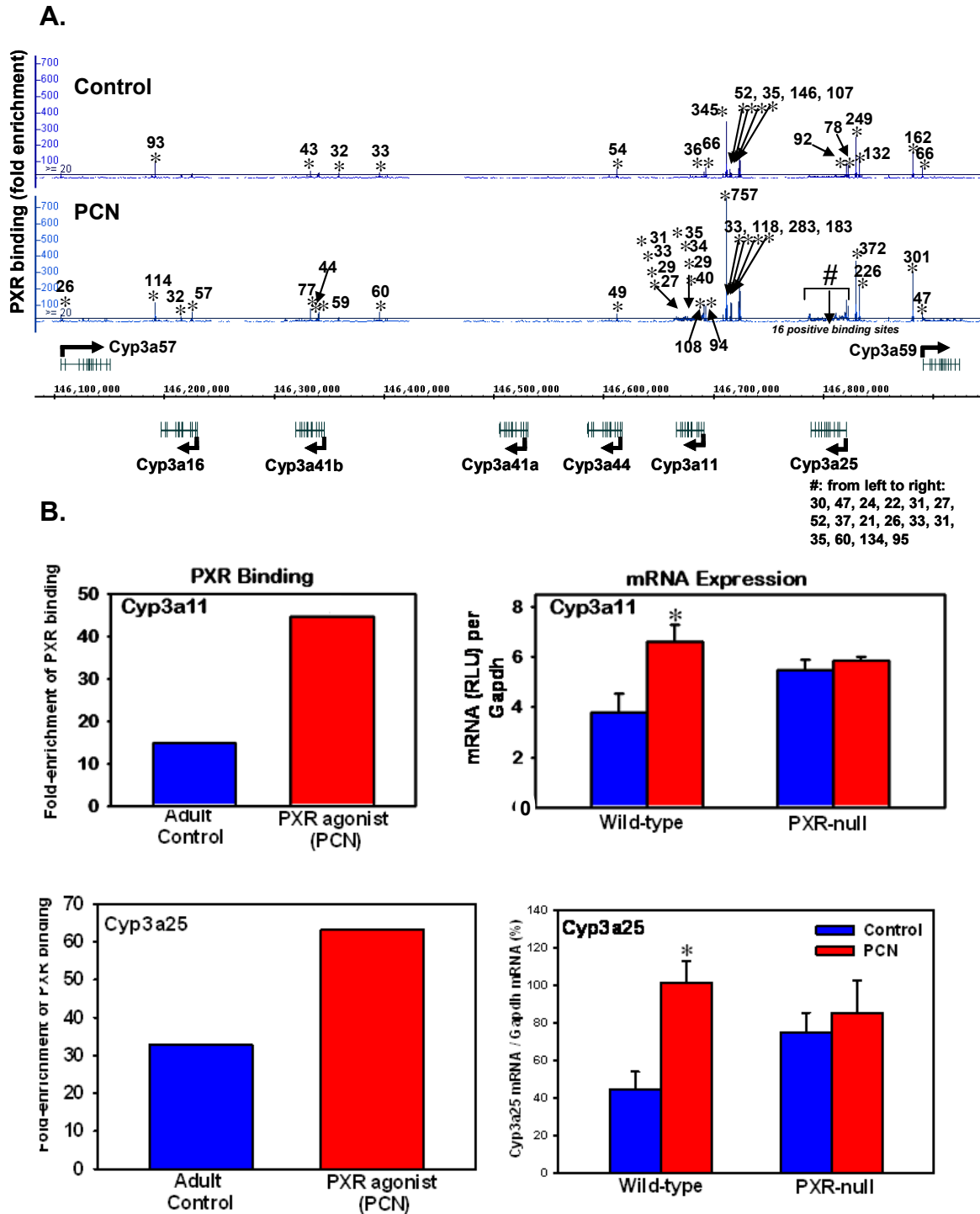


Figure 5.8. A: Location and fold enrichment of PXR binding to the Cyp3a gene locus during liver development. Image was generated by the Affymetrix Integrated Genome Browser (IGB). Line: threshold values (20-fold of background based on calculations of false discovery rate). Asterisks (*) represent positive enrichment of epigenetic marks at a certain genomic location. B: mRNA expression of Cyp3a11 and Cyp3a25 in livers of WT and PXR-null mice. Asterisks (*) represent significant differences between control and PCN-treatment.

Cyp3a gene cluster, and provide strong evidence that a permissive epigenetic environment marked with H3K4Me2 and absence of H3K27Me3, is critical in recruiting PXR to the Cyp3a genes (Figure 5.8).

DISCUSSION

The present study has systematically characterized the ontogenic expression signatures of over seventy cytochrome P450 genes within the Cyp1-4 family during postnatal liver maturation in mice, and identified four distinct ontogeny patterns using cluster analysis. The majority of Cyps form a total of 8 genomic clusters, and certain segments of the Cyps within the same cluster on a chromosome tended to show a similar ontogenic expression pattern, indicating that neighboring Cyps may be regulated by common pathways during liver maturation.

As many as 54 novel Cyps have been examined in the present study, and they were not included in a previous study we performed (Hart et al., 2009). These novel Cyps include Cyp2a5, 2a22, 2b9, 2b13, 2b19, 2b23, 2c37, 2c38, 2c40, 2c44, 2c50, 2c54, 2c55, 2c67-70, 2d9-12, 2d26, 2d34, 2d40, 2g1, 2j5, 2j7-9, 2j11-13, 2t4, 2u1, 2w1, 3a59, 3a41a, 3a44, 4a12a, 4a12b, 4a14, 4a29, 4a30b, 4a31-32, 4b1, 4f13-17, 4f39-40, 4v3, and 4x1. If a Cyp mRNA is higher than 1% of Gapdh mRNA at one or multiple ages examined during liver development, I designated that Cyp gene as a liver-enriched Cyp at that age. Using the threshold of above 1% Gapdh mRNA as defined in **MATERIALS AND METHODS**, among these newly characterized Cyps, 44 out of 54 Cyp mRNAs are enriched in liver during development. Interestingly, several novel Cyps, including Cyp2c37, 2c50, 2c70, 2d26, and 3a59, even showed more than 200% of Gapdh mRNA levels at 20 days of age, indicating they are extremely enriched

in adolescent liver and may be functionally critical for normal development. Cyp3a59, which is highly conserved in numerous species, including drosophila, rat, mice, chimpanzees, and humans according to the NCBI database, was expressed at twice the Gapdh mRNA at 20 days of age (Figure 5.4 right panel 2). However, surprisingly, very little is known about the function of this Cyp. This suggests that although the state of characterization of Cyp genes is generally considered finished at the DNA level, there are still many unresolved issues in terms of their expression patterns and functional significance.

The relative percentages of the Cyp mRNAs at selected ages namely, day 1 representing neonatal age, day 15 representing adolescent age, and day 45 representing adult age, are shown in Figure 5.9. Although caution needs to be made while interpreting the percentages of Cyp gene expression, considering the potential differences in the hybridization efficiency of the probe sets, it appears that compared with the mRNAs of other Cyps, Cyp2e1 and 3a11 are the two most enriched Cyp isoforms at all ages and in both genders. Cyp3a41b, 2d26, and 4a31 are highly expressed in newborn livers, Cyp2c37, 2c70, and 2d26 in adolescent livers, as well as Cyp2c29, 2c37, and 2f2 in adult livers. Nevertheless, the low expression of the other novel Cyps during development does not necessarily indicate that they are not important in liver. For example, Cyp2c39, although very lowly expressed in liver throughout development (0.4% of Gapdh mRNA at the highest level at 45 days of age, Figure 5.2 right panel 5), has recently been found critical for retinoic acid hydroxylation in liver, and its

down-regulation offers a molecular basis for liver retinoid accumulation and fibrosis in AhR-null mice (Andreola et al., 2004). Therefore, the present study has set an example of investigating both highly and lowly expressed Cyps unbiasedly in liver maturation, and we suggest that future studies need to focus on characterizing the potentially critical functions of novel Cyps in liver at an age when they are highly expressed.

During evolution, over half of the mouse Cyps within the 1-4 family are conserved for humans, but mice display more sequence variations in Cyp gene isoforms than humans (Table 3.1). In addition, the other half of the mouse Cyps has no human homologs. The CYP2D/Cyp2d subfamily is an interesting example, in that humans only have one active CYP2D gene, namely CYP2D6, which determines the efficacy of tamoxifen in breast cancer (Dezentje et al., 2009) and is responsible for the debrisoquine hydroxylase polymorphism (Coughlin and Piper, 1999). In contrast, mice have nine different functional Cyp2d genes. It has become clear in the genomic era that lower species generally tend to have more Cyp isoforms. For example, whereas humans have only 57 Cyps, mice have 102, mosquitoes have 106, sea urchin have 120, and drosophila have 83 functional CYPs, according to the current Cyp database (<http://drnelson.utmem.edu/CytochromeP450.html>). It can be hypothesized that as the species evolves, the higher species has more anatomical and physiological advantages than the lower species, so that the environment

becomes less harsh for the higher species in many ways, and this may contribute to the decreased isoforms in higher species.

For many years, mice have been a common research model to recapitulate pharmacological and toxicological responses in humans. The beginning of the 21st century is an exciting era of generating not only the Cyp gene-knockout mice, but also transgenic mice that carry a human cytochrome P450 gene (van Herwaarden et al., 2007; Lofgren et al., 2009; Zhou et al., 2010). These humanized CYP transgenic mice hold great promise for *in vivo* studies on human P450 functions. However, their utility is often compromised by the presence of relatively high levels, and more subfamily members of endogenous mouse Cyps. For example, to investigate the physiological and pharmacological roles of human CYP3A, Cyp3a-null mice have been generated that lack all functional Cyp3a genes, but there is an up-regulation of Cyp2b9, Cyp2b10, and Cyp2c55 in liver (van Herwaarden et al., 2007).

Caution needs to be made when extrapolating results from mice to humans. Interestingly, most of the Cyp isoforms within the same subfamily are clustered together on a chromosome, and certain Cyps within the same cluster showed similar ontogeny patterns (Figure 5.1-5). The coordinate expression and multiplicity of mouse Cyp genes in many subfamilies have provided more challenges for translating the molecular mechanisms of gene regulation and

functions into humans, even though mice and human are generally considered to have similar pharmacological and toxicological responses.

Another interesting finding is the postnatal enrichment of all Cyps in the 1-4 families, and their gender-divergent gene expression. Functionally speaking, the postnatal enrichment of Cyps is an adaptive mechanism to biotransform an increased amount of xenobiotics from the environment, compared to the prenatal period when the fetus is largely protected from these chemicals by the placenta, and fetal membranes. Nuclear receptors may contribute to the the age- and gender-specific gene expression of Cyp isoforms during development, considering that many nuclear receptors, which are well known to regulate Cyp gene expression in adults, begin to be expressed in liver after birth in both rat and mice (Balasubramanian et al., 2005). Female-predominant expression was observed for many genes in Cyp2b and 2c subfamilies (such as Cyp2b9, 2b10, 2b13, 2c40, 2c67, 2c68, and 2c69). The present findings are generally consistent with the gender differences observed for these genes in literature (Kawamoto et al., 2000; Lofgren et al., 2009; Waxman and Holloway, 2009). To note, the expression of CAR protein shows a female-predominant pattern, and it has been found to be responsible for the female-predominant expression of Cyp2b10 in mouse liver (Kawamoto et al., 2000). Very recent findings indicate that CAR also regulates the basal expression of Cyp2c29 and Cyp2b13 (Hernandez et al., 2009). Therefore, it is possible that the postnatal enrichment and female-predominant expression of CAR also contributes to the female-specific

expression of other novel Cyp isoforms in the 2b and 2c subfamilies, including Cyp2b9, 2b13, 2c39, 2c40, 2c67, 2c68, and 2c69 (Figure 5.2 and 3). In addition, Drs. Waxman and Ingelman-Sundberg's groups have recently examined the roles of sex and growth hormones in Cyp gene expression, and demonstrated that androgen-dependent pituitary growth hormone secretory pattern is the primary regulator of male-specific expression in liver (Lofgren et al., 2009), suggesting that there is a higher order of gene regulation mediated by pituitary hormones beyond the local regulation of Cyps by nuclear receptors.

The spatial organization of the genome is thought to play an important part in the coordination of gene regulation, and the coordinate expression of the Cyps in certain segments of genomic clusters indicates that common spatial regulatory mechanisms may exist. Conversely, on the boundary regions between segments in the same Cyp cluster, there may be distinct regulators that prevent the spread of transcription from one segment to the other at certain ages. It is critical to understand the molecular mechanisms underlying the developmental switch of cytochrome P450 isoforms, so as to better predict the altered drug responses in pediatric pharmacology. It is well known that the two human CYP3A members, namely CYP3A4 and 3A7, exhibit a developmental switch in gene expression during liver maturation (Schuetz et al., 1994). In mice, using ChIP-on-chip for three epigenetic marks for gene regulation, namely DNA and histone H3 lysine-27 tri-methylation (H3K27Me3) for gene suppression, and histone H3 lysine-4 dimethylation (H3K4Me2) for gene activation, we recently characterized that the

developmental switch between the perinatal Cyp3a isoform to adult Cyp3a genes is likely due to the dynamic changes of H3K4Me2 and H3K27Me3 during postnatal liver maturation, but not likely due to DNA methylation (Li et al., 2009). It is possible that distinct chromatin epigenetic marks may also modify other Cyp gene loci with segment-specific signatures within a certain cluster, resulting in common expression patterns within the same segment. Another possible mechanism for differential expression patterns between segments of Cyps is the presence of insulators. It was only recently identified that a ubiquitously expressed transcription factor, CCCTC-binding factor (CTCF), can act as an enhancer-blocking protein, which binds to boundary elements between genes to prevent spreading of transcription, thereby isolating genes from the influence of their neighbors (Williams and Flavell, 2008). Direct evidence for CTCF-mediated gene expression is the β -globin locus (Splinter et al., 2006). It is an intriguing hypothesis that CTCF might also contribute to the differential expression of the Cyps in the neighboring regions. Recent technological advancement, including ChIP-Seq (chromatin immunoprecipitation coupled with the next generation sequencing) and 3C (chromosome conformation capture), have made such investigations possible for future studies.

Although much progress has been made in characterizing the Cyp gene isoforms, there are still many unresolved issues. For example, are there any novel splice-isoforms of Cyp mRNAs during liver development? What transcription factors contribute to the temporal and spatial regulation of various

Cyp isoforms? Fifty years ago, people thought there were only two Cyp isoforms. The completion of the Human Genome Project in the late 20th century has broadened our point of view of a relatively complete assembly of cytochrome P450s. Next-generation sequencing has opened the door to rapid characterization of the transcriptome as well as the transcription factor-DNA binding landscape (Werner, 2010). The characterization of age-dependent Cyp mRNA splicing isoforms and the regulatory factors for transcription will be determined in future studies.

CHAPTER SIX
GENETIC AND EPIGENETIC REGULATION AND EXPRESSION
SIGNATURES OF GLUTATHIONE S-TRANSFERASES IN DEVELOPING
MOUSE LIVER

ABSTRACT

The hepatic glutathione *S*-transferases (Gsts) are critical phase-II enzymes in protecting cellular macromolecules against electrophiles and oxidative stress. Little is known about the ontogeny of Gsts and the underlying regulatory mechanisms during liver development. Therefore, in the present study, the ontogeny and the regulatory mechanisms of 19 known Gst isoforms were investigated in mouse liver from 2 days before birth to postnatal day 45. With the exception of Gstm5 and MGst2, which showed a progressive decline in postnatal mRNA expression, most other Gst isoforms showed a progressive increase in postnatal mRNA expression. Two-way hierarchical clustering revealed three distinct expression patterns of these Gsts isoforms: perinatal-, adolescent-, and adult-enriched. The expression signatures of certain Gst isoforms showed positive association with the ontogeny of critical xenobiotic-sensing transcription factors, including AhR, PXR, CAR, PPAR α , and Nrf2. Specifically, genome-wide ChIP-seq revealed direct PXR-binding sites to the Gsta, Gstm, Gstt, and Gstp polycistron clusters, as well as to the Mgst1 gene locus. ChIP-on-chip analysis demonstrated that DNA methylation and histone-H3K27-trimethylation (H3K27me3), two gene expression-suppressing epigenetic marks, were consistently low around the Gstz1 gene locus. In contrast, enrichment of histone-H3K4-dimethylation (H3K4me2), a hallmark for gene activation, increased 60% around the Gstz1 gene locus from prenatal to the young adult period. Regression analysis revealed a strong correlation between the enrichment of H3K4me2 and Gstz1 mRNA expression ($r=0.76$). In conclusion,

the present study characterized three distinct ontogenic expression signatures of the 19 Gst isoforms, and examined some genetic and epigenetic mechanisms inducing their transcription during liver development.

INTRODUCTION

The glutathione *S*-transferases (Gsts) are thought to play important roles in protecting macromolecules against electrophiles and products of oxidative stress, thus providing an efficient detoxification mechanism. The ability of Gst(s) to metabolize cancer chemotherapeutic drugs, insecticides, herbicides, and carcinogens suggests that their expression can influence the efficacy and detoxification capacity of drugs, as well as an individual's susceptibility to cancer (Hayes and Pulford, 1995; Board et al., 1997). Previous studies in this laboratory have examined the tissue distribution and chemical induction of various Gst isoforms in adult mice (Knight et al., 2007; Knight et al., 2008). For example, multiple Gsts are enriched in adult mouse liver (Gsta3, k1, m1, m4, m6, p1/2, t1, z1, and Mgst1). In addition, many hepatic Gst mRNAs are inducible by ligands of critical xenobiotic-sensing transcription factors. For example, Gstm1 by the aryl hydrocarbon receptor (AhR); Gsta1/2, m1, m2, m3, m4, and t1 by the constitutive androstane receptor (CAR); Gsta1/2, m1, m2, m3, m4, m5, m6, and MGst1 by the pregnane X receptor (PXR); Gstk1, m5, t1, t2, z1, MGst1, and MGst3 by the peroxisome proliferator-activated receptor α (PPAR α); and Gsta1/2, a4, m1, m2, m3, m4, m6, o1, t1, MGst1, and MGst3 by the NF-E2-related factor-2 (Nrf2) (Knight et al., 2008). In addition, it has been shown that the mouse hepatic Gstp1 and p2 gene expression was induced in a Nrf2-dependent manner (Sato et al., 2002; Yeager et al., 2009).

Maturation of the drug metabolizing capacity of the liver is essential during liver development to protect the children from environmental toxicants that they may be exposed to. It is known that developing embryos, fetuses and newborns, all face challenges from the environment that are different from that of adults. For example, *in utero* growth and development of eutherian mammals requires flow of nutrients from the mother through the placenta. But after birth, the newborn is gradually exposed to various xenobiotics through food and drink, and the expression of drug metabolizing enzymes and transporters are not the same between newborns and adults.

It is becoming increasingly evident that gene expression during development is also tightly regulated by epigenetic mechanisms, such as DNA methylation and histone modifications (Jaenisch and Bird, 2003; Kiefer, 2007). In general, changes in DNA methylation profiles and histone code determine whether there is a permissive chromatin state for the transcription machinery to access gene promoter regions and initiate transcription. DNA methylation is a covalent modification resulting in stable gene silencing (Bird, 2002; Reik, 2007). Histone modifications, such as histone H3 lysine-4 dimethylation (H3K4me₂) is present in promoters and transcribed regions of many active genes, and is positively associated with gene transcription (Bernstein et al., 2005; Kim et al., 2005; Roh et al., 2006), whereas H3 lysine-27 trimethylation (H3K27me₃) is usually associated with suppression of gene transcription, because H3K27me₃ is a target for the chromodomain protein Polycomb, which silences genes by yet

unknown mechanisms (Boyer et al., 2006; Lee et al., 2006; Kiefer, 2007). The epigenetic regulation of the Gst ontogenic expression by DNA and histone modifications has not been investigated; thus such studies are needed to fill the critical knowledge gap in understanding the epigenetic mechanisms underlying the maturation of drug metabolizing capacity of the developing liver.

Differential expression of cytochrome p-450s and xenobiotic transporters during developmental stages has been reported ((Hakkola et al., 1998; Gonzalez et al., 1986; Omiecinski et al., 1990; Pineau et al., 1991; Buist et al., 2002; Li et al., 2002; Slitt et al., 2002). However, little is known about the ontogenic expression of various Gst isoforms and its genetic and epigenetic regulatory mechanisms. Therefore, the purpose of the present study is to characterize the ontogenic expression of 19 known Gst isoforms in mouse liver, and determine the genetic and epigenetic mechanisms for the ontogeny of Gsts. For the genetic regulation of Gst ontogeny, direct PXR-binding signatures to all the Gst gene loci were characterized by ChIP-seq, a recently developed high-throughput technique to identify genome-wide transcription factor binding sites. The choice of PXR is dictated by the fact that it is instrumental in the regulation of many important genes associated with drug metabolism and transport. For the epigenetic regulation of Gst gene expression, Gstz1, the Gst isoform most highly expressed in liver (Knight et al., 2007) was used as a model for investigating the association between its developmental expression and specific epigenetic

signatures of gene expression, namely DNA methylation and histone modifications (H3K4me2, and H3K27me3).

RESULTS

Three expression signatures of Gst mRNAs in developing mouse liver:

The Gsta family: As shown in Figure 6.1A, the mRNAs of all four Gsta family members (Gsta1/2, a3, and a4) showed a similar expression pattern, which was low before birth, but gradually increased and peaked from day 15 to day 45 of age in both male and female livers. Interestingly, male-predominant expression patterns were observed for Gsta1/2 mRNA from day 0 to day 10 of age, whereas the female Gsta1/2 mRNA expression was very low for the first 15 days of age.

Gstk1, o1, p1/2 and Gstz1: The Gstk1, o1, and z1 are all isolated Gsts that do not form clusters with other Gst isoforms, and all of these three Gsts gradually increased during liver development (Figure 6.1A). Gsto1 mRNA was relatively higher in males than females at birth. Due to high homology, the bDNA probes were unable to differentiate Gstp1 and p2 in the same cluster, therefore the expression of these two genes were combined together as “Gstp1/2”. Gstp1/2 showed a distinct male-predominant expression pattern from day 30 onwards in adult mice. The expression in females was low, and it showed little variation at all time points studied.

The Gstm family: Gstm1, m2, m3, m4, and m6, which are all transcribed from the minus strand, displayed similar expression patterns, a gradual increase in their mRNA expression during liver development (Figure 6.1B). In contrast, Gstm5, which is the only Gstm transcribed from the plus strand, i.e., in the

Figure 6.1. ■ Male
□ Female

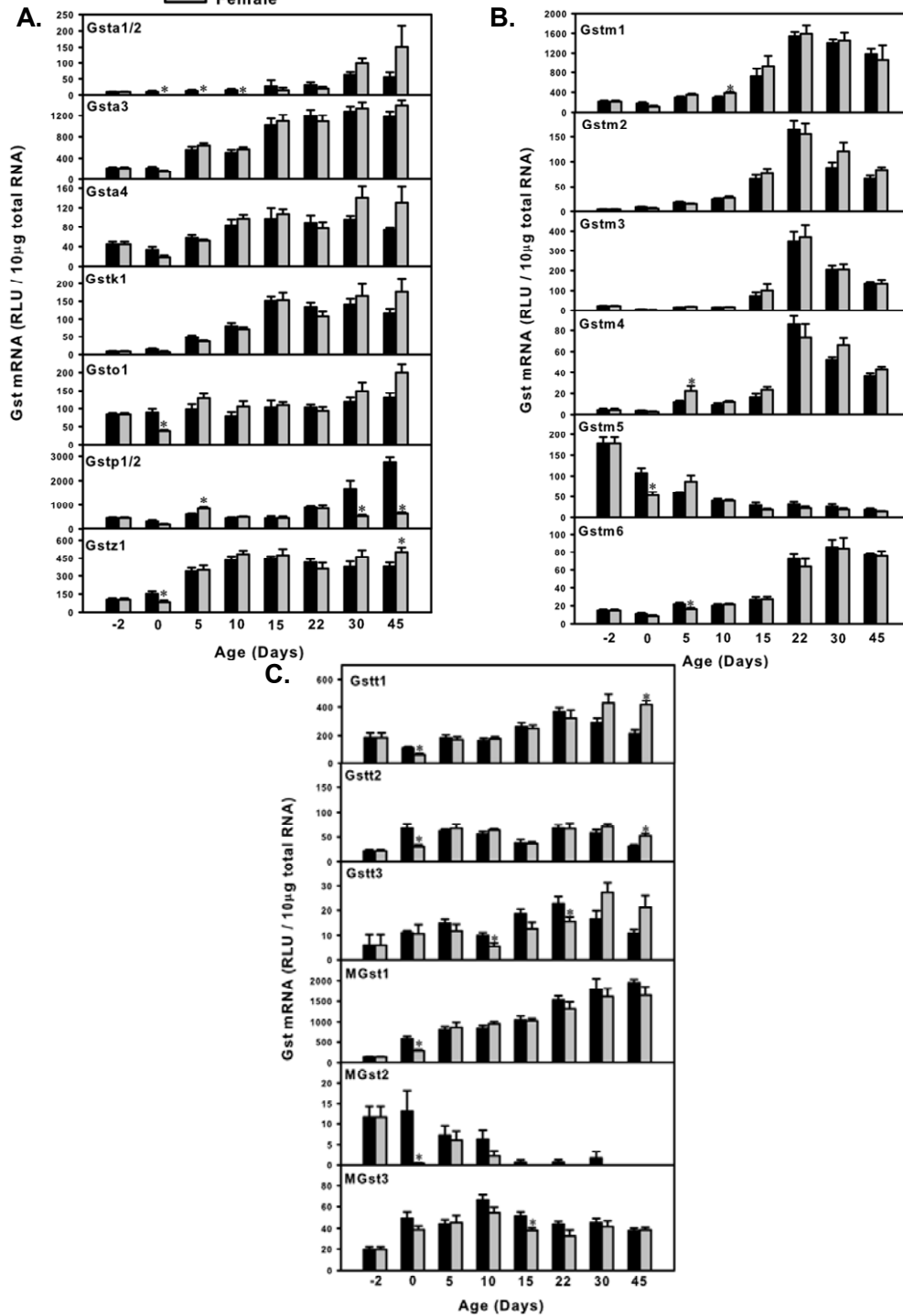


Figure 6.1: The mRNA ontogenic expression of the 19 Gst isoforms. **A:** Ontogeny of Gsta polycistron cluster (Gsta1/2, a3, a4), as well as Gstk1, o1, Gst p1/2 cluster, and Gstz1, in male and female livers from day -2 to day 45 of age. **B:** The mRNA ontogenic expression of the Gstm polycistron cluster (Gstm1, m2, m3, m4, m5 and m6) in male and female livers from day -2 to day 45 of age. **C:** The mRNA ontogenic expression of the Gstt polycistron cluster (Gstt1, t2, and t3), as well as microsomal Gsts (MGst1, MGst2, and MGst3) in male and female livers from day -2 to day 45 of age. Total RNA was isolated from liver at each age and analyzed by the single-plex bDNA assay as described in MATERIALS and METHODS. Data are presented as mean RLU \pm S.E.M. (n = 6 animals per gender, i.e. n=12 per age). Asterisks (*) represent significant differences (p < 0.05) between male and female mRNAs at each age.

opposite direction, showed a progressive decrease in its mRNA expression with age. Gender differences were observed for Gstm4 mRNA at day 5 (female-predominant), Gstm5 at day 0 (male-predominant), and Gstm6 at day 5 of age (male-predominant).

The Gstt family: Gstt1, t2, and t3 are members of the Gstt polycistron cluster on mouse chromosome 10. Interestingly, all of these three genes showed a postnatal enrichment pattern (Figure 6.1C). For Gstt1 and t2, male-predominant expression was observed at day 0 of age; whereas for Gstt3, male-predominant pattern was observed at day 10 and day 22 of age.

The microsomal Gsts: The three microsomal Gsts (MGsts) in mice are located on different chromosomes and do not form clusters with each other or other Gst isoforms (data not shown). These three MGsts showed three distinct expression patterns (Figure 6.1C). Whereas MGst1 mRNA progressively increased with age in both male and female livers, MGst2 displayed a perinatal-enriched pattern in both male and female mouse livers that decreased with age, and MGst3 was highly expressed in every postnatal time point studied with no distinct expression patterns. For MGst2, a large difference in expression between male and female livers was observed in day 0, the expression in females being negligible. The regulatory mechanism for such a temporal drop in expression in females is yet to be identified.

In order to perform an unbiased classification of the expression patterns of the mouse Gst isoforms, as well as to identify critical transcription factors for the developmental regulation of these Gsts in mouse liver, the mRNA ontogenic expression of the 19 Gst isoforms, as well as the mRNAs of five important xenobiotic-sensing transcription factors, namely AhR, CAR, PXR, PPAR α , and Nrf2, were analyzed in developing mouse liver by a two-way hierarchical clustering method (JMP v. 7.0) and visualized as heatmaps. As shown in Figure 6.2A, male Gst isoforms had three distinct ontogenic patterns: (1) two perinatal-enriched Gst isoforms, Gstm5 and MGst2; (2) ten adolescent-enriched Gst isoforms, Gsta4, k1, z1, t2, t3, m2, m3, m4, t1, and t3; and (3) seven adult-enriched Gst isoforms, Gsta1/2, o1, p1/2, a3, MGst1, m1, and m6. Interestingly, all the five transcription factors exhibited an adolescent-enriched pattern in developing liver of males, suggesting their potential functions in regulating the ontogeny of the Gsts in postnatal period.

The female-predominant Gst isoforms also showed three distinct ontogenic patterns (Figure 6.2B). However, the perinatal-enriched Gsts in female livers include not only Gstm5 and MGst2, but also MGst3. Fewer Gst isoforms were adolescent-enriched in females compared to males, and these include Gstp1/2, t2, m1, m2, m3, and m4. Most Gsts in females were adult-enriched in adulthood in female livers, including Gsta1/2, o1, m6, t1, t3, a3, k1, MGst1, Gsta4, and Gstz1. Interestingly, all the five transcription factors showed a perinatal-enriched pattern in female livers, with only three Gst isoforms in the same category.

Figure 6.2.

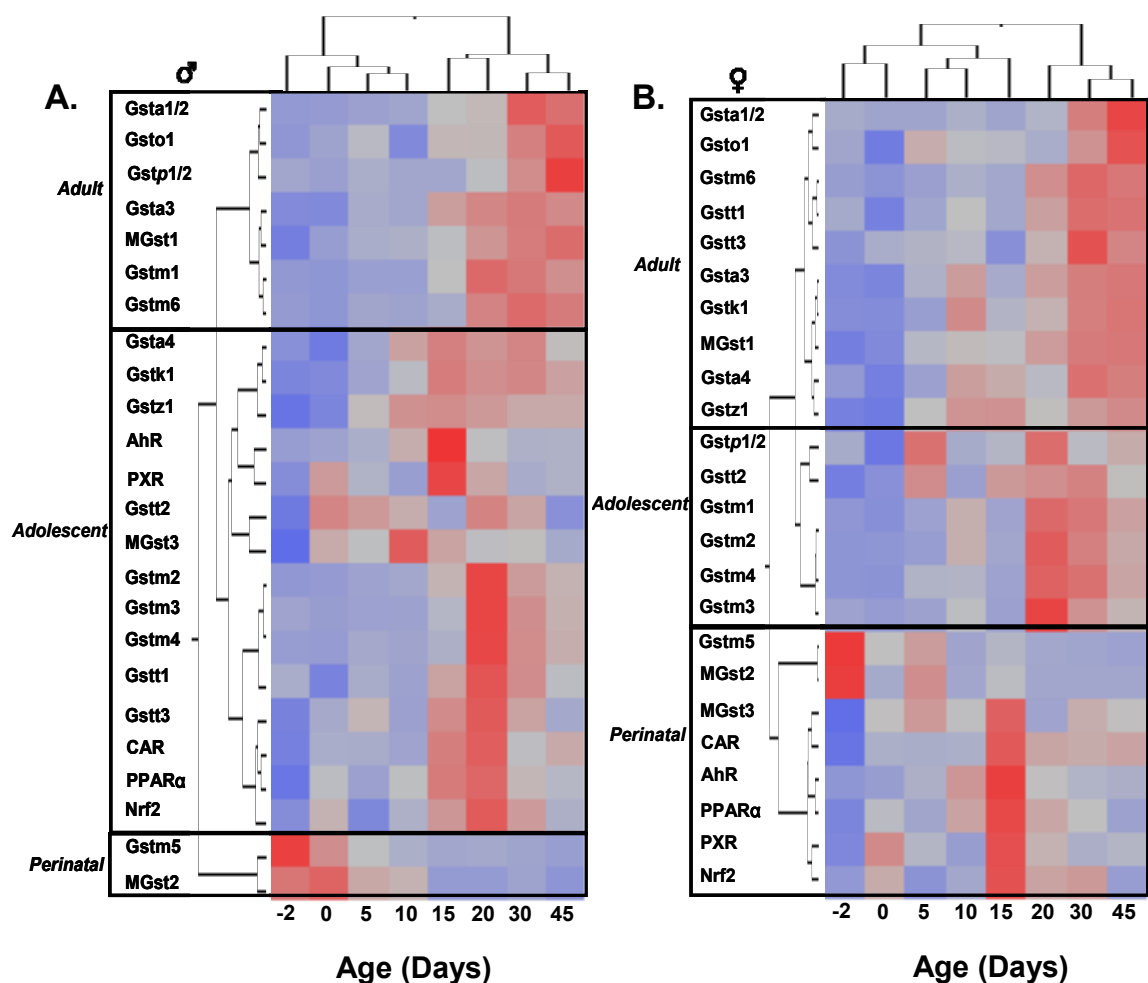


Figure 6.2: Heatmaps of the mRNA ontogeny of all the Gst isoforms as well as five xenobiotic-sensing transcription factors (AhR, CAR, PXR, PPAR α , and Nrf2) in male (A) and female (B) mouse liver. The ontogenic expression of these mRNAs from day -2 to day 45 of age was analyzed by a two-way hierarchical clustering method (JMP v. 7.0) using Ward's minimum variance and visualized by a dendrogram, that revealed three distinct patterns: perinatal-, adolescent-, and adult-enriched. Distances between genes reflect significance of associations. Red color represents relative high expression, and blue color represents relative low expression.

In summary, there were three distinct expression patterns of the mouse Gst mRNAs in developing mouse liver. Gst genes in the same polycistron clusters tended to have similar expression patterns. Most Gst isoforms were enriched postnatally in both male and female livers. However, the ontogeny of the five transcription factors only positively associated with most Gst mRNAs in male but not in female livers.

PXR-mediated regulation of Gst mRNA expression in mouse liver: To further elucidate the mechanisms of the transcription factor-mediated ontogenic expression of Gsts, the major xenobiotic sensor PXR was selected to examine whether it directly trans-activates Gst expression. Young adult mice were selected (8-week-old) to determine the bindings of PXR to Gst genes in liver, because both PXR and the Gst genes are highly expressed at this age. Using Genome-wide ChIP-Seq analysis revealed three positive PXR-binding sites within the Gsta1/a4 polycistron cluster, and the PXR-DNA binding fold-enrichments were 51-fold, 39-fold, and 40-fold above background values respectively (threshold: 20-fold) (Figure 6.3A). Gsta2 is transcribed from the opposite strand, and is located more than 100kb from the closest PXR-binding site. For the Gstm cluster (Figure 6.3B), one positive PXR-binding site was observed between Gstm1 and m4 (41-fold), and three sites between Gstm2 and m3 (95-fold, 58-fold, and 25-fold). To note, Gstm5 gene locus is on the boundary of the Gstm cluster, and it is approximately 80kb away from the closest PXR-binding site. Multiple PXR-binding sites were also observed within the Gstt

Figure 6.3.

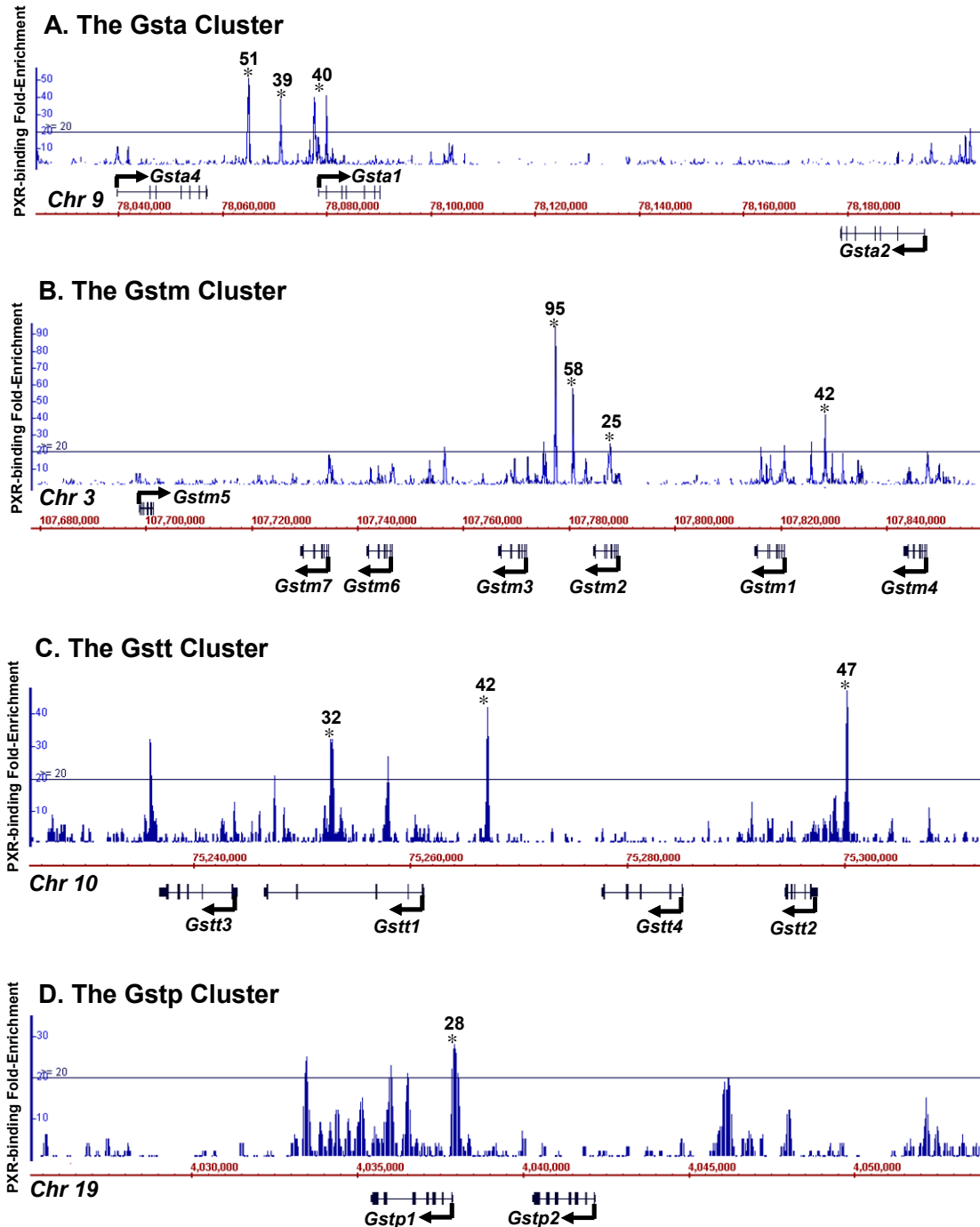


Figure 6.3: Location and fold enrichment of PXR binding sites to various Gst polycistron clusters in adult male mouse liver by ChIP-Seq as described in MATERIALS and METHODS: A. The Gsta cluster on chr 9; B. The Gstm cluster on chr 3; C. The Gstt cluster on chr 10; and D. The Gstp cluster on chr 19. Image was generated by the Affymetrix Integrated Genome Browser (IGB). Line: twenty-fold of background signal was used as the threshold value based on calculations of false discovery rate. Asterisks (*) represent positive enrichment of PXR bindings at a certain genomic location.

polycistron cluster (Figure 6.3C), one upstream of *Gstt2* (47-fold), one between *Gstt4* and *t1* (42-fold), and one in the intronic region of *Gstt1* (32-fold). For the *Gstp* cluster, one positive PXR binding site was observed at the promoter region of *Gstp1*, and it is downstream of *Gstp2* (Figure 6.3D). For the *Gst* genes that are not part of a cluster, a PXR-binding site 418-bp upstream of the *MGst1* gene locus was observed (Figure 6.4A), but not in any regions within ± 10 kb of the *MGst2* or *MGst3* gene loci (Figure 6.4B-C). Interestingly, only *MGst1* is highly expressed in liver, corresponding to enriched PXR binding. In addition, we have also identified one positive PXR-binding site 8.5kb upstream of the *Gsta3* gene locus (30-fold) (Figure 6.4D). There were no observed PXR-bindings to *Gstk1*, *o1*, *z1* (data not shown). NHR-scan revealed 18 consensus PXR-DNA binding motifs (DR-3, DR-4, ER-6, ER-8, or IR-0) present in 9 of the 13 ChIP-DNA sequences (3 DR-3, 7 DR-4, 4 ER-6, 3 ER-8, and 1 IR-0) within ± 10 kb of *Gst* gene loci with positive PXR-bindings (Table 6.1).

In summary, in addition to identifying strong associations between the postnatal enriched PXR mRNA and multiple *Gst* mRNAs, the present study also demonstrated that the *Gsta*, *Gstm*, *Gstt*, and *Gstp* clusters, as well as *MGst1*, are direct target genes of the PXR protein.

Figure 6.4.

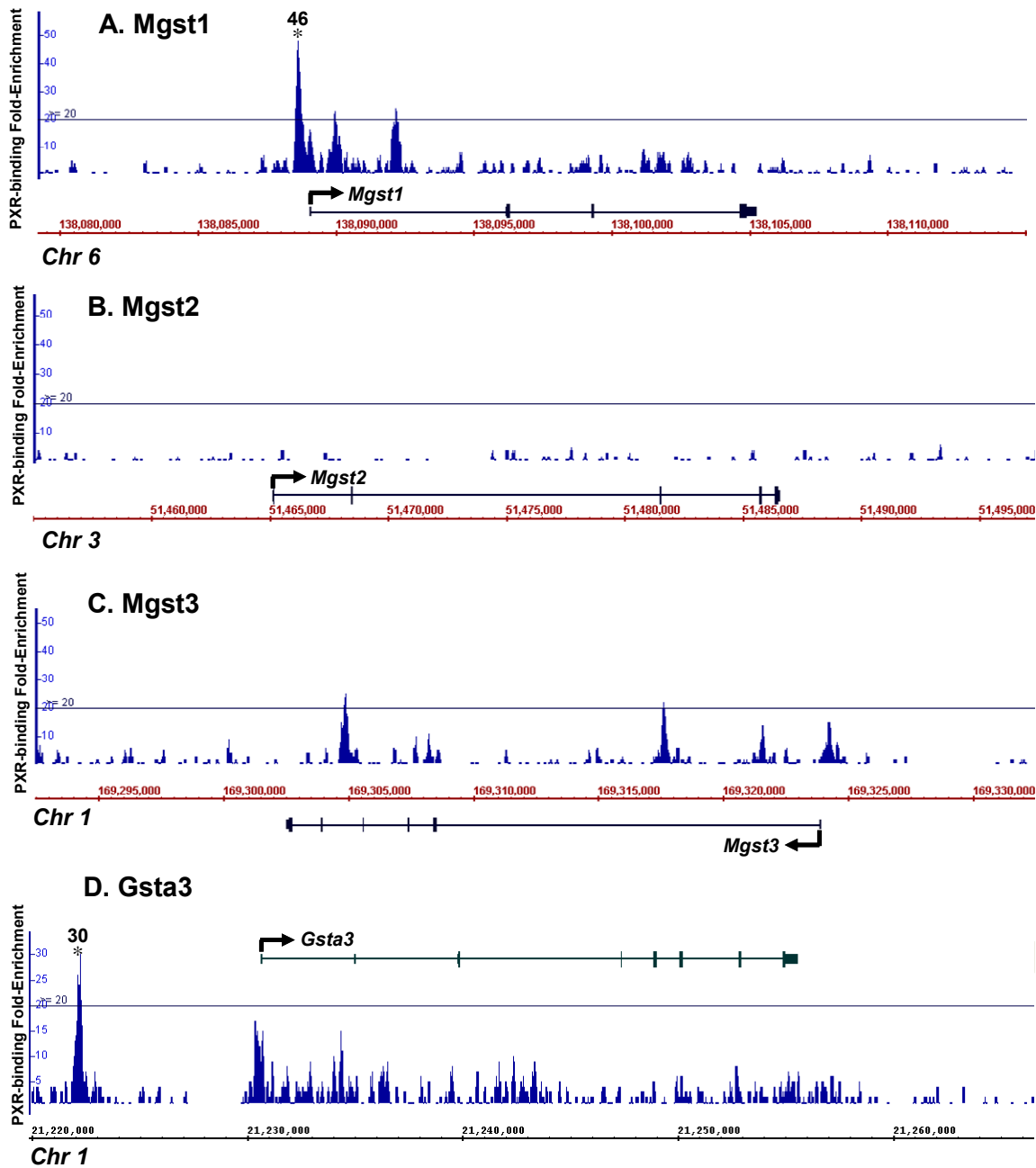


Figure 6.4: Location and fold enrichment of PXR binding sites to MGst1 (A), MGst2 (B), MGst3 (C), and Gsta3 (D) in adult male mouse liver by ChIP-Seq as described in MATERIALS and METHODS. Image was generated by the Affymetrix Integrated Genome Browser (IGB). Line: twenty-fold of background signal was used as the threshold value based on calculations of false discovery rate. Asterisks (*) represent positive enrichment of PXR bindings at a certain genomic location.

Table 6.1 . Consensus PXR-DNA binding motifs within the ChIP-DNA sequences for PXR

Chromosome Coordinates	PXR Binding Peak Value	ChIP-DNA Sequences (5' → 3')	PXR Consensus Sequences	Genes
chr1:21222117-21222301	30	CAGGGATGAGAGCAATCATCAAGAATGAAGTAAATCGATAAAAAAAAAAAGTTGGACATTGATTAAGAAA AAAACATAGCCCTGCAAAATGTAAGTGGAAAGTTTCTG GATGTTTCTAAGCACACTTTGACTTTGGGCCATTAT ATAACACTGTGGGAAATATGTAATCATTGTAGC	N/A	Tmem14a, Gsta3
chr3:10777317-10777565	95	CAAGAGAGTCCAAGCTCCCAATGTGGTCTGAGGT CATTCTACTGAGCCAAAGCTGACCTCATCTCCAGGC CTGATAAGGGACCATACTGGATGATACCCACATATGC CATTGACCTTCTACTAGAATGGTAAGTGTACAGAGTT TAAAGAGTTCAAGATACCCATGACTTTGTCCTCCA AAATCTAGGTCAGCGAGCTCAAGTGCATCCTGAA TGGTCCCTCTGACCCTCTCTCTCC	DR-3 DR-4 ER-8	Gstm3, LOC624701, Gstm2
chr3:107780677-107780861	58	CCGAAATGCACAGCCAGCATGAATCAGCTAGACCG GAGCCCTTGGCTGGGGCTGAGGCCAGAGGTAGAGAG AGTTCTGGACAGGACTTTACTCTCTGGGAAGTGGAG TCCACTCTGGGAAGGACAAGCCACTGTGTTGAGATAGG AGGGCCCTGATAACAGTGTCTACTGTATACAGGGGTT TG	DR-4 ER-6	Gstm3, LOC624701, Gstm2
chr3:107787749-107787901	25	GAACTCTGTCTCTATCAGGGACTAAAGTGTCACT GTGAGAGTCTGGACTGGACCTTAGGCCAATGACTGG AAGTTTCAATTTGGCAAACTAAGCTTTGAGGTTACTCT GTTGGCAATTTCAAACACTGTGCCATGACGACACTG AGAG	N/A	LOC624701, Gstm2
chr3:107828325-107828509	42	CTGATTGAGCCTGTCTAACCCAGAAATGCACAGGCAG CATGAATCAGCTAGACCCGAGCCCTTGGCTGGGGCC TGAGGCCAGAGTTAAGAGAGTTCAAGGACAGGACTT TACTCTCTGGGAAGTGGAGTCCACTCTGGGAAGGAC AACACTGTGTTGAGATAGGAGGGCCCTGATAACAGT GC	DR-4 ER-6	Gstm1, LOC100043641
chr6:138088517-138088765	48	ACTGGTAAAGTCCCGAGTGAATGTTGCAGATGGGA ACTTATCAACCTTAGAGCTCTCAGAGCTGGAGCTGG CCATTACTGTGGGCTCTGTGATGTGCAATAGCTTTGA TGTGGCCATAACGACCTGCCCTTGCACACTTTCC TAAGTCACTGTAAACAAGTTAGTTGCCTAACAGACT CATAAATTCGCAGGTTTCACTTTGCACCCTGAAGGTAT TCACAGCAATAGAGCCCTCCCC	N/A	Mgst1
chr9:78064805-78065181	51	TTTAAGCCAGGAGAAGGAATCAACTACTCAAGAAGTT GAATATGGTCAAGTTTCGTTTTGCTCTGAAGCTCAAT GCCCTTCTCTGCTAATGCGATTCTAATGACTATGCCCTA GGTTGTTTGTAGAAGGGAGAGTCACTGTTAGATATCA CAGTGAATGATAAAAAAGGTGTGGGCCACAGCAAA AATCTAATCTCTGGCCTCATTGTGTTGCCAGCAA AACTTATGCCACCTTTGTCCTGTCTGGCTGGGCCCT CTGGAAAGCCCATATTGCAACTGGGAAAAGTTACTT AATAGAAAGACAATTTGATAAGCTGTATGACAATCA AAGTTCAGATCTACTGTAGCAGGACCTTCAGTCAAT GA	DR-3 DR-4	Gsta4
chr9:78071141-78071293	39	TTCCTTTAAAGCCCCACATTAACCTTGAACCTTGGAC CTCTGCTTCTGGCAGTACCATCTCCACTGGTCTT ACTGAGCTCAGATGAGCCCAACTGCCAGACGATGAG ATTTGACTTCGAGTCCCTTTGTTCTGAAACCCAGAACT TG	DR-4	Gsta1
chr9:78077541-78077853	40	AGGGTATACAGCCTTAGGATGTGACAGGCATCCCG AGGCCAGCCAGATCATCAGGTAATGATTAAACCAA GACCCATGAACCAAGGATTAACATAAATCATGATCA GCTTGTGGGTGTGTGAGTGAAGTCAGCGAGAATGACC TTGTTGGATAAGAGCCATGCTGAAGTTGGCAGGA AGGATCAGTAATTCTCATTAGCTTGAATGACATTGC TAATGTTGACAAAGCAACTTTCCACAGGAGTAACCTG CAGGGACTCACAGGCTGACTGAGACCTAGAGCAGG CTGGACAGAATGTGCT	ER-6 ER-8	Gsta1
chr10:75252613-75252925	32	ATTACAAGCTTGCACCATGACTGAAGCTCAGCTTCTTA CCTCCGGCTTAGAACCGCTGTGTACTGAAGCATGGC TGGCTCAGGTCACCTGATAAAAAGTGGTCCATGTTAC TCATTAAACAGAGCCACAGGACAGCTAGATGACACCCA TCTGACTTTTCTGGAGCTGTGATAGAACACTTGCAA AGCAACTGAAGGGAGCGAGGCCACAGTTCCAGGGT ACAGCTGGTCAATGGATGTCATGGCAGCAGGAACCT GAGGGACCCGGTACACTGTGTCCACACTGAGGTC CACTGTGCCACTGA	DR-4 ER-6	Gstt3, Gstt1
chr10:75267045-75267229	42	ATTAATACTACAAGACCTTATTGACCGACTCCTAGA GGTATGATAAAGGTCAGACAAAGGCACTCTGGCTCCA GATCAGTAAGGTCAAGTCAAAGGTTAGGCAAGGACAT CTAGCTCCAGGTCATTAACAAAGTCAAAGACCTT CACCTGTTGACTGTCTTAAAAATCTGCTTGCAAT	DR-3 DR-4 ER-8	Gstt1
chr10:75300133-75300349	47	TTCCCGCCCTCCTCGAGAGTCCGCTGCGCAAAGCAT GCTGGGAATCCTACACTGCAAGGAGGAGAGTCAAGC GCCTGTTGGTTGCTTGGCAACTGCTCACGCGAGCAA CGGGCGTGAAGTGTGCGTTAGGGGCAAGTAGACTAG CTGCCACAACCTCTAGAGGTGATTGCTCCCGGATTG GAAGGGTTGATTGTGGGAAACTCCCGCAACCG	IR-0	Gstt2
chr19:4037861-4038045	28	ACTGCCTGCTGGGTGGGATTCAGTCTGCTGAGACA GAGGGTACTCAGAGTGAAGGAGCCACCGTAGGCCA CCGGCCCGCAGCCTTATAAGGGGATCGGCTCCG CCCCGATCTGACTCAACACTTTGGAGAGAAAGC CGGTAGCGGAGCTCTGAGCTCCCGCTCTGCGCG GGAC	N/A	Gstp1, Gstp2

Epigenetic aspects of regulation of Gst mRNA expression in developing

mouse liver: To identify whether the ontogeny is also regulated by epigenetic mechanisms, three distinct epigenetic signatures, namely DNA methylation, histone H3K4 dimethylation (H3K4me2), and histone H3K27 trimethylation (H3K27me3), were characterized by ChIP-on-chip around the Gstz1 locus, as Gstz1 mRNA is highly expressed in liver. Positive enrichment of the gene activation signal H3K4me2 was observed at all 4 selected ages (day -2, 1, 7, and 45, threshold: 4.0-fold), with more H3K4me enrichment sites at day 45 in the adult liver (Figure 6.5A). The overall average H3K4me2 enrichment gradually increased during liver maturation (Figure 6.5B), and this ontogenic expression pattern was strongly associated with the postnatal-enriched pattern of Gstz1 mRNA ($r= 0.76$) (Figure 6.5C). In contrast, there was no enrichment in the two suppression signals, DNA methylation or histone H3K27me3 within ± 10 kb of the Gstz1 gene locus (Figure 6.6). Together these data indicate that epigenetic modifications, such as the absence of transcription-repressing epigenetic marks, combined with the presence of H3K4me2 (transcription-activating epigenetic mark), might play a role in facilitating a permissive chromatin state that activates Gstz1 gene transcription during mouse liver development.

Figure 6.5.

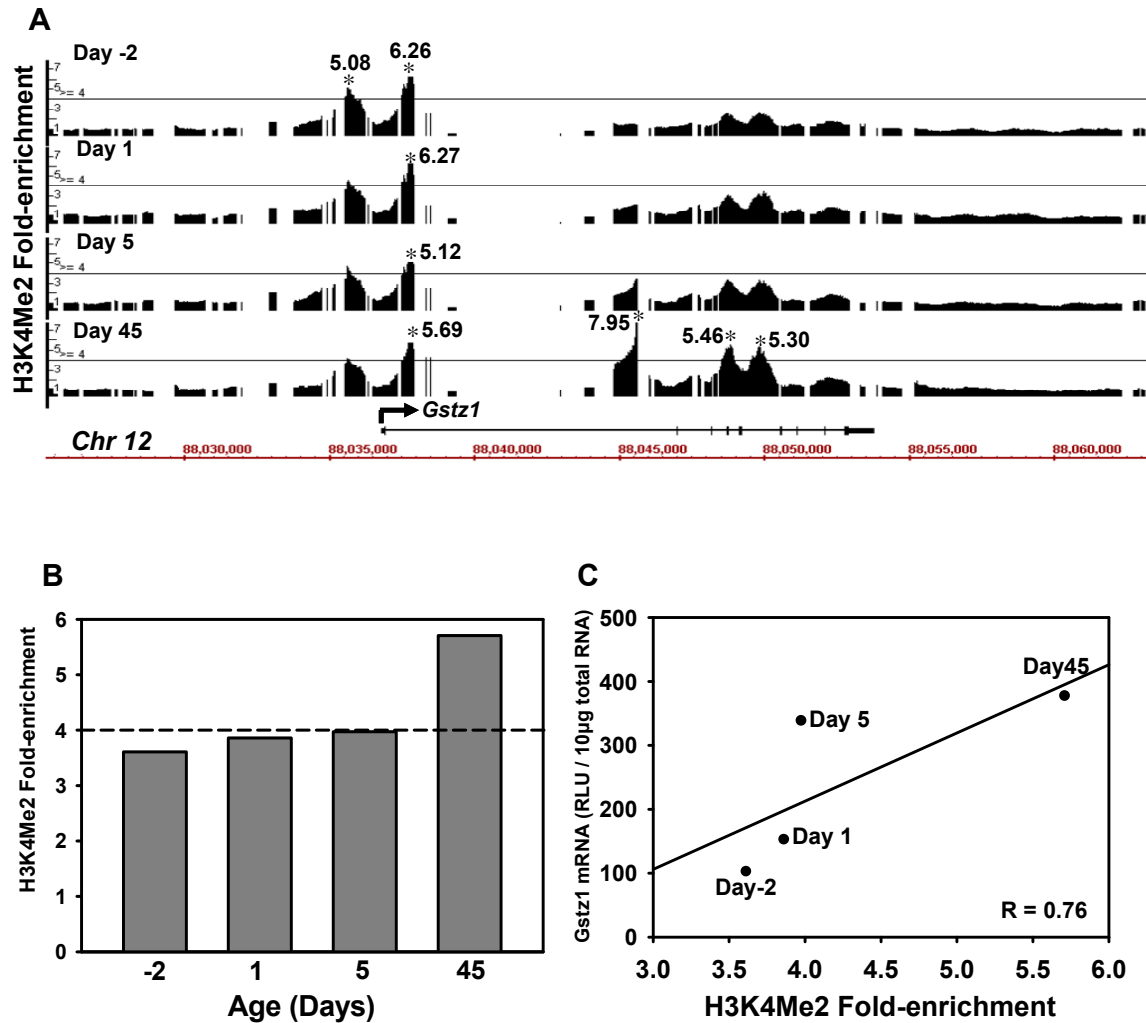


Figure 6.5: Dimethylation of histone H3 at lysine-4 (H3K4me2) at the *Gstz1* gene locus during mouse liver development. **A**: Histone H3K4me2 fold changes at the *Gstz1* gene locus at day -2, 1, 5, and 45 of age (equal amount of pooled samples from $n=5$ at each age). Solid lines through the signal enrichment peaks indicate the threshold value (4.0) for enriched intervals. Bars under the peaks of each age indicate the existence and length of active regions for H3K4me2. Asterisks (*) indicate the peak center. **B**: Average peak values of H3K4me2 at day -2, 1, 5, and 45 of age. The dashed line indicates the threshold value (4.0) for enriched intervals. **C**: Regression analysis of the correlation (r) between *Gstz1* mRNA and the fold changes of the three epigenetic marks (DNA and histone di- and tri-methylations) at day -2, 1, 5, and 45 of age during liver development in mice.

Figure 6.6.

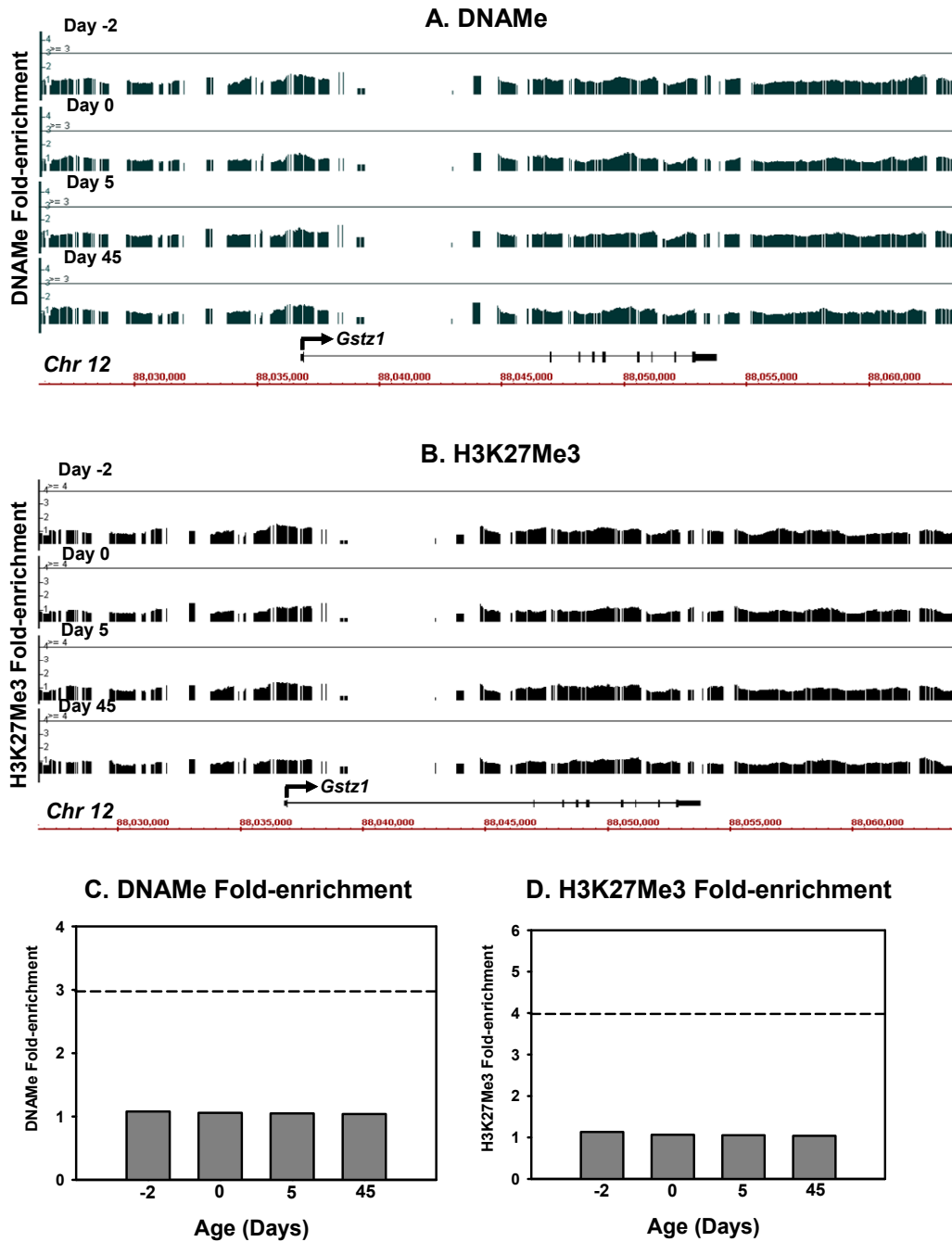


Figure 6.6: A: DNA methylation status of hepatic *Gstz1* gene locus at day -2, 1, 5, and 45 of age. Solid lines through the signal enrichment peaks indicate the threshold value (3.0) for positive DNA methylation. B: Trimethylation of histone H3 at lysine-27 (H3K27me3) of the hepatic *Gstz1* gene locus at day -2, 1, 5, and 45 of age. Solid lines through the signal enrichment peaks indicate the threshold value (4.0) for enriched intervals. C: Average peak values of DNA methylation at day -2, 1, 5, and 45 of age. The dashed line indicates the threshold value (3.0) for enriched intervals. D: Average peak values of H3K27me3 at the *Ahr* gene locus at day -2, 1, 5, and day 45 of age. The dashed line indicates the threshold value (4.0) for enriched intervals.

DISCUSSION

The present study is among the first to identify the age-specific mRNA expression signatures of the 19 glutathione-S-transferase isoforms in developing mouse liver. Using recent technological advancements, such as ChIP-seq and ChIP-on-chip, the present study has provided new insights in characterizing the Gst genes that are direct targets of the critical xenobiotic sensor PXR, and revealed potential epigenetic regulators for the ontogeny of Gstm1 in liver maturation. Our data suggest that the developmental regulation of Gst genes is a sequential event regulated by transcription factors and alterations of the chromatin structure. Both the genetic and epigenetic factors may play important roles in forming the age-specific expression signatures of Gst mRNA in mouse liver.

It has been proposed that changes in expression of liver-specific proteins generally occur at three specific developmental stages: (i) late gestation; (ii) at or directly after birth; or (iii) just before weaning (Greengard, 1970). During these periods, the liver undergoes significant anatomical and physiological changes associated with maturation. Thus, investigation of the age-specific ontogenic expression of Gsts will help understand differences in chemical detoxification abilities between adult and neonatal livers. In the current study, hepatic Gst mRNA expression was lowest or absent at prenatal day -2 and at birth except for Gstm5 and MGst2, which showed highest expression at prenatal day -2 followed by a gradual decrease over age. Embryonic development and fetal growth

depends on nutrients obtained from the mother and such exchange occurs through the placenta. Although placenta is capable of metabolism and detoxification of xenobiotics and endogenous chemicals, it does not entirely exclude or metabolize all chemicals in the mother's blood. Consequently, many drugs and other xeno- or endobiotic metabolites reach fetal organs from the mother's blood. The unique expression profiles of Gstm5 and MGst2 need further study because their expression profiles suggest that they may have special functional significance during gestation.

Our findings of lower Gst expression at birth and early postnatal period are consistent with an earlier report in rats where a low total hepatic Gst enzyme activity was observed in neonatal period, but was higher in adults (Tee et al., 1992). In that study, total Gst activity was determined using CDNB (1-chloro-2,4-dinitrobenzene) as the universal Gst substrate. Perhaps the most intriguing results are the marked differences in the expression profiles of the Gsts between day 15 and 20. One can envision that these gene expression changes observed around weaning may be in response to dietary changes, because mice transition from milk to chow during this period. Dietary factors have been shown to be critical regulators for liver gene expression. For example, both the mRNA and activities of lipogenic enzymes increase in rat liver after weaning in response to a high-carbohydrate diet (Girard et al., 1994). If the hypothesis that dietary factors regulate Gst gene expression is true, it can be argued that they may serve as critical signaling molecules to initiate a cascade whereby the liver becomes more

capable of detoxifying electrophilic chemicals and reactive oxygen species, highlighting the importance of diet on drug metabolizing enzyme gene expression patterning and detoxification capacity.

Interestingly, Tee et al. (1992) reported that in rats, Gstps are abundant in 18-day fetal livers, but are almost absent postnatally. In contrast, in the present study in mice, postnatal hepatic Gstp1/2 expression increased between 15 and 45 days of age in male mice, whereas female Gstp1/2 expression was similar to that in male mice until 22 days of age, but did not increase thereafter as in male mice. Such differences in Gstp gene ontogeny could be due to species differences, and/or detection methods. For example, for species differences, it has been demonstrated that rat GST-P gene has a strong enhancer element GPE1 (GST-P enhancer-1) that specifically regulates the GST-P gene by interacting with certain transcription factors such as C/EBP α and Nrf2/MafK. In contrast, the mouse GST-P1 gene does not contain a GPE1 or related element (Sakai and Muramatsu, 2007). For differences in detection method, the study by Tee et al. in rats used immunocytochemistry and HPLC identification of Gst subunits, whereas the study by Raijmaker et al. (2001) in humans used western blot to study specific isoforms. Tee et al. also used northern blot to determine the mRNA expression of Gst alpha, mu and pi class, using longer cDNA probes. Obviously, the ability to distinguish all 19 isoforms using such long probes was limited. In contrast, the present study reveals additional information because of

the ability to investigate the expression of individual isoforms by using isoform-specific short oligonucleotide probes.

Among all the 19 Gst isoforms, the most predominant gender difference was observed in the ontogeny of the Gstp1/2 gene, which had higher levels of mRNA in livers of male than female mice at 30 and 45 days of age. Our observation for the male-predominant expression of Gstp1/2 is consistent with previous findings (Bammler et al., 1994; Knight et al. 2007; Townsend et al., 2008). Gender differences were also observed at early postnatal ages, with Gsta1/2, o1, z1, m5, and p1/2. Such neonatal gender differences suggest that distinct molecular mechanisms might also exist in regulating the gender-divergent gene expression at early ages. The gender specific gene expression of Gsts suggests that males and females may have different capacities in metabolizing and detoxifying chemicals that are Gst substrates.

Yijia et al. (2008) studied the expression of MAPEG (membrane associated proteins in eicosanoid and glutathione metabolism) in an *in vitro* system of mouse embryonic stem (ES) cell-derived hepatic tissue. The protein expression of MGst1 was not detected until postnatal day 14 and gradually increased with the maturation of hepatic tissue. This finding is consistent with MGst1 mRNA expression observed in the present study. The membrane-associated enzyme activities involved in eicosanoid and glutathione metabolism are important in both

inflammation and cell protection, and therefore a part of the tissue's defense mechanism.

Certain Gst/GSTs exist as polycistron clusters in both mice and humans. For example, Gsta1 and a2 cluster together on chromosome 9 in mice and transcribe from the opposite strands; whereas Gsta1 transcribes from the plus strand, and Gsta2 transcribes from the minus strand. In humans, five members of the GSTA family (GSTA1-A5) also form a polycistron cluster on chromosome 6; the human GSTA5 is homologous to both Gsta1 and a2 in mice (Figure 6.8). Other examples of Gst/GST family members forming polycistron clusters include Gstm/GSTM clusters on mouse chromosome 3 and human chromosome 1, with multiple homologous genes between the two species (Figure 6.9); as well as Gstt/GSTT and Gstp/GSTP clusters in mice and humans (Figure 6.10). From an evolutionary standpoint, the formation of Gst/GST polycistron clusters suggests a possible fine-tuning of gene expression through coordinate regulation that should produce cluster-specific gene expression signatures. Therefore, the ontogenic expression signatures of the clustered Gst isoforms was investigated in the present study.

Figure 6.7.

The GSTA/Gsta Cluster

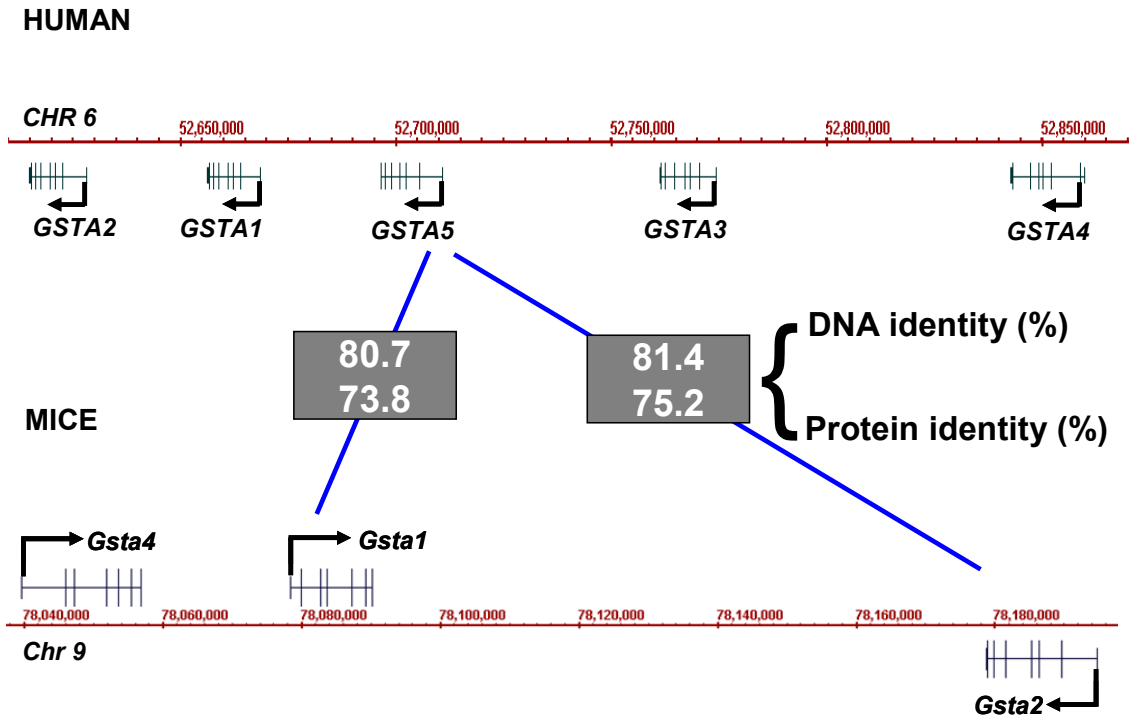


Figure 6.7: Human GSTA polycistron cluster and their homologous mouse Gsta cluster family. Image was obtained from the Affymetrix Integrated Genome Browser (IGB). DNA and protein identities (%) were calculated based on the NCBI database.

Figure 6.8.

GSTM/Gstm Cluster

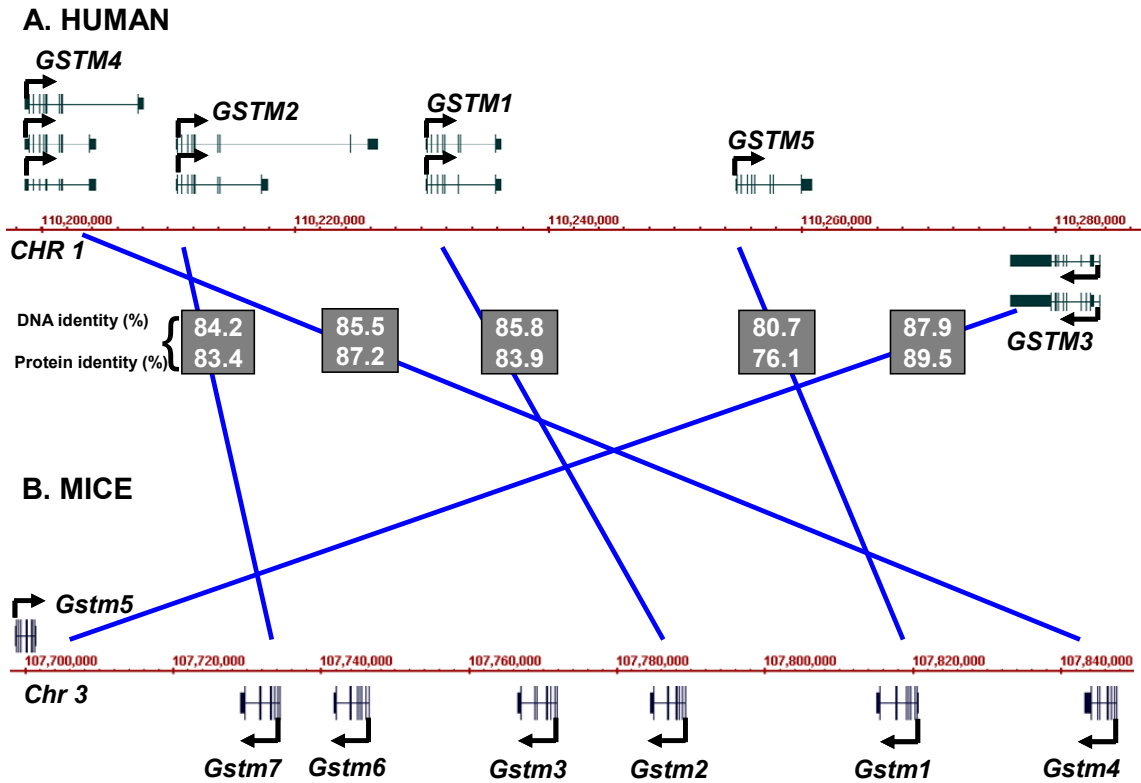
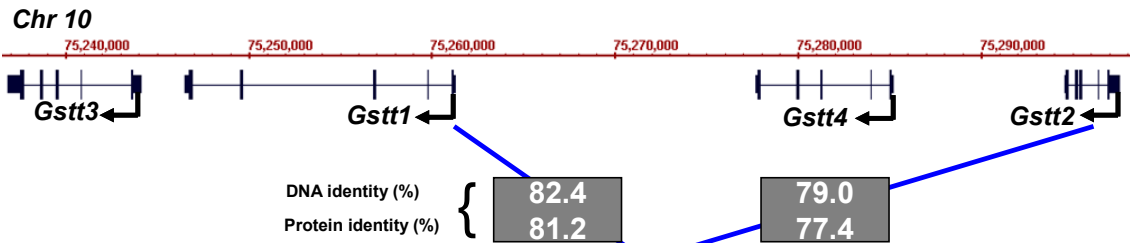


Figure 6.8: Human GSTM polycistron cluster and their homologous mouse Gstm cluster family. Image was obtained from the Affymetrix Integrated Genome Browser (IGB). DNA and protein identities (%) were calculated based on the NCBI database.

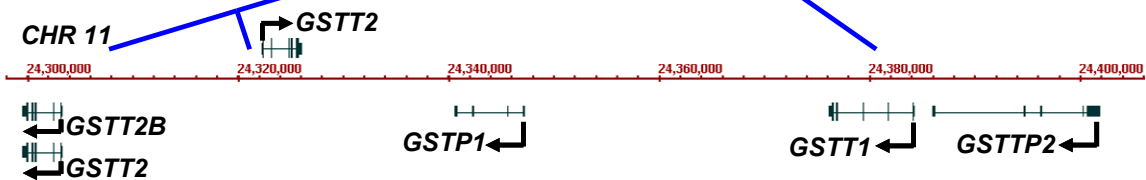
Figure 6.9.

The GSTT/Gstt Cluster and the GSTP/Gstp Cluster

MOUSE *Gstt*



HUMAN *GSTT* and *GSTP*



MOUSE *Gstp*

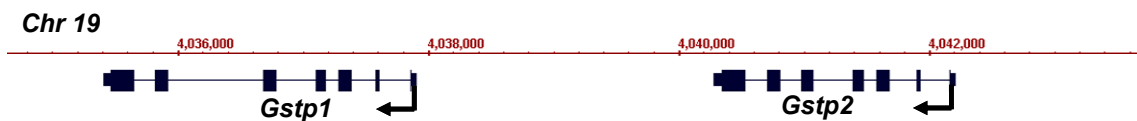


Figure 6.9: Human *GSTT* and *GSTP* polycistron clusters and their homologous mouse *Gstt* and *Gstp* cluster families. Image was obtained from the Affymetrix Integrated Genome Browser (IGB). DNA and protein identities (%) were calculated based on the NCBI database.

Previous studies in this laboratory have shown that several Gsts were induced following PCN administration (Cheng et al., 2005b; Maher et al., 2005a; Alnouti et al., 2008b; Alnouti and Klaassen, 2008; Knight et al., 2008), but only a few genes have been shown to be direct PXR targets. The present study is among the first to identify that multiple Gst genes are direct PXR-targets, including a few genes in the Gsta, Gstm, Gstt, Gstp clusters, and the microsomal MGst1. Similar ontogenic expression of genes in the same Gst polycistron clusters indicate they share common regulatory mechanisms, likely mediated by PXR protein binding. Gstm5 is the only Gstm isoform that showed a different ontogenic pattern. This might be due to the fact that Gstm5 transcribes from the opposite strand, and thus may be under separate regulatory control.

Recently, a large body of data has been generated to characterize histone modifications in the genomes of various organisms (Hawkins and Ren, 2006). A current area of research is to understand how histone marks correlate and/or regulate gene transcription. High-resolution profiling of histone methylations in the entire human genome has demonstrated that active genes are characterized by high levels of H3K4me₂; in contrast, inactive genes are characterized by low or negligible levels of H3K4me₂ of the promoter regions, and high levels of H3K27me₃ (Barski et al., 2007). It has been shown that the H3K4me₂ signals are usually localized close to transcription start sites, providing a permissive chromatin environment to trigger gene transcription (Barski et al., 2007). In the

present study, the strong postnatal enrichment of H3K4me2 in the close vicinity of the *Gstz1* gene promoter indicates H3K4Me2 is likely a mechanism to trigger the increase in *Gstz1* gene activation during mouse liver development.

In conclusion, the present study identified three distinct ontogenic expression patterns among the 19 hepatic *Gst* isoforms in both male and female mice, characterized the occurrence of gender differences in the expression of certain *Gsts* during liver maturation, identified that certain *Gsts* are direct target genes by the xenosensor PXR, and revealed positive associations between the *Gstz1* ontogeny and enrichment of the epigenetic mark H3K4Me2. By combining genome-scale investigations and *Gst* gene expression profiling, our study has provided novel insights in understanding the genetic and epigenetic mechanisms in regulating the maturation of drug metabolism in developing liver.

CHAPTER SEVEN

DEVELOPMENTAL REGULATION OF LIVER TRANSPORTERS IN MICE

Part One

Bile acids via FXR Initiate the Expression of Major Transporters involved in the Enterohepatic Circulation of Bile acids in Newborn Mice

ABSTRACT

The enterohepatic circulation (EHC) of bile acids plays a pivotal role in facilitating lipid absorption. Therefore, initiation of the EHC in newborns is of crucial importance for lipid absorption from milk. The purpose of this study was to determine at what age bile-acid transporters in liver are expressed, and the mechanism for their initiation. Samples were collected from C57BL/6 mice at 2 days before birth and various postnatal ages. Messenger RNA assays revealed a dramatic increase at birth in the expression of the bile-acid transporters Ntcp, Bsep, Mrp4, Ost β , as well as the phospholipid flipase Mdr2 in mouse liver, with the highest expression at 1 day of age. The mRNA expression of the ileal bile-acid transporters, Ost α and Ost β , also increased markedly at birth. Meanwhile, taurine-conjugated cholic acid increased markedly in both serum and liver of newborns, suggesting that an up-regulation of the classic pathway of bile-acid biosynthesis occurs in newborn liver. The mRNA levels of the major bile-acid sensors, FXR and PXR, were increased at day 1 of age, and their prototypical target genes were up-regulated in liver. The mRNA expression of transporters involved in the EHC of bile acids was similar in wild-type and PXR-null mice. In contrast, in FXR-null mice, the “day-1 surge” pattern of Ntcp, Bsep, Ost β , and Mdr2 was blocked in newborn mouse liver, and the induction of Ost α and Ost β was also abolished in ileum of FXR-null mice. In conclusion, at birth, bile acids from the classic pathway of synthesis appear to trigger the induction of transporters involved in enterohepatic circulation of bile acids, through activation of the nuclear receptor FXR.

INTRODUCTION

Enterohepatic circulation (EHC) is the circulation of bile acids between liver and intestine and back to the liver. Bile acids are synthesized from cholesterol in the liver and excreted into intestine. Once in the intestine, bile acids facilitate the absorption of fat and fat-soluble vitamins by emulsifying the lipophilic substances in the diet. Most of the bile acids in the intestine are recycled back to the liver, with only 5% of bile acids eliminated into feces daily. Conservation of bile acids ensures efficient nutrient and energy supply to the organism. During postnatal development, initiation of the enterohepatic circulation of bile acids is crucial for nutrient and energy acquisition, in order to facilitate the rapid growth of developing tissues. In humans, there is a phase of physiological immaturity of the EHC of bile acids during the neonatal period, resulting in delayed hepatic clearance of bile acids and bilirubin, as well as altered clearance of some exogenous chemicals. Immaturity of EHC results in inefficient lipid digestion, and a cholestatic period of liver. This immaturity of EHC is termed “physiological cholestasis” (Suchy et al., 1981). Clinically, newborns that have defects in bile-acid transport systems develop deficiencies in fat-soluble vitamins (vitamins A, D, E, K), severe diarrhea (Heubi et al., 1979), and progressive cholestasis (Scheimann et al., 2007), which can be lethal if untreated.

Transporters play essential roles in maintaining the EHC of bile acids. The sodium-taurocholate cotransporting polypeptide (Ntcp) is the major basolateral bile-acid uptake transporter in liver (Hagenbuch et al., 1996), and the bile- salt

export pump (Bsep) is the rate-limiting canalicular transporter for bile-acid excretion into bile (Wang et al., 2003). Although most bile acids are sequestered in the EHC under physiological conditions, during cholestasis, bile acids are also excreted into blood from the liver via the basolateral transporters, including the multidrug resistance-associated protein 4 (Mrp4) (Mennone et al., 2006), as well as the organic solute transporters α and β (Ost α and Ost β) that function as a heterodimer (Ballatori et al., 2005). In addition to bile-acid transporters, the multidrug resistance protein 2 (Mdr2) in liver flips phospholipids from the inner to the outer lipid bilayer of the canalicular membrane. Phospholipids enter bile and form micelles with bile acids, thereby protecting the biliary tree from injury (Smit et al., 1993), as well as facilitating nutrient absorption. In the ileum, there is an active uptake system that brings bile acids from the intestinal lumen back into the blood, and the transporters involved include the ileal apical sodium-dependent bile-acid transporter (Asbt), as well as the basolateral transporters Ost α and Ost β in enterocytes (Ballatori et al., 2005). Despite the crucial functions of the transporters in regulating the EHC, the ontogenic expression patterns of these transporters are poorly characterized.

Recently, it has been demonstrated that bile acids are signaling molecules that activate certain nuclear receptors called “bile-acid sensors” (Chiang, 2002). Farnesoid X Receptor (FXR) is the major bile-acid sensor, but the Pregnane X Receptor (PXR) may also regulate bile-acid metabolism. Once activated by bile acids, FXR in liver down-regulates the major bile-acid uptake transporter, Ntcp

(Zollner et al., 2005), up-regulates the main bile-acid efflux transporter, Bsep (Plass et al., 2002), and up-regulates the basolateral bile-acid efflux transporters, Ost α and β (Zollner et al., 2006). FXR in ileum induces the expression of Ost α and β on the basolateral membrane of the enterocytes to promote bile-acid re-absorption (Zollner et al., 2006). In mouse enterocytes, bile acids activate FXR, which results in the synthesis and secretion of fibroblast growth factor 15 (Fgf15) into blood (the human analog of Fgf15 is FGF19). Fgf15 is then delivered to the liver where it activates the FgfR4 signaling pathway, which inhibits bile-acid synthesis via down-regulation of Cyp7a1 mRNA expression (Inagaki et al., 2005). It has been suggested, using a human hepatocyte culture system, that the mechanism of Cyp7a1 down-regulation involves the FGF19-MAPK pathway (Song et al., 2008). In addition, the nuclear receptor PXR increases the expression of Cyp enzymes, conjugation enzymes, and transporters involved in the metabolism and elimination of potentially toxic chemicals, including bile acids from the body (Chiang, 2002). The physiological roles of FXR and PXR in regulating bile-acid homeostasis during postnatal liver development are not well characterized.

Bile-acid synthesis mainly involves two pathways, namely the classic and the alternative pathway (Chiang, 2004). The major enzymes involved in the classic pathway of bile-acid synthesis include Cyp7a1, which is the rate-limiting enzyme for bile-acid synthesis, as well as Cyp8b1, and these two enzymes catalyze the formation of cholic acid (CA). In the absence of Cyp8b1, chenodeoxycholic acid

(CDCA) is the major bile-acid (Chiang, 2004). Therefore CA and CDCA are the major primary bile acids synthesized via the classic pathway. The enzymes in the alternative bile-acid biosynthesis pathway include Cyp27a1, Cyp7b1, as well as Cyp39a1 (relatively lowly expressed in liver), with CDCA as the primary product formed (Russell, 2003). The two primary bile acids synthesized by humans are CA and CDCA. In contrast, mice convert CDCA to α - and β -muricholic acid (MCA), therefore, the main primary bile acids in mice are CA and MCA (Elliott and Hyde, 1971). CA and MCA are then conjugated with taurine (major co-substrate in mice) and excreted into bile. The alternative pathway is the major route of bile-acid synthesis in the prenatal period (Yamato et al., 2001), whereas the classic pathway predominates in the adult period, except in certain diseases (Crosignani et al., 2007). However, when the switch from the alternative to the classic pathway of bile-acid synthesis occurs during liver development remains unknown. This is partially due to the lack of a valid and simple analytical method for the quantification of individual bile acids, as well as their taurine and glycine conjugates. Recently, a simple and sensitive UPLC-MS/MS method for the simultaneous quantification of bile acids was developed in our laboratory (Alnouti et al., 2008a), and this method was modified and used in the present study to determine the composition of bile acids at various ages in mice.

Because of the importance of EHC in mediating the absorption of fat-soluble nutrients, it is crucial to determine the mechanisms underlying the regulation of

bile-acid transport systems in the EHC during postnatal liver development.

Therefore, the purpose of the present study was to determine at what age the liver bile-acid transporters are expressed, and the mechanism for their initiation.

Because bile acids are substrates for many liver transporters involved in the EHC, the working hypothesis is that certain bile acids initiate the expression of these transporters in liver after birth, via activating bile-acid sensor-mediated pathways.

RESULTS

Ontogeny of major transporters in mice involved in EHC of bile acids. The mRNA expression of major hepatic and ileal transporters involved in the EHC of bile acids was determined from day -2 to day 45 of age in mice as shown in Figure 7.1.1 and 2. The Ntcp mRNA was low at day -2 of age (Figure 7.1.1A). At birth, the Ntcp mRNA increased approximately 2 fold, then peaked at day 1 of age (5-fold prenatal levels), followed by a decrease at day 3 and 5 of age, and returned to prenatal levels at day 10 and 15 of age. After day 20 of age, Ntcp mRNA gradually approached adult levels (approximately 2-fold higher than prenatal levels) till 45 days of age. The basolateral bile-acid efflux transporters, Ost α and β , function as a dimer. Interestingly, although Ost α mRNA is lowly expressed in liver throughout development (Figure 7.1.1B), Ost β mRNA was induced markedly in newborn liver, which peaked at day 1 of age (4.5-fold of prenatal levels) (Figure 7.1.1C). After day 5, Ost β mRNA decreased to adult levels at about 10 days of age. The mRNA expression of hepatic Mrp4 was consistent from day -2 to day 45 of age, except for a moderate increase at day 1 of age (Figure 7.1.1D).

The mRNAs of both Bsep and Mdr2 were increased markedly in mouse liver after birth (approximately 3-4-fold higher at day 1 of age than before birth). The expression of Bsep and Mdr2 then returned to before birth levels at day 10 and 15 of age, and then gradually increased to adult levels by approximately 30 days of age (Figure 7.1.1E and F).

Figure 7.1.1

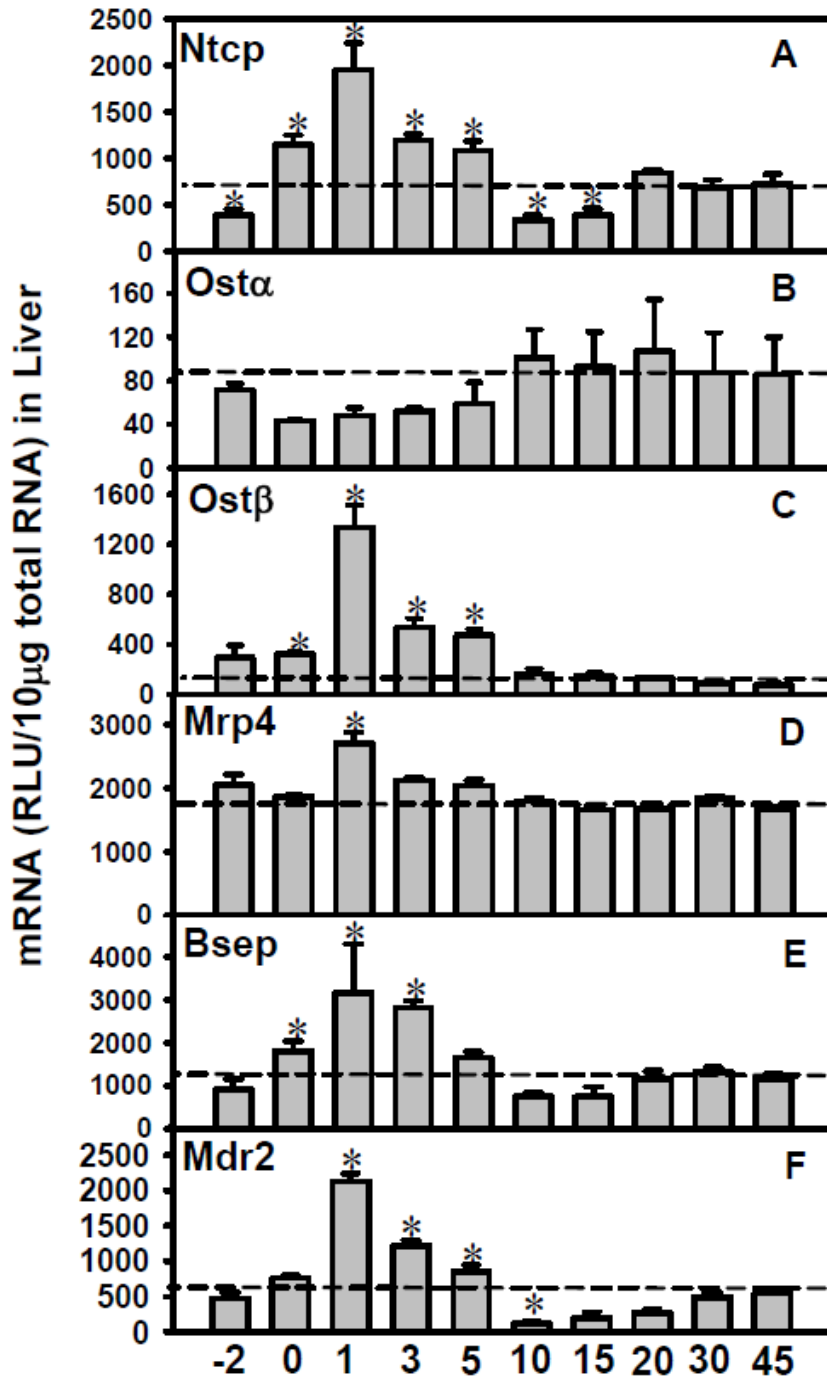


Figure 7.1.1. Ontogeny of liver transporters: Ntcp (basolateral uptake), Ost α , Ost β , and Mrp4 (basolateral efflux), Bsep and Mdr2 (canalicular efflux) in wild-type mice from day -2 to day 45 of age. Total RNA was isolated from liver at each age and analyzed by the bDNA assay as described in MATERIALS AND METHODS. Data are presented as mean RLU \pm S.E.M. (n = 5 animals). Asterisks (*) represent significant differences (p < 0.05) compared with values at day 45 of age.

In summary, the liver transporters Ntcp, Bsep, Mrp4, Mdr2, and Ost β , which all play important roles in EHC, share a common “day-1 surge” pattern in their mRNA expression during development. Other liver transporters, including the basolateral uptake transporters for xenobiotics (the Oatps, Oct1, Oat2, and Ent1), the basolateral efflux transporters (Mrp3 and 6, Abca1), and many canalicular transporters for xenobiotics and other chemicals (Mrp2, Bcrp, Mate1, Abcg5, g5, and Atp8b1), do not have a “day-1 surge” pattern in their mRNA expression in liver development, and the majority of these transporters are enriched between day 15 to day 45 of age, except for Bcrp, which is enriched prenatally (see Chapter VII, Part Two, Figure 7.2.1 to 7.2.3). In addition, the house-keeping gene glyceraldehyde-3-phosphate dehydrogenase (Gapdh), used for normalization of some mRNA assays in the present study, is consistently expressed during liver development (data not shown). Therefore, the “day-1 surge” pattern appears to be a specific phenomenon for the expression of transporters involved in the EHC of bile acids.

In ileum, a marked increase in the mRNA expression of the basolateral bile-acid transporters, Ost α and β , was observed shortly after birth (Figure 7.1.2). The ileal Ost α mRNA at day 1 was 6.4-fold higher than before birth, and then peaked at day 15 of age (19.4-fold) (Figure 7.1.2A). The ileal Ost β mRNA peaked at day 1 of age (20.9-fold of prenatal levels), and remained relatively similar thereafter (Figure 7.1.2B). Therefore, the neonatal increase in the expression of the major bile-acid efflux transporters, Ost α and Ost β , in ileum

Figure 7.1.2

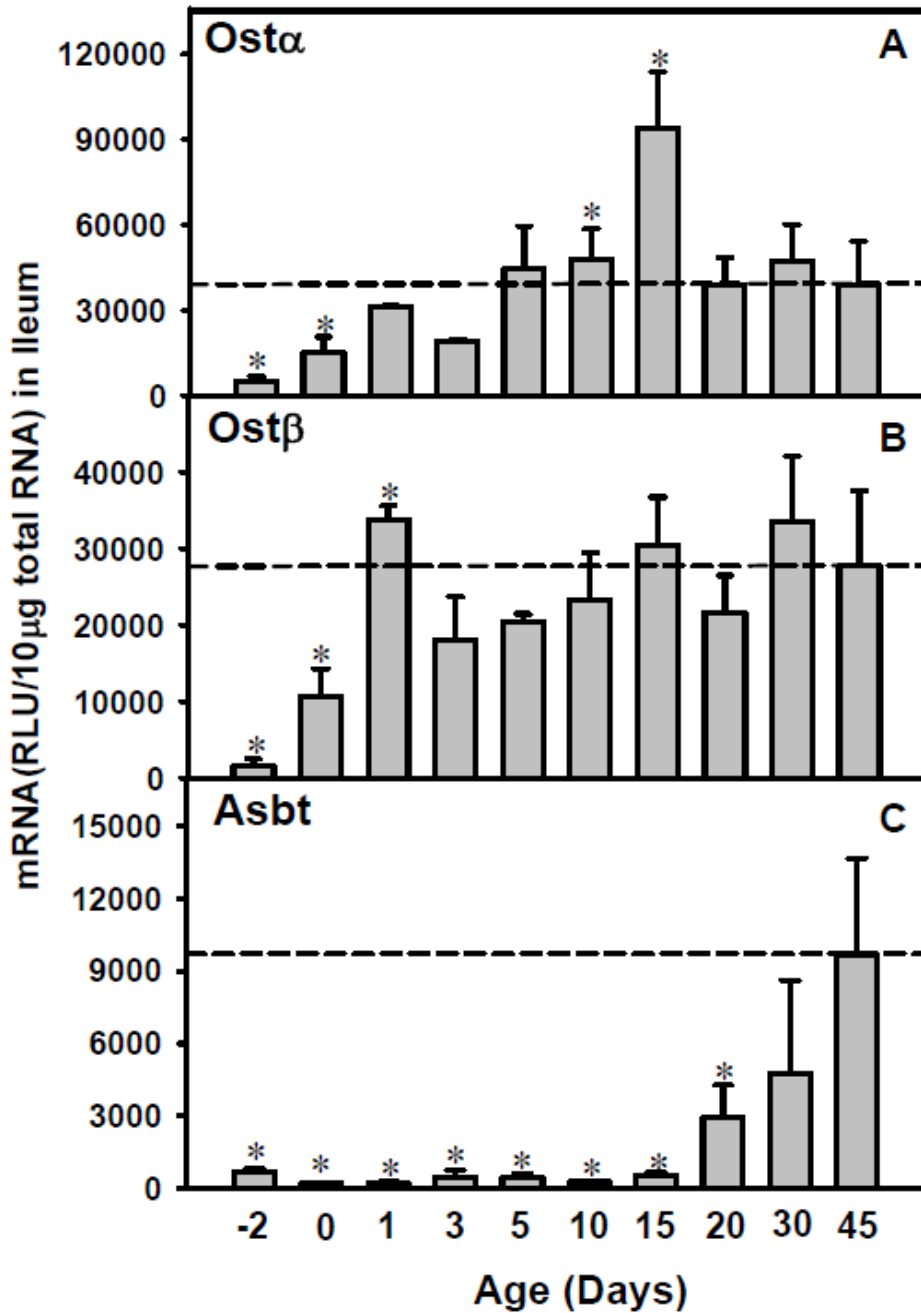


Figure 7.1.2. Ontogeny of ileal transporters: Ost α and Ost β (basolateral efflux), and Asbt (apical uptake) in wild-type mice from day -2 to day 45 of age. Total RNA was isolated from ileum at each age and analyzed by the bDNA assay as described in MATERIALS AND METHODS. Data are presented as mean RLU \pm S.E.M. (n = 5 animals). Asterisks (*) represent significant differences (p < 0.05) compared with values at day 45 of age.

correlates with the up-regulation of liver bile-acid uptake and efflux transporters, however, the ileal apical bile-acid uptake transporter, Asbt, was low both before birth and the first 15 days of age, and then gradually increased during development, and peaked at day 45 of age (14.8-fold of prenatal levels) (Figure 7.1.3C).

Because the peak mRNA levels of most transporters involved in the EHC of bile acids were observed at day 1 of age, the present phenomenon was termed the “day-1 surge” pattern. To determine whether the protein expression of some of these transporters is also up-regulated shortly after birth, immunofluorescence staining was performed in the following experiments.

Immunofluorescence staining of Ntcp and Bsep in livers of wild-type mice during development. To determine the expression and localization of Ntcp and Bsep, immunofluorescence staining was performed on frozen liver sections at day -2, day 1, and day 45 of age for these two proteins (Figure 7.1.3). Ntcp protein was low but detectable at day -2 of age. At day 1 of age, enhanced basolateral Ntcp staining (green) throughout the liver lobule was observed, and the fluorescence intensity is comparable to that at day 45 of age (Figure 7.1.3 left column). Bsep protein was barely detectable at day -2 of age, but at day 1 of age, the staining of Bsep protein (green) was enhanced markedly. Mrp4 and Ost β immunofluorescence staining were not detectable, probably due to low protein expression levels in liver (data now shown). In summary, the “day-1

Figure 7.1.3

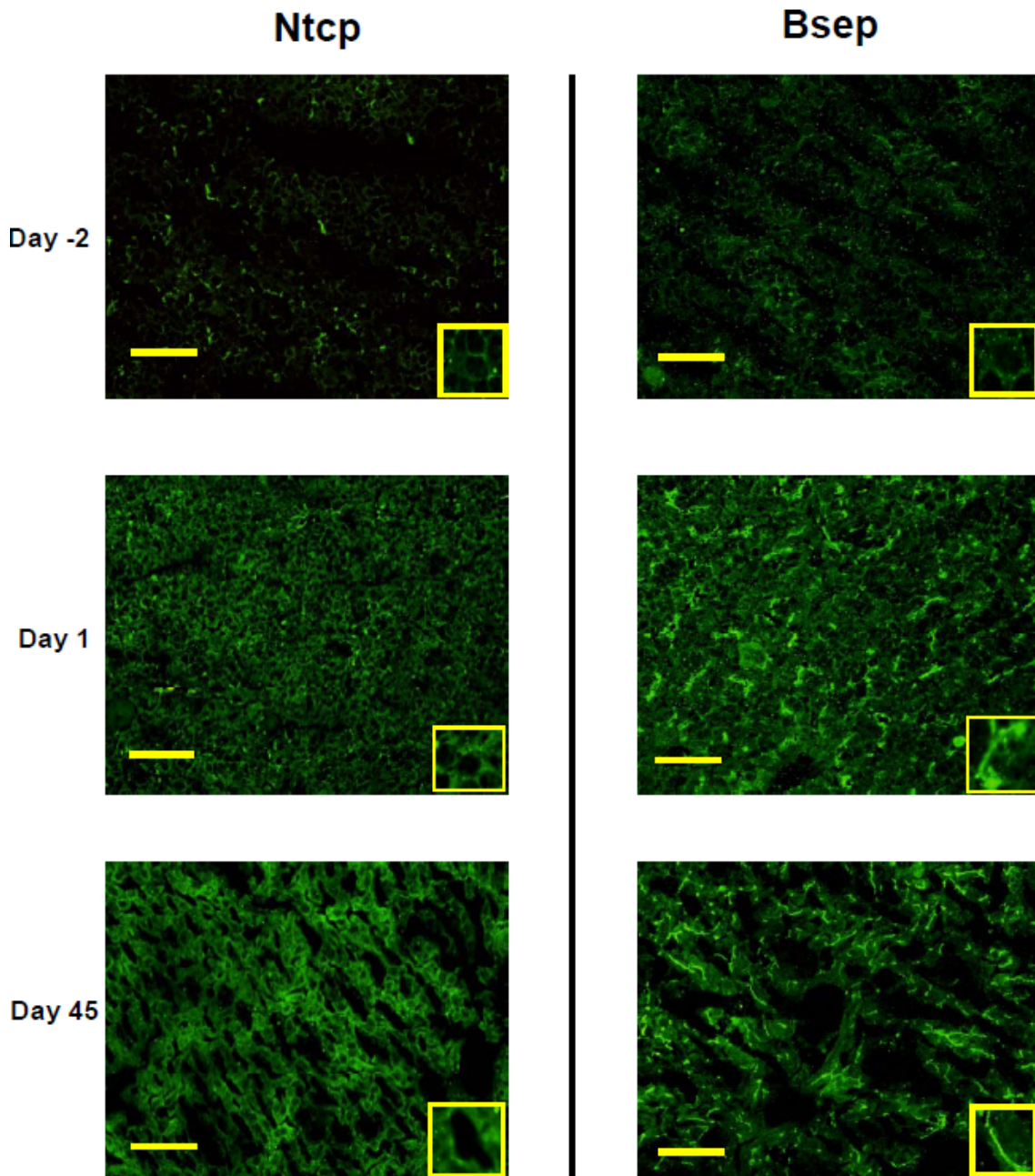


Figure 7.1.3. Immunofluorescence of Ntcp and Bsep protein in livers from day -2, day 1, and day 45 of age. Immunofluorescence against basolateral Ntcp as well as canalicular Bsep (green) was conducted on liver cryosections as described in MATERIALS AND METHODS. Portions of images were enlarged and provided as inserts. Representative images are shown. Bar, 50 μ m.

surge” pattern in the mRNA expression of hepatic transporters, Ntcp and Bsep, was detected at both the mRNA and protein levels in liver at day 1 of age.

Because bile acids are substrates for many hepatic transporters that share the “day-1 surge” pattern, we hypothesized that an elevation in bile acids due to their increased de novo biosynthesis in newborns initiate the mRNA increase of these transporters during development.

Ontogeny of bile-acid biosynthesizing enzymes during liver development.

To determine whether bile-acid biosynthesizing enzymes are increased in liver during development, the mRNA expression of major enzymes from both the classic and alternative pathways of bile-acid biosynthesis were quantified (Figure 7.1.4). For the classic pathway of bile-acid synthesis, both Cyp7a1 and 8b1 mRNAs were low before birth, but increased markedly at birth (14.4-fold and 8.1-fold of prenatal levels, respectively) (Figure 7.1.4A and B). After one day of age, both Cyp7a1 and 8b1 mRNAs decreased, but they increased again after 10 days of age. Cyp7a1 mRNA peaked at 20 days of age and decreased thereafter, whereas Cyp8b1 mRNA peaked at 30 days of age and remained stable thereafter. In contrast, for the alternative pathways of bile-acid synthesis, Cyp27a1 mRNA increased markedly after 20 days of age, and remained stable until 45 days of age (between day 20 and 45: approximately 50 fold higher than before birth). Cyp7b1 mRNA was also consistently low before 20 days of age,

Figure 7.1.4

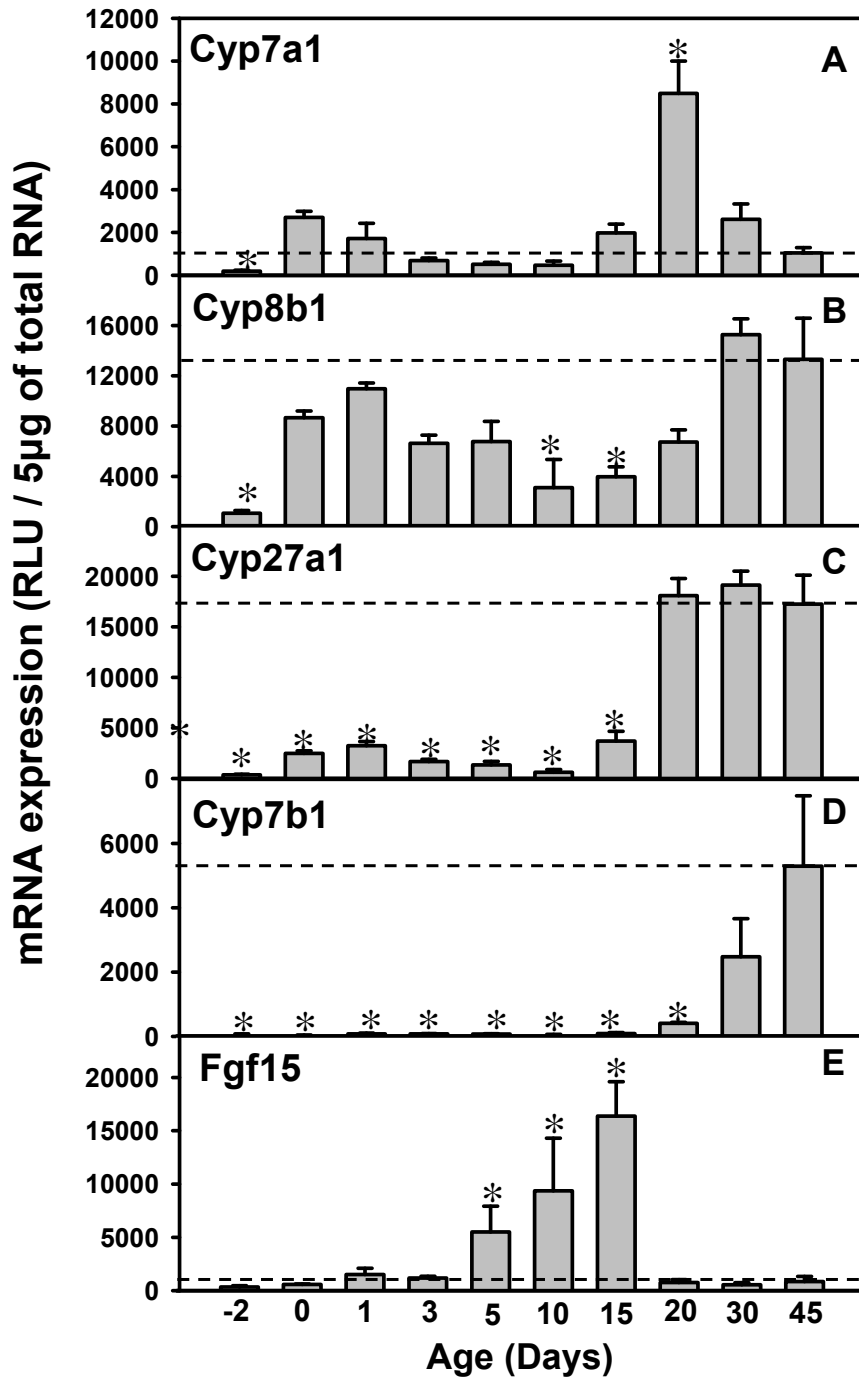


Figure 7.1.4. A-D. Messenger RNA expression of bile-acid synthesizing enzymes (Cyp7a1, 8b1, 27a1, and 7b1) in livers of wild-type mice during development. E. Ontogeny of the mRNA expression of ileal Fgf15 and in wild-type mice. Total RNA was isolated from liver at each age and analyzed as described in MATERIALS AND METHODS. Individual samples (n=5) analyzed by bDNA assay. Data are presented as mean RLU normalized to 5µg total RNA. Asterisks (*) represent statistically significant differences compared to day 45 adult levels ($p < 0.05$).

then increased markedly to adult levels (46 fold of day -2 levels at day 30, and 99-fold at day 45) (Figure 7.1.4 C and D).

In addition to the liver enzymes contributing to bile-acid biosynthesis, Fgf15 is secreted from the ileum and thought to be transported by the blood to the liver, where it binds to the FgfR4 receptor, and subsequently decreases the transcription of the bile-acid synthesizing enzyme, Cyp7a1. To determine the contribution of Fgf15-signaling on bile-acid synthesis in development, the ontogeny of FgfR4 mRNA in liver, as well as the ontogeny of Fgf15 mRNA in ileum, were determined. FgfR4 mRNA was consistently low throughout liver development (data not shown). The ileal Fgf15 mRNA was expressed lowly from day -2 to day 3, and started to increase after day 5 of age, and peaked at 15 days of age (49-fold prenatal levels) (Figure 7.1.4 E). It decreased markedly by day 20. The low perinatal expression of Fgf15 likely provides a permissive environment for the first induction of Cyp7a1 mRNA in newborns. In addition, the low expression of Fgf15 in intestine may contribute to the second peak of Cyp7a1 expression after day 15 of age.

In summary, the neonatal induction of bile-acid synthesizing enzymes, Cyp7a1 and 8b1, together with the low expression of the suppression signal Fgf15, promote an increase in bile-acid biosynthesis in newborns. Because the major bile-acid synthesized by Cyp7a1 and 8b1 in the classic pathway is cholic acid, and the major bile-acid synthesized by the alternative pathway enzymes in

mice is muricholic acid and cholic acid, we hypothesized that cholic acid is the predominant type of bile acid in newborns that contribute to the “day-1 surge” pattern of liver transporters.

Bile-acid concentrations in serum and liver during development. As a first approach to determine the association between bile-acid concentrations and the expression of major liver transporters involved in the enterohepatic circulation, bile acids in serum and liver were quantified during development as described in MATERIAL AND METHODS (Figure 7.1.5). Total bile-acid concentrations in serum were highest in newborns (day 1), and the total bile-acid concentrations at day 1 were 15.8-fold higher than adult levels. After day 15, the serum bile acids decreased markedly (Figure 7.1.5A upper panel). In liver, the total bile-acid concentrations were lowest before birth (7.5% of day 45 levels), followed by a marked increase at birth (1.88-fold higher than day 45 levels). The total bile acid concentrations in liver continued to increase till day 3. At 5 days of age, the total liver bile-acid concentrations moderately decreased to 2.8-fold higher than day 45 levels, but increased again after 10 days of age, and peaked at 15 days of age (7.2-fold higher than day 45 levels) and decreased thereafter (Figure 7.1.5B upper panel).

To determine whether bile-acids synthesized from the classic pathway are responsible for the “day-1 surge” of transporters, serum and liver bile-acid concentrations were quantified by LC-MS/MS (Figure 7.1.5). The taurine-conjugated cholic acid (T-CA) and the unconjugated cholic acid (CA) were

Figure 7.1.5

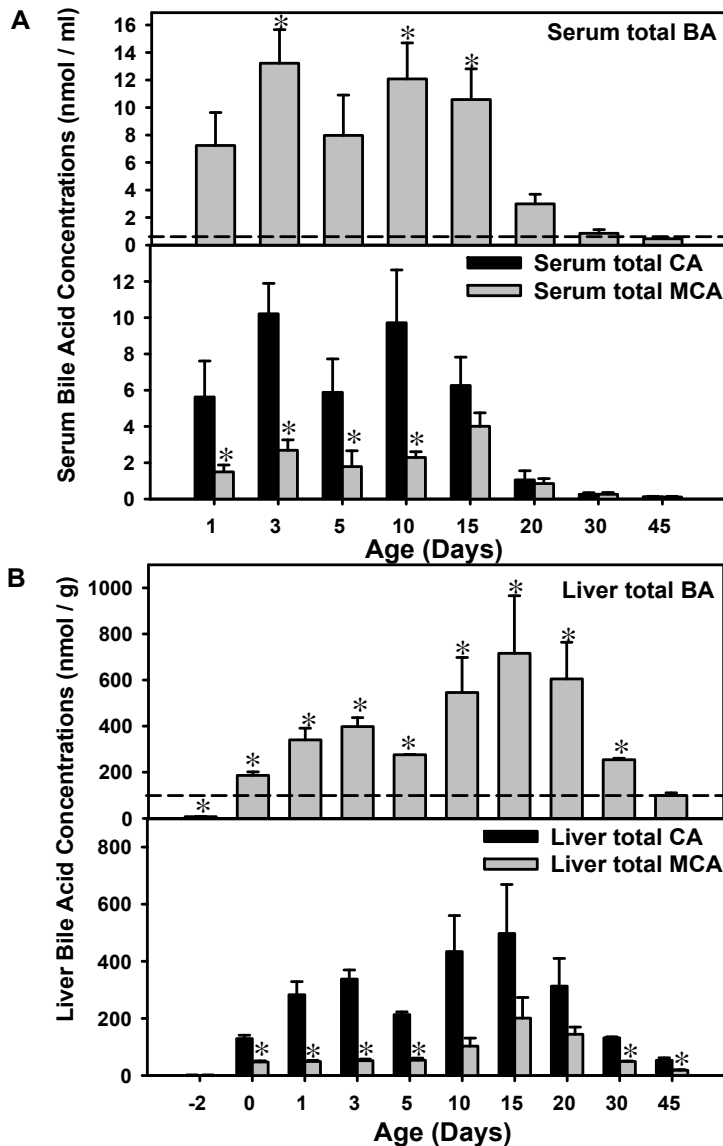


Figure 7.1.5. A. Serum total bile-acid concentrations (upper panel), as well as concentrations of total cholic acid (taurine-conjugated CA and unconjugated CA), and total primary muricholic acid (T- α MCA, T- β MCA, α MCA, and β MCA) (lower panel) during development (n=3 per age). The ω MCA was excluded because it is a secondary bile-acid. B. Liver total bile-acid concentrations (upper panel), as well as concentrations of total cholic acid (taurine-conjugated CA and unconjugated CA), and total primary muricholic acid (T- α MCA, T- β MCA, α MCA, and β MCA) during development (n=3 per age). Bile acids from serum and liver were quantified by LC-MS/MS as described in MATERIALS AND METHODS. For serum, data are expressed as nmol of bile acids per ml. For liver, data are expressed as nmol / g. Asterisks (*) in the upper panels of A and B represent significant differences ($p < 0.05$) compared to levels at 45 days of age. Asterisks (*) in the lower panels of A and B represent significant differences ($p < 0.05$) between total CA and MCA levels at the same age.

defined as total CA, and represent the primary product from the classic pathway of bile-acid biosynthesis. Taurine-conjugated α MCA and β MCA (T- α MCA and T- β MCA), as well as their unconjugated forms (α MCA and β MCA), were defined as total MCA, which represents the total primary bile acids synthesized from the alternative pathway and classic pathway. In serum, both total CA and MCA concentrations were markedly higher before 15 days of age than their concentrations thereafter (Figure 7.1.5A lower panel). As shown in Figure 7.1.5A lower panel, total CA was significantly higher than total MCA in serum from 1 day of age to 10 days of age. After day 15, both CA and MCA concentrations decreased markedly till 45 days of age.

In liver, both total CA and MCA concentrations were low before birth, followed by a marked increase right after birth (Figure 7.1.5B lower panel). The total CA concentrations in liver continued to increase at day 1 and day 3, but moderately decreased at 5 days of age. After day 5, the total CA concentrations increased again, peaked at 15 days of age, and decreased thereafter. For total MCA, the concentrations remained constant from day 0 to 5 days of age, and moderately increased after 10 days of age, peaked at 15 days of age, and decreased thereafter. Interestingly, similar to serum bile-acid concentrations, total liver CA was higher than total MCA during the neonatal period. In addition, from day 10 to day 20, total CA concentrations in liver tended to be higher than MCA, although statistical significance was not achieved. The total CA concentrations were also higher than total MCA in the livers of adult mice.

The concentrations of individual bile acids in serum and liver are shown in Figure 7.1.6 and 7.1.7. In serum, LC-MS/MS detected 11 bile acids, including T-CA, T- α MCA, T- β MCA, T- ω MCA, T-CDCA, T-DCA, as well as unconjugated bile acids, including CA, α MCA, β MCA, ω MCA, and DCA (Figure 7.1.6). In general, taurine-conjugated bile acids in serum were high from 1 to 20 days of age, and decreased after 30 days of age. However, the unconjugated bile acids in liver were low from 1 to 5 days of age, but increased after 10 days of age, and then decreased in adults. In liver, LC-MS/MS detected 17 bile acids, including 9 taurine-conjugated bile acids (T-CA, T- α MCA, T- β MCA, T- ω MCA, T-CDCA, T-DCA, T-HDCA, T-MDCA, and T-UDCA) (Figure 7.1.7A), and 9 unconjugated bile acids (CA, α MCA, β MCA, ω MCA, CDCA, DCA, HDCA, and UDCA) (Figure 7.1.7B). For conjugated bile acids, T-CA and T-CDCA tended to be high in livers up to 20-days of age; T- α MCA was only present in the neonatal period (day 0 to day 3), whereas the other bile acids were high in the adolescent period (around day 10 to 20). For unconjugated bile acids, α MCA, ω MCA, HDCA, and UDCA were present in livers only after 20 days of age. DCA was detected in livers immediately right after birth, and remained constant thereafter. CA, β MCA, and CDCA were detected right after birth, gradually increased, and peaked at 30 days of age, but decreased moderately by day 45.

Figure 7.1.6

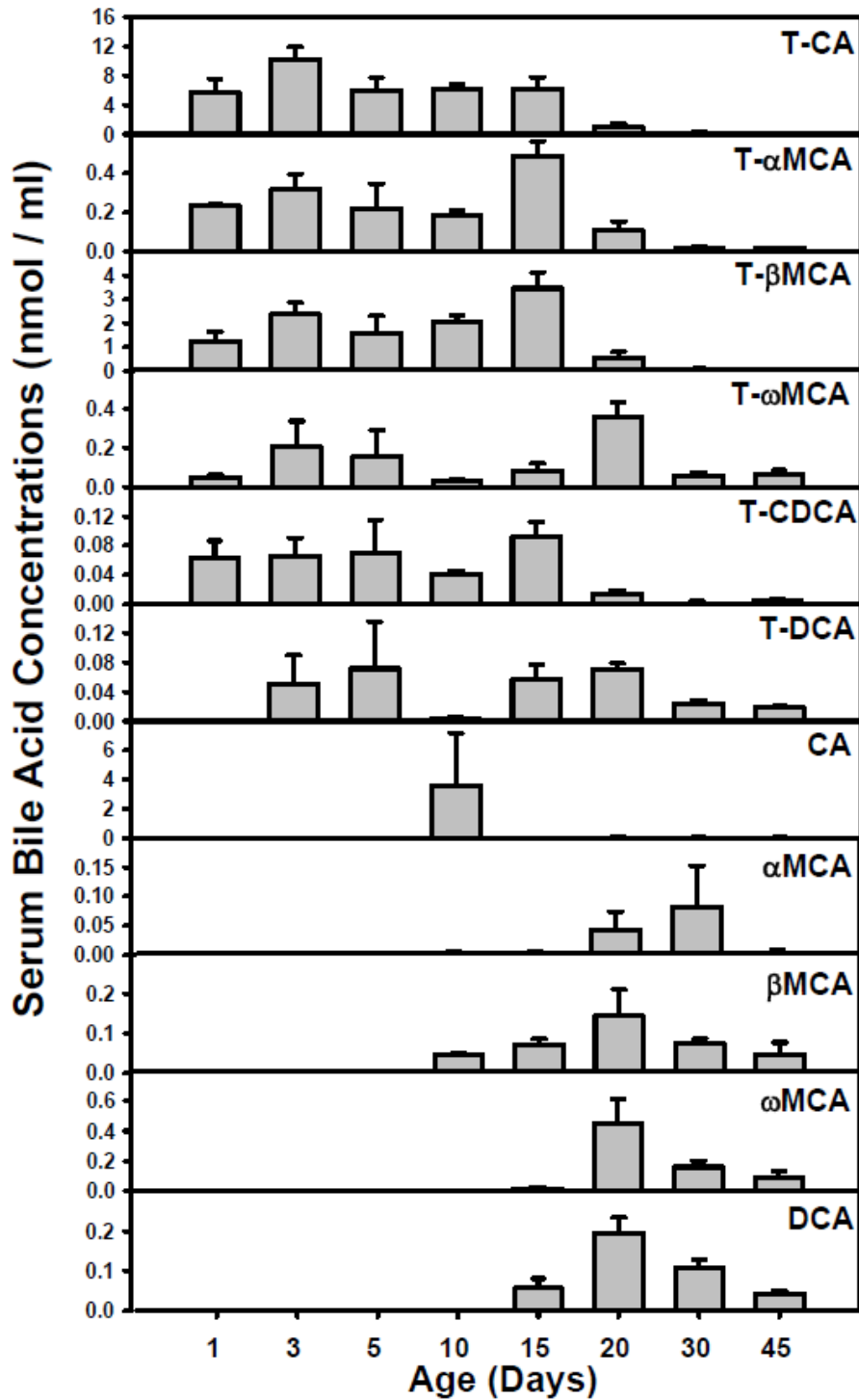


Figure 7.1.6. Serum unconjugated bile-acid concentrations during development (n=3 per age). Bile acids from serum were quantified by LC-MS/MS as described in MATERIALS AND METHODS. Data are expressed as nmol of bile acids per ml.

Figure 7.1.7

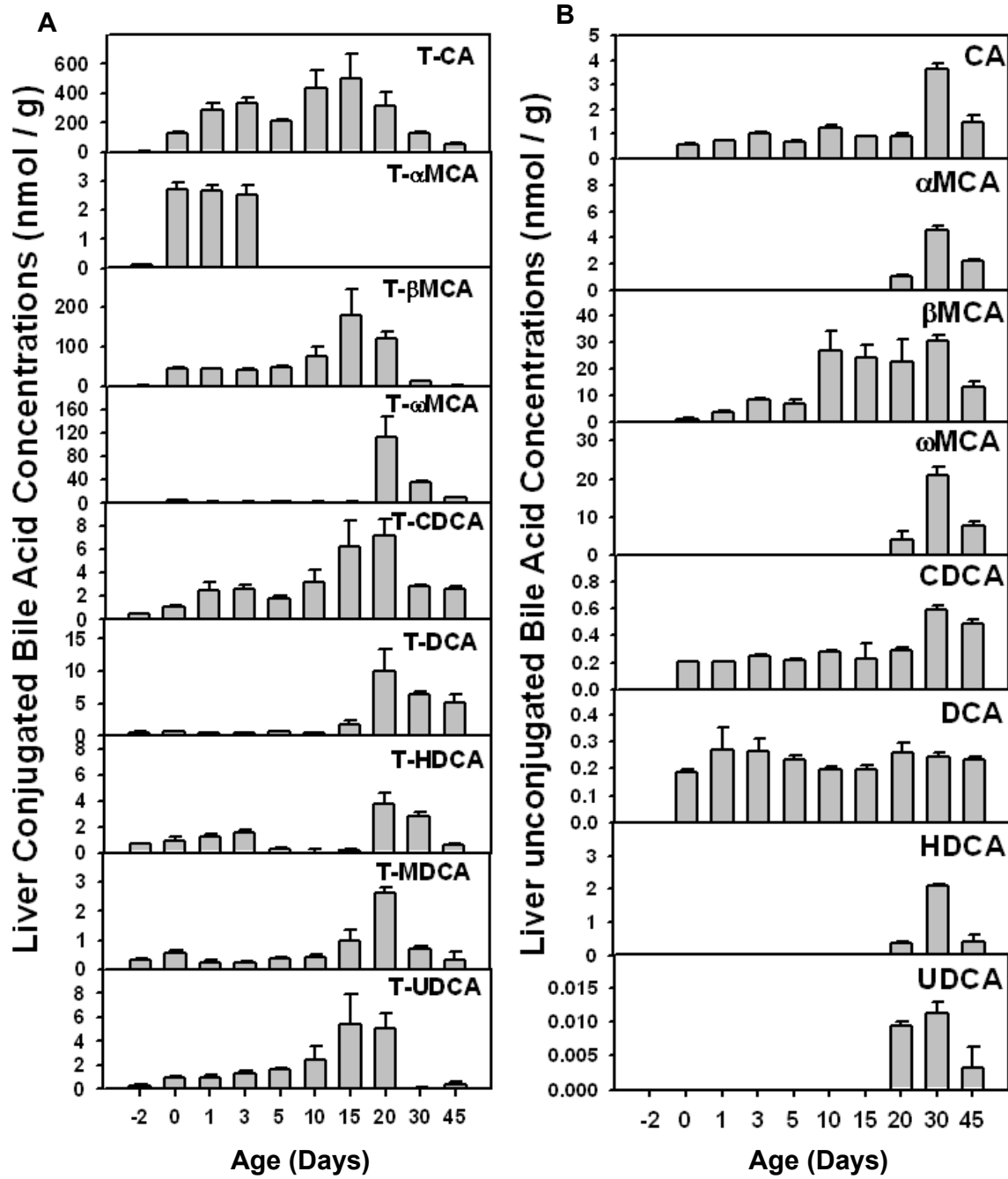


Figure 7.1.7. Liver conjugated (A) and unconjugated (B) bile-acid concentrations during development (n=3 per age). Bile acids from liver were quantified by LC-MS/MS as described in MATERIALS AND METHODS. Data are expressed as nmol / g.

To further consolidate the hypothesis that the classic pathway of bile-acid biosynthesis predominates in the neonatal period, percentages of bile acids in serum and liver were calculated at day 1 of age in comparison to day 45 (Figure 7.1.8). In both serum and liver, T-CA was the predominant bile-acid at day 1 of age (77.8% of total bile acids in serum, and 82.9% of total bile acids in liver). In contrast, at 45 days of age, although T-CA was still a major bile-acid, it decreased to 22% in serum, and 52.3% in liver. In addition, there was an increase in both the variety and percentages of other bile acids increased in adults.

In summary, both serum and liver bile acids increased right after birth, and the high bile acid concentrations associate with the high mRNA expression of liver transporters involved in the enterohepatic circulation of bile acids. The major bile acids in both serum and liver are taurine conjugates, and T-CA is the predominant bile-acid in newborns, providing strong evidence that the classic pathway of bile-acid biosynthesis predominates during the neonatal period (from day 0 to 5).

Neonatal up-regulation of FXR and PXR pathways in liver. FXR and PXR are major bile-acid sensors in liver. To determine whether FXR and PXR are expressed in newborns, and whether FXR- and PXR-mediated pathways are activated by high concentrations of bile acids in newborns, the mRNA expression

Figure 7.1.8

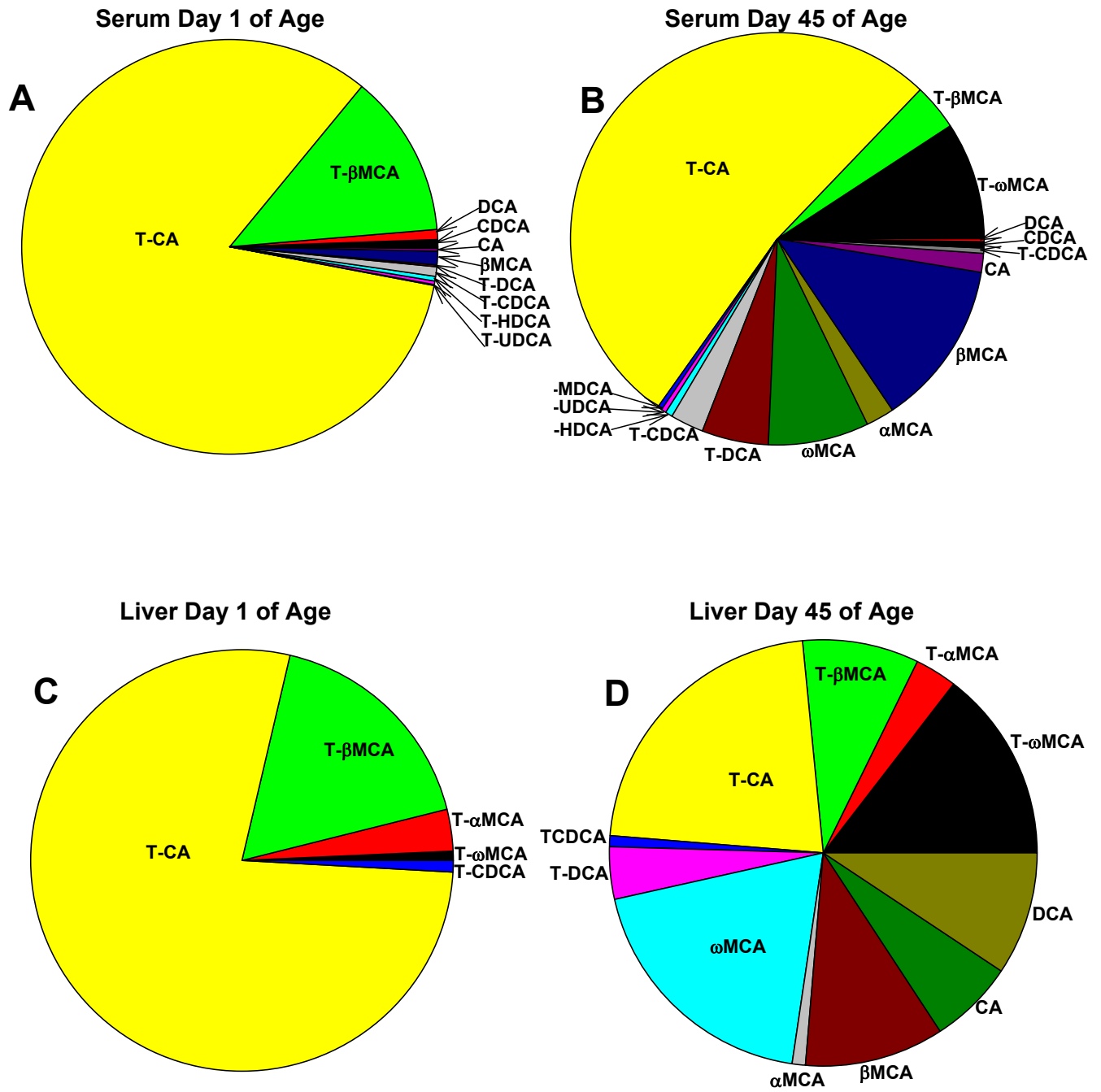


Figure 7.1.8. Percentage of various components of bile acids in serum (A and B) and liver (C and D) at day 1 (A and C) and 45 days of age (B and D). Bile acids were quantified by LC-MS/MS as described in MATERIALS AND METHODS.

of both FXR and PXR, as well as their prototypical target genes were quantified from day -2 to day 5 of age (Figure 7.1.9). FXR mRNA was low before birth, followed by an increase at birth (1.5-fold higher than prenatal levels), then peaked at day 1 of age (3.4-fold), but decreased at day 3 (1.6-fold) and day 5 (1.6-fold) of age (Figure 7.1.9A). Correlated with the “day-1 surge” pattern of FXR-mRNA expression, the mRNA of the prototypical FXR-target gene, SHP, also increased in newborns and peaked at day 1 of age (20 times of prenatal levels) (Figure 7.1.9B). Similar to the expression pattern of FXR, PXR mRNA also increased after birth, and peaked at day 1 of age (4.3-fold of prenatal levels) (Figure 7.1.9C). The prototypical PXR-target gene, Cyp3a11, also peaked at day 1 of age (18-fold prenatal levels) (Figure 7.1.9D). In summary, the “day-1 surge” pattern was observed in both FXR and PXR mRNA in liver, as well as in their prototypical target genes, indicating not only the major bile-acid sensors are highly expressed in newborn liver, but also the FXR- and PXR-mediated pathways are functionally activated. In contrast, although the ileal FXR and PXR mRNA expression were increased in newborns, their target genes were not readily activated in ileums of newborns (Figure 7.1.10), indicating a delayed maturation of FXR and PXR pathways in newborn ileum compared to fully functioning FXR and PXR pathways in newborn liver.

Expression of liver transporters in FXR and PXR-null mice at day 1 of age.

To determine whether FXR and PXR contribute to the “day-1 surge” pattern of hepatic transporters (Ntcp, Bsep, Mdr2, Mrp4, and Ost β), the mRNA of these

Figure 7.1.9

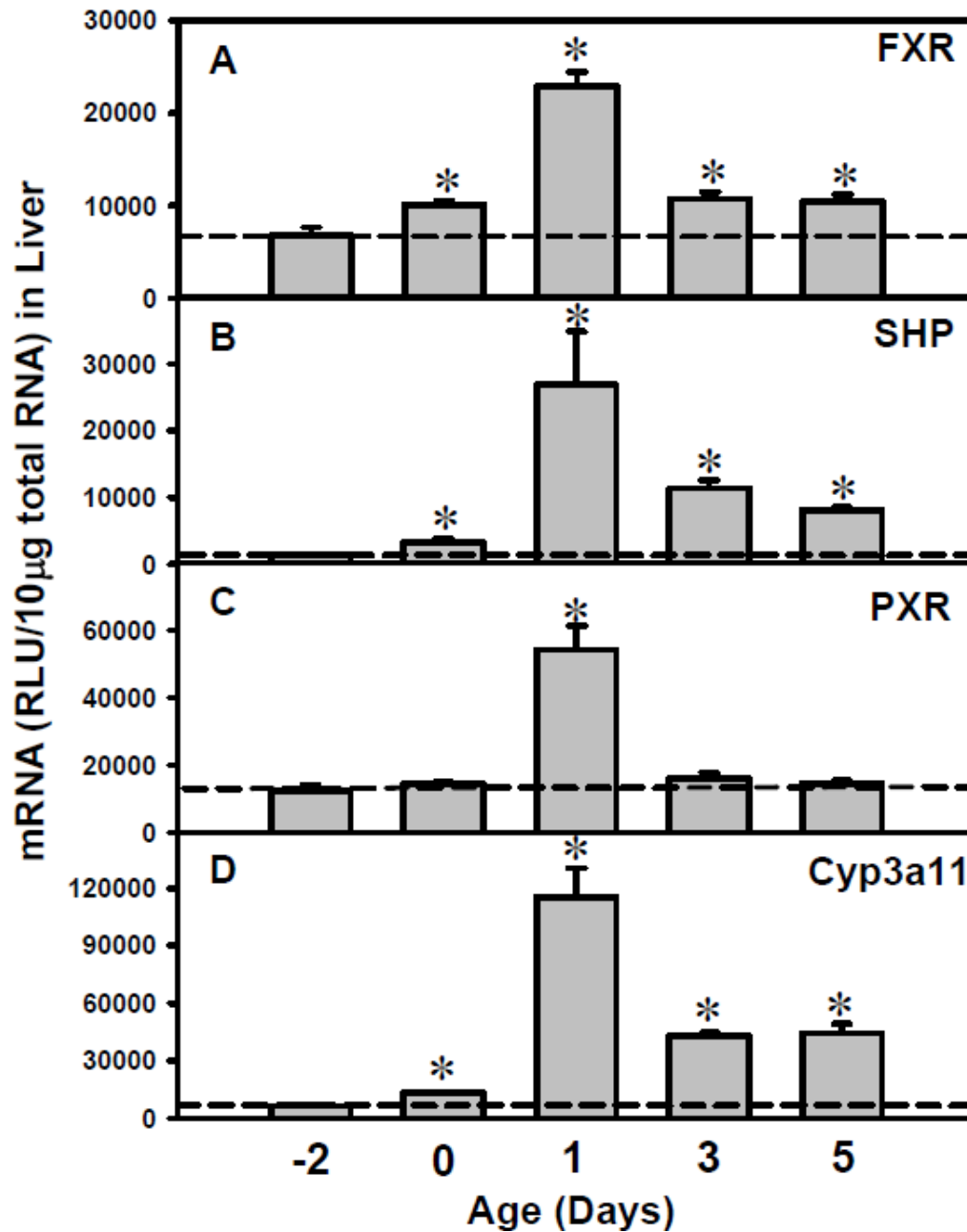


Figure 7.1.9. Up-regulation of the mRNA expression of FXR, SHP (prototypical target gene of FXR), PXR, and Cyp3a11 (prototypical target gene of PXR) in neonatal wild-type mouse livers. Total RNA was isolated from liver at each age and analyzed by the bDNA assay as described in MATERIALS AND METHODS. Data are presented as mean RLU \pm S.E.M. (n = 5 animals). Asterisks (*) represent significant differences (p < 0.05) compared with values at day -2 of age.

Figure 7.1.10

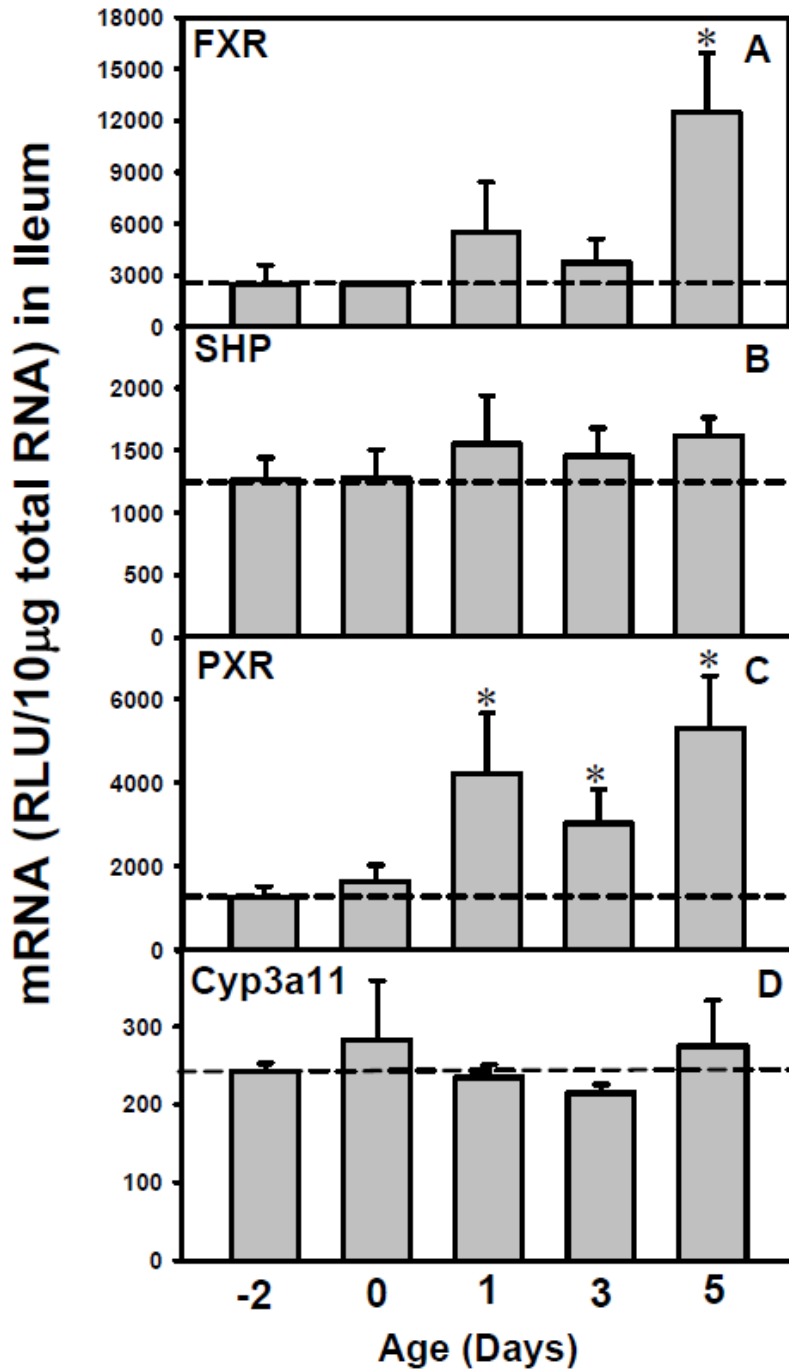


Figure 7.1.10. Messenger RNA expression of FXR, SHP (prototypical target gene of FXR), PXR, and Cyp3a11 (prototypical target gene of PXR) in neonatal wild-type mouse ileum. Total RNA was isolated from ileum at each age and analyzed by the bDNA assay as described in MATERIALS AND METHODS. Data are presented as mean RLU \pm S.E.M. (n = 5 animals). Asterisks (*) represent significant differences (p < 0.05) compared with values at day -2 of age.

transporters was quantified in livers from FXR- and PXR-null mice at day 1 of age (Figure 7.1.11A). In PXR-null mice, the “day-1 surge” pattern of all five hepatic transporters was still maintained. In contrast, in FXR-null mice, except for Mrp4, which remained unchanged, the mRNA expression in liver at day 1 was attenuated for Ntcp, Bsep, Mdr2, and Ost β , which were 66%, 18%, 56%, and 45% of wild-type levels, respectively, but Mrp4 mRNA remained unchanged (Figure 7.1.11A). At day 3 and 5 of age, the expression of Bsep and Ost β in FXR-null mouse liver was still lower than that in wild-type mice, whereas the expression of Ntcp and Bsep was similar between FXR-null and wild-type mice (data not shown). To determine whether FXR and PXR contribute to the neonatal up-regulation of the ileal bile-acid efflux transporters, Ost α and Ost β , the mRNA of these transporters was quantified in livers from FXR- and PXR-null mice at day 1 of age (Figure 7.1.11B). In PXR-null mice, the “day-1 surge” pattern of Ost α and β transporters was maintained. In contrast, in FXR-null mice at 1 day of age, the expression of both Ost α and β was decreased, which were 39% and 32% of wild-type levels, respectively. In summary, the “day-1 surge” pattern of the liver transporters Ntcp, Bsep, Mdr2, and Ost β , as well as the ileal transporters, Ost α and β , was attenuated in FXR-null mice, but not in PXR-null mice.

Immunofluorescence staining of Ntcp and Bsep in livers of wild-type and

FXR-null mice at day 1 of age. To determine whether the protein expression and membrane localization of transporters were also impaired in FXR-null mice

Figure 7.1.11

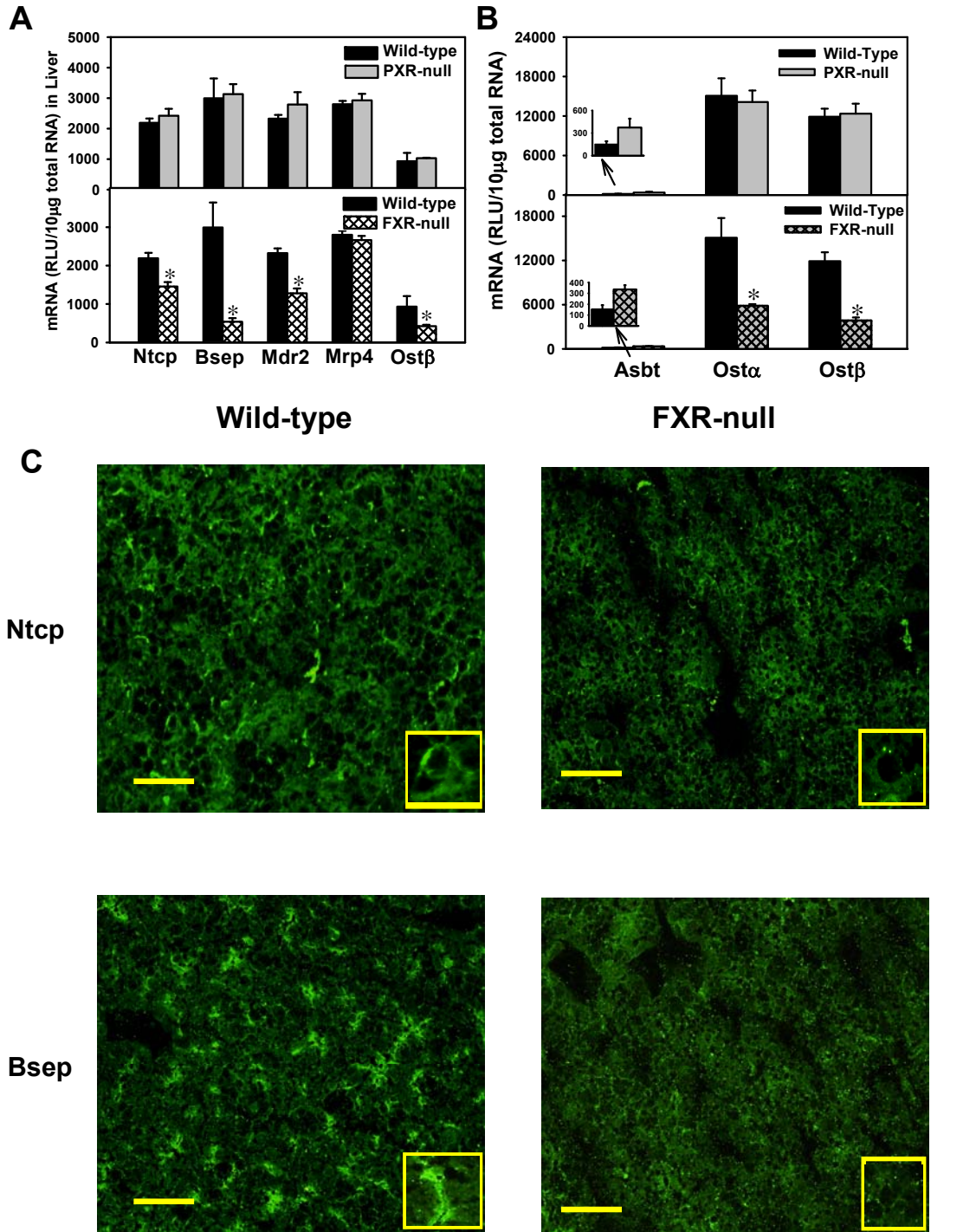


Figure 7.1.11. A. The mRNA expression of liver transporters Ntcp, Bsep, Mdr2, Mrp4, and Ostβ in wild-type, PXR-null (upper panel), and FXR-null mice (lower panel) at 1 day of age. B. The mRNA expression of ileal transporters Asbt, Ostα, and Ostβ in wild-type, PXR-null (upper panel), and FXR-null mice (lower panel) at 1 day of age. C. Immunofluorescence of Ntcp and Bsep protein in livers from wild-type and FXR-null mice at day 1 of age. Immunofluorescence against basolateral Ntcp protein as well as canalicular Bsep (green) was conducted on liver cryosections as described in MATERIALS AND METHODS. Portions of images were enlarged and provided as inserts. Representative images are shown. Bar, 50 μm.

in newborns, immunofluorescence staining of Ntcp and Bsep was performed on frozen liver sections of wild-type and FXR-null mice at day 1 of age (Figure 7.1.11C). The staining of Ntcp protein was reduced, but still detectable in livers of FXR-null mice, indicating FXR at least partially contributes to the “day-1 surge” pattern of Ntcp in liver. The canalicular staining of Bsep protein was decreased in livers of FXR-null mice, suggesting FXR is important in maintaining the neonatal surge of Bsep expression.

Expression of liver transporters and bile-acid synthesizing enzymes in human liver during development. To determine the clinical significance of the present findings, the mRNA expression of the following genes was determined in human liver during development from gestational day 96, to 21 years of age. The major bile-acid uptake transporter NTCP, the rate-limiting bile-acid efflux transporter BSEP, the phospholipid transporter MDR3 (the ortholog for mouse Mdr2), as well as the mRNAs of CYP7A1 and 8B1 for the classic pathway of bile-acid biosynthesis were quantified in human livers (Figure 7.1.12). Minimal mRNA expression of these genes was observed between gestational day 96 to 108, followed by a marked increase within 1 year of age. For example, the mRNA of NTCP increased 14.7-fold in the neonatal period (from birth to 1 year of age), the mRNA of BSEP increased 2.4-fold, the mRNA of MDR3 increased 9.6-fold, the mRNA of CYP7A1 increased 27.7-fold, and the mRNA of CY8B1 increased 11.3-fold. The levels of these genes appear to remain high between 1 to 4 years of age, followed by another increase between 7 to 14 years of age, but

Figure 7.1.12

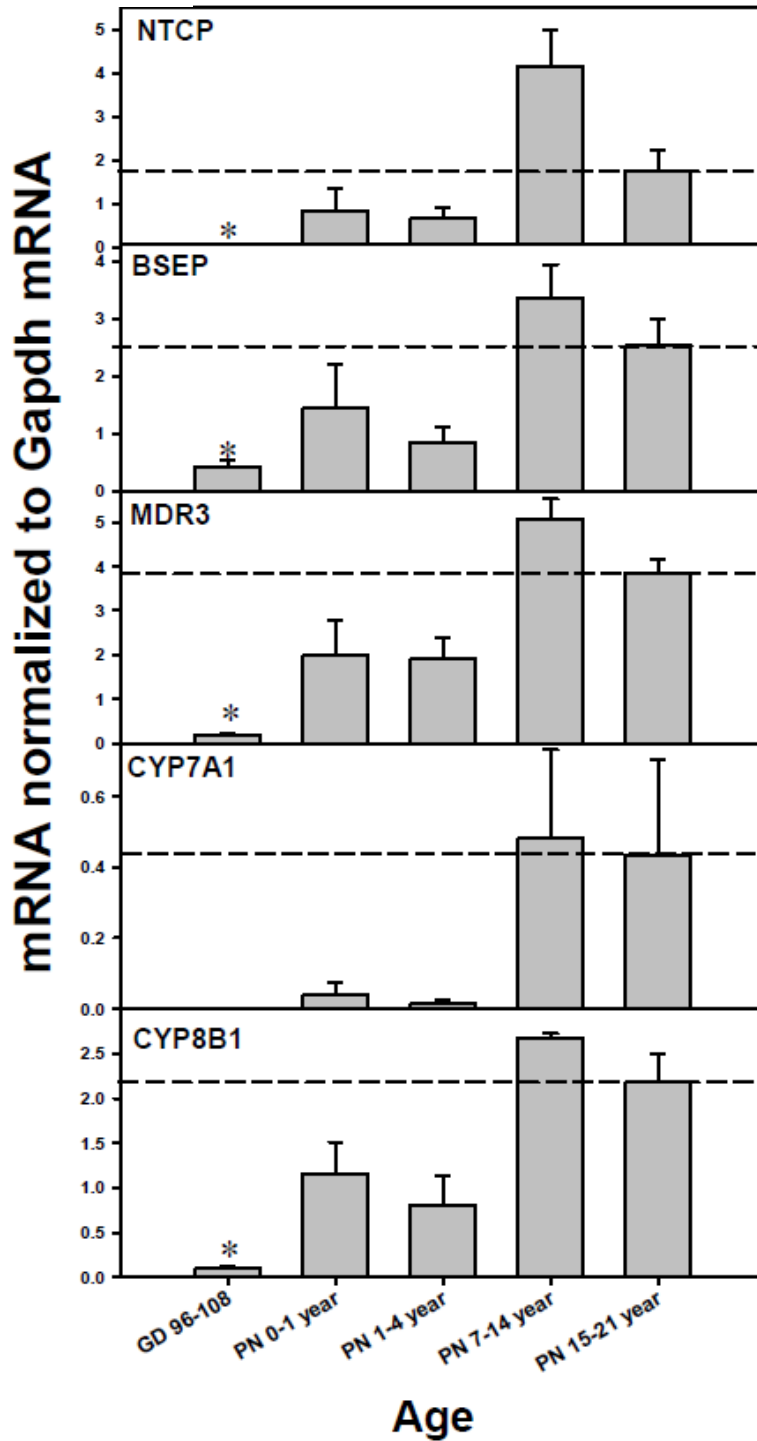


Figure 7.1.12. Messenger RNA expression of human transporters (NTCP, BSEP, and MDR3), as well as bile-acid bio-synthetic enzymes (CYP7A1 and 8B1) in human livers during development. Total RNA was isolated from liver at each age and analyzed as described in MATERIALS AND METHODS.

decreased to adult levels thereafter (15 to 21 years of age). These data indicate that in humans, there is also a marked increase in the expression of bile-acid transporters and synthesizing enzymes for the classic pathway in newborn liver, although there seemed to be a secondary increase of these genes in the adolescent period.

DISCUSSION

In conclusion, the present study revealed a “day-1 surge” pattern in the expression of major transporters involved in the enterohepatic circulation of bile acids in newborns. Increased bile acids via the classic pathway of biosynthesis correlated with the "day-1 surge" pattern of these transporters, through activating the FXR-mediated pathway. Our working model is that during development, increased bile-acid biosynthesis occurs in liver during the neonatal period primarily by the classic pathway, and this contributes to the increased bile acids in newborns. In turn, high concentrations of bile acids activate both the FXR and PXR receptors, but FXR is responsible for the "day-1 surge" pattern of hepatic transporters for the EHC of bile acids (Figure 7.1.13).

Transporters are essential in maintaining the enterohepatic circulation of bile acids, evidenced by numerous clinical cases in pediatrics and animal studies using gene knock-out mice. For example, Bsep is the major bile-acid efflux transporter in liver that determines bile flow, and inborn errors in human BSEP results in severe progressive familial intrahepatic cholestasis (PFIC type II) (Wang et al., 2002), as well as hepatocellular carcinoma in young children (Knisely et al., 2006). In addition, although the phospholipid transporter Mdr2 in liver does not transport bile acids, the defect in its human analog MDR3 results in progressive familial intrahepatic cholestasis (PFIC type III) (de Vree et al., 1998). Mdr2-null mice develop hepatocyte degeneration and focal necrosis, as well as abnormalities in bile composition (Smit et al., 1993), indicating the importance of

Figure 7.1.13

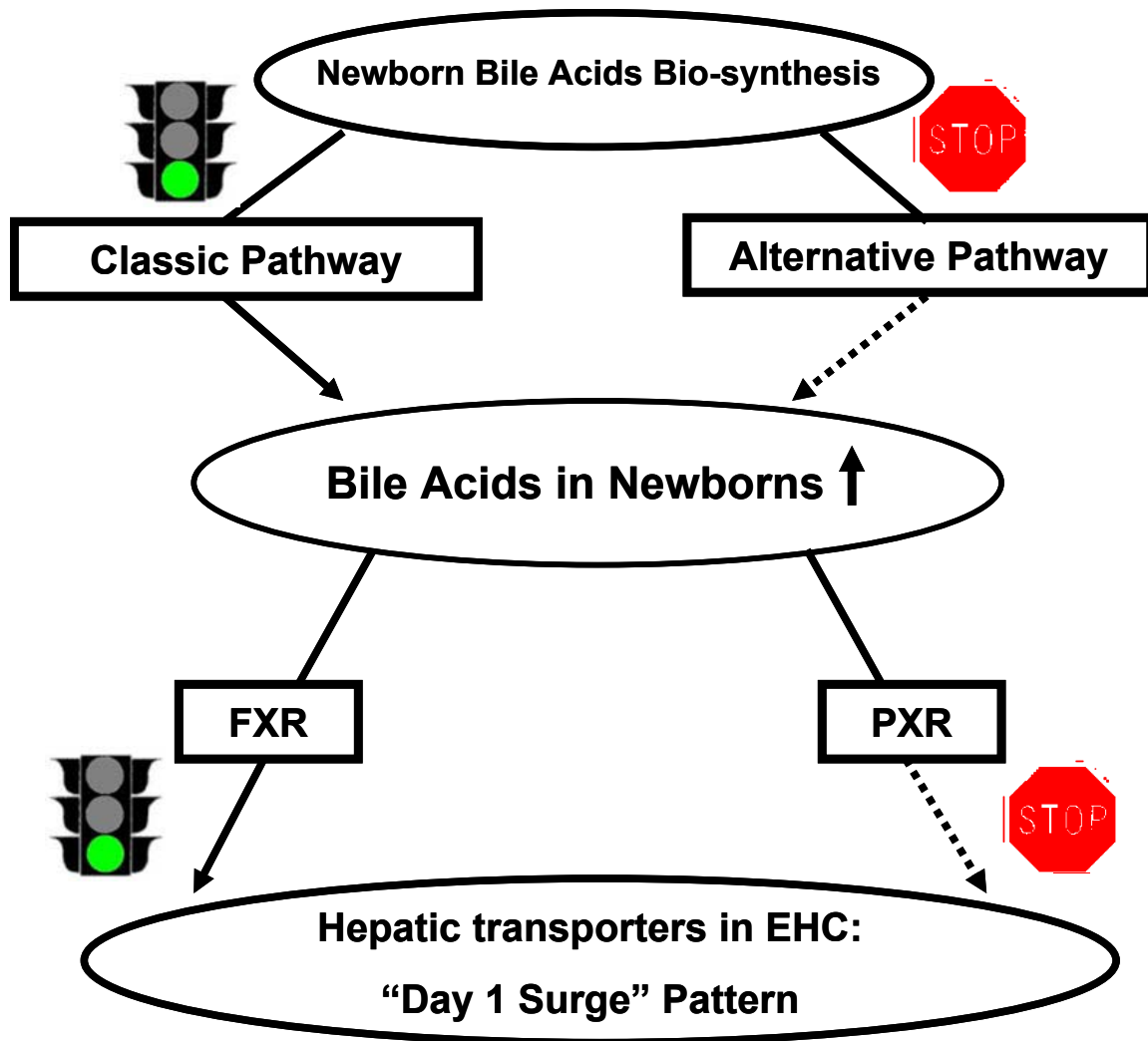


Figure 7.1.13. A schematic of the working hypothesis for the molecular mechanisms underlying the neonatal induction of hepatic transporters involved in EHC.

Mdr2/MDR3 in maintaining bile-acid circulation and liver protection. On the basolateral membrane of hepatocytes, Ntcp is the major bile-acid uptake transporter that brings serum bile-acids back into hepatocytes, evidenced by a 95% blockade of sodium-dependent bile-acid uptake following a Ntcp-specific antisense oligonucleotide administration (Hagenbuch et al., 1996). By transporting the bile acids back into liver, Ntcp keeps bile acids in the EHC for the next cycle of nutrient absorption, and prevents toxicity to extrahepatic organs.

The basolateral bile-acid efflux transporters, Mrp4, Ost α , and Ost β are very lowly expressed in liver (Maher et al., 2005b). The low expression of basolateral efflux transporters reflects a conservative mechanism to minimize the leakage of bile acids into the systemic circulation, so as to preserve most bile acids in the EHC for nutrient absorption. To note, these basolateral bile-acid efflux transporters are often induced during cholestasis for hepatic protection. For example, Mrp4-null mice have more severe liver injury than wild-type mice following bile-duct ligation (Mennone et al., 2006).

The general dogma for the regulation of Ntcp states that high levels of bile acids decrease Ntcp mRNA expression through activating the FXR-SHP signaling pathway in liver, as observed in various cholestasis models (Liu et al., 2003; Slitt et al., 2007) and bile-acid feeding studies (Zollner et al., 2005) performed in adult mice or rats. Teleologically this may be protective, because unrestricted hepatic influx of bile acids from serum might lead to accumulation of

toxic bile acids in hepatocytes. However, the present study challenges the existing paradigm by demonstrating that both Ntcp mRNA and protein immunofluorescence staining are high in newborn livers, despite approximately 2-fold higher bile-acid concentrations at birth than that at 45 days of age, and up-regulated hepatic FXR-SHP pathway in newborns. In addition, the present study also demonstrates that the “day-1 surge” pattern of Ntcp is dependent on the presence of the FXR- signaling pathway in newborns. Evidence from clinical studies demonstrates that children with severe hypercholanemia had normal expression of NTCP, even though the serum concentrations of bile acids were extremely high (Shneider et al., 1997). Thus the regulation of Ntcp by bile acids is not as simple as anticipated. It can be speculated that the FXR-SHP signaling pathway is not the major pathway in regulating the expression of Ntcp in newborns, but FXR may be involved in certain neonatal-predominant signaling pathways that promote the “day-1 surge” pattern of Ntcp in newborns. It is well-known that before birth, liver is mainly a haematopoietic organ, whereas after birth, it becomes the major organ for chemical metabolism and detoxification. Therefore, functionally speaking, during the neonatal period when bile acids are high in serum and liver due to the immaturity in EHC, it is necessary to up-regulate Ntcp in liver to reduce bile-acid concentrations in the systemic circulation, even at the cost of stressing the hepatocytes, so as to protect extrahepatic organs that are critical for survival, including the brain where the blood-brain barrier is not completely functioning, as well as other developing organs that are vulnerable to bile-acid-induced toxicity.

Previous studies have determined the ontogenic expression of Ntcp and Bsep in rat livers. It has been shown that Ntcp mRNA was detectable by northern blot as early as gestation day 18 in rat liver when sodium-dependent bile-acid transport already occurs (Boyer et al., 1993). The present study has shown that the mouse Ntcp mRNA was very low before birth (day -2), but increased markedly after birth. In addition, the expression of Bsep was undetectable in prenatal rat livers, but a marked up-regulation of Bsep protein occurred in newborn rat livers (Zinchuk et al., 2002). The present study further demonstrates that the induction of Bsep in newborn mouse liver might be due to activation of FXR, likely by direct activation, because it has been demonstrated that Bsep is a FXR-target gene (Plass et al., 2002).

A large body of evidence indicates that FXR is important in regulating bile-acid homeostasis, lipid metabolism, and glucose metabolism in adults (Chiang, 2004). FXR-null mice have elevated serum bile-acid concentrations in adults (Sinal et al., 2000), indicating the important role of FXR in bile-acid synthesis and/or disposition. Less is known of the role of FXR during development. Clinically, decreased FXR expression in ileum was observed in children with progressive familial intrahepatic cholestasis type I (Chen et al., 2004), and functional variants of FXR in liver have been identified in intrahepatic cholestasis of pregnancy (Van Mil et al., 2007), indicating FXR is important for both perinatal and maternal bile-acid homeostasis. The present study demonstrates that FXR is at least partially involved in mediating the “day-1 surge” of hepatic and ileal

transporters to promote the enterohepatic circulation of bile acids, so as to facilitate the absorption of fat-soluble nutrients in newborns. Mrp4 is the only transporter whose neonatal surge is independent of FXR. It has been shown that the constitutive androstane receptor (CAR) can induce Mrp4 expression in mouse liver (Assem et al., 2004; Maher et al., 2005a; Slitt et al., 2006), and the expression of CAR mRNA is up-regulated right after birth (our lab's unpublished data). Therefore, it can be speculated that CAR contributes to the moderate induction of hepatic Mrp4 at 1 day of age.

It has been suggested that “physiological cholestasis” in newborns is due to the immaturity of the EHC and delayed hepatic clearance of bile acids (Suchy et al., 1981). However, how the neonatal bile-acid concentrations are elevated remains poorly understood. It has been demonstrated that maternal cholestasis in rat does not affect the expression of Ntcp in pups (Arrese et al., 1998), indicating the high levels of bile acids in newborns is not likely from the mother through placental transfer. The present study demonstrates that the increase in bile-acid concentrations in newborns is likely due to up-regulation of the classic pathway of bile-acid synthesis, as evidenced by the marked increase in Cyp7a1 and 8b1 mRNAs, as well as increase in taurine-conjugated cholic acid in newborns. It is well known that oxysterols, which are metabolized from cholesterol, serve as ligand for the liver X receptor (LXR), and in turn, LXR transcriptionally up-regulates Cyp7a1 in mice (Chiang, 2004). Therefore, it is possible that the up-regulation of the classic pathway of bile-acid synthesis is

triggered by cholesterol-enriched milk from the mother. In addition, the low expression of the suppression signal Fgf15 from the intestine also provides a permissive environment to allow the induction of Cyp7a1. Although Cyp39a1 from the alternative pathway was also induced in newborns, the significance of this 24-hydroxysterol 7-hydroxylase in producing bile acids in liver is not well understood.

Various bile acids have different affinities towards FXR. Chenodeoxycholic acid has been shown to be the most potent FXR agonist in cell cultures (Pellicciari et al., 2005). In addition, 6 α -ethyl-chenodeoxycholic acid (6-ECDCA) is a potent and selective FXR agonist endowed with anti-cholestatic activity when given to an *in vivo* rat model of cholestasis (Pellicciari et al., 2002). However, CDCA and 6-ECDCA are either very low or not synthesized in mice. Another study showed that the FXR target gene Bsep in mice can be induced by cholic-acid feeding in a FXR-dependent manner, indicating that cholic acid might also be a ligand for FXR (Zollner et al., 2005). Therefore, during neonatal period, the increased concentrations of cholic acid are likely the mechanism for the FCR-mediated pathway.

At later ages (from day 20 to day 30), serum bile-acid concentrations decreased in wild-type mice, whereas liver bile-acid concentrations remained high, and correlated with high mRNA levels of the bile-acid synthesizing enzymes (Cyp7a1, 8b1, and 27a1). The decrease in serum bile-acid concentrations

probably reflects maturation of other bile-acid uptake transport systems in liver at later ages, for example, the basolateral uptake transporters Oatp1a1, 1a4, and 1b2 increase gradually, and reach adult levels at around day 30 of age (Cheng et al., 2005a). The Oatps may act in concert with Ntcp to further reduce serum bile acids and thus protect other organs from bile-acid toxicity.

During the neonatal period, the expression profiles of a gene can be different in liver and ileum. For example, the prototypical target genes of FXR and PXR (SHP and Cyp3a11) were only up-regulated in liver but not in ileum, even though FXR and PXR mRNAs were increased in both tissues. *Ost α* , a well-known FXR target gene (Zollner et al., 2006), was only induced in newborn ileum but not in liver. In addition, the intestinal *Fgf15*, which is a target of FXR, was not induced at day 1 even though FXR mRNA is induced at this age. The mechanism for the tissue-specific regulation of these genes is not clearly understood, but it can be speculated that certain epigenetic mechanisms, like microRNAs, might regulate the expression of certain genes in the intestine, like FXR and PXR, and either inhibit the formation of a functional protein, or decrease mRNA stability. The post-transcriptional modifications of these genes in liver and ileum will be determined in future studies.

The present study provides some insights in understanding the mechanisms for the maturation of enterohepatic circulation of bile acids in the neonatal period,

and demonstrates that FXR might be a therapeutic target in regulating bile acids and nutrient homeostasis in pediatric patients.

CHAPTER SEVEN

DEVELOPMENTAL REGULATION OF LIVER TRANSPORTERS IN MICE

Part Two

Regulation of Xenobiotic Transporters by PXR

In Part One of this chapter, I characterized that the bile-acid sensor FXR is important in triggering the neonatal upregulation of several transporters involved in the enterohepatic circulation of bile acids. These transporters are mainly endobiotic transporters, including the bile-acid transporters Ntcp, Bsep, and Ost β , as well as the phospholipid transporter Mdr2. However, the ontogenic expression patterns and regulatory mechanisms of transporters involved in the disposition of xenobiotics remain to be determined. Therefore, in this chapter, the ontogeny and mechanisms underlying the regulation of these genes will be discussed. One example will be given for each class of transporters (basolateral uptake, basolateral efflux, and canalicular efflux) for regulatory mechanisms.

Based on their critical roles in chemical disposition in liver, for basolateral uptake transporters, Oatp1a1, Oatp1a4, Oatp1b2, Oatp2b1, Oct1, Oat2, and Ent1 have been selected (Klaassen and Lu, 2008). For canalicular transporters, Bcrp, Mrp2, Mate1, Atp8b1, Abcg5, and Abcg8 have been selected. For basolateral efflux transporters, Mrp3, Mrp6, and Abca1 have been selected. As shown from Figure 7.2.1 to 7.2.3, the majority of these transporters was low before birth, and then increased from adolescent to adult ages. The only exception is Bcrp mRNA, which was enriched in perinatal ages and decreased markedly after birth, corresponding to its critical role as a heme efflux transporter during the fetal to neonatal functional transition during liver maturation. Figure 7.2.4A is a heatmap of the associations of these transporter mRNAs, and the

Figure 7.2.1

Ontogeny of Mouse Liver Basolateral Uptake Transporters

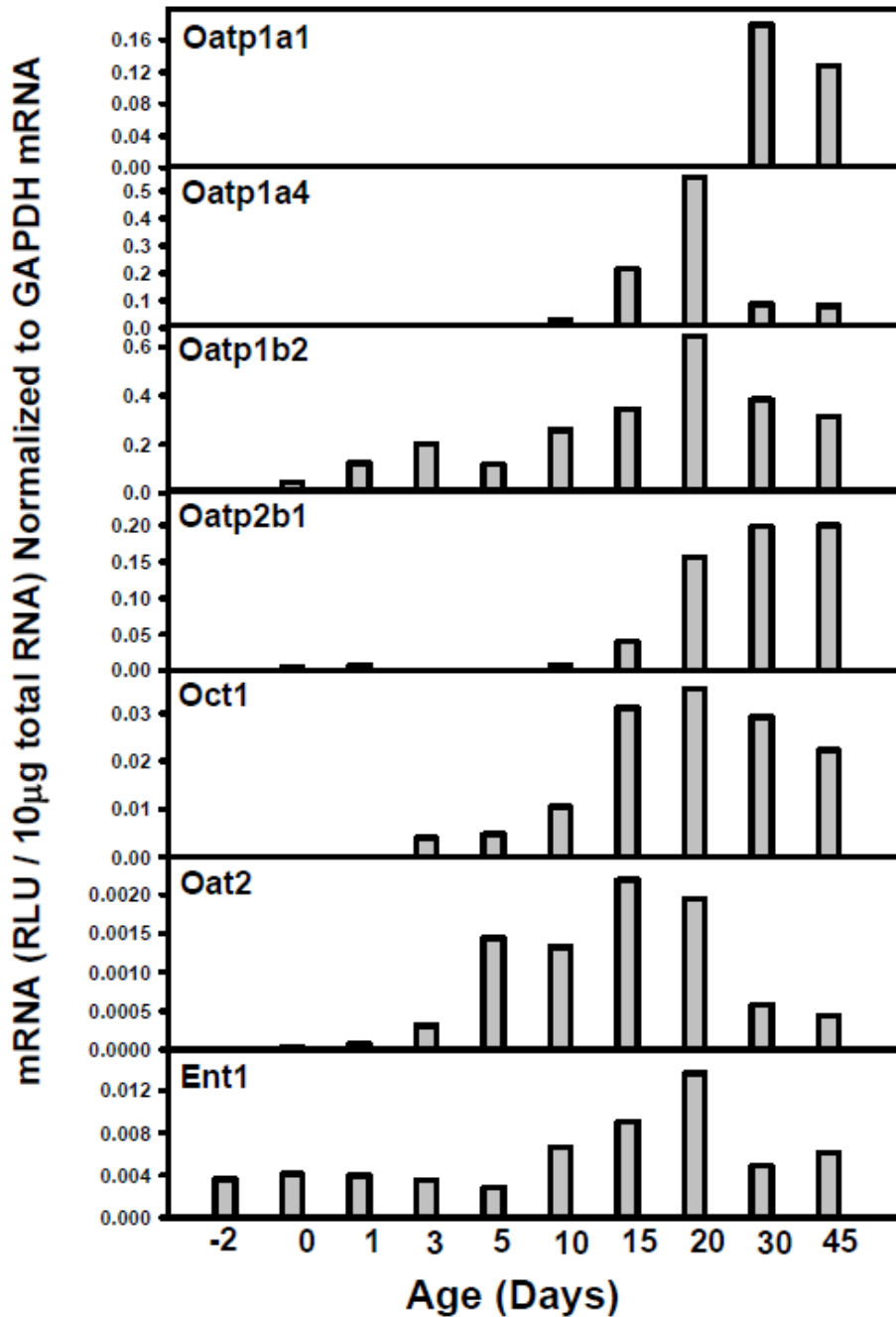


Figure 7.2.1. Messenger RNA expression of other basolateral update transporters in livers of wild-type mice during development. Total RNA was isolated from liver at each age and analyzed as described in MATERIALS AND METHODS. Individual samples (n=5) were pooled at each age, and data were analyzed by bDNA assay. Data are presented as RLU normalized to Gapdh mRNA.

Figure 7.2.2

Ontogeny of Mouse Liver Basolateral Efflux Transporters

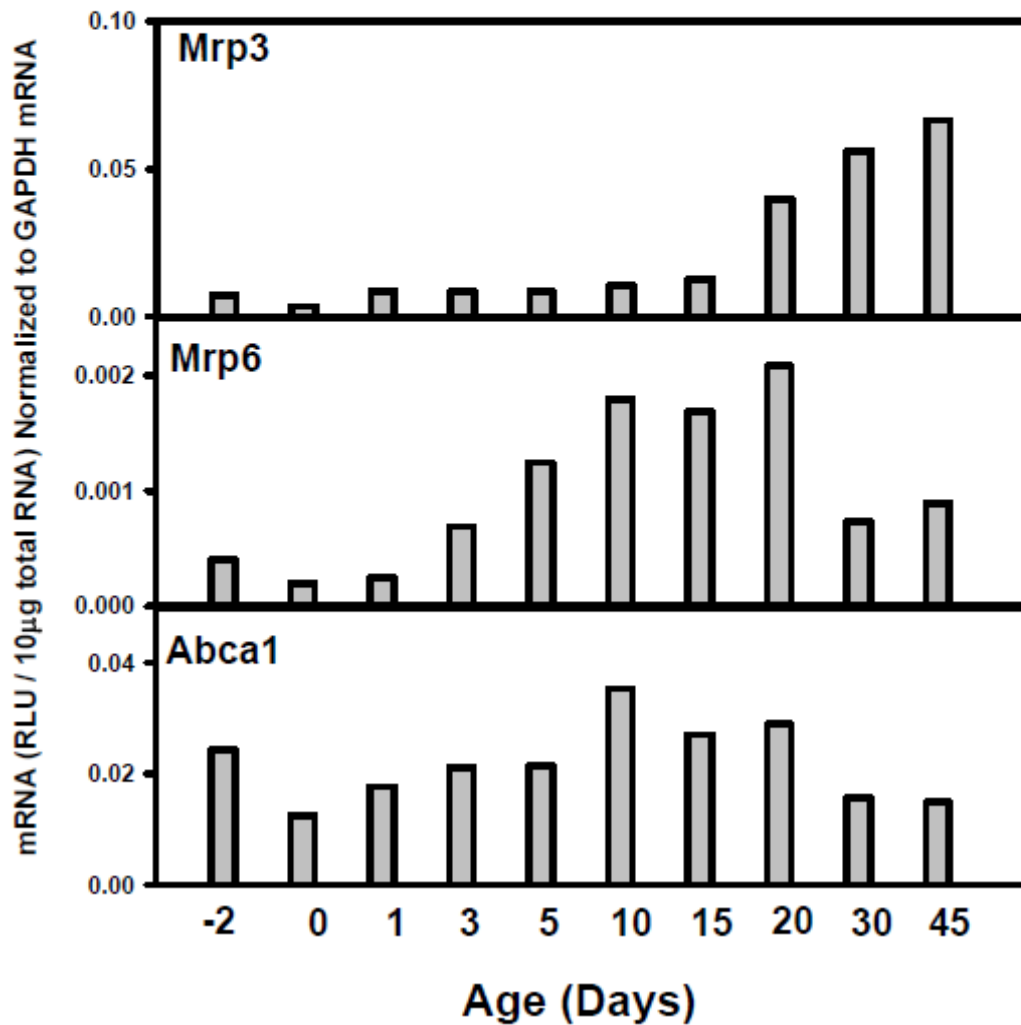


Figure 7.2.2. Messenger RNA expression of other basolateral efflux transporters in livers of wild-type mice during development. Total RNA was isolated from liver at each age and analyzed as described in MATERIALS AND METHODS. Individual samples (n=5) were pooled at each age, and data were analyzed by bDNA assay. Data are presented as RLU normalized to Gapdh mRNA.

Figure 7.2.3

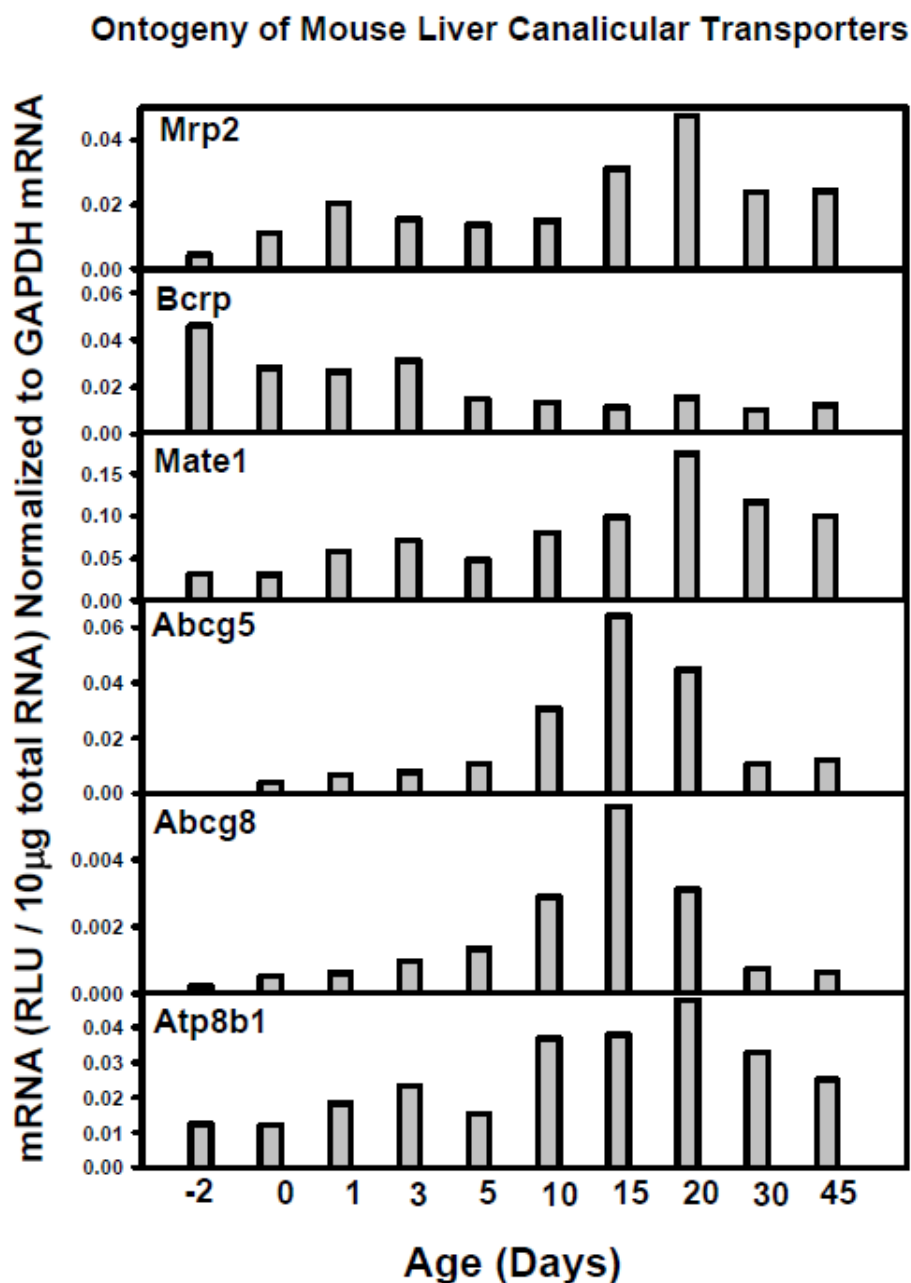


Figure 7.2.3. Messenger RNA expression of other canalicular efflux transporters in livers of wild-type mice during development. Total RNA was isolated from liver at each age and analyzed as described in MATERIALS AND METHODS. Individual samples (n=5) were pooled at each age, and data were analyzed by bDNA assay. Data are presented as RLU normalized to Gapdh mRNA.

data demonstrated that except for Bcrp mRNA, they all tended to be highly expressed after 10 days of age.

For the majority of these postnatal-enriched xenobiotic transporters, PXR appears to be good candidate transcription factor to trigger their increased expression during liver maturation. First, PXR is a critical sensor for xenobiotics. Second, PXR mRNA is markedly increased after birth and peaked around adolescent period (Figure 7.2.4). Therefore, I hypothesize that PXR is a critical regulator of these xenobiotic transporters, either by direct binding to DNA, or by indirect effects.

The postnatal enrichment of the xenobiotic sensor PXR during development appears to be a good candidate for the postnatal enrichment of the basolateral uptake transporter Oatp1a4 mRNA in mice. Oatp1a4 has been reported to be a direct PXR-target gene in rat liver by Guo et al. (Guo et al., 2002). They demonstrated that treatment of rats with the PXR agonist, PCN, significantly enhanced the rat Oatp1a4 mRNA expression, and eletrophoretic mobility shift assays showed that PXR binds to a DR-3 consensus sequence with the highest affinity around 8kb upstream of the transcription start site, and binds to two other DR-3 motifs (-5kb and -8kb, respectively) with a lower affinity (Guo et al., 2002).

In mice, using HNR-scan and NUBI-scan, we detected 4 PXR consensus sequences (DR-3 or ER-6) within 10kb upstream of the transcription start site of

Figure 7.2.4

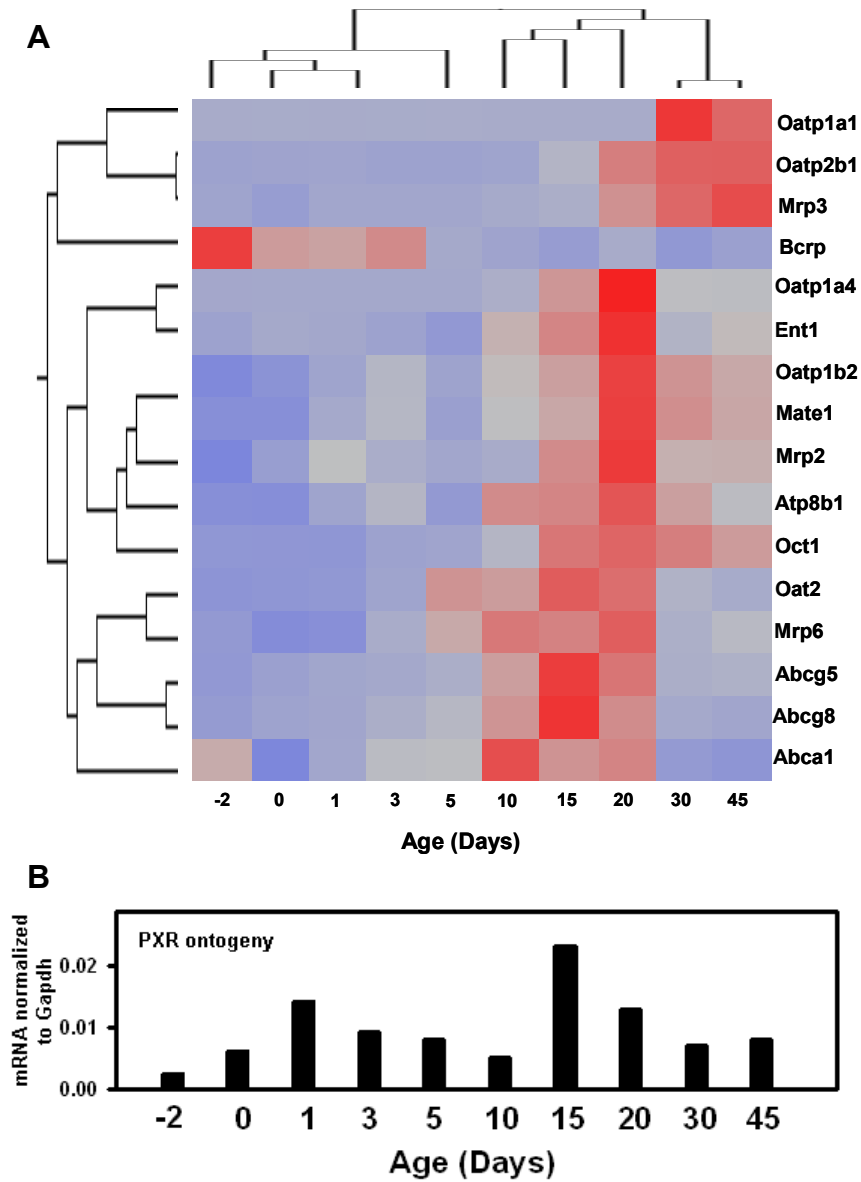


Figure 7.2.4. A. Heatmap of the mRNA ontogeny of xenobiotic transporters in liver during development (male). The ontogenetic expression of these mRNAs from day -2 to day 45 of age was analyzed by a two-way hierarchical clustering method (JMP v. 7.0) using Ward's minimum variance and visualized by a dendrogram. Distances between genes reflect significance of associations. Red color represents relative high expression, and blue color represents relative low expression. B. The mRNA expression of PXR during liver development (male).

Oatp1a4 (-3258, -3721, -6251, and -7429bp). To our surprise, none of these consensus sequences appeared to bind to PXR in control or PCN-treated conditions (data not shown). In addition, we blasted the response elements of the *Oatp1a4* gene and found little conservation during evolution. These pieces of evidence suggest that either the mouse Oatp1a4 is an indirect target, or we missed the real PXR-DNA binding sites due to the biased detection method, or species-specific PXR-DNA binding patterns. Therefore, in the next step, we examined the entire Oatp1a4 gene locus including ± 10 kb using the unbiased ChIP-sequencing approach. Interestingly, we identified one site at 10kb upstream of the TSS with strong enrichment of PXR binding in control liver (277-fold compared to background; threshold: 20-fold). After PCN treatment, PXR binding was still only observed at this site, but with a further increase in signal enrichment (549-fold) (Figure 7.2.5A). Although there were no known PXR-consensus sequences (DR-3, DR-4, ER-6, and ER-8) observed in this region using conventional methods, which have limited settings for the spacer distance (NHR-scan and NUBI-scan, data not shown), using our novel and unbiased motif detection algorithm, we have identified one DR-9 like consensus sequence present in the PXR-binding site for *Oatp1a4*. Corresponding to increased PXR bindings after PCN treatment, we observed PXR-dependent mRNA induction of Oatp1a4 in mouse liver (Figure 7.2.6B). To validate our findings from ChIP-sequencing, and to fill the gap between *in silico* analysis and the actual biological functions of PXR, we performed an ELISA-based transcription factor DNA-binding assay in control and PCN-treated mouse liver samples, and showed for

Figure 7.2.5

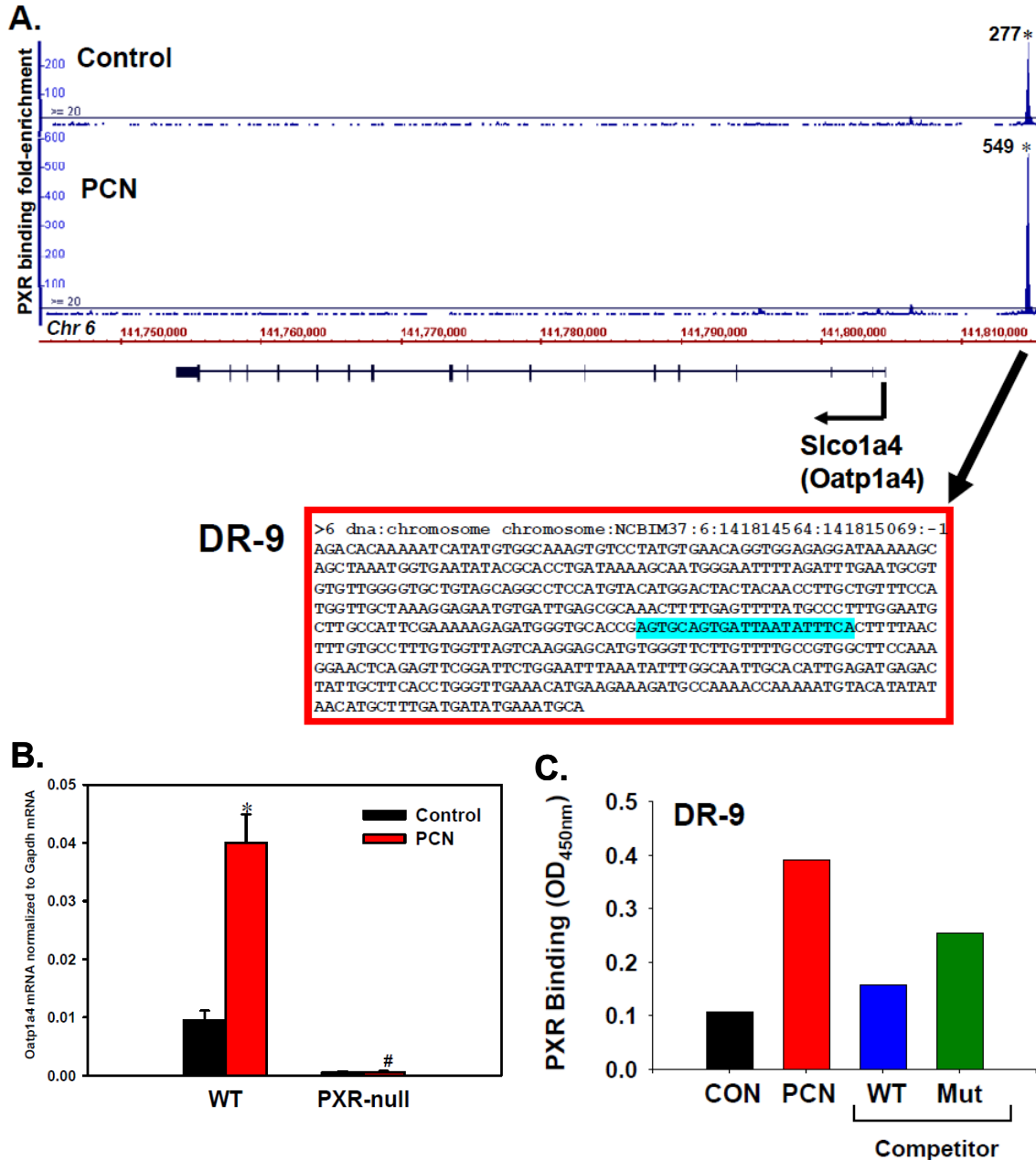


Figure 7.2.5. PXR-DNA binding signatures to the *Oatp1a4* gene locus. A. location and fold enrichment of PXR binding to the *Oatp1a4* gene locus (± 10 kb included). Image was generated by the Integrated Genome Browser. Upper panel: control. Lower panel: PCN-treatment. Asterisks: positive enrichment of PXR binding. Arrow points to the novel DR-9 consensus sequence present in the ChIP-DNA fragment. B. *Oatp1a4* mRNA expression in livers of control and PCN-treated WT and PXR-null mice. Asterisk: statistical significance between control and PCN-treatment. Pound: statistical significance between PCN-treated WT and PXR-null mice. C. Quantification of PXR binding to DR-9 DNA-binding motif. Nuclear protein extracts from the livers of mice treated with corn oil vehicle control (CON) or the PXR agonist, PCN, were incubated with oligonucleotides corresponding DR-9. The binding of PXR to the various DNA-binding motifs was quantified using an ELISA-based transcription-factor binding assay, as detailed in the Methods section. An unlabeled oligonucleotide competitor was included for DR-9 DNA binding motif to confirm the specificity of the assay (WT Comp) as well as a mutated oligonucleotide competitor that should not compete effectively with the positive control (PCN treatment).

the first time that PXR protein from the liver extract indeed prefers to DR-9 like sequences, which is the same sequence found to be bound by PXR protein upstream of the *Oatp1a4* gene locus from the ChIP-Seq motif analysis. Competition assays using unlabeled wild-type (WT) and mutated oligos further confirmed the specificity of the interaction between DR-9 and PXR protein (Figure 7.2.5C). Taken together, data from ChIP-Seq, motif analysis, ELISA-based transcription-factor binding assay, and mRNA assays in WT and PXR-null mice, have provided strong evidence that *Oatp1a4* is indeed a direct PXR-target gene, and highlighted the functional significance of the novel DR-9 in inducing the trans-activation of PXR-target gene *in vivo*.

For the basolateral efflux transporter, *Mrp3* was selected as an example to demonstrate novel PXR-DNA binding patterns. Interestingly, *Mrp3* has three positive PXR-binding sites only inside the gene (45,538bp, 30,722bp, and 3,810bp downstream of TSS), with further enriched PXR binding at approximately the same regions after PCN treatment (45,586bp, 30,722bp, and 3,778bp downstream of TSS) (Figure 7.2.6A). Prior to this work, most studies have limited the detection range for PXR binding to the gene promoter regions. Such designs are inherently biased, in that they do not seek to detect novel genomic PXR-binding sites that may be equally important for gene regulation. The novel intronic PXR-DNA bindings to the *Mrp3* gene locus has highlighted the importance of using unbiased approaches to search for nuclear receptor consensus sequences. Corresponding to increased PXR bindings after PCN

Figure 7.2.6

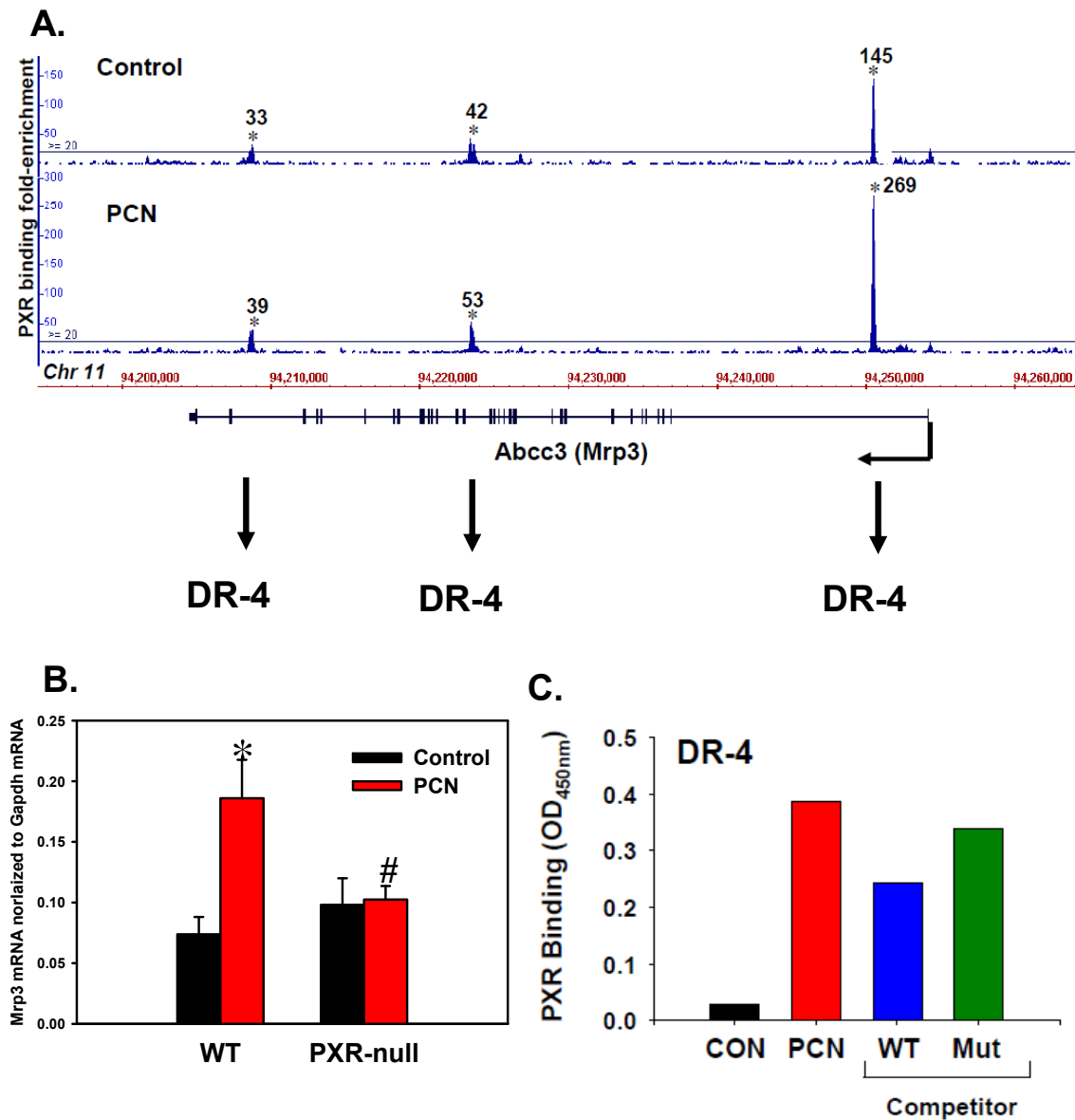


Figure 7.2.6. PXR-DNA binding signatures to the Mrp3 gene locus. A. location and fold enrichment of PXR binding to the Mrp3 gene locus (± 10 kb included). Image was generated by the Integrated Genome Browser. Upper panel: control. Lower panel: PCN-treatment. Asterisks: positive enrichment of PXR binding. Arrow points to the DR-4 consensus sequence present in the CHIP-DNA fragment. B. Mrp3 mRNA expression in livers of control and PCN-treated WT and PXR-null mice. Asterisk: statistical significance between control and PCN-treatment. Pound: statistical significance between PCN-treated WT and PXR-null mice. C. Quantification of PXR binding to DR-4 DNA-binding motif. Nuclear protein extracts from the livers of mice treated with corn oil vehicle control (CON) or the PXR agonist, PCN, were incubated with oligonucleotides corresponding DR-4. The binding of PXR to the various DNA-binding motifs was quantified using an ELISA-based transcription-factor binding assay, as detailed in the Methods section. An unlabeled oligonucleotide competitor was included for DR-4 DNA binding motif to confirm the specificity of the assay (WT Comp) as well as a mutated oligonucleotide competitor, which should not compete effectively with the positive control (PCN treatment).

treatment, we observed PXR-dependent mRNA induction of Mrp3 in mouse liver (Figure 7.2.6B). Motif analysis detected the presence of DR-4 at all of the PXR-DNA binding sites, and ELISA-based transcription factor DNA-binding validated that PXR protein indeed binds to DR-4-like sequences *in vitro* (Figure 7.2.6C).

For the canalicular transporters, it is well known that the xenobiotic efflux transporter family MDR1/Mdr1a/b are PXR direct target genes from *in vitro* evidence and in intestine (Geick et al., 2001; Synold et al., 2001). Surprisingly, my previous work has demonstrated that *in vivo* liver, PXR does not appear to induce either Mdr1a or Mdr1b, in addition, the basal expression of Mdr1a and 1b is very low in liver, in contrast to the phospholipid transporter Mdr2, which is highest in liver (Cui et al., 2009a). It should be noted that three of these Mdr genes form a polycistron cluster on chr 5 in mice. CHIP-on-chip identified strong enrichment of H3K4Me2 around the Mdr2 gene locus, but not around the *Mdr1a* or *1b* gene loci (Figure 7.2.7). The suppressive mark, H3K27Me3, was consistently low around the *Mdr* gene loci. For DNA methylation, strong enrichment of DNAMe was observed at the 3'-UTR regions of both *Mdr1a* and *1b* gene loci. In contrast, the DNAMe for *Mdr2* gene showed a different pattern, in that the DNAMe was observed within the intronic region of *Mdr2*, and its fold enrichment was much lower than that within the *Mdr1a* and *1b* genes. Interestingly, corresponding to the epigenetic signatures, positive PXR-DNA binding was not observed around the *Mdr1a* or *1b* gene locus, whereas strong enrichment of PXR was identified around the *Mdr2* gene locus. In summary, pre-

Figure 7.2.7

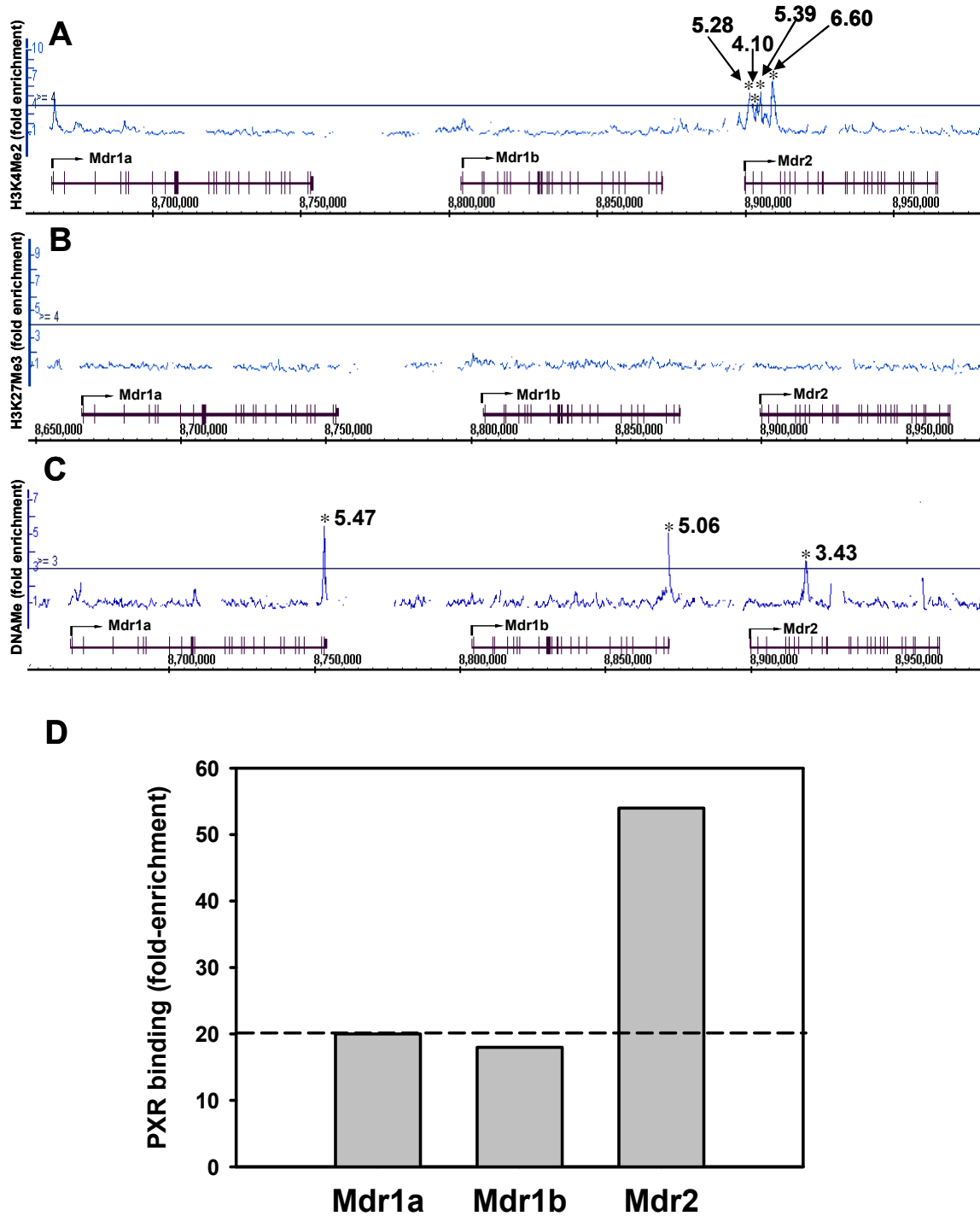


Figure 7.2.7. Location and fold enrichment of H3K4Me2 (A), H3K27Me3 (B), and DNAMe (C) to the *Mdr* gene loci (*Mdr1a*, *Mdr1b*, and *Mdr2*) at 45 days of age. Asterisks: positive enrichment of an epigenetic mark. Solid lines through the signal enrichment peaks indicate the threshold value (4.0-fold of input background for histone H3K4Me2 and H3K27Me3, and 3.0-fold for DNAMe). Data were generated by ChIP-on-chip and visualized by the Integrated Genome Browser. D. Overall PXR binding fold-enrichment to *Mdr1a*, *1b*, and *Mdr2* gene loci under basal conditions.

existence of a permissive chromatin environment appears to be important for recruiting PXR protein to the target *Mdr* genes.

In conclusion, most of the xenobiotic transporters are enriched between adolescent and adult ages. In addition, using genome-wide location analysis, we have identified novel PXR-binding profiles to some of these transporter genes, suggesting that PXR is a critical regulator for the xenobiotic transporters.

CHAPTER EIGHT
ONTOGENIC REGULATION OF TRANSCRIPTION FACTORS AHR, PPAR α ,
AND PGC-1 α IN MOUSE LIVER

ABSTRACT

The aryl hydrocarbon receptor (Ahr) is a xenobiotic sensor that regulates the expression of a battery of drug-metabolizing genes. However, Ahr is also important for normal liver development. The purpose of the first part of the study in this chapter was to examine the ontogeny of Ahr mRNA in mouse liver, and determine the epigenetic mechanisms regulating Ahr gene transcription during postnatal liver development. There was a 224% increase in hepatic Ahr mRNA from 2 days before birth to 45 days after birth. CHIP-on-chip analysis demonstrated that DNA methylation and histone H3K27 tri-methylation (H3K27Me3), two epigenetic marks for gene suppression, were consistently low around the *Ahr* gene locus. In contrast, enrichment of histone H3K4 di-methylation (H3K4Me2), a hallmark for gene activation, increased 182% from prenatal to the young adult period (45 days of age) around the *Ahr* gene locus. Regression analysis revealed a strong correlation between enrichment of H3K4Me2 and Ahr mRNA ($r=0.91$).

Postnatal liver development is critical for newborns to obtain sufficient nutrient and energy for survival. Peroxisome proliferator-activated receptor α (PPAR α) and peroxisome proliferator-activated receptor γ coactivator 1 α (PGC-1 α) are two important metabolic regulators in liver for nutrient homeostasis. Whereas PPAR α is a liver-enriched nuclear receptor that regulates lipid metabolism, PGC-1 α is an essential coactivator to promote gluconeogenesis in liver. Little is known about the ontogeny of PPAR α and PGC-1 α in liver, nor the epigenetic

mechanism of their transcriptional activation during development. Therefore the purpose of the second part of the chapter is to determine the mRNA expression of PPAR α and PGC-1 α in developing mouse liver at day -2, 1, 5, and 45 of age, and determine its correlation with changes in chromatin epigenetic signatures (DNA and histone methylations). Multichannel suspension array revealed postnatal increases in both PPAR α and PGC-1 α mRNA in mouse liver. The postnatal increase in PPAR α mRNA correlates with an increase in histone H3K4 di-methylation, a hallmark for gene activation, coupled by a decrease in histone H3K27 tri-methylation, a hallmark for gene suppression (Chip-on-chip). The high neonatal expression of PGC-1 α mRNA correlates with high histone H3K4 dimethylation, and the low expression of PGC-1 α mRNA in adult liver correlates with DNA methylation. The postnatal decrease in serum triglycerides and serum glucose indicate that in addition to the up-regulation of the mRNA levels of the PPAR α and PGC-1 α , these pathways were also functionally activated. In summary, postnatal H3K4Me2 enrichment positively associates with *Ahr* mRNA in developing mouse liver, providing a permissive chromatin state allowing *Ahr* gene transactivation in postnatal liver development.

In conclusion, the postnatal increase in mRNA expression of *Ahr*, PPAR α and PGC-1 α correlates with distinct epigenetic signatures during mouse liver development. The increased expression of both xeno-sensors and nutrient-sensors in liver is critical for normal postnatal development.

INTRODUCTION

The aryl hydrocarbon receptor (Ahr) is well recognized as a ligand-activated transcription factor for aromatic hydrocarbons, including TCDD (2,3,7,8-tetrachlorodibenzo-*p*-dioxin) and polycyclic aromatic hydrocarbons. In mice, Ahr mRNA is highly expressed in lung, and expressed at intermediate levels in liver and gastrointestinal tract (Petrick and Klaassen, 2007). In the absence of a ligand, the Ahr is sequestered in the cytosol by two molecules of heat-shock protein 90 (HSP90). Upon ligand binding, Ahr is released from HSP90, translocates into the nucleus, and dimerizes with the Ahr nuclear translocator (ARNT). The Ahr-ARNT heterodimer then binds to the xenobiotic response element of target genes, and usually results in increased gene transcription (Li et al., 1994; Ma et al., 1995).

Ahr regulates the expression of a large battery of drug-metabolizing genes, including the prototypical target genes cytochrome P450 1A1, 1A2, and 1B1 (Rowlands and Gustafsson, 1997), several liver aldehyde dehydrogenases in mice (Alnouti and Klaassen, 2008), some liver UDP glucuronosyltransferases in rats (Shelby and Klaassen, 2006) and mice (Buckley and Klaassen, 2009), the organic anion transporting polypeptides 2b1 and 3a1 (Cheng et al., 2005), and some multidrug resistance-associated protein efflux transporters in mice (Cheng et al., 2005b; Maher et al., 2005a).

In addition to its role in drug metabolism, the Ahr is also important for normal liver development. Ahr-null mice have been engineered, either by deleting Ahr exon 1 (Fernandez-Salguero et al., 1995; Gonzalez and Fernandez-Salguero, 1998) or exon 2 (Schmidt et al., 1996; Harstad et al., 2006). Common phenotypes of the two lines of Ahr-null mice include a marked decrease in liver size per gram of body weight, moderate hepatic portal fibrosis, and decreased constitutive expression of certain xenobiotic-metabolizing enzymes, such as Cyp1a2 (Lahvis and Bradfield, 1998). In addition to the common liver phenotypes, Ahr-null mice with exon 1 deletion also have increased mortality within the first 2 weeks of age, hyper-proliferative blood vessels in the portal areas of the liver, glycogen depletion in liver, inflammation of bile ducts, and adenocarcinomas with aging (Gonzalez and Fernandez-Salguero, 1998). In contrast, Ahr-null mice with exon 2 deletion are viable and fertile, but exhibit a spectrum of hepatic defects including transient microvesicular fatty metamorphosis, prolonged extramedullary hematopoiesis, and portal hypercellularity with thickening and fibrosis (Schmidt et al., 1996).

Although Ahr plays important roles in both drug metabolism and normal development, the mechanisms underlying the developmental regulation of the *Ahr* gene *in vivo* are poorly characterized. Recently, it has become increasingly evident that developmental gene regulation is controlled by epigenetic mechanisms (Jaenisch and Bird, 2003; Kiefer, 2007). DNA methylation and histone modifications are the ultimate regulatory epigenetic mechanisms of gene

expression during development. In general, changes in DNA methylation profiles and chromatin structure determine whether there is a permissive chromatin environment for the transcription machinery to access gene promoter regions and initiate transcription. DNA methylation is a covalent modification that results in stable silencing of genes during development, either by interfering directly with transcription factor binding to response elements of target genes, or by recruiting corepressor complexes and reinforcing gene silencing (Bird, 2002; Reik, 2007). Histone H3 lysine-4 di-methylation (H3K4Me₂) is present in promoters and transcribed regions of many active genes, and is positively associated with gene transcription (Bernstein et al., 2005; Kim et al., 2005; Roh et al., 2006). In contrast, H3 lysine-27 tri-methylation (H3K27Me₃) is associated with suppression of gene transcription, because H3 lysine-27 tri-methylated histone is a target for the chromodomain protein Polycomb, that silences genes by yet unknown mechanisms (Boyer et al., 2006; Lee et al., 2006; Kiefer, 2007). Other types of histone modifications, like the most extensively studied epigenetic mark histone acetylation, not only regulate gene transcription, but are also involved in DNA repair, replication, and condensation (Kouzarides, 2007). In comparison, histone methylations are more specific for regulation of gene expression. Nevertheless, the co-occurrence between certain types of histone acetylation and methylation of H3K4 is very high (Bernstein et al., 2005; Pokholok et al., 2005).

Little is known of either the ontogeny of the *Ahr* mRNA in mouse liver during development, or the epigenetic mechanism of *Ahr* gene transcriptional activation

during development. Therefore, the purpose of the present study was to reveal the ontogeny of hepatic Ahr mRNA expression in mice, and determine the epigenetic mechanisms mediating the Ahr mRNA expression during liver development. Because alterations of chromatin structure by epigenetic modifications is a critical mechanism to regulate gene expression, it is hypothesized in the present study that specific epigenetic marks associate with changes in Ahr mRNA expression during liver development in mice.

Mammals have highly regulated systems to maintain nutrient homeostasis although they have intermittent access to food. Liver is an essential organ for nutrient homeostasis including lipid and glucose biosynthesis and metabolism. Postnatal liver development is therefore critical for newborns to maintain sufficient nutrient and energy for survival and further development. Peroxisome proliferator-activated receptor α (PPAR α , NR1C1) and peroxisome proliferator-activated receptor γ coactivator 1 (PGC-1 α) are two important metabolic regulators in liver for nutrient homeostasis. PPAR α is an essential nuclear receptor that regulates lipid metabolism. PPAR α was first identified by Issemann and Green in 1990, and was named “PPAR” because its activation increases hepatic peroxisome volume and density, or peroxisome proliferation. PPAR α -null mice are resistant to peroxisome proliferation in response to administration of PPAR α ligands (Lee et al., 1995).

PPAR α is abundantly expressed in liver where it regulates fatty-acid catabolism, as well as a few other organs including heart, muscle, and kidney.

Upon activation, PPAR α hetero-dimerizes with the retinoid X receptor (RXR), and binds to the response elements of a large battery of target genes involved in lipid homeostasis. For example, PPAR α stimulates peroxisomal β -oxidation of fatty acids to produce energy, shortens long-chain fatty acids and thus prevents lipid accumulation and toxicity, up-regulates fatty acid transport protein and long-chain acyl-CoA synthetase genes in liver, induces the expression of mitochondrial HMG-CoA synthetase to form ketone bodies, and increases apolipoproteins apoA-I and apoA-II and decreases apoC-III (Li and Glass, 2004). Consequently, PPAR α activators increase HDL and decrease triglyceride levels. PPAR α also regulates cholesterol homeostasis in macrophages, for example, PPAR α activation can lead to the induction of LXR α expression (Chinetti et al., 2001). PPAR α can also inhibit esterification and increase the efflux of free cholesterol in human macrophages (Chinetti et al., 2000; Chinetti et al., 2003). The endogenous ligands for PPAR α are fatty acids that bind PPAR α with relatively low affinities, whereas exogenous PPAR α ligands include fibrates, like gemfibrozil, that are used to treat hypertriglyceridemia in patients, as well as a few potent agonists used in the laboratory for non-human studies (GW7647, Wy-14643).

Whereas PPAR α is generally considered a lipid sensor, PGC-1 α is a critical transcriptional coactivator in liver to promote gluconeogenesis (Yoon et al., 2001). PGC-1 α was first identified in brown-adipose tissue as a key regulator of adipocyte differentiation (Puigserver et al., 1998), and was later found to be is a

versatile metabolic regulator for adaptive thermogenesis, mitochondrial biogenesis, and fuel homeostasis (Puigserver and Spiegelman, 2003) in various organs. Although the basal levels of PGC-1 α is low in liver, which is the major producer of glucose, the hepatic expression of PGC-1 α is increased markedly by fasting (Yoon et al., 2001) and in type I diabetes (Puigserver and Spiegelman, 2003). It has been shown that PGC-1 α activates glucose biosynthesis by inducing all the three key genes of gluconeogenesis in primary hepatocytes, namely phosphoenol-pyruvate carboxykinase (PEPCK), fructose 1,6-bisphosphatase, and glucose 6-phosphatase (Yoon et al., 2001). PGC-1 α stimulates a 3-fold increase in glucose secretion by hepatocytes when provided with gluconeogenic precursors (Puigserver and Spiegelman, 2003). In addition to promoting glucose biosynthesis, PGC-1 α also cooperates with PPAR α in the transcriptional control of genes encoding mitochondrial fatty acid oxidation enzymes (Vega et al., 2000). As a coactivator for transcription, PGC-1 α exerts its function by direct interaction with transcription factors after recruited to specific sequences in gene promoters, and it has been shown that PGC-1 α can recruit proteins that contain histone acetyl-transferase activities, and consequently unwind the chromatin to promote gene transcription (Puigserver et al., 1999).

Accumulating evidence during recent years suggests that PPAR α and PGC-1 α may be important during development, as they may mediate adaptations to changes in nutrient supply. It has been demonstrated that PPAR α -null mice have severe fatty infiltration and elevated triglycerides in liver under fasting

conditions (Lee et al., 2004a). In humans, a genetic defect in PGC-1 α signaling results in a defect in hepatic energy metabolism, and death usually occurs between 6 months and 12 years of age (Cooper et al., 2006). In mice, PGC-1 α -genetic depletion results in fasting hypoglycemia in response to impaired gluconeogenic gene expression and hepatic glucose production (Lin et al., 2004; Leone et al., 2005).

It has become increasingly evident that gene regulation during development is under stringent epigenetic control (Kiefer, 2007). Current studies on epigenetic modifications focus on DNA methylation and histone modifications. In general, alterations in DNA methylation status and chromatin environment are the ultimate regulatory mechanisms of gene transcription. DNA methylation is a covalent modification that results in stable silencing of genes, either by interfering directly with transcription factor binding to response element of target genes, or by recruiting corepressor complexes and reinforcing gene silencing. Histone H3 lysine-4 di-methylation (H3K4Me₂) is related to initiation of gene transcription, evidenced by the presence of H3K4Me₂ in promoters and transcribed regions of many active genes; whereas H3 lysine-27 tri-methylation (H3K27Me₃) is associated with suppression of gene transcription. H3 lysine-27 tri-methylated histone is a target for the chromodomain protein Polycomb that silences genes by yet unknown mechanisms (Kiefer, 2007). Among the various modifications of histones, namely, methylation, acetylation, ubiquitination, phosphorylation, poly-ADP-ribosylation, and sumoylation, histone methylations are more stable and the

enzymes that catalyze the histone methylation are implicated in playing essential roles during development (Barski et al., 2007). Therefore, methylations were selected in the present study over other types of histone modifications.

Little is known of the expression of PPAR α and PGC-1 α in mice during liver development, nor the epigenetic mechanism of their transcriptional activation during development. Therefore, the purpose of the present study is to reveal the ontogeny of hepatic PPAR α and PGC- α mRNA expression in mice, and determine its correlation with changes in chromatin epigenetic signatures (DNA and histone methylations) during development.

RESULTS

Ahr expression during mouse liver development. The ontogenic expression of mouse liver Ahr mRNA is shown in Figure 8.1A. Ahr mRNA expression was low before birth, increased after birth (216% of prenatal levels at day 1, and 162% at day 5 of age), and peaked at 45 days of age (293%). Compared to levels at day 45 of age, Ahr mRNA expression was significantly lower at day -2 and 5. The Ahr mRNA expression at 1 day of age also appeared lower than adult levels, although the difference was not statistically significant.

Corresponding to an increase in the Ahr mRNA, the protein expression of Ahr also increased during postnatal liver development (Figure 8.1B). The Ahr protein in adult lungs were stained as a positive control, and there was no Ahr protein detected in livers of Ahr-null mice (negative control).

Methylation of the *Ahr* gene during liver development. DNA methylation is generally considered a mechanism for gene suppression, and it usually occurs in a GC-rich region called the CpG island. The *Ahr* gene is approximately 36.9kb long on chromosome 12. Within 10kb upstream and 1kb downstream of the *Ahr* gene promoter region, *in silico* analysis identified one CpG island slightly upstream of the TSS site, and this CpG island is 1635bp in length ($[(C+G) / \text{total bases}] = 57.68\%$). However, despite the presence of a GC-rich region, DNA-methylation signal enrichment within the CpG island did not reach the threshold value of 3.0-fold for positive DNA methylation, and there was also no enrichment in DNA methylation throughout the *Ahr* gene locus (Figure 8.2, upper panel). In

Figure 8.1

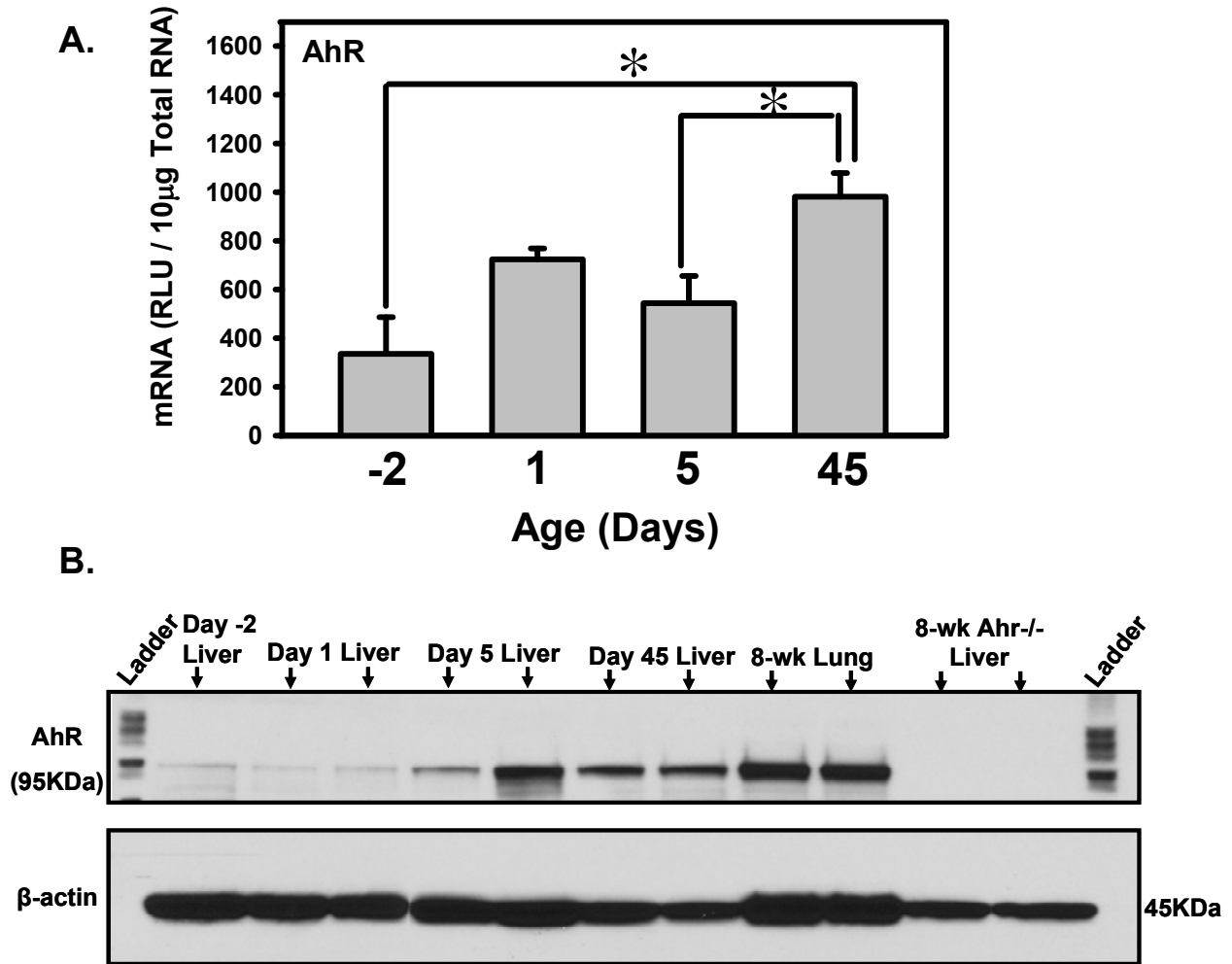


Figure 8.1A. Ontogenic expression of Ahr mRNA in mouse liver. Ahr mRNA ontogenic expression was determined by bDNA assay as described in MATERIALS AND METHODS (n=5). Data were expressed as RLU / 10µg total RNA. Asterisks (*) indicate statistical significance compared to day 45 levels ($p < 0.05$, one way ANOVA followed by Duncan's multiple range post hoc test). B. Ontogenic expression of Ahr protein in liver during development. Adult Ahr^{+/+} lung: positive control; Adult Ahr^{-/-} liver: negative control.

Figure 8.2

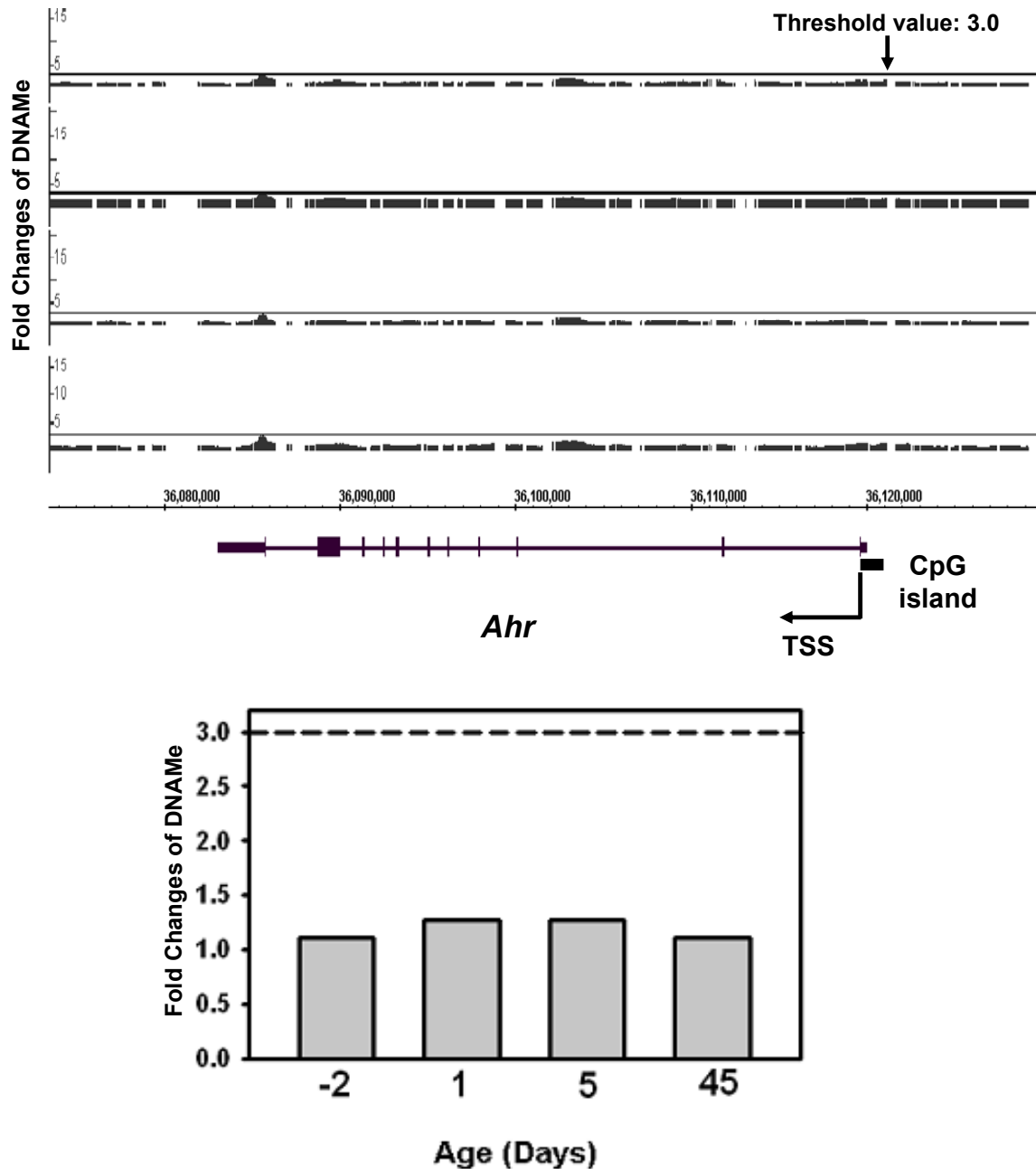


Figure 8.2. DNA methylation status of *Ahr* gene during mouse liver development. Upper panel: DNA methylation fold changes at the *Ahr* gene locus at day -2, 1, 5, and 45 of age (equal amounts of pooled samples from $n=5$ at each age). Solid lines through the signal enrichment peaks indicate the threshold value (3.0) for positive DNA methylation. Lower panel: Average peak values of DNA methylation at day -2, 1, 5, and 45 of age. The dashed line indicates the threshold value (3.0) for enriched intervals.

addition, there was no DNA methylation enrichment upstream of the *Ahr* gene start site or downstream of the end of the *Ahr* gene (detection limit: 10kb up and down, data not shown). The fold changes were all below the threshold of 3-fold (day -2, 1.12-fold; day 1, 1.27-fold; day 5, 1.28-fold; and day 45, 1.14-fold). In summary, *Ahr* DNA methylation signals were consistently low in the developing mouse liver, and therefore do not appear to mediate the changes in the ontogenic expression of *Ahr* mRNA.

Di-methylation at lysine-4 of histone H3 (H3K4Me2) of the *Ahr* gene during liver development. Histone H3K4 di-methylation generally associates with gene activation. There was no H3K4Me2 enrichment upstream of the *Ahr* gene start site or downstream of the *Ahr* gene locus (detection limit: 10kb up and down, data not shown). The fold change of H3K4Me2 was lower than the 4.0 threshold value at day -2 of age with no positive H3K4Me2 regions of the *Ahr* gene locus (Figure 8.3, upper panel) (average peak value at day -2: 2.3-fold, Figure 8.3, lower panel). At 1 day of age, there was an increase in the fold change of H3K4Me2 of the *Ahr* gene, with one interval identified in the gene (peak value: 6.03-fold), and it is located 1350bp downstream of the promoter region (Figure 8.3, upper panel), although the overall average fold changes still did not reach the 4.0 threshold (3.3-fold, Figure 8.3, lower panel). At 5 days of age, there was another positive H3K4Me2 region identified in the gene, and it is 1405bp downstream of the promoter region (peak value: 6.02-fold, Figure 8.3, upper panel), but still, the overall average fold change was below the threshold (3.7-fold,

Figure 8.3

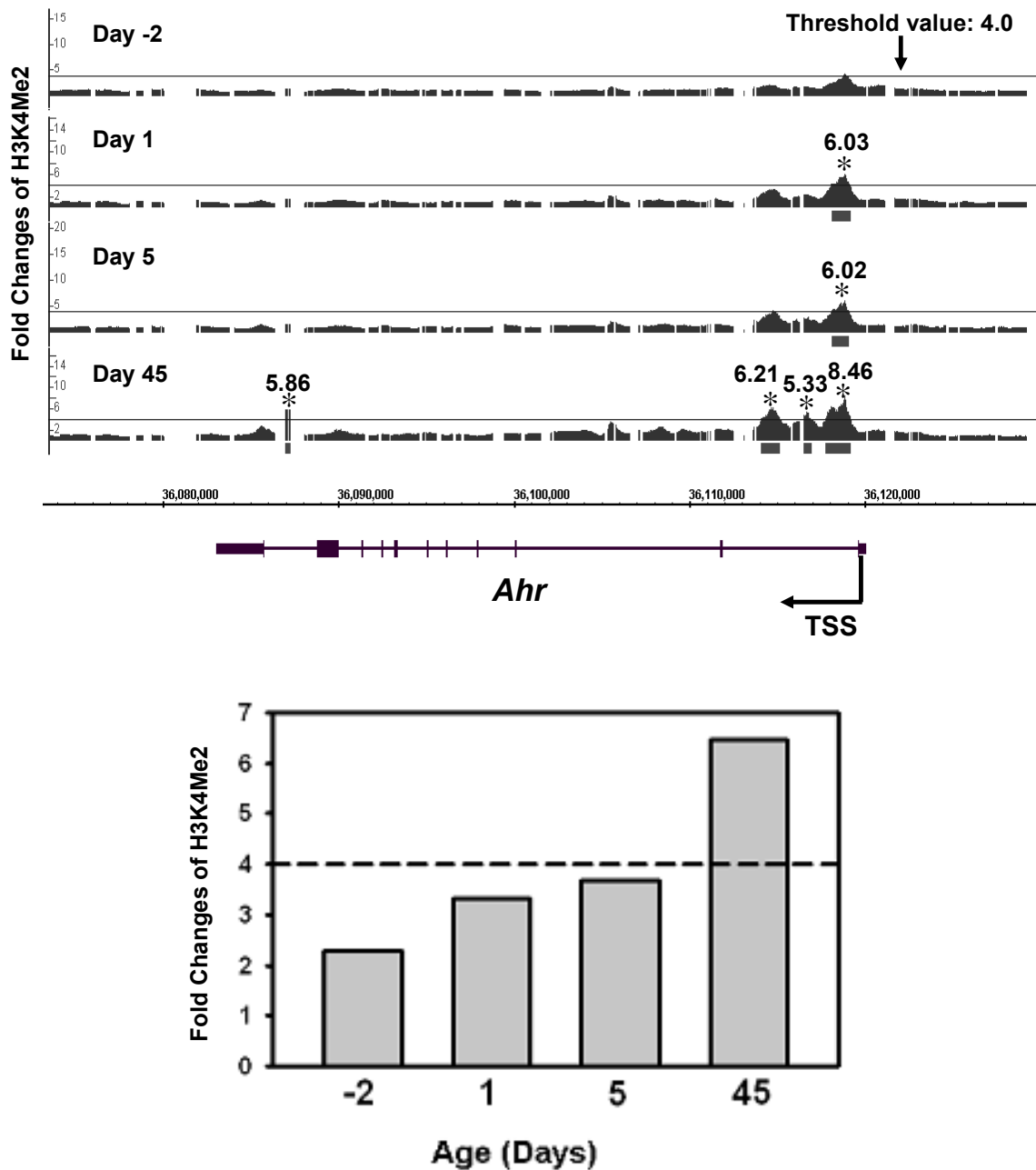


Figure 8.3. Di-methylation of histone H3 at lysine-4 (H3K4Me2) at the *Ahr* gene locus during mouse liver development. Upper panel: histone H3K4Me2 fold changes at the *Ahr* gene locus at day -2, 1, 5, and 45 of age (equal amount of pooled samples from $n=5$ at each age). Solid lines through the signal enrichment peaks indicate the threshold value (4.0) for enriched intervals. Bars under the peaks of each age indicate the existence and length of active regions for H3K4Me2. Asterisks (*) indicate the peak center. Lower panel: Average peak values of H3K4Me2 at day -2, 1, 5, and 45 of age. The dashed line indicates the threshold value (4.0) for enriched intervals.

Figure 8.3 lower panel). At 45 days of age, there was a strong enrichment of histone H3K4 di-methylation that exceeded the threshold, with four active regions in the *Ahr* gene locus, at 1522bp (8.46-fold), 3271bp (5.33-fold), 5374bp (6.21-fold), and 32.85kb (5.86-fold) downstream of from the TSS, respectively (Figure 8.3, upper panel), and the overall average fold change was as high as 6.5-fold (Figure 8.3, lower panel). In summary, there was an enrichment in the histone H3K4 di-methylation of the *Ahr* gene locus from prenatal to the young adult period in mouse liver, and the value in young adults was approximately 280% of the prenatal value.

Tri-methylation at lysine-27 of histone 3 (H3K27Me3) at the *Ahr* gene in liver during development. Histone H3K27 tri-methylation generally correlates with gene suppression. There was no H3K27Me3 enrichment upstream of the *Ahr* gene start site or downstream of the end of the *Ahr* gene (detection limit: 10kb up and down, data not shown). As shown in the upper panel, the H3K4Me3 average values for the *Ahr* gene locus gradually decreased during development, however, all values were below the 4.0-fold at any age examined (-2, 1, 5, and 45 days of age). The average fold changes of H3K27Me3 of the *Ahr* gene locus were computed and shown in the lower panel of Figure 8.4. The histone H3K27 tri-methylation values for *Ahr* were approximately 1.23-fold at day -2 of age, followed by 1.08-fold at day 1, 0.99-fold at day 5, and 0.87-fold at day 45. In summary, the histone H3K27 tri-methylation signals of *Ahr* gradually decreased

Figure 8.4

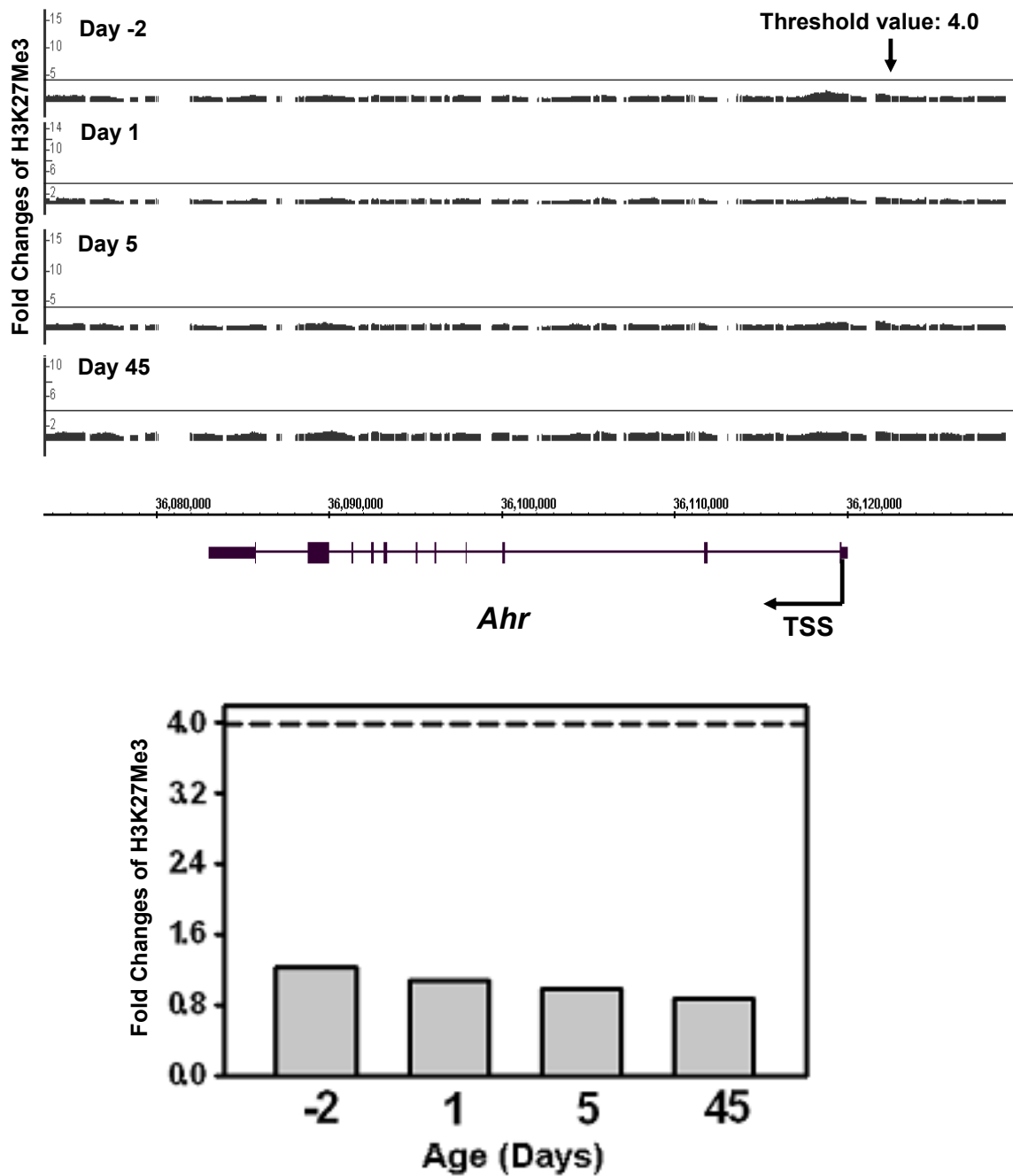


Figure 8.4. Tri-methylation of histone H3 at lysine-27 (H3K27Me3) at the *Ahr* gene locus during mouse liver development. Upper panel: histone H3K27Me3 fold changes at the *Ahr* gene locus at day -2, 1, 5, and 45 of age (equal amount of pooled samples from $n=5$ at each age). Solid lines through the signal enrichment peaks indicate the threshold value (4.0) for enriched intervals. Lower panel: Average peak values of H3K27Me3 at the *Ahr* gene locus at day -2, 1, 5, and day 45 of age. The dashed line indicates the threshold value (4.0) for enriched intervals.

and were lower than threshold throughout liver development, and provide a permissive environment for *Ahr* gene activation.

Regression analysis of *Ahr* mRNA expression and epigenetic marks.

Regression analysis demonstrated no correlation between DNA methylation of the *Ahr* gene locus and *Ahr* mRNA ($R = 0.06$), whereas histone di-methylation and histone tri-methylation each exhibited a strong correlation with *Ahr* mRNA expression ($R = 0.91$ and -0.86 , respectively). However, histone di-methylation of the *Ahr* gene locus was the only methylation profile to exceed the threshold value (4.0-fold) (Figure 8.5). In summary, among the three epigenetic marks, H3K4Me2 is the only enriched mark above the threshold that strongly correlated with *Ahr* mRNA expression during mouse liver development.

Figure 8.5

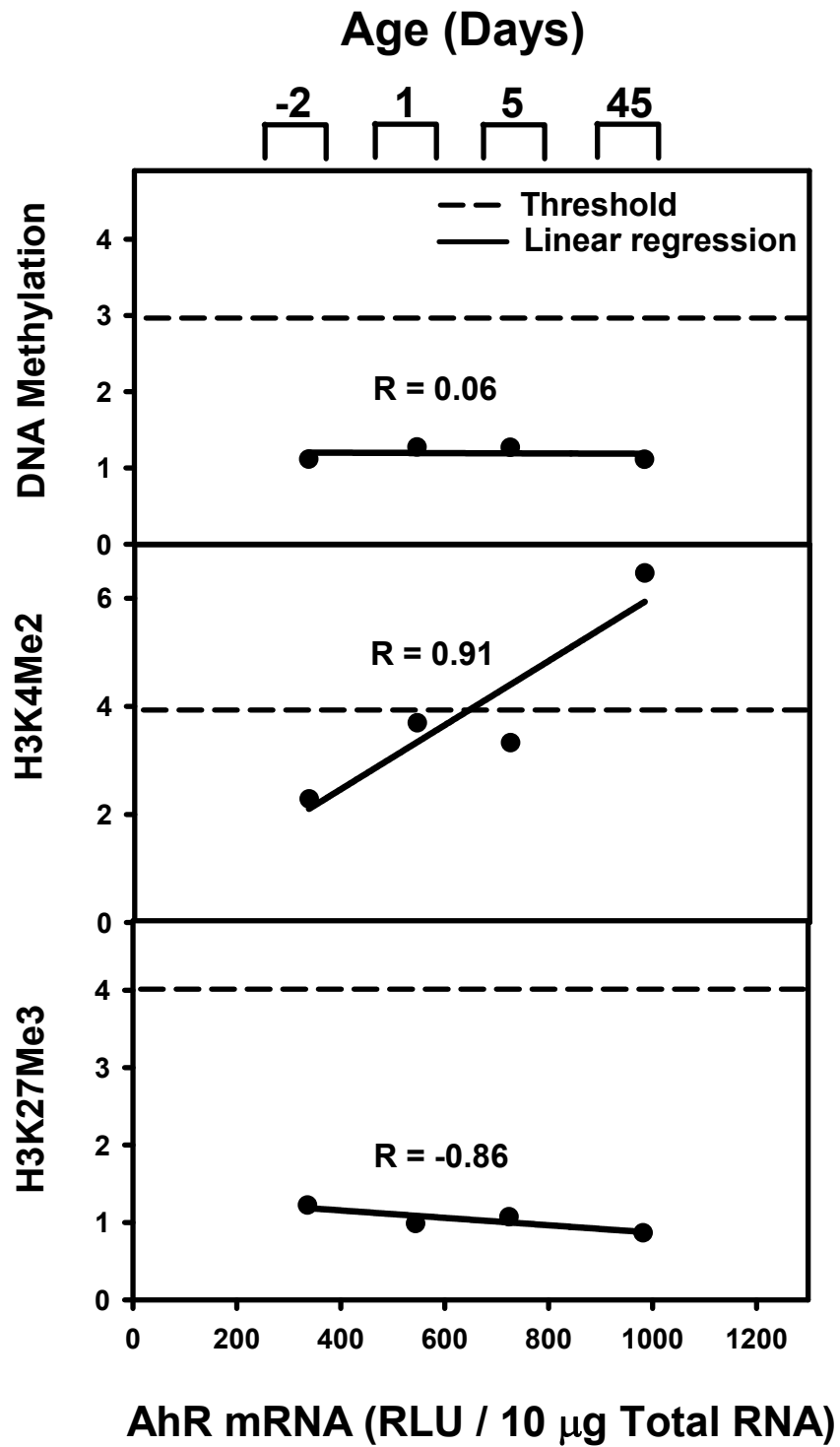


Figure 8.5. Regression analysis of the correlation (R) between Ahr mRNA and the fold changes of the three epigenetic marks (DNA and histone di- and tri-methylations) at day -2, 1, 5, and 45 of age during liver development in mice.

PPAR α and PGC-1 α mRNA expression during mouse liver development.

The ontogeny of mouse liver PPAR α and PGC-1 α mRNA levels was determined by Multiplex suspension array and is shown in Figure 8.6. Low mRNA expression of PPAR α was observed two days before birth, followed by a postnatal increase, which was 3.4-fold higher than prenatal levels at day 1, 2.5-fold higher at day 5, and 3.2-fold higher at day 45 of age (Figure 8.6, upper panel). There was also a postnatal increase in the mRNA expression of PGC-1 α , which was 7.2-fold higher than prenatal levels at day 1 (peak value), 3.2-fold higher at day 5, and 2.5-fold higher at day 45 of age. In summary, there was a postnatal increase in the mRNA expression of both PPAR α and PGC-1 α , with peak levels observed at day 1 of age.

To determine the epigenetic mechanisms for the postnatal mRNA enrichment of PPAR α and PGC-1 α , three epigenetic marks, namely DNA methylation (DNAMe), histone H3K4 di-methylation (H3K4Me2), and histone H3K27 tri-methylation (H3K27Me3) were quantified in both *PPAR α* and *PGC-1 α* gene loci, as shown in the following experiments. Overall, ChIP-on-chip analysis identified ten active regions within ± 10 kb of *PPAR α* gene locus, and two active regions within ± 10 kb of *PGC-1 α* gene locus. These active regions have positive enrichment of at least one epigenetic mark during liver development, and the details will be described in the following sections.

Figure 8.6

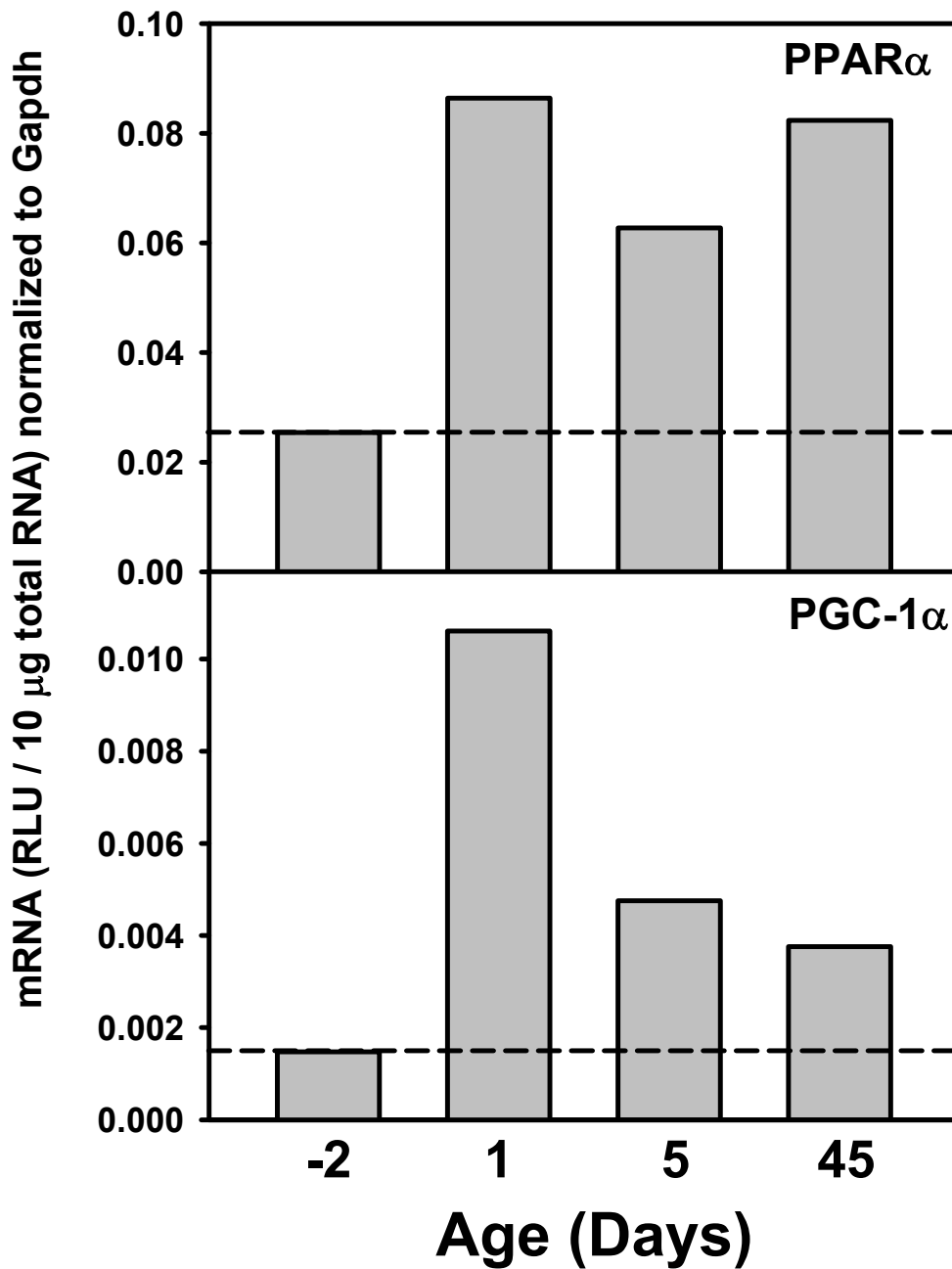


Figure 8.6. Ontogenic expression of PPAR α and PGC-1 α mRNA in mouse liver (equal weight of pooled samples from n=5 at each age). The mRNA levels from different ages are quantified by the Multiplex suspension array, and data are expressed at fluorescent signal intensities of PPAR α mRNA normalized to Gapdh.

DNA methylation (DNAMe) of the *PPAR α* gene during liver development.

DNA methylation is generally considered a mechanism for gene suppression and it usually occurs in GC-rich regions (defined by composition of bases: $[C+G] / \text{total bases} > 50\%$) near the promoter. The signal intensities of DNA methylation of the *PPAR α* gene in livers of mice at 4 different ages were determined by ChIP-on-chip analysis. As shown in the upper panel of Figure 8.7, there is a CpG island spanning from 1kb upstream to 2kb downstream from the transcription start site of the mouse *PPAR α* gene. However, DNA-methylation signal intensity of the *PPAR α* locus did not reach the threshold value of 3.0 for positive DNA methylation at this region, or at any other active regions (Figure 8.7 upper panel). The average peak values of DNAMe were calculated among all the 10 active regions of the *PPAR α* gene locus (approximately 1.5-fold from day -2 to 45 days of age) (Figure 8.7 bottom panel). This value is less than the threshold value of 3.0. In summary, *PPAR α* DNA methylation signals were consistently low in the developing mouse liver, and therefore do not appear to mediate changes in *PPAR α* mRNA ontogenic expression.

Di-methylation at lysine-4 of histone H3 (H3K4Me2) of the *PPAR α* gene

during liver development. Histone H3K4 di-methylation is generally considered a mechanism of gene activation, because it “relaxes” the chromosome and thus favors the recruitment of transcription machinery to the DNA. The H3K4Me2

Figure 8.7

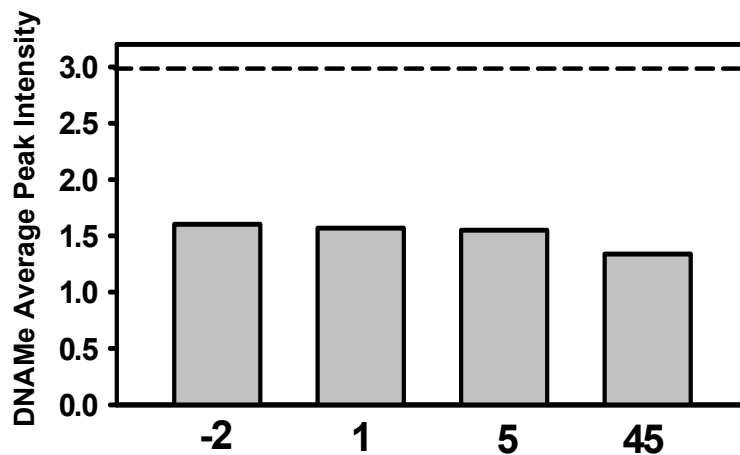
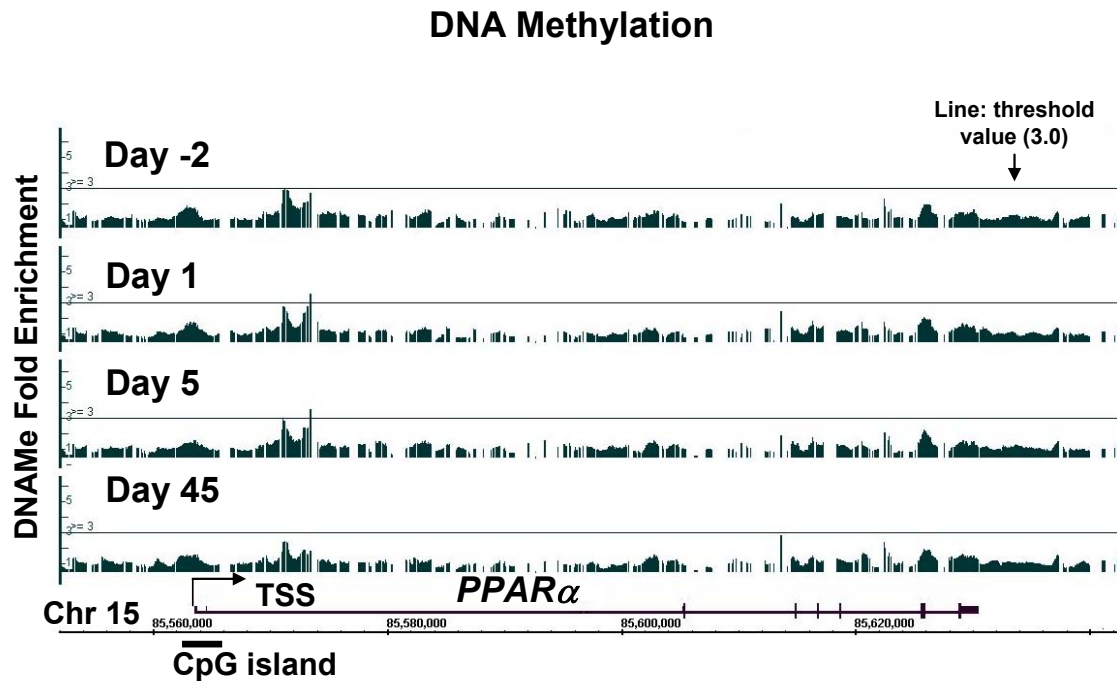


Figure 8.7. DNA methylation status of *PPARα* gene during mouse liver development. Upper panel: DNA methylation signal intensity at the *PPARα* gene locus at day -2, 1, 5, and 45 of age (equal weight of pooled samples from $n=5$ at each age). The line indicates the threshold value (3.0) for positive DNA methylation. An *in silico* analysis of CpG islands within 10kb upstream plus 5kb downstream of the *PPARα* promoter region was performed using the Methyl Primer Express Software v1.0. According to the parameters set by the software, CpG island is a GC rich region with a minimal length of 300bp, and a maximum length of 2kb. Lower panel: average peak values of DNA methylation at day -2, 1, 5, and day 45 of age, line: 3.0 threshold value.

signal intensity around the *PPAR α* gene locus is shown in Figure 8.8. From day -2 to 5 days of age, positive enrichment peaks of H3K4Me2 was identified at approximately 75kb downstream of the transcription start site (TSS) of the *PPAR α* gene, and were 6.3-fold of input background at day -2, 5.6-fold at day 1, and 6.6-fold at day 5 (Figure 8.8 upper panel). At 45 days of age, all ten active regions had positive enrichment of H3K4Me2 within ± 10 kb of the *PPAR α* gene locus (gene length: 67kb), one positive peak was observed 2.1kb upstream of TSS (4.9-fold), and 8 peaks were found inside the genes (4.5-fold at 1.4kb, 6.8-fold at 4.0kb, 9.2-fold at 6.0kb, 5.7-fold at 8.1kb, 6.5-fold at 9.8-kb, 4.9-fold at 25.9kb, 4.7-fold at 31.6kb, and 6.5-fold at 37.9kb downstream of TSS). In addition, another positive peak was found 75kb downstream of TSS (4.8-fold) (Figure 8.8, upper panel). The overall average signal intensity of H3K4Me2 was calculated based on the average peak values of all the active regions. As shown in the bottom panel of Figure 8.8, from day -2 to day 5, although positive H3K4Me2 enrichments were identified in the active region 75kb downstream of TSS, the overall average signal intensity of H3K4Me2 among all the active regions was lower than the 4.0 threshold value. The overall average peak values of H3K4Me2 were approximately 2.4-fold at day -2 of age, followed by 3.2-fold at day 1 (133% of day -2), 3.4-fold at day 5 (142% of day -2), and 5.9-fold at day 45, and the day 45 average peak values exceed the 4.0 threshold value (246% of day -2). In summary, there was an increase in H3K4Me2 from prenatal to young adult period in mouse liver, with strong signal enrichment occurring in the young adults.

Figure 8.8

Histone H3K4 Di-methylation

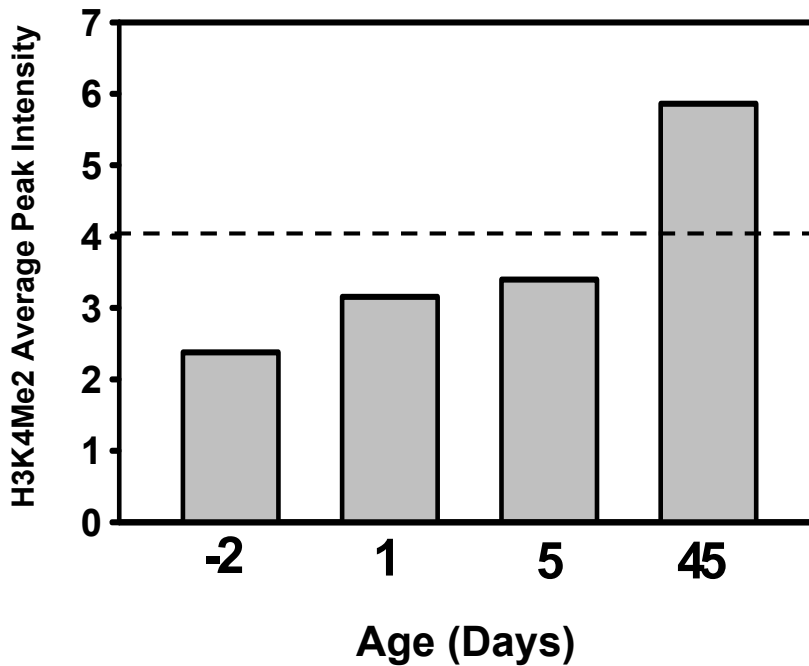
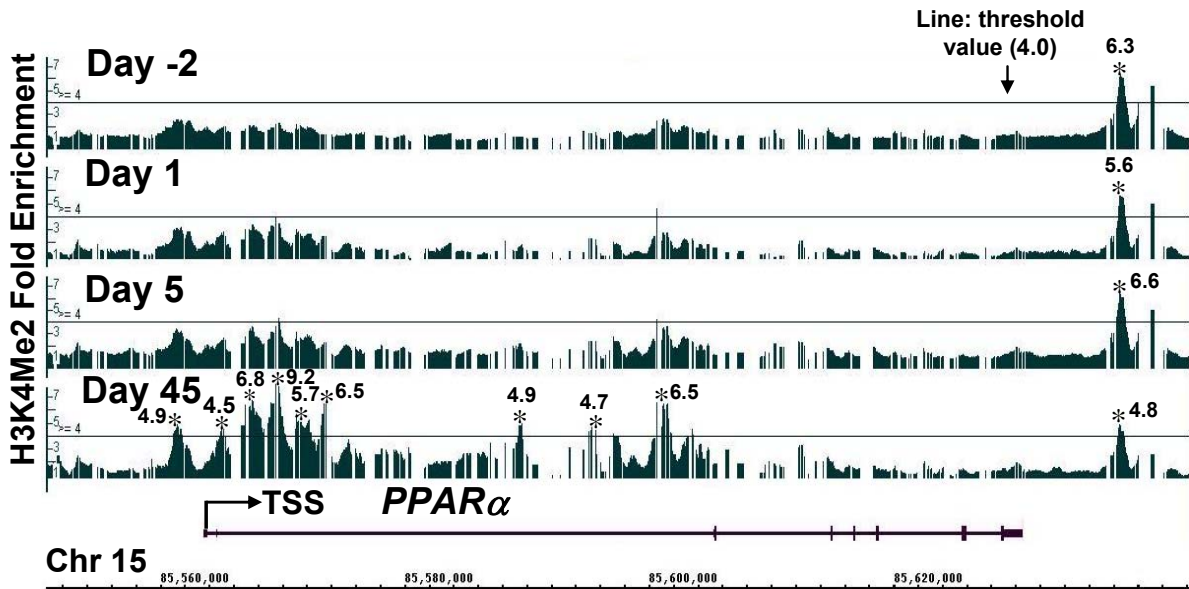


Figure 8.8. Di-methylation of histone H3 at lysine-4 (H3K4Me2) of *PPAR α* gene locus during mouse liver development. Upper panel: histone H3K4Me2 signal intensity at the *PPAR α* gene locus at day -2, 1, 5, and 45 of age (equal weight of pooled samples from n=5 at each age). The line indicates the threshold value (4.0) for enriched intervals. Lower panel: average peak values of H3K4Me2 at day -2, 1, 5, and day 45 of age, line, 4.0 threshold value.

Tri-methylation at lysine-27 of histone 3 (H3K27Me3) of the *PPAR α* gene in liver during development. Histone H3K27 tri-methylation generally correlates with gene suppression. At day -2 of age, an age with low *PPAR α* mRNA expression, there was one active region with positive enrichment of H3K27Me3, that is 1.8kb upstream of the TSS of the *PPAR α* gene (average peak value: 5.3-fold of input background values, threshold: 4.0-fold of input background values) (Figure 8.9, upper panel). At 1 day of age, the H3K27Me3 peak value at this region decreased markedly to 4.2-fold. There was no other positive enrichment of H3K27Me3 in any active regions during development. The average peak values of H3K27Me3 at this active region are shown in the lower panel of Figure 8.9, that was 5.3-fold at day -2 of age, followed by 4.2-fold at day 1 (79% of day -2), 3.1-fold at day 5 (58% of day -2), and 1.2-fold at day 45 (23% of day -2). In summary, the overall histone H3K27 tri-methylation signals of *PPAR α* were below threshold values at all ages, although one positive peak was identified at 2 days before birth.

In summary, whereas DNA methylation does not appear to play a major role in regulating *PPAR α* gene expression, the strong postnatal increase of *PPAR α* mRNA is likely a result of the distinct epigenetic signature of histone methylation profiles, characterized by a postnatal increase in the gene activation signal H3K4Me2, and a postnatal decrease in the gene suppression signal H3K27Me3.

Figure 8.9

Histone H3K27 Tri-methylation

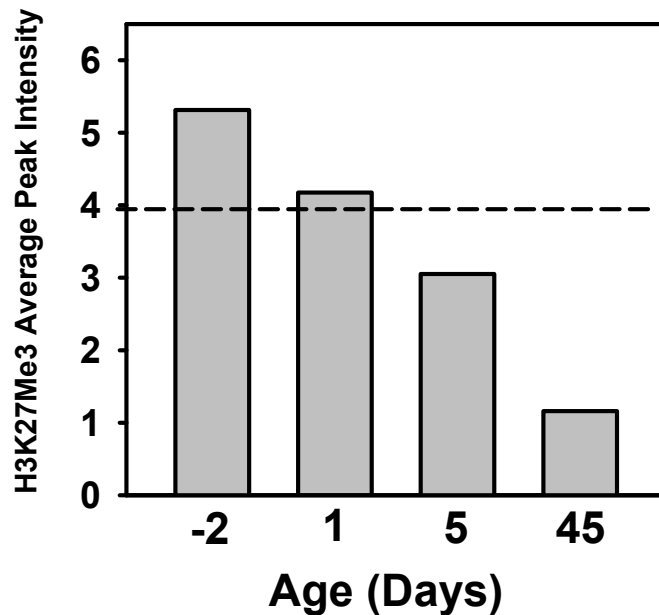
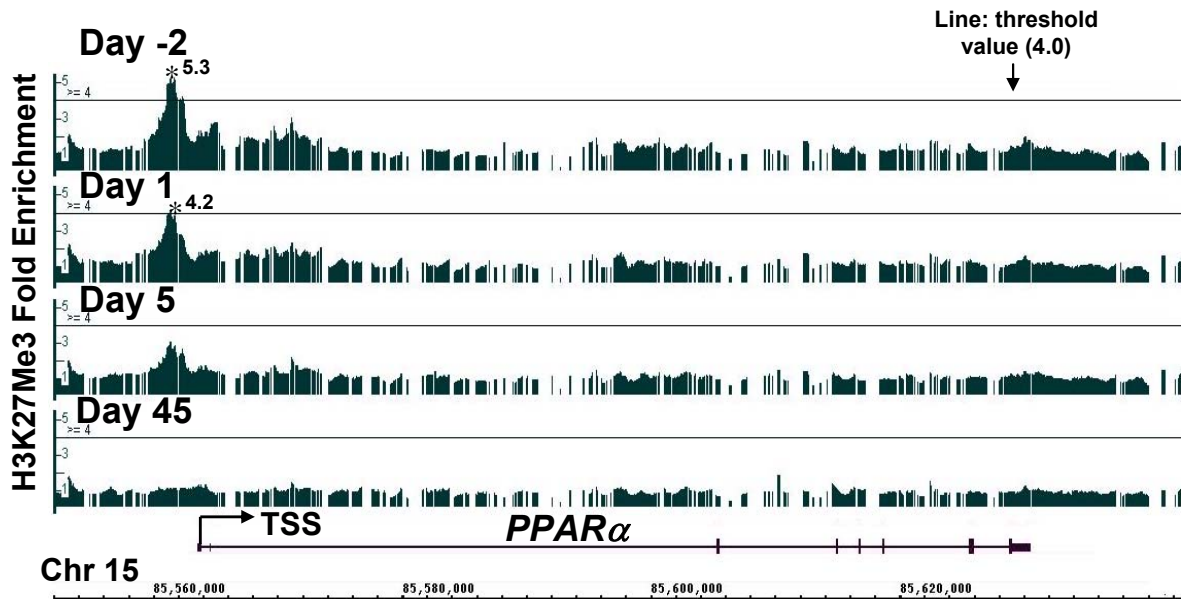


Figure 8.9. Tri-methylation of histone H3 at lysine-27 (H3K27Me3) of *PPARα* gene locus during mouse liver development. Upper panel: histone H3K27Me3 signal intensity at the *PPARα* gene locus at day -2, 1, 5, and 45 of age (equal weight of pooled samples from n=5 at each age). The line indicates the threshold value (4.0) for enriched intervals. Lower panel: average peak values of H3K27Me3 at day -2, 1, 5, and day 45 of age, line, 4.0 threshold value.

DNA methylation of the *PGC-1 α* gene during liver development. The signal intensities of DNA methylation of the *PGC-1 α* gene in livers of mice at 4 different ages were determined by ChIP-on-chip analysis. As shown in the upper panel of Figure 8.10, there is a CpG island spanning from 14.65 to 15.28kb downstream of the transcription start site of the mouse *PGC-1 α* gene (CpG island length: 608bp; gene length: 96.3kb). However, the DNA-methylation signal intensity at the CpG island of the *PGC-1 α* locus did not reach the 3.0 threshold value at any age. Interestingly, at day 45 of age, there was one active region for DNA methylation inside the *PGC-1 α* gene (58.5kb downstream of the TSS), where there was no CpG island (Figure 8.10 upper panel). There was no other enrichment in DNA methylation at any other ages. The average peak values at the active region for DNA methylation (58.5kb downstream of TSS) were calculated as shown in the lower panel of Figure 8.10, that were 1.9-fold at day -2, 2.4 at day 1, 2.2 at day 5, and 3.8-fold at day 45 of age. In summary, *PGC-1 α* DNA methylation signals were low in perinatal period (from day -2 to day 5), but increased and enriched significantly in adults.

Di-methylation at lysine-4 of histone H3 (H3K4Me2) of the *PGC-1 α* gene during liver development. The signatures of the gene activation mark H3K4Me2 around *PGC-1 α* gene locus were visualized from day -2 to day 45 of age (Figure 8.11, upper panel). H3K4Me2 signal intensities were low before birth, but increased right after birth with a positive peak at day 1 of age (4.5-fold, 2kb

Figure 8.10

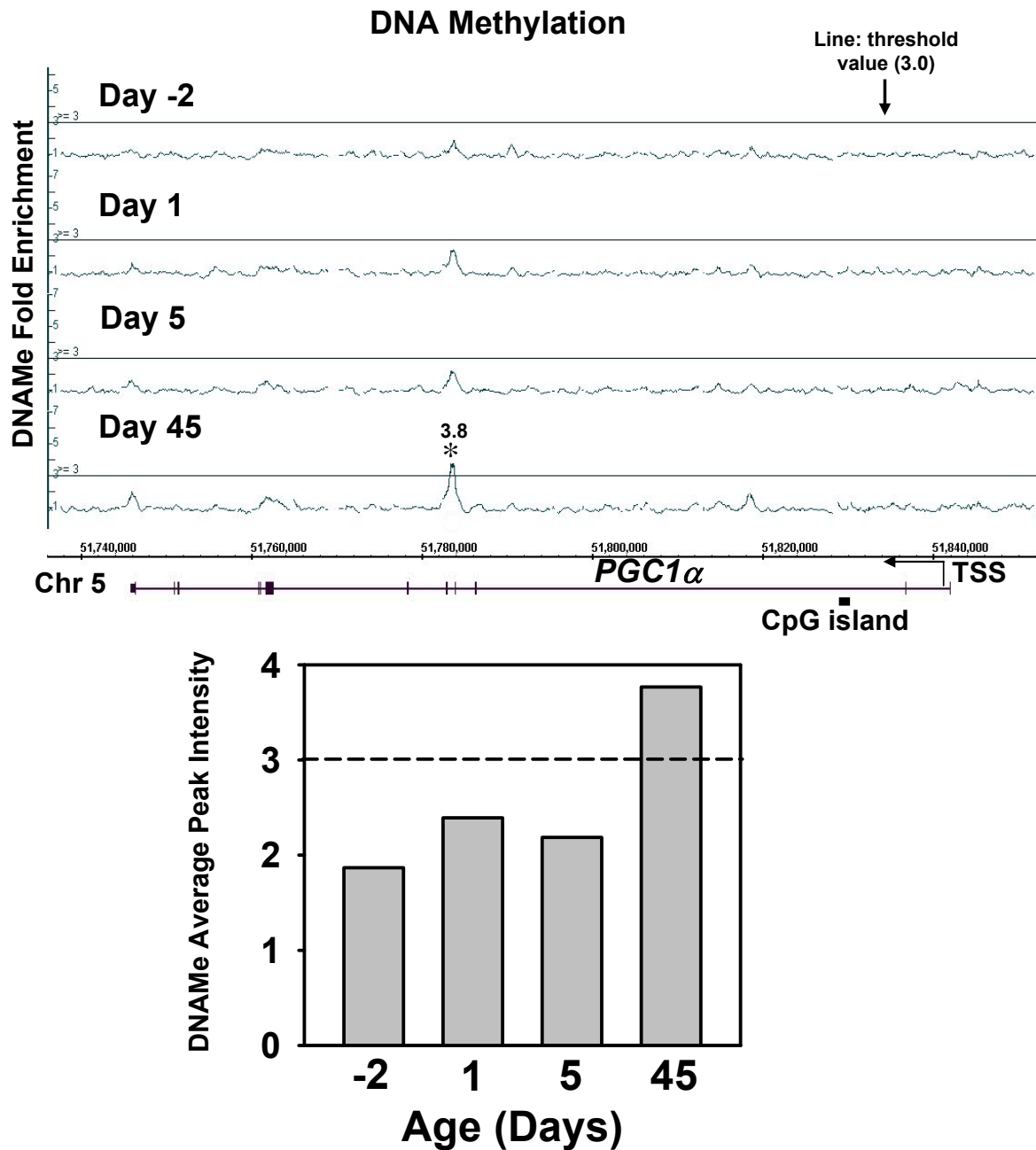


Figure 8.10. DNA methylation status of *PGC-1α* gene during mouse liver development. Upper panel: DNA methylation signal intensity at the *PGC-1α* gene locus at day -2, 1, 5, and 45 of age (equal weight of pooled samples from $n=5$ at each age). The line indicates the threshold value (3.0) for positive DNA methylation. An *in silico* analysis of CpG islands within 10kb upstream plus 5kb downstream of the *PGC-1α* promoter region was performed using the Methyl Primer Express Software v1.0. According to the parameters set by the software, CpG island is a GC rich region with a minimal length of 300bp, and a maximum length of 2kb. Lower panel: average peak values of DNA methylation at day -2, 1, 5, and day 45 of age, line: 3.0 threshold value.

downstream of TSS). The signal then moderately decreased at day 5 of age, but then peaked at day 45 of age (5.5-fold). The average values for H3K27Me3 at this active region were calculated as shown in the lower panel of Figure 8.11, that were 2.9-fold at day -2, 4.5-fold at day 1, 3.8-fold at day 5, and 5.5-fold at day 45 of age. In summary, H3K4Me2 was enriched in 1 and 45 days of age.

Tri-methylation at lysine-27 of histone 3 (H3K27Me3) of the *PGC-1 α* gene in liver during development. As shown in the upper panel of Figure 8.12, the average peak values of the suppressive mark H3K27Me3 were below the 4.0-fold threshold in all active regions and at all ages, and were 1.7-fold at day -2, 1.5-fold at day 1, 1.1-fold at day 5, and 0.8-fold at day 45. Therefore, H3K27Me3 does not appear to mediate changes in PPAR α mRNA ontogenic expression.

In summary, the postnatal increase in PGC-1 α mRNA associates with a postnatal increase in the gene activation signal H3K4Me2. The peak in PGC-1 α mRNA expression at day 1 of age is likely a result of the enrichment of H3K4Me2 signal and the absence of both gene suppression signals (DNAMe and H3K27Me3). At day 45 of age, in addition to the presence of H3K4Me2, there was also a strong enrichment in DNAMe for gene suppression in the *PGC-1 α* gene, and this might contribute to the lower mRNA levels in adult than in newborns.

Figure 8.11

Histone H3K4 Di-methylation

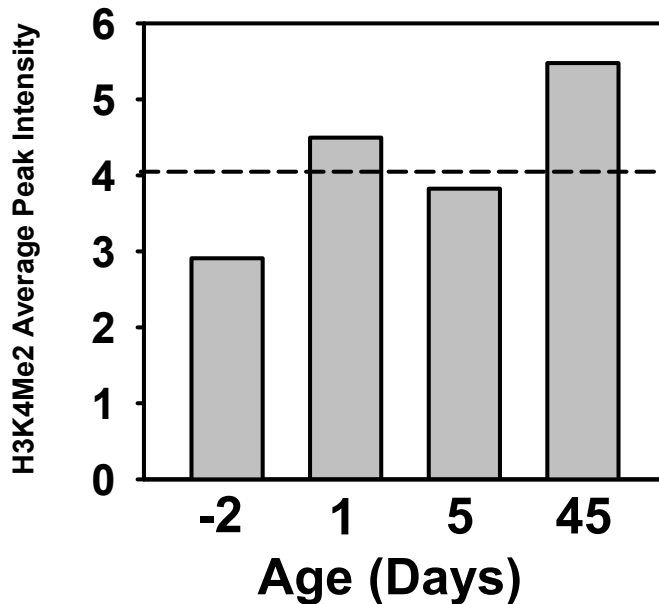
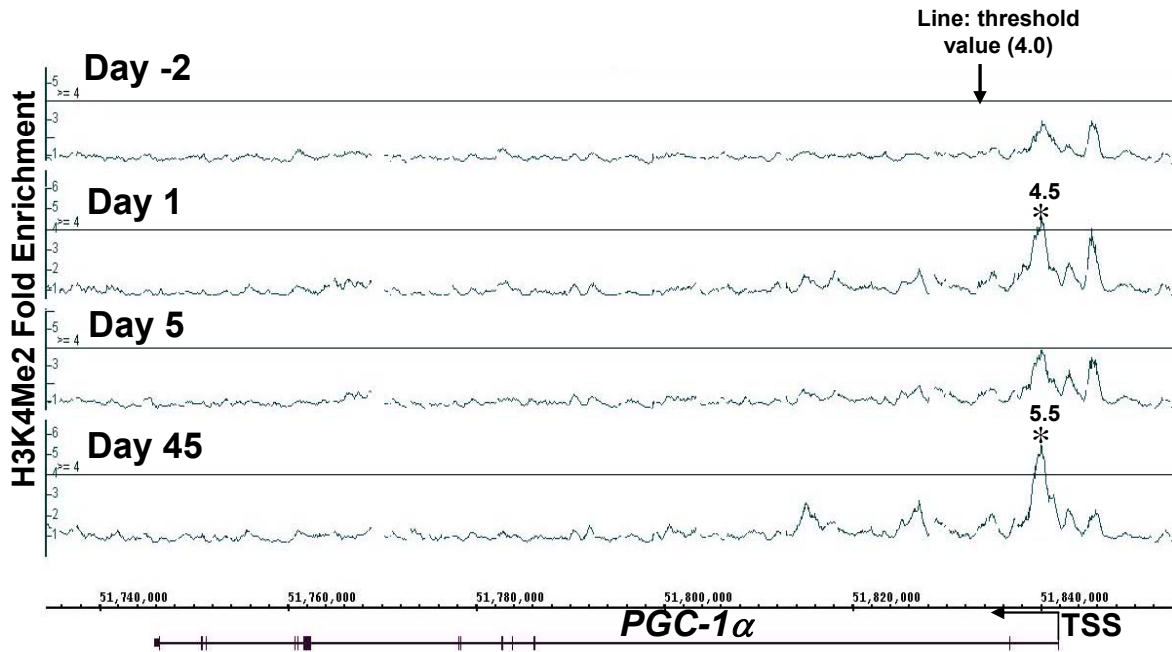


Figure 8.11. Di-methylation of histone H3 at lysine-4 (H3K4Me2) of PGC-1 α gene locus during mouse liver development. Upper panel: histone H3K4Me2 signal intensity at the PGC-1 α gene locus at day -2, 1, 5, and 45 of age (equal weight of pooled samples from n=5 at each age). The line indicates the threshold value (4.0) for enriched intervals. Lower panel: average peak values of H3K4Me2 at day -2, 1, 5, and day 45 of age, line, 4.0 threshold value.

Figure 8.12

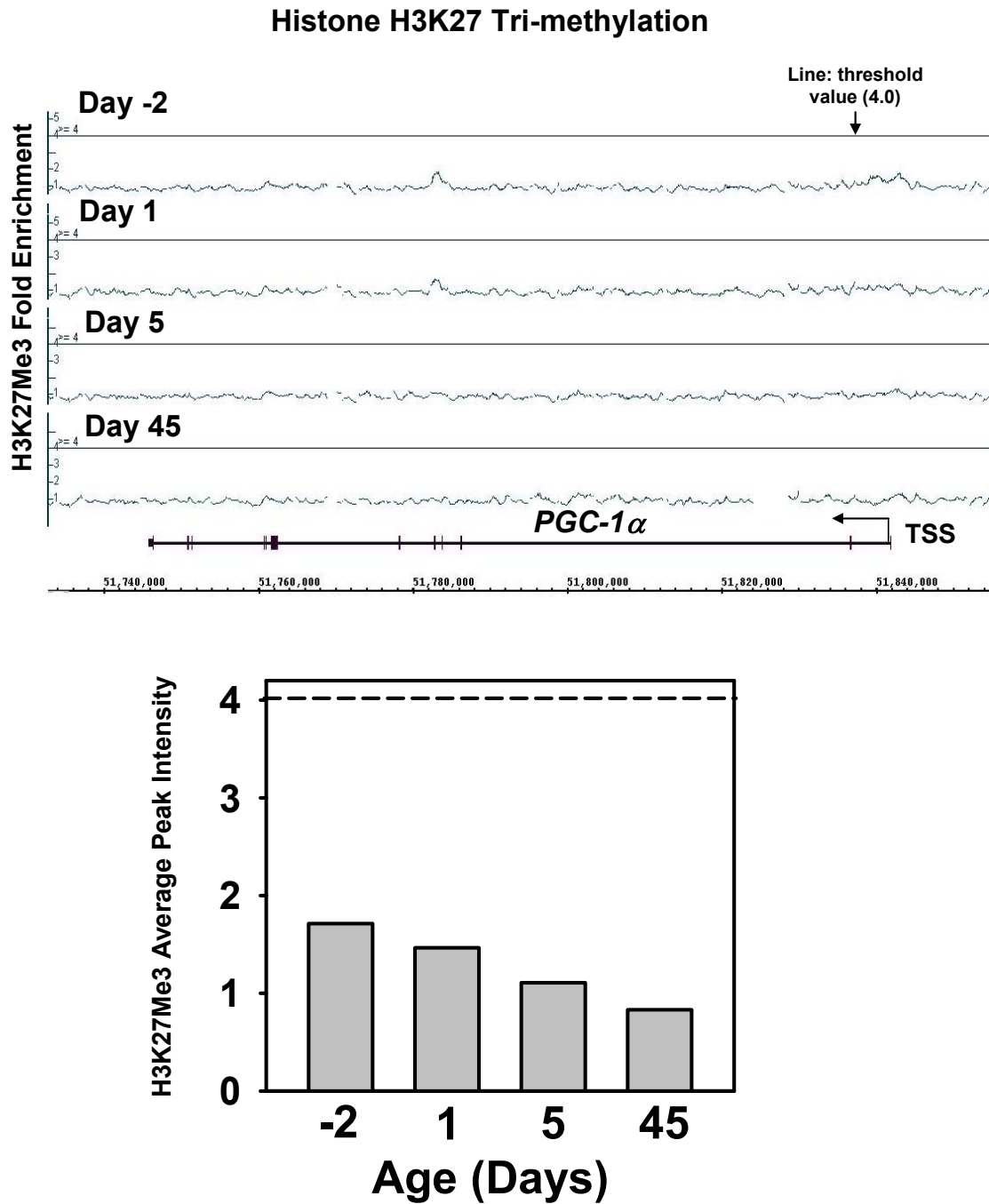


Figure 8.12. Tri-methylation of histone H3 at lysine-27 (H3K27Me3) of PGC-1 α gene locus during mouse liver development. Upper panel: histone H3K27Me3 signal intensity at the PGC-1 α gene locus at day -2, 1, 5, and 45 of age (equal weight of pooled samples from n=5 at each age). The line indicates the threshold value (4.0) for enriched intervals. Lower panel: average peak values of H3K27Me3 at day -2, 1, 5, and day 45 of age, line, 4.0 threshold value.

Serum triglyceride and glucose levels during development. A hallmark of activation of the PPAR α pathway is a decrease in serum triglyceride concentrations. Serum triglyceride levels were low right after birth, followed by a sharp increase at day 1 and 5 when pups are feeding on milk from their mothers (about 2.3-fold of prenatal level at both neonatal ages) (Figure 8.13, upper panel). The transient peak of serum triglyceride levels returned to adult levels by 10 days of age, and the plasma triglyceride concentrations were relatively constant thereafter. Activation of the PGC-1 α -signaling pathway leads to increased gluconeogenesis and more secretion of glucose from the liver into serum. Serum glucose levels were also low right after birth and at day 1 of age, followed by a marked increase at day 5 of age (3-fold of prenatal level), and remained high thereafter (Figure 8.13, bottom panel). The postnatal decrease in serum triglyceride and increase in serum glucose together indicate that in addition to the up-regulation of mRNA expression, the PPAR α and PGC-1 α pathways were also functionally activated.

Figure 8.13

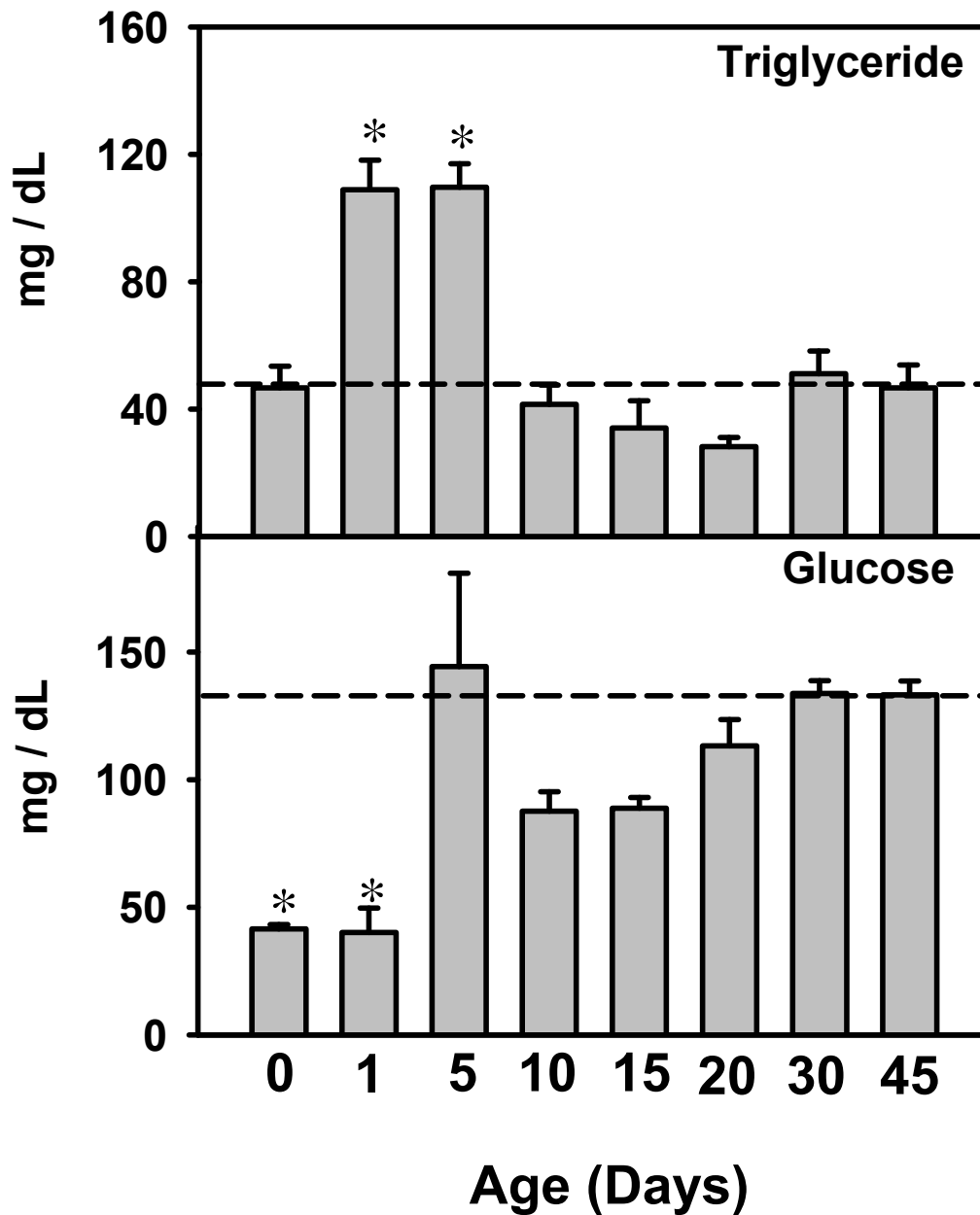


Figure 8.1.13. Serum triglyceride and glucose levels during mouse development. Data are expressed at mg of triglyceride or glucose per deci-liter serum at different ages. Asterisks (*) indicate significant differences from adult levels ($p < 0.05$).

DISCUSSION

The first part of the present study revealed a postnatal increase in the Ahr mRNA expression in mouse liver during development, and demonstrated the role of histone H3K4 di-methylation in triggering the postnatal increase of Ahr mRNA during mouse liver development.

The methylation of DNA at cytosine residues is a well-established epigenetic mechanism that regulates tissue-specific gene expression. DNA methylation usually silences gene transcription, by preventing the recruitment of the transcription complex, or by indirect mechanisms involving changes in chromatin structure (Jaenisch and Bird, 2003). It has been suggested that the interplay between methylation and demethylation dictates the distinct DNA methylation patterns of genes and consequently influences their transcriptional activity. Much attention has been paid to the association between DNA methylation patterns and Ahr target genes. For example, mouse Cyp1a2 gene expression coincides well with the methylation status of DNA during liver development (Jin et al., 2004). However, little is known of the role of DNA methylation in the ontogenic expression of mouse Ahr in liver. The present study is the first to demonstrate that despite the presence of a CpG island, DNA methylation is consistently low at the *Ahr* gene locus from 2 days before birth to 45 days of age, and therefore does not appear to play a significant role in regulating Ahr mRNA expression in liver development.

Recently, a large body of data has been generated for histone marks on the genomes of various organisms, primarily focusing on yeast (Hawkins and Ren, 2006). A current area of research is to understand how these histone modifications correlate and/or regulate transcriptional activity. A remarkable pattern has emerged for histone H3K4 di-methylation of actively transcribed genes, and H3K27 tri-methylation of silenced genes. Among the various modifications, histone methylations are more stable and the enzymes that catalyze the histone methylation are implicated in playing essential roles in the function of the human genome (Barski et al., 2007). High-resolution profiling of histone methylations in the entire human genome has demonstrated that active genes are characterized by high levels of H3K4Me₂, and in contrast, inactive genes are characterized by low or negligible levels of H3K4 methylation of the promoter regions, and high levels of H3K27 tri-methylations (Barski et al., 2007). Therefore, histone methylations were selected in the present study rather than other types of histone modifications. It has been shown that the H3K4Me₂ signals are usually localized to the vicinity of transcription start site, providing a permissive chromatin environment to trigger gene transcription (Barski et al., 2007). In the present study, the strong postnatal enrichment of H3K4Me₂ in the close vicinity of the *Ahr* gene promoter indicates histone H3K4 di-methylation is likely a mechanism to trigger the increase in *Ahr* gene activation during liver development in mice. In contrast, although the gene suppression mark H3K27Me₃ gradually decreases during development around the *Ahr* gene locus, corresponding to increased *Ahr* mRNA, the signals of H3K27Me₃ are well below

threshold at all ages. Therefore, it is difficult to ascertain the importance of the histone tri-methylation profile with regard to Ahr mRNA expression despite the strong correlation between histone tri-methylation and hepatic Ahr mRNA expression.

Interestingly, it appears that Ahr target genes also undergo regulation by histone modifications. For example, it has been shown in the mouse Hepa-1 cell line that the chromatin structure plays an essential role in Cyp1a1 gene transcription. Specifically, Cyp1a1 gene induction by the Ahr/ARNT complex is strongly associated with modifications of specific chromatin marks of Cyp1a1, including hyperacetylation of histone H3K14 and H4K16, tri-methylation of histone H3K4, and phosphorylation of H3S10 (Schnekenburger et al., 2007). Taken together, analyzing distinct histone epigenetic signatures in Ahr and its target genes might become an essential approach in future research on Ahr-mediated drug metabolism and disposition. However, lack of specific inhibitors for histone modification enzymes makes it more challenging to establish a causative role of histone modifications in regulating Ahr gene transcription. Nevertheless, the strong association between the increase in Ahr gene expression and H3K4 di-methylation enrichment provides a direction for future studies that may explore specific upstream factors regulating Ahr gene expression during development.

In summary, the lack of all epigenetic marks, as observed in the *Ahr* gene locus in fetal liver, associate with a low basal expression of *Ahr* mRNA. In contrast, high levels of H3K4Me2 in the absence of suppressor signals of H3K27Me3 and DNA methylation triggers the increase in *Ahr* expression in adult mouse liver. Moreover, the increase in *Ahr* mRNA correlates with the dynamic enrichment of H3K4Me2 during liver development. Epigenetic regulation of *Ahr* gene transcription by histone H3K4 di-methylation is a strong candidate to be considered in the developmental programming of *Ahr* expression in mouse liver. Future studies will determine the causative mechanisms of the ontogeny of *Ahr* by altering the epigenetic signatures during liver development.

The second part of the study is among the first to reveal the postnatal increase of the nutrient sensors PPAR α and PGC-1 α in mouse liver during development, and establishes the correlations between their postnatal increases with distinct epigenetic signatures in liver development. The postnatal increase in the permissive mark H3K4Me2 and decrease in the suppressive mark H3K27Me3 together provide a permissive environment for the postnatal increase of PPAR α mRNA, whereas enrichment of H3K4Me2 correlates with the neonatal surge of PGC-1 α , and DNAm enrichment seems to have inhibitory effects on the PGC-1 α mRNA expression. The postnatal decrease in serum triglycerides indicates that in addition to the up-regulation of mRNA expression, the PPAR α signaling pathway was also functionally activated. In addition, although other pathways might also participate in the regulation of glucose homeostasis during liver maturation, the postnatal increase in serum glucose levels appears to be at

least in part due to the activation of the PGC-1 α pathway, which consequently provides sufficient energy for the postnatal development of various organs.

It is well-known that the composition of the human diet in western society has changed profoundly during the last century, characterized by an increase in fat and sugar consumption (usually coupled with decreased physical activity). The excessive intake of fat and sugar results in a combination of medical disorders termed the “metabolic syndrome”, characterized by increased risk of cardiovascular diseases and diabetes. The metabolic syndrome is not just a “privilege” for adults, in that the prevalence and magnitude of childhood obesity have dramatically increased recently, and the prevalence of metabolic syndrome is high among obese children and adolescents, and this prevalence increases with worsening obesity (Weiss et al., 2004). Therefore, it is crucially important to understand the mechanism for the ontogeny of critical “nutrient sensors” (PPAR α and PGC-1 α) in children, so as to identify novel targets that could potentially be used in treating childhood metabolic syndrome clinically. The present study provides the first evidence that the mRNA expression of PPAR α and PGC-1 α are associated by distinct epigenetic signatures during liver development. In addition, the ontogeny of serum triglyceride and glucose levels indicate that both PPAR α and PGC-1 α signaling pathways were functionally activated, suggesting also a maturation of the expression of the two proteins in postnatal liver development, in addition to an increase in mRNA levels.

It has been demonstrated in rat liver by real-time PCR that PPAR α mRNA is very low during the embryonic period, starts to increase by the end of gestation, and peaks close to adulthood (Balasubramanian et al., 2005). The present data in mice were consistent with the ontogeny data in rats, and the similarities in PPAR α mRNA expression between the two species probably reflect the similarities in their biological cycles for nutrient acquisition. The ontogeny of PGC-1 α in mouse liver has been shown by northern blot to be high during both the prenatal and neonatal period, but decreased in adults (Yubero et al., 2004). In contrast, the present study indicates that PGC-1 α mRNA was low prenatally, peaked in newborns, and then decreased but was still above prenatal levels in adults. The different observations are likely a result of the method for mRNA quantification (northern blot vs. multiplex suspension bead array), or the mouse strains (Swiss vs. C57BL/6). It has been shown that the PGC-1 α target genes for gluconeogenesis, namely phosphoenol-pyruvate carboxykinase (PEPCK), fructose 1,6-bisphosphatase, and glucose 6-phosphatase, were all up-regulated in neonatal mouse liver (Yubero et al., 2004), and the present study also revealed an increase in serum glucose levels after birth. Therefore, it seems that PGC-1 α is higher in livers of newborns than fetus.

PPAR α plays important roles during postnatal liver development. Although PPAR α -null mice are viable, PPAR α deficiency in feed-deprived mice leads to enhanced accumulation of hepatic triglyceride levels, as well as dysregulation of hepatic lipid and carbohydrate metabolism, emphasizing the importance of

precise control role of PPAR α in regulating lipid oxidation for hepatic fuel homeostasis (Sugden et al., 2002). In addition to its effect on lipid homeostasis, PPAR α also exerts antidiabetic effects by increasing insulin sensitivity, and mediates anti-inflammatory responses in endothelial cells, smooth muscle cells, and macrophages. In high fat diet-fed rats and lipoatrophic mice, activation of PPAR α led to a significant improvement in insulin sensitivity (Ye et al., 2001; Chou et al., 2002).

The significance of PPAR α in developmental programming for nutrient homeostasis has become more evident recently, and several studies have determined the regulation of PPAR α during liver development. For example, maternal diets can influence PPAR α expression in offspring, evidenced by the fact that maternal dietary protein restriction in rats results in decreased PPAR α gene methylation and increased PPAR α mRNA in rat offspring. This has been suggested to contribute to the long-term changes in the stable expression of PPAR α and its target genes, associated with impaired lipid homeostasis in the adult. In addition, aging decreases hepatic expression of PPAR α , and decreased PPAR α expression associates with decreased response to lipid-lowering drugs in the aged rats (Sanguino et al., 2005).

The present study adds to the current knowledge of the regulation of PPAR α in development, by demonstrating a strong association of the postnatal increase in PPAR α mRNA expression, with an increase in histone H3K4Me2 and a

decrease in histone H3K27Me3. The methylation of histones at two distinct lysine positions provides a permissive chromatin environment for the initiation of gene transcription. The causative mechanisms for the regulation of PPAR α transcription by histone methylations are currently unknown.

PGC-1 α is a critical metabolic regulator in liver and other organs. As a transcriptional coactivator, PGC-1 α interacts with many transcription factors, including PPAR α , to alter local chromatin structure to initiate gene transcription (Rees et al., 2008). It has been shown that a genetic deficiency in a component of PGC-1 α in humans results in Leigh syndrome with a defect in hepatic energy metabolism, and death occurring between 6 months and 12 years of age (Cooper et al., 2006). In contrast, activation of PGC-1 α by resveratrol increases SIRT1 (silent mating type information regulation 2, homolog 1) and AMPK (AMP-activated protein kinase) activity, which alleviates alcoholic fatty liver in mice (Ajmo et al., 2008).

It has been shown that PGC-1 α gene expression is induced in livers of fasted or diabetic mice, and the increased PGC-1 α in turn activates gluconeogenesis, as well as induces genes of β -oxidation and ketogenesis in hepatocytes (Rhee et al., 2003). The induction of PGC-1 α by fasting also results in an increase in several basolateral uptake transporters in livers as a compensatory response (Dietrich et al., 2007). During liver development, PGC-1 α interacts with HNF6 and participates in the regulation of time-specific gene expression, including up-regulating glucose-6-phosphatase, which is a late marker for hepatocyte

maturation (Beaudry et al., 2006). It has been shown that there are close interactions between PGC-1 α and PPAR α for nutrient homeostasis.

In addition to being a coactivator of PPAR α , PGC-1 α also up-regulates the expression of PPAR α mRNA. PGC-1 α and PPAR α together induce the expression of glycerol kinase, which may promote a futile cycle of triglyceride hydrolysis and fatty acid reesterification in human adipocytes (Mazzucotelli et al., 2007). In addition, single nucleotide polymorphism of both PPAR α and PGC-1 α increase the risk of type II diabetes (Andrulionyte et al., 2007). Upon interacting with various transcription factors, PGC-1 α protein alters the chromatin epigenetic signatures by recruiting histone acetyl-transferases to the gene promoter region and initiate transcription. However, the epigenetic regulation of the PGC-1 α gene itself is poorly understood. It has been shown in heart that PGC-1 α gene expression is down-regulated in mice by histone deacetylase. The present study is among the first to determine the correlations between PGC-1 α ontogeny in liver with regard to histone H3K4Me2, and DNA methylation patterns.

It has become increasingly evident that gene regulation during development is under stringent epigenetic control (Kiefer, 2007). Critical epigenetic signatures include modifications, such as DNA methylation and histone H3K27 trimethylation, which result in gene suppression, as well as histone H3K4 dimethylation, which elicits gene activation. Little is known of these epigenetic signatures for PPAR α expression during development. The present study is the

first to demonstrate that it is the activation of histone H3K4 di-methylation, rather than the suppression by DNA and H3K27 tri-methylation, that correlates strongly with the dynamic increase of PPAR α mRNA expression patterns over time.

DNA methylation usually occurs in GC-enriched regions, and these regions are termed “CpG islands”. The present study identified one CpG island spanning from 1kb upstream to 2kb downstream of the transcription start site of the PPAR α gene. It has been shown that unbalanced prenatal nutrition decreases PPAR α DNA methylation at the CpG island, correlated with an increase in PPAR α mRNA expression in rat offspring (Lillycrop et al., 2005), as noted in the model where restricted-protein diet are given to their mothers during pregnancy. However, as shown in the present study during normal development, the intensity of the DNA methylation of the entire PPAR α gene locus region was consistently low or hypomethylated from day -2 to day 45 of age, and the CpG island was also not methylated at any selected age using the suggested threshold value (3.0-fold of probe intensity) Therefore DNA methylation does not seem to be the mechanism for the differences in PPAR α mRNA expression with age. In addition, another CpG island was identified 14.65 to 15.28kb downstream of the transcription start site of the mouse PGC-1 α gene. Interestingly, the CpG island was not methylated at any age during liver development, in contrast, there was an enrichment in DNA methylation signals in a different region within the PGC-1 α gene locus, that is not considered a CpG

island (Figure 8.10, upper panel). Therefore, DNA methylation does not necessarily mean the presence of CpG island.

High-resolution profiling of histone methylations in the entire human genome demonstrates that active genes are characterized by high levels of H3K4Me₂, and in contrast, inactive genes are characterized by low or negligible levels of H3K4 methylation in their promoter regions, and high levels of H3K27 trimethylations (Barski et al., 2007). In the present study, H3K27Me₃ signal decreased around the PPAR α gene locus with age, whereas H3K4Me₂ increased with age. Thus, together the decreased H3K27Me₃ and increased H3K4Me₂ may contribute to the up-regulation of PPAR α gene expression in postnatal liver development. It has been shown that H3K4Me₂ signal is localized more to the vicinity of the transcription start site and in actively-transcribed genes (Barski et al., 2007). In the present study, enrichment of H3K4Me₂ signals was observed near the TSS region for both PPAR α and PGC-1 α genes in the adult period. Therefore, the close vicinity of H3K4Me₂ to the TSS region indicates that histone H3K4 di-methylation is likely a mechanism to trigger the postnatal increase in PPAR α and PGC-1 α gene activation. However, the causative mechanisms remain yet to be determined.

Epigenetic regulation of PPAR α and PGC-1 α gene transcription by DNA and histone methylations provides a strong candidate mechanism for the

developmental programming of nutrient homeostasis in postnatal liver development.

Taken together, the present study suggests that epigenetic modifications are a probable mechanism facilitating a permissive chromatin state that activates the transcription of Ahr, PPAR α and PGC-1 α during liver development in mice.

CHAPTER NINE. GENERAL SUMMARY AND CONCLUSIONS

The present dissertation has systemically characterized the ontogenic expression signatures and molecular regulatory mechanisms of numerous drug-processing genes. Both the nuclear receptor-mediated regulation and epigenetic regulation of these genes have been addressed.

There are profound changes during development in the hepatic expression of drug processing genes, and they may have significant impact on the risk of adverse drug reactions in children. Through multi-disciplinary approaches, the present study has demonstrated that the hepatic expression of drug-processing genes is hierarchically regulated by multiple mechanisms. Bile acids have attracted great interest in recent years due to the discovery of bile acids as endogenous ligands for two nuclear receptors, FXR and PXR. In the immediate perinatal period, newborns need to synthesize and secrete bile acids into bile to facilitate the absorption of milk. Consistently, data from my dissertation showed that hepatic expression of bile-acid synthetic enzymes and transporters was markedly induced right after birth, and the increased expression of bile acid transporters appears to be mediated by FXR activation.

In addition to maturation of the bile acid processing system during postnatal liver development, weaning and food intake will result in absorption of an increasing amount of xenobiotics. Increased absorption of xenobiotics requires the activation of detoxification systems. PXR is a classic xenobiotic sensor in the

liver. Because of its large and expandable ligand binding pocket, PXR is able to accommodate a large variety of xenobiotics as ligands. Using the ChIP-Seq approach combined with bioinformatics analysis and *in vitro* validations, I have examined direct target genes of PXR in the entire genome in the mouse liver. I have identified a novel DR-(5n+4) periodic DNA-binding motif for the PXR protein. This finding has challenged the existing paradigm of our current understandings on the consensus sequences that PXR recognizes.

Briefly, for phase-I metabolic processes, a systematic investigation of the ontogeny of novel isoforms of the first 4 Cyp families was performed, using messenger RNA assays (high throughput multiplex bDNA assays and RT-qPCR). The genetic and epigenetic regulatory mechanisms for the ontogeny of these Cyps were determined by the ChIP-Seq and ChIP-on-chip. All of these Cyp mRNAs increased after birth, forming 4 distinct ontogeny patterns identified by cluster analysis. Distinct segments of the Cyp isoforms within the same chromosomal cluster showed similar ontogenic patterns. In summary, the present study has revealed 4 patterns of the ontogeny of novel Cyps in liver, and showed that certain Cyps within a genomic cluster shared similar ontogeny patterns, suggesting that the Cyps are regulated by common pathways within the clusters in liver development. The ontogeny of Cyp3a genes seem to be regulated by distinct histone methylation patterns (H3K4Me2 and H3K27Me3), and positive enrichment of PXR binding was observed at multiple regions within the *Cyp3a* gene locus.

For phase-II metabolism, using the glutathione S-transferases as an example, I have investigated the ontogeny and the regulatory mechanisms of all known Gst isoforms during liver development. Similar to the phase-I P450 enzymes, the Gst isoforms also showed distinct ontogenic expression patterns, and genome-wide ChIP-seq revealed direct PXR-binding sites in the *Gsta*, *Gstm*, *Gstt*, and *Gstp* polycistron clusters, as well as in the *Mgst1* gene locus. ChIP-on-chip analysis demonstrated that DNA methylation and histone-H3K27-trimethylation (H3K27me3), two hallmarks for gene transcriptional suppression, were consistently low around the *Gstz1* gene locus. In contrast, enrichment of histone-H3K4-dimethylation (H3K4me2), a hallmark for gene transcriptional activation, increased at this gene locus from the prenatal to the young adult period.

For transporters, first, the present study has demonstrated that the initiation of bile-acid signaling mediated by the nuclear receptor FXR, may be responsible for the neonatal upregulation of critical bile-acid and phospholipid transporters in the liver. The expression of the genes in classic pathway of bile-acid biosynthesis was increased right after birth, and appears to be responsible for the activation of FXR in the neonatal liver. Secondly, the expression of the genes encoding xenobiotic transporters tended to be enriched in later developmental ages (after adolescent ages), and multiple transporter genes appear to be direct genes regulated by PXR, including *Oatp1a4* and *Mrp3*. In addition, novel PXR-DNA binding sites and PXR-DNA binding motifs have been characterized using ChIP-

Seq and motif analysis, validated by ELISA-based transcription factor binding assays.

Finally, the ontogeny and regulatory mechanisms of the xeno-sensor AhR, the lipid sensor PPAR α , as well as the glucose sensor PGC-1 α , have been characterized. H3K4Me2 seems to be the choice of nature to induce their gene expression during postnatal liver maturation.

In conclusion, through integrating various research models and technologies, the present dissertation has examined the expression patterns as well as the genetic and epigenetic mechanisms for the regulation of phase-I and –II drug metabolizing enzymes as well as transporters during liver development. Our studies have provided novel insights into identifying and further understanding the molecular targets for efficacious and safe drug treatments in children.

CHAPTER TEN. REFERENCES

- Ajmo JM, Liang X, Rogers CQ, Pennock B and You M (2008) Resveratrol alleviates alcoholic fatty liver in mice. *Am J Physiol Gastrointest Liver Physiol* **295**:G833-842.
- Aleksunes LM, Slitt AM, Cherrington NJ, Thibodeau MS, Klaassen CD and Manautou JE (2005) Differential expression of mouse hepatic transporter genes in response to acetaminophen and carbon tetrachloride. *Toxicol Sci* **83**:44-52.
- Alnouti Y, Csanaky IL and Klaassen CD (2008a) Quantitative-profiling of bile acids and their conjugates in mouse liver, bile, plasma, and urine using LC-MS/MS. *J Chromatogr B Analyt Technol Biomed Life Sci* **873**:209-217.
- Alnouti Y and Klaassen CD (2006) Tissue distribution and ontogeny of sulfotransferase enzymes in mice. *Toxicol Sci* **93**:242-255.
- Alnouti Y and Klaassen CD (2008b) Tissue distribution, ontogeny, and regulation of aldehyde dehydrogenase (Aldh) enzymes mRNA by prototypical microsomal enzyme inducers in mice. *Toxicol Sci* **101**:51-64.
- Andreola F, Hayhurst GP, Luo G, Ferguson SS, Gonzalez FJ, Goldstein JA and De Luca LM (2004) Mouse liver CYP2C39 is a novel retinoic acid 4-hydroxylase. Its down-regulation offers a molecular basis for liver retinoid accumulation and fibrosis in aryl hydrocarbon receptor-null mice. *J Biol Chem* **279**:3434-3438.
- Andrulionyte L, Kuulasmaa T, Chiasson JL and Laakso M (2007) Single nucleotide polymorphisms of the peroxisome proliferator-activated

- receptor-alpha gene (PPARA) influence the conversion from impaired glucose tolerance to type 2 diabetes: the STOP-NIDDM trial. *Diabetes* **56**:1181-1186.
- A Armstrong RN (1997) Structure, catalytic mechanism, and evolution of the glutathione transferases. *Chem Res Toxicol* **10**:2-18.
- Arrese M, Trauner M, Ananthanarayanan M, Boyer JL and Suchy FJ (1998) Maternal cholestasis does not affect the ontogenic pattern of expression of the Na⁺/taurocholate cotransporting polypeptide (ntcp) in the fetal and neonatal rat liver. *Hepatology* **28**:789-795.
- Assem M, Schuetz EG, Leggas M, Sun D, Yasuda K, Reid G, Zelcer N, Adachi M, Strom S, Evans RM, Moore DD, Borst P and Schuetz JD (2004) Interactions between hepatic Mrp4 and Sult2a as revealed by the constitutive androstane receptor and Mrp4 knockout mice. *J Biol Chem* **279**:22250-22257.
- Balasubramanian N, Shahid M, Suchy FJ and Ananthanarayanan M (2005) Multiple mechanisms of ontogenic regulation of nuclear receptors during rat liver development. *Am J Physiol Gastrointest Liver Physiol* **288**:G251-260.
- Baldwin WS, Marko PB and Nelson DR (2009) The cytochrome P450 (CYP) gene superfamily in *Daphnia pulex*. *BMC Genomics* **10**:169.
- Ballatori N, Christian WV, Lee JY, Dawson PA, Soroka CJ, Boyer JL, Madejczyk MS and Li N (2005) OSTalpha-OSTbeta: a major basolateral bile acid and

- steroid transporter in human intestinal, renal, and biliary epithelia.
Hepatology **42**:1270-1279.
- Bammler TK, Smith CA and Wolf CR (1994) Isolation and characterization of two mouse Pi-class glutathione S-transferase genes. *Biochem J* **298** (Pt 2):385-390.
- Barker EV, Hume R, Hallas A and Coughtrie WH (1994)
Dehydroepiandrosterone sulfotransferase in the developing human fetus: quantitative biochemical and immunological characterization of the hepatic, renal, and adrenal enzymes. *Endocrinology* **134**:982-989.
- Barski A, Cuddapah S, Cui K, Roh TY, Schones DE, Wang Z, Wei G, Chepelev I and Zhao K (2007) High-resolution profiling of histone methylations in the human genome. *Cell* **129**:823-837.
- Beaudry JB, Pierreux CE, Hayhurst GP, Plumb-Rudewiez N, Weiss MC, Rousseau GG and Lemaigre FP (2006) Threshold levels of hepatocyte nuclear factor 6 (HNF-6) acting in synergy with HNF-4 and PGC-1alpha are required for time-specific gene expression during liver development. *Mol Cell Biol* **26**:6037-6046.
- Beilke LD, Aleksunes LM, Holland RD, Besselsen DG, Beger RD, Klaassen CD and Cherrington NJ (2009) Constitutive androstane receptor-mediated changes in bile acid composition contributes to hepatoprotection from lithocholic acid-induced liver injury in mice. *Drug Metab Dispos* **37**:1035-1045.

- Bernstein BE, Kamal M, Lindblad-Toh K, Bekiranov S, Bailey DK, Huebert DJ, McMahon S, Karlsson EK, Kulbokas EJ, 3rd, Gingeras TR, Schreiber SL and Lander ES (2005) Genomic maps and comparative analysis of histone modifications in human and mouse. *Cell* **120**:169-181.
- Bird A (2002) DNA methylation patterns and epigenetic memory. *Genes Dev* **16**:6-21.
- Bjorkhem I (1994) Inborn errors of metabolism with consequences for bile acid biosynthesis. A minireview. *Scand J Gastroenterol Suppl* **204**:68-72.
- Blake MJ, Castro L, Leeder JS and Kearns GL (2005) Ontogeny of drug metabolizing enzymes in the neonate. *Semin Fetal Neonatal Med* **10**:123-138.
- Board PG, Baker RT, Chelvanayagam G and Jermiin LS (1997) Zeta, a novel class of glutathione transferases in a range of species from plants to humans. *Biochem J* **328 (Pt 3)**:929-935.
- Boyer JL, Hagenbuch B, Ananthanarayanan M, Suchy F, Stieger B and Meier PJ (1993) Phylogenic and ontogenic expression of hepatocellular bile acid transport. *Proc Natl Acad Sci U S A* **90**:435-438.
- Boyer LA, Plath K, Zeitlinger J, Brambrink T, Medeiros LA, Lee TI, Levine SS, Wernig M, Tajonar A, Ray MK, Bell GW, Otte AP, Vidal M, Gifford DK, Young RA and Jaenisch R (2006) Polycomb complexes repress developmental regulators in murine embryonic stem cells. *Nature* **441**:349-353.

- Buckley DB and Klaassen CD (2009) Induction of Mouse UDP-Glucuronosyltransferase mRNA Expression in Liver and Intestine by Activators of AhR, CAR, PXR, PPAR{alpha}, and Nrf2. *Drug Metab Dispos.* **37**: 847-56
- Buist SC, Cherrington NJ, Choudhuri S, Hartley DP and Klaassen CD (2002) Gender-specific and developmental influences on the expression of rat organic anion transporters. *J Pharmacol Exp Ther* **301**:145-151.
- Caldwell J (2004) Pharmacogenetics and individual variation in the range of amino acid adequacy: the biological aspects. *J Nutr* **134**:1600S-1604S; discussion 1630S-1632S, 1667S-1672S.
- Cappiello M, Giuliani L, Rane A and Pacifici GM (1991) Dopamine sulphotransferase is better developed than p-nitrophenol sulphotransferase in the human fetus. *Dev Pharmacol Ther* **16**:83-88.
- Chen F, Ananthanarayanan M, Emre S, Neimark E, Bull LN, Knisely AS, Strautnieks SS, Thompson RJ, Magid MS, Gordon R, Balasubramanian N, Suchy FJ and Shneider BL (2004) Progressive familial intrahepatic cholestasis, type 1, is associated with decreased farnesoid X receptor activity. *Gastroenterology* **126**:756-764.
- Cheng X and Klaassen CD (2006) Regulation of mRNA expression of xenobiotic transporters by the pregnane x receptor in mouse liver, kidney, and intestine. *Drug Metab Dispos* **34**:1863-1867.

- Cheng X, Maher J, Chen C and Klaassen CD (2005a) Tissue distribution and ontogeny of mouse organic anion transporting polypeptides (Oatps). *Drug Metab Dispos* **33**:1062-1073.
- Cheng X, Maher J, Dieter MZ and Klaassen CD (2005b) Regulation of mouse organic anion-transporting polypeptides (Oatps) in liver by prototypical microsomal enzyme inducers that activate distinct transcription factor pathways. *Drug Metab Dispos* **33**:1276-1282.
- Chiang JY (2002) Bile acid regulation of gene expression: roles of nuclear hormone receptors. *Endocr Rev* **23**:443-463.
- Chiang JY (2004) Regulation of bile acid synthesis: pathways, nuclear receptors, and mechanisms. *J Hepatol* **40**:539-551.
- Chinetti G, Gbaguidi FG, Griglio S, Mallat Z, Antonucci M, Poulain P, Chapman J, Fruchart JC, Tedgui A, Najib-Fruchart J and Staels B (2000) CLA-1/SR-BI is expressed in atherosclerotic lesion macrophages and regulated by activators of peroxisome proliferator-activated receptors. *Circulation* **101**:2411-2417.
- Chinetti G, Lestavel S, Bocher V, Remaley AT, Neve B, Torra IP, Teissier E, Minnich A, Jaye M, Duverger N, Brewer HB, Fruchart JC, Clavey V and Staels B (2001) PPAR-alpha and PPAR-gamma activators induce cholesterol removal from human macrophage foam cells through stimulation of the ABCA1 pathway. *Nat Med* **7**:53-58.

- Chinetti G, Lestavel S, Fruchart JC, Clavey V and Staels B (2003) Peroxisome proliferator-activated receptor alpha reduces cholesterol esterification in macrophages. *Circ Res* **92**:212-217.
- Chou CJ, Haluzik M, Gregory C, Dietz KR, Vinson C, Gavrilova O and Reitman ML (2002) WY14,643, a peroxisome proliferator-activated receptor alpha (PPARalpha) agonist, improves hepatic and muscle steatosis and reverses insulin resistance in lipoatrophic A-ZIP/F-1 mice. *J Biol Chem* **277**:24484-24489.
- Choudhary D, Jansson I, Schenkman JB, Sarfarazi M and Stoilov I (2003) Comparative expression profiling of 40 mouse cytochrome P450 genes in embryonic and adult tissues. *Arch Biochem Biophys* **414**:91-100.
- Choudhary D, Jansson I, Stoilov I, Sarfarazi M and Schenkman JB (2005) Expression patterns of mouse and human CYP orthologs (families 1-4) during development and in different adult tissues. *Arch Biochem Biophys* **436**:50-61.
- Choudhuri S, Cherrington NJ, Li N and Klaassen CD (2003) Constitutive expression of various xenobiotic and endobiotic transporter mRNAs in the choroid plexus of rats. *Drug Metab Dispos* **31**:1337-1345.
- Choudhuri S, Cui Y and Klaassen CD (2010) Molecular targets of epigenetic regulation and effectors of environmental influences. *Toxicol Appl Pharmacol* **245**:378-393.
- Choudhuri S, Ogura K and Klaassen CD (2001) Cloning, expression, and ontogeny of mouse organic anion-transporting polypeptide-5, a kidney-

- specific organic anion transporter. *Biochem Biophys Res Commun* **280**:92-98.
- Cooper MP, Qu L, Rohas LM, Lin J, Yang W, Erdjument-Bromage H, Tempst P and Spiegelman BM (2006) Defects in energy homeostasis in Leigh syndrome French Canadian variant through PGC-1alpha/LRP130 complex. *Genes Dev* **20**:2996-3009.
- Coughlin SS and Piper M (1999) Genetic polymorphisms and risk of breast cancer. *Cancer Epidemiol Biomarkers Prev* **8**:1023-1032.
- Crosignani A, Del Puppo M, Longo M, De Fabiani E, Caruso D, Zuin M, Podda M, Javitt NB and Kienle MG (2007) Changes in classic and alternative pathways of bile-acid synthesis in chronic liver disease. *Clin Chim Acta* **382**:82-88.
- Cui JY, Choudhuri S, Knight TR and Klaassen CD (2010) Genetic and Epigenetic Regulation and Expression Signatures of Glutathione S-Transferases in Developing Mouse Liver. *Toxicol Sci* **116**: 32-43
- Cui YJ, Cheng X, Weaver YM and Klaassen CD (2009a) Tissue distribution, gender-divergent expression, ontogeny, and chemical induction of multidrug resistance transporter genes (Mdr1a, Mdr1b, Mdr2) in mice. *Drug Metab Dispos* **37**:203-210.
- Cui YJ, Yeager RL, Zhong XB and Klaassen CD (2009b) Ontogenic expression of hepatic Ahr mRNA is associated with histone H3K4 di-methylation during mouse liver development. *Toxicol Lett* **189**:184-190.

- Davit-Spraul A, Fabre M, Branchereau S, Baussan C, Gonzales E, Stieger B, Bernard O and Jacquemin E ATP8B1 and ABCB11 analysis in 62 children with normal gamma-glutamyl transferase progressive familial intrahepatic cholestasis (PFIC): phenotypic differences between PFIC1 and PFIC2 and natural history. *Hepatology* **51**:1645-1655.
- de Vree JM, Jacquemin E, Sturm E, Cresteil D, Bosma PJ, Aten J, Deleuze JF, Desrochers M, Burdelski M, Bernard O, Oude Elferink RP and Hadchouel M (1998) Mutations in the MDR3 gene cause progressive familial intrahepatic cholestasis. *Proc Natl Acad Sci U S A* **95**:282-287.
- de Wildt SN, Kearns GL, Leeder JS and van den Anker JN (1999) Cytochrome P450 3A: ontogeny and drug disposition. *Clin Pharmacokinet* **37**:485-505.
- Dezentje VO, Guchelaar HJ, Nortier JW, van de Velde CJ and Gelderblom H (2009) Clinical implications of CYP2D6 genotyping in tamoxifen treatment for breast cancer. *Clin Cancer Res* **15**:15-21.
- Dietrich CG, Martin IV, Porn AC, Voigt S, Gartung C, Trautwein C and Geier A (2007) Fasting induces basolateral uptake transporters of the SLC family in the liver via HNF4alpha and PGC1alpha. *Am J Physiol Gastrointest Liver Physiol* **293**:G585-590.
- Douet V, Heller MB and Le Saux O (2007) DNA methylation and Sp1 binding determine the tissue-specific transcriptional activity of the mouse Abcc6 promoter. *Biochem Biophys Res Commun* **354**:66-71.

- Dunn RT, 2nd, Gleason BA, Hartley DP and Klaassen CD (1999) Postnatal ontogeny and hormonal regulation of sulfotransferase SULT1B1 in male and female rats. *J Pharmacol Exp Ther* **290**:319-324.
- Elliott WH and Hyde PM (1971) Metabolic pathways of bile acid synthesis. *Am J Med* **51**:568-579.
- Estabrook RW (2003) A passion for P450s (remembrances of the early history of research on cytochrome P450). *Drug Metab Dispos* **31**:1461-1473.
- Falany CN, Johnson MR, Barnes S and Diasio RB (1994) Glycine and taurine conjugation of bile acids by a single enzyme. Molecular cloning and expression of human liver bile acid CoA:amino acid N-acyltransferase. *J Biol Chem* **269**:19375-19379.
- Fernandez-Salguero P, Pineau T, Hilbert DM, McPhail T, Lee SS, Kimura S, Nebert DW, Rudikoff S, Ward JM and Gonzalez FJ (1995) Immune system impairment and hepatic fibrosis in mice lacking the dioxin-binding Ah receptor. *Science* **268**:722-726.
- Fouts JR and Adamson RH (1959) Drug metabolism in the newborn rabbit. *Science* **129**:897-898.
- Gaedigk A, Baker DW, Totah RA, Gaedigk R, Pearce RE, Vyhldal CA, Zeldin DC and Leeder JS (2006) Variability of CYP2J2 expression in human fetal tissues. *J Pharmacol Exp Ther* **319**:523-532.
- Geick A, Eichelbaum M and Burk O (2001) Nuclear receptor response elements mediate induction of intestinal MDR1 by rifampin. *J Biol Chem* **276**:14581-14587.

- Girard J, Perdereau D, Foufelle F, Prip-Buus C and Ferre P (1994) Regulation of lipogenic enzyme gene expression by nutrients and hormones. *FASEB J* **8**:36-42.
- Glatt H (2000) Sulfotransferases in the bioactivation of xenobiotics. *Chem Biol Interact* **129**:141-170.
- Gonzalez FJ and Fernandez-Salguero P (1998) The aryl hydrocarbon receptor: studies using the AHR-null mice. *Drug Metab Dispos* **26**:1194-1198.
- Gonzalez FJ, Song BJ and Hardwick JP (1986) Pregnenolone 16 alpha-carbonitrile-inducible P-450 gene family: gene conversion and differential regulation. *Mol Cell Biol* **6**:2969-2976.
- Guo GL, Staudinger J, Ogura K and Klaassen CD (2002) Induction of rat organic anion transporting polypeptide 2 by pregnenolone-16alpha-carbonitrile is via interaction with pregnane X receptor. *Mol Pharmacol* **61**:832-839.
- Guzelian J, Barwick JL, Hunter L, Phang TL, Quattrochi LC and Guzelian PS (2006) Identification of genes controlled by the pregnane X receptor by microarray analysis of mRNAs from pregnenolone 16alpha-carbonitrile-treated rats. *Toxicol Sci* **94**:379-387.
- Hagenbuch B, Scharschmidt BF and Meier PJ (1996) Effect of antisense oligonucleotides on the expression of hepatocellular bile acid and organic anion uptake systems in *Xenopus laevis* oocytes. *Biochem J* **316 (Pt 3)**:901-904.
- Hakkola J, Tanaka E and Pelkonen O (1998) Developmental expression of cytochrome P450 enzymes in human liver. *Pharmacol Toxicol* **82**:209-217.

- Harstad EB, Guite CA, Thomae TL and Bradfield CA (2006) Liver deformation in Ahr-null mice: evidence for aberrant hepatic perfusion in early development. *Mol Pharmacol* **69**:1534-1541.
- Hart SN, Cui Y, Klaassen CD and Zhong XB (2009) Three patterns of cytochrome P450 gene expression during liver maturation in mice. *Drug Metab Dispos* **37**:116-121.
- Hartley DP and Klaassen CD (2000) Detection of chemical-induced differential expression of rat hepatic cytochrome P450 mRNA transcripts using branched DNA signal amplification technology. *Drug Metab Dispos* **28**:608-616.
- Hawkins RD and Ren B (2006) Genome-wide location analysis: insights on transcriptional regulation. *Hum Mol Genet* **15 Spec No 1**:R1-7.
- Hayes JD, Flanagan JU and Jowsey IR (2005) Glutathione transferases. *Annu Rev Pharmacol Toxicol* **45**:51-88.
- Hayes JD and Pulford DJ (1995) The glutathione S-transferase supergene family: regulation of GST and the contribution of the isoenzymes to cancer chemoprotection and drug resistance. *Crit Rev Biochem Mol Biol* **30**:445-600.
- Hernandez JP, Mota LC, Huang W, Moore DD and Baldwin WS (2009) Sexually dimorphic regulation and induction of P450s by the constitutive androstane receptor (CAR). *Toxicology* **256**:53-64.

- Heubi JE, Balistreri WF, Partin JC, Schubert WK and McGraw CA (1979) Refractory infantile diarrhea due to primary bile acid malabsorption. *J Pediatr* **94**:546-551.
- Heubi JE, Setchell KD and Bove KE (2007) Inborn errors of bile acid metabolism. *Semin Liver Dis* **27**:282-294.
- Hines RN (2007) Ontogeny of human hepatic cytochromes P450. *J Biochem Mol Toxicol* **21**:169-175.
- Hirschfield GM and Alexander GJ (2006) Gilbert's syndrome: an overview for clinical biochemists. *Ann Clin Biochem* **43**:340-343.
- Hunter AL and Klaassen CD (1975) Biliary excretion of colchicine in newborn rats. *Drug Metab Dispos* **3**:530-535.
- Inagaki T, Choi M, Moschetta A, Peng L, Cummins CL, McDonald JG, Luo G, Jones SA, Goodwin B, Richardson JA, Gerard RD, Repa JJ, Mangelsdorf DJ and Kliewer SA (2005) Fibroblast growth factor 15 functions as an enterohepatic signal to regulate bile acid homeostasis. *Cell Metab* **2**:217-225.
- Jaenisch R and Bird A (2003) Epigenetic regulation of gene expression: how the genome integrates intrinsic and environmental signals. *Nat Genet* **33 Suppl**:245-254.
- Jin B, Park DW, Nam KW, Oh GT, Lee YS and Ryu DY (2004) CpG methylation of the mouse CYP1A2 promoter. *Toxicol Lett* **152**:11-18.
- Johnson DR, Guo GL and Klaassen CD (2002) Expression of rat Multidrug Resistance Protein 2 (Mrp2) in male and female rats during normal and

- pregnenolone-16alpha-carbonitrile (PCN)-induced postnatal ontogeny. *Toxicology* **178**:209-219.
- Johnson WE, Li W, Meyer CA, Gottardo R, Carroll JS, Brown M and Liu XS (2006) Model-based analysis of tiling-arrays for ChIP-chip. *Proc Natl Acad Sci U S A* **103**:12457-12462.
- Kang HS, Angers M, Beak JY, Wu X, Gimble JM, Wada T, Xie W, Collins JB, Grissom SF and Jetten AM (2007) Gene expression profiling reveals a regulatory role for ROR alpha and ROR gamma in phase I and phase II metabolism. *Physiol Genomics* **31**:281-294.
- Kawamoto T, Kakizaki S, Yoshinari K and Negishi M (2000) Estrogen activation of the nuclear orphan receptor CAR (constitutive active receptor) in induction of the mouse Cyp2b10 gene. *Mol Endocrinol* **14**:1897-1905.
- Kearns GL, Abdel-Rahman SM, Alander SW, Blowey DL, Leeder JS and Kauffman RE (2003) Developmental pharmacology--drug disposition, action, and therapy in infants and children. *N Engl J Med* **349**:1157-1167.
- Keen JH and Jakoby WB (1978) Glutathione transferases. Catalysis of nucleophilic reactions of glutathione. *J Biol Chem* **253**:5654-5657.
- Kershaw WC, Lehman-McKeeman LD and Klaassen CD (1990) Hepatic isometallothioneins in mice: induction in adults and postnatal ontogeny. *Toxicol Appl Pharmacol* **104**:267-275.
- Kiefer JC (2007) Epigenetics in development. *Dev Dyn* **236**:1144-1156.
- Kikuchi R, Kusuhara H, Hattori N, Shiota K, Kim I, Gonzalez FJ and Sugiyama Y (2006) Regulation of the expression of human organic anion transporter 3

- by hepatocyte nuclear factor 1alpha/beta and DNA methylation. *Mol Pharmacol* **70**:887-896.
- Kim TH, Barrera LO, Zheng M, Qu C, Singer MA, Richmond TA, Wu Y, Green RD and Ren B (2005) A high-resolution map of active promoters in the human genome. *Nature* **436**:876-880.
- Klaassen CD (1972) Immaturity of the newborn rat's hepatic excretory function for ouabain. *J Pharmacol Exp Ther* **183**:520-526.
- Klaassen CD (1973a) Comparison of the toxicity of chemicals in newborn rats to bile duct-ligated and sham-operated rats and mice. *Toxicol Appl Pharmacol* **24**:37-44.
- Klaassen CD (1973b) Hepatic excretory function in the newborn rat. *J Pharmacol Exp Ther* **184**:721-728.
- Klaassen CD (1974) Stimulation of the development of the hepatic excretory mechanism for ouabain in newborn rats with microsomal enzyme inducers. *J Pharmacol Exp Ther* **191**:212-218.
- Klaassen CD (1975a) Biliary excretion of drugs: role of ligandin in newborn immaturity and in the action of microsomal enzyme inducers. *J Pharmacol Exp Ther* **195**:311-319.
- Klaassen CD (1975b) Hepatic uptake of cardiac glycosides in newborn rats, rabbits and dogs. *Biochem Pharmacol* **24**:923-925.
- Klaassen CD and Aleksunes LM Xenobiotic, bile acid, and cholesterol transporters: function and regulation (2010). *Pharmacol Rev* **62**:1-96.

- Klaassen CD and Lehman-McKeeman LD (1989) Regulation of the isoforms of metallothionein. *Biol Trace Elem Res* **21**:119-129.
- Klaassen CD and Lu H (2008) Xenobiotic transporters: ascribing function from gene knockout and mutation studies. *Toxicol Sci* **101**:186-196.
- Kliwer SA, Goodwin B and Willson TM (2002) The nuclear pregnane X receptor: a key regulator of xenobiotic metabolism. *Endocr Rev* **23**:687-702.
- Kliwer SA, Moore JT, Wade L, Staudinger JL, Watson MA, Jones SA, McKee DD, Oliver BB, Willson TM, Zetterstrom RH, Perlmann T and Lehmann JM (1998) An orphan nuclear receptor activated by pregnanes defines a novel steroid signaling pathway. *Cell* **92**:73-82.
- Knapen MF, Peters WH, Mulder TP, Merkus HM, Jansen JB and Steegers EA (1999) Glutathione and glutathione-related enzymes in decidua and placenta of controls and women with pre-eclampsia. *Placenta* **20**:541-546.
- Knight TR, Choudhuri S and Klaassen CD (2007) Constitutive mRNA expression of various glutathione S-transferase isoforms in different tissues of mice. *Toxicol Sci* **100**:513-524.
- Knight TR, Choudhuri S and Klaassen CD (2007) Constitutive mRNA expression of various glutathione S-transferase isoforms in different tissues of mice. *Toxicol Sci* **100**:513-524.
- Knight TR, Choudhuri S and Klaassen CD (2008) Induction of hepatic glutathione S-transferases in male mice by prototypes of various classes of microsomal enzyme inducers. *Toxicol Sci* **106**:329-338.

- Knisely AS, Strautnieks SS, Meier Y, Stieger B, Byrne JA, Portmann BC, Bull LN, Pawlikowska L, Bilezikci B, Ozcay F, Laszlo A, Tiszlavicz L, Moore L, Raftos J, Arnell H, Fischler B, Nemeth A, Papadogiannakis N, Cielecka-Kuszyk J, Jankowska I, Pawlowska J, Melin-Aldana H, Emerick KM, Whittington PF, Mieli-Vergani G and Thompson RJ (2006) Hepatocellular carcinoma in ten children under five years of age with bile salt export pump deficiency. *Hepatology* **44**:478-486.
- Kouzarides T (2007) Chromatin modifications and their function. *Cell* **128**:693-705.
- Krauer B and Dayer P (1991) Fetal drug metabolism and its possible clinical implications. *Clin Pharmacokinet* **21**:70-80.
- Lahvis GP and Bradfield CA (1998) Ahr null alleles: distinctive or different? *Biochem Pharmacol* **56**:781-787.
- Lam P, Wang R and Ling V (2005) Bile acid transport in sister of P-glycoprotein (ABCB11) knockout mice. *Biochemistry* **44**:12598-12605.
- Lee SS, Chan WY, Lo CK, Wan DC, Tsang DS and Cheung WT (2004a) Requirement of PPARalpha in maintaining phospholipid and triacylglycerol homeostasis during energy deprivation. *J Lipid Res* **45**:2025-2037.
- Lee SS, Pineau T, Drago J, Lee EJ, Owens JW, Kroetz DL, Fernandez-Salguero PM, Westphal H and Gonzalez FJ (1995) Targeted disruption of the alpha isoform of the peroxisome proliferator-activated receptor gene in mice results in abolishment of the pleiotropic effects of peroxisome proliferators. *Mol Cell Biol* **15**:3012-3022.

- Lee TI, Jenner RG, Boyer LA, Guenther MG, Levine SS, Kumar RM, Chevalier B, Johnstone SE, Cole MF, Isono K, Koseki H, Fuchikami T, Abe K, Murray HL, Zucker JP, Yuan B, Bell GW, Herbolsheimer E, Hannett NM, Sun K, Odom DT, Otte AP, Volkert TL, Bartel DP, Melton DA, Gifford DK, Jaenisch R and Young RA (2006) Control of developmental regulators by Polycomb in human embryonic stem cells. *Cell* **125**:301-313.
- Lee YL, Lin YC, Lee YC, Wang JY, Hsiue TR and Guo YL (2004b) Glutathione S-transferase P1 gene polymorphism and air pollution as interactive risk factors for childhood asthma. *Clin Exp Allergy* **34**:1707-1713.
- Leeder JS, Gaedigk R, Marcucci KA, Gaedigk A, Vyhldal CA, Schindel BP and Pearce RE (2005) Variability of CYP3A7 expression in human fetal liver. *J Pharmacol Exp Ther* **314**:626-635.
- Lehman-McKeeman LD, Andrews GK and Klaassen CD (1988) Ontogeny and induction of hepatic isometallothioneins in immature rats. *Toxicol Appl Pharmacol* **92**:10-17.
- Leone TC, Lehman JJ, Finck BN, Schaeffer PJ, Wende AR, Boudina S, Courtois M, Wozniak DF, Sambandam N, Bernal-Mizrachi C, Chen Z, Holloszy JO, Medeiros DM, Schmidt RE, Saffitz JE, Abel ED, Semenkovich CF and Kelly DP (2005) PGC-1alpha deficiency causes multi-system energy metabolic derangements: muscle dysfunction, abnormal weight control and hepatic steatosis. *PLoS Biol* **3**:e101.

- Li AC and Glass CK (2004) PPAR- and LXR-dependent pathways controlling lipid metabolism and the development of atherosclerosis. *J Lipid Res* **45**:2161-2173.
- Li H, Dong L and Whitlock JP, Jr. (1994) Transcriptional activation function of the mouse Ah receptor nuclear translocator. *J Biol Chem* **269**:28098-28105.
- Li N, Hartley DP, Cherrington NJ and Klaassen CD (2002) Tissue expression, ontogeny, and inducibility of rat organic anion transporting polypeptide 4. *J Pharmacol Exp Ther* **301**:551-560.
- Li X, Schuler MA and Berenbaum MR (2007) Molecular mechanisms of metabolic resistance to synthetic and natural xenobiotics. *Annu Rev Entomol* **52**:231-253.
- Li Y, Cui Y, Hart SN, Klaassen CD and Zhong XB (2009) Dynamic patterns of histone methylation are associated with ontogenic expression of the Cyp3a genes during mouse liver maturation. *Mol Pharmacol* **75**:1171-1179.
- Lillicrop KA, Phillips ES, Jackson AA, Hanson MA and Burdge GC (2005) Dietary protein restriction of pregnant rats induces and folic acid supplementation prevents epigenetic modification of hepatic gene expression in the offspring. *J Nutr* **135**:1382-1386.
- Lin J, Wu PH, Tarr PT, Lindenberg KS, St-Pierre J, Zhang CY, Mootha VK, Jager S, Vianna CR, Reznick RM, Cui L, Manieri M, Donovan MX, Wu Z, Cooper MP, Fan MC, Rohas LM, Zavacki AM, Cinti S, Shulman GI, Lowell BB, Krainc D and Spiegelman BM (2004) Defects in adaptive energy

- metabolism with CNS-linked hyperactivity in PGC-1alpha null mice. *Cell* **119**:121-135.
- Liu L and Klaassen CD (1996a) Ontogeny and hormonal basis of female-dominant rat hepatic sulfotransferases. *J Pharmacol Exp Ther* **279**:386-391.
- Liu L and Klaassen CD (1996b) Ontogeny and hormonal basis of male-dominant rat hepatic sulfotransferases. *Mol Pharmacol* **50**:565-572.
- Liu Y, Binz J, Numerick MJ, Dennis S, Luo G, Desai B, MacKenzie KI, Mansfield TA, Kliewer SA, Goodwin B and Jones SA (2003) Hepatoprotection by the farnesoid X receptor agonist GW4064 in rat models of intra- and extrahepatic cholestasis. *J Clin Invest* **112**:1678-1687.
- Lofgren S, Baldwin RM, Carleros M, Terelius Y, Fransson-Steen R, Mwinyi J, Waxman DJ and Ingelman-Sundberg M (2009) Regulation of human CYP2C18 and CYP2C19 in transgenic mice: influence of castration, testosterone, and growth hormone. *Drug Metab Dispos* **37**:1505-1512.
- Ma Q, Dong L and Whitlock JP, Jr. (1995) Transcriptional activation by the mouse Ah receptor. Interplay between multiple stimulatory and inhibitory functions. *J Biol Chem* **270**:12697-12703.
- Maher JM, Cheng X, Slitt AL, Dieter MZ and Klaassen CD (2005a) Induction of the multidrug resistance-associated protein family of transporters by chemical activators of receptor-mediated pathways in mouse liver. *Drug Metab Dispos* **33**:956-962.

- Maher JM, Slitt AL, Cherrington NJ, Cheng X and Klaassen CD (2005b) Tissue distribution and hepatic and renal ontogeny of the multidrug resistance-associated protein (Mrp) family in mice. *Drug Metab Dispos* **33**:947-955.
- Margolin AA, Palomero T, Sumazin P, Califano A, Ferrando AA and Stolovitzky G (2009) ChIP-on-chip significance analysis reveals large-scale binding and regulation by human transcription factor oncogenes. *Proc Natl Acad Sci U S A* **106**:244-249.
- Mazzucotelli A, Viguerie N, Tiraby C, Annicotte JS, Mairal A, Klimcakova E, Lepin E, Delmar P, Dejean S, Tavernier G, Lefort C, Hidalgo J, Pineau T, Fajas L, Clement K and Langin D (2007) The transcriptional coactivator peroxisome proliferator activated receptor (PPAR)gamma coactivator-1 alpha and the nuclear receptor PPAR alpha control the expression of glycerol kinase and metabolism genes independently of PPAR gamma activation in human white adipocytes. *Diabetes* **56**:2467-2475.
- McCarver DG and Hines RN (2002) The ontogeny of human drug-metabolizing enzymes: phase II conjugation enzymes and regulatory mechanisms. *J Pharmacol Exp Ther* **300**:361-366.
- McDonagh PD, Judah DJ, Hayes JD, Lian LY, Neal GE, Wolf CR and Roberts GC (1999) Determinants of specificity for aflatoxin B1-8,9-epoxide in alpha-class glutathione S-transferases. *Biochem J* **339 (Pt 1)**:95-101.
- Meech R and Mackenzie (2010) PI UGT3A: novel UDP-glycosyltransferases of the UGT superfamily. *Drug Metab Rev* **42**:43-52.

- Mennone A, Soroka CJ, Cai SY, Harry K, Adachi M, Hagey L, Schuetz JD and Boyer JL (2006) Mrp4^{-/-} mice have an impaired cytoprotective response in obstructive cholestasis. *Hepatology* **43**:1013-1021.
- Nelson DR, Zeldin DC, Hoffman SM, Maltais LJ, Wain HM and Nebert DW (2004) Comparison of cytochrome P450 (CYP) genes from the mouse and human genomes, including nomenclature recommendations for genes, pseudogenes and alternative-splice variants. *Pharmacogenetics* **14**:1-18.
- Niehrs C, Beisswanger R and Huttner WB (1994) Protein tyrosine sulfation, 1993--an update. *Chem Biol Interact* **92**:257-271.
- Noble SM, Carnahan VE, Moore LB, Luntz T, Wang H, Ittoop OR, Stimmel JB, Davis-Searles PR, Watkins RE, Wisely GB, LeCluyse E, Tripathy A, McDonnell DP and Redinbo MR (2006) Human PXR forms a tryptophan zipper-mediated homodimer. *Biochemistry* **45**:8579-8589.
- Omicinski CJ, Hassett C and Costa P (1990) Developmental expression and in situ localization of the phenobarbital-inducible rat hepatic mRNAs for cytochromes CYP2B1, CYP2B2, CYP2C6, and CYP3A1. *Mol Pharmacol* **38**:462-470.
- Pacyniak EK, Cheng X, Cunningham ML, Crofton K, Klaassen CD and Guo GL (2007) The flame retardants, polybrominated diphenyl ethers, are pregnane X receptor activators. *Toxicol Sci* **97**:94-102.
- Pellicciari R, Costantino G and Fiorucci S (2005) Farnesoid X receptor: from structure to potential clinical applications. *J Med Chem* **48**:5383-5403.

- Pellicciari R, Fiorucci S, Camaioni E, Clerici C, Costantino G, Maloney PR, Morelli A, Parks DJ and Willson TM (2002) 6alpha-ethyl-chenodeoxycholic acid (6-ECDCA), a potent and selective FXR agonist endowed with anticholestatic activity. *J Med Chem* **45**:3569-3572.
- Petrick JS and Klaassen CD (2007) Importance of hepatic induction of constitutive androstane receptor and other transcription factors that regulate xenobiotic metabolism and transport. *Drug Metab Dispos* **35**:1806-1815.
- Pineau T, Daujat M, Pichard L, Girard F, Angevain J, Bonfils C and Maurel P (1991) Developmental expression of rabbit cytochrome P450 CYP1A1, CYP1A2 and CYP3A6 genes. Effect of weaning and rifampicin. *Eur J Biochem* **197**:145-153.
- Plass JR, Mol O, Heegsma J, Geuken M, Faber KN, Jansen PL and Muller M (2002) Farnesoid X receptor and bile salts are involved in transcriptional regulation of the gene encoding the human bile salt export pump. *Hepatology* **35**:589-596.
- Pokholok DK, Harbison CT, Levine S, Cole M, Hannett NM, Lee TI, Bell GW, Walker K, Rolfe PA, Herbolzheimer E, Zeitlinger J, Lewitter F, Gifford DK and Young RA (2005) Genome-wide map of nucleosome acetylation and methylation in yeast. *Cell* **122**:517-527.
- Poschl G and Seitz HK (2004) Alcohol and cancer. *Alcohol Alcohol* **39**:155-165.

- Puigserver P, Adelmant G, Wu Z, Fan M, Xu J, O'Malley B and Spiegelman BM (1999) Activation of PPARgamma coactivator-1 through transcription factor docking. *Science* **286**:1368-1371.
- Puigserver P and Spiegelman BM (2003) Peroxisome proliferator-activated receptor-gamma coactivator 1 alpha (PGC-1 alpha): transcriptional coactivator and metabolic regulator. *Endocr Rev* **24**:78-90.
- Puigserver P, Wu Z, Park CW, Graves R, Wright M and Spiegelman BM (1998) A cold-inducible coactivator of nuclear receptors linked to adaptive thermogenesis. *Cell* **92**:829-839.
- Radomska-Pandya A, Czernik PJ, Little JM, Battaglia E and Mackenzie PI (1999) Structural and functional studies of UDP-glucuronosyltransferases. *Drug Metab Rev* **31**:817-899.
- Raijmakers MT, Steegers EA and Peters WH (2001) Glutathione S-transferases and thiol concentrations in embryonic and early fetal tissues. *Hum Reprod* **16**:2445-2450.
- Rees WD, McNeil CJ and Maloney CA (2008) The Roles of PPARs in the Fetal Origins of Metabolic Health and Disease. *PPAR Res* **2008**:459030.
- Reik W (2007) Stability and flexibility of epigenetic gene regulation in mammalian development. *Nature* **447**:425-432.
- Rhee J, Inoue Y, Yoon JC, Puigserver P, Fan M, Gonzalez FJ and Spiegelman BM (2003) Regulation of hepatic fasting response by PPARgamma coactivator-1alpha (PGC-1): requirement for hepatocyte nuclear factor 4alpha in gluconeogenesis. *Proc Natl Acad Sci U S A* **100**:4012-4017.

- Rodriguez-Antona C, Gomez A, Karlgren M, Sim SC and Ingelman-Sundberg M
Molecular genetics and epigenetics of the cytochrome P450 gene family
and its relevance for cancer risk and treatment. *Hum Genet* **127**:1-17.
- Roh TY, Cuddapah S, Cui K and Zhao K (2006) The genomic landscape of
histone modifications in human T cells. *Proc Natl Acad Sci U S A*
103:15782-15787.
- Rowlands JC and Gustafsson JA (1997) Aryl hydrocarbon receptor-mediated
signal transduction. *Crit Rev Toxicol* **27**:109-134.
- Russell DW (2003) The enzymes, regulation, and genetics of bile acid synthesis.
Annu Rev Biochem **72**:137-174.
- Sanguino E, Roglans N, Alegret M, Sanchez RM, Vazquez-Carrera M and
Laguna JC (2005) Atorvastatin reverses age-related reduction in rat
hepatic PPAR α and HNF-4. *Br J Pharmacol* **145**:853-861.
- Satoh K, Itoh K, Yamamoto M, Tanaka M, Hayakari M, Ookawa K, Yamazaki T,
Sato T, Tsuchida S and Hatayama I (2002) Nrf2 transactivator-
independent GSTP1-1 expression in "GSTP1-1 positive" single cells
inducible in female mouse liver by DEN: a preneoplastic character of
possible initiated cells. *Carcinogenesis* **23**:457-462.
- Scheimann AO, Strautnieks SS, Knisely AS, Byrne JA, Thompson RJ and
Finogold MJ (2007) Mutations in bile salt export pump (ABCB11) in two
children with progressive familial intrahepatic cholestasis and
cholangiocarcinoma. *J Pediatr* **150**:556-559.

- Schmidt D, Wilson MD, Spyrou C, Brown GD, Hadfield J and Odom DT (2009) ChIP-seq: using high-throughput sequencing to discover protein-DNA interactions. *Methods* **48**:240-248.
- Schmidt JV, Su GH, Reddy JK, Simon MC and Bradfield CA (1996) Characterization of a murine Ahr null allele: involvement of the Ah receptor in hepatic growth and development. *Proc Natl Acad Sci U S A* **93**:6731-6736.
- Schnekenburger M, Peng L and Puga A (2007) HDAC1 bound to the Cyp1a1 promoter blocks histone acetylation associated with Ah receptor-mediated trans-activation. *Biochim Biophys Acta* **1769**:569-578.
- Schuetz JD, Beach DL and Guzelian PS (1994) Selective expression of cytochrome P450 CYP3A mRNAs in embryonic and adult human liver. *Pharmacogenetics* **4**:11-20.
- Sheehan D, Meade G, Foley VM and Dowd CA (2001) Structure, function and evolution of glutathione transferases: implications for classification of non-mammalian members of an ancient enzyme superfamily. *Biochem J* **360**:1-16.
- Shelby MK and Klaassen CD (2006) Induction of rat UDP-glucuronosyltransferases in liver and duodenum by microsomal enzyme inducers that activate various transcriptional pathways. *Drug Metab Dispos* **34**:1772-1778.
- Shneider BL, Fox VL, Schwarz KB, Watson CL, Ananthanarayanan M, Thevananther S, Christie DM, Hardikar W, Setchell KD, Mieli-Vergani G,

- Suchy FJ and Mowat AP (1997) Hepatic basolateral sodium-dependent-bile acid transporter expression in two unusual cases of hypercholanemia and in extrahepatic biliary atresia. *Hepatology* **25**:1176-1183.
- Sinal CJ, Tohkin M, Miyata M, Ward JM, Lambert G and Gonzalez FJ (2000) Targeted disruption of the nuclear receptor FXR/BAR impairs bile acid and lipid homeostasis. *Cell* **102**:731-744.
- Slitt AL, Allen K, Morrone J, Aleksunes LM, Chen C, Maher JM, Manautou JE, Cherrington NJ and Klaassen CD (2007) Regulation of transporter expression in mouse liver, kidney, and intestine during extrahepatic cholestasis. *Biochim Biophys Acta* **1768**:637-647.
- Slitt AL, Allen K, Morrone J, Aleksunes LM, Chen C, Maher JM, Manautou JE, Cherrington NJ and Klaassen CD (2007) Regulation of transporter expression in mouse liver, kidney, and intestine during extrahepatic cholestasis. *Biochim Biophys Acta* **1768**:637-647.
- Slitt AL, Cherrington NJ, Dieter MZ, Aleksunes LM, Scheffer GL, Huang W, Moore DD and Klaassen CD (2006) trans-Stilbene oxide induces expression of genes involved in metabolism and transport in mouse liver via CAR and Nrf2 transcription factors. *Mol Pharmacol* **69**:1554-1563.
- Smit JJ, Schinkel AH, Oude Elferink RP, Groen AK, Wagenaar E, van Deemter L, Mol CA, Ottenhoff R, van der Lugt NM, van Roon MA and et al. (1993) Homozygous disruption of the murine mdr2 P-glycoprotein gene leads to a complete absence of phospholipid from bile and to liver disease. *Cell* **75**:451-462.

- Song KH, Li T, Owsley E, Strom S and Chiang JY (2008) Bile acids activate fibroblast growth factor 19 signaling in human hepatocytes to inhibit cholesterol 7 α -hydroxylase gene expression. *Hepatology*. **49**: 297-305
- Sonoda J, Xie W, Rosenfeld JM, Barwick JL, Guzelian PS and Evans RM (2002) Regulation of a xenobiotic sulfonation cascade by nuclear pregnane X receptor (PXR). *Proc Natl Acad Sci U S A* **99**:13801-13806.
- Splinter E, Heath H, Kooren J, Palstra RJ, Klous P, Grosveld F, Galjart N and de Laat W (2006) CTCF mediates long-range chromatin looping and local histone modification in the beta-globin locus. *Genes Dev* **20**:2349-2354.
- Staudinger JL, Goodwin B, Jones SA, Hawkins-Brown D, MacKenzie KI, LaTour A, Liu Y, Klaassen CD, Brown KK, Reinhard J, Willson TM, Koller BH and Kliewer SA (2001) The nuclear receptor PXR is a lithocholic acid sensor that protects against liver toxicity. *Proc Natl Acad Sci U S A* **98**:3369-3374.
- Stellaard F and Wolthers BG (1993) [Inborn errors of bile acid metabolism]. *Tijdschr Kindergeneesk* **61**:125-134.
- Suchy FJ, Balistreri WF, Heubi JE, Searcy JE and Levin RS (1981) Physiologic cholestasis: elevation of the primary serum bile acid concentrations in normal infants. *Gastroenterology* **80**:1037-1041.
- Sugden MC, Bulmer K, Gibbons GF, Knight BL and Holness MJ (2002) Peroxisome-proliferator-activated receptor-alpha (PPARalpha) deficiency leads to dysregulation of hepatic lipid and carbohydrate metabolism by fatty acids and insulin. *Biochem J* **364**:361-368.

- Synold TW, Dussault I and Forman BM (2001) The orphan nuclear receptor SXR coordinately regulates drug metabolism and efflux. *Nat Med* **7**:584-590.
- Tee LB, Gilmore KS, Meyer DJ, Ketterer B, Vandenberghe Y and Yeoh GC (1992) Expression of glutathione S-transferase during rat liver development. *Biochem J* **282 (Pt 1)**:209-218.
- Teotico DG, Frazier ML, Ding F, Dokholyan NV, Temple BR and Redinbo MR (2008) Active nuclear receptors exhibit highly correlated AF-2 domain motions. *PLoS Comput Biol* **4**:e1000111.
- Thier R, Bruning T, Roos PH and Bolt HM (2002) Cytochrome P450 1B1, a new keystone in gene-environment interactions related to human head and neck cancer? *Arch Toxicol* **76**:249-256.
- Townsend DM, Tew KD, He L, King JB and Hanigan MH (2009) Role of glutathione S-transferase Pi in cisplatin-induced nephrotoxicity. *Biomed Pharmacother* **63**:79-85.
- Tukey RH and Strassburg CP (2000) Human UDP-glucuronosyltransferases: metabolism, expression, and disease. *Annu Rev Pharmacol Toxicol* **40**:581-616.
- van Herwaarden AE, Wagenaar E, van der Kruijssen CM, van Waterschoot RA, Smit JW, Song JY, van der Valk MA, van Tellingen O, van der Hoorn JW, Rosing H, Beijnen JH and Schinkel AH (2007) Knockout of cytochrome P450 3A yields new mouse models for understanding xenobiotic metabolism. *J Clin Invest* **117**:3583-3592.

- Van Mil SW, Milona A, Dixon PH, Mullenbach R, Geenes VL, Chambers J, Shevchuk V, Moore GE, Lammert F, Glantz AG, Mattsson LA, Whittaker J, Parker MG, White R and Williamson C (2007) Functional variants of the central bile acid sensor FXR identified in intrahepatic cholestasis of pregnancy. *Gastroenterology* **133**:507-516.
- Vega RB, Huss JM and Kelly DP (2000) The coactivator PGC-1 cooperates with peroxisome proliferator-activated receptor alpha in transcriptional control of nuclear genes encoding mitochondrial fatty acid oxidation enzymes. *Mol Cell Biol* **20**:1868-1876.
- Waalkes MP and Klaassen CD (1984) Postnatal ontogeny of metallothionein in various organs of the rat. *Toxicol Appl Pharmacol* **74**:314-320.
- Wang L, Soroka CJ and Boyer JL (2002) The role of bile salt export pump mutations in progressive familial intrahepatic cholestasis type II. *J Clin Invest* **110**:965-972.
- Wang R, Lam P, Liu L, Forrest D, Yousef IM, Mignault D, Phillips MJ and Ling V (2003) Severe cholestasis induced by cholic acid feeding in knockout mice of sister of P-glycoprotein. *Hepatology* **38**:1489-1499.
- Wang W, Prosser WW, Chen J, Taremi SS, Le HV, Madison V, Cui X, Thomas A, Cheng KC and Lesburg CA (2008) Construction and characterization of a fully active PXR/SRC-1 tethered protein with increased stability. *Protein Eng Des Sel* **21**:425-433.
- Watson JD and Crick FH (1953) The structure of DNA. *Cold Spring Harb Symp Quant Biol* **18**:123-131.

- Waxman DJ and Holloway MG (2009) Sex differences in the expression of hepatic drug metabolizing enzymes. *Mol Pharmacol* **76**:215-228.
- Wei P, Zhang J, Egan-Hafley M, Liang S and Moore DD (2000) The nuclear receptor CAR mediates specific xenobiotic induction of drug metabolism. *Nature* **407**:920-923.
- Weiss R, Dziura J, Burgert TS, Tamborlane WV, Taksali SE, Yeckel CW, Allen K, Lopes M, Savoye M, Morrison J, Sherwin RS and Caprio S (2004) Obesity and the metabolic syndrome in children and adolescents. *N Engl J Med* **350**:2362-2374.
- Werner T (2010) Next generation sequencing in functional genomics. *Brief Bioinform.*
- Williams A and Flavell RA (2008) The role of CTCF in regulating nuclear organization. *J Exp Med* **205**:747-750.
- Xie W, Radominska-Pandya A, Shi Y, Simon CM, Nelson MC, Ong ES, Waxman DJ and Evans RM (2001) An essential role for nuclear receptors SXR/PXR in detoxification of cholestatic bile acids. *Proc Natl Acad Sci U S A* **98**:3375-3380.
- Yamato Y, Kimura A, Inoue T, Kurosawa T and Kato H (2001) Fetal bile acid metabolism: analysis of urinary 3beta-monohydroxy-delta(5) bile acid in preterm infants. *Biol Neonate* **80**:19-25.
- Ye JM, Doyle PJ, Iglesias MA, Watson DG, Cooney GJ and Kraegen EW (2001) Peroxisome proliferator-activated receptor (PPAR)-alpha activation lowers

- muscle lipids and improves insulin sensitivity in high fat-fed rats:
comparison with PPAR-gamma activation. *Diabetes* **50**:411-417.
- Yeager RL, Reisman SA, Aleksunes LM and Klaassen CD (2009) Introducing the
"TCDD-inducible AhR-Nrf2 gene battery". *Toxicol Sci* **111**:238-246.
- Yijia L, Danyan Z, Yue D, Meiyuan G, Xin H, Kuifen M and Yu Y (2008) MAPEG
expression in mouse embryonic stem cell-derived hepatic tissue system.
Stem Cells Dev. **17**: 775-783
- Yoon JC, Puigserver P, Chen G, Donovan J, Wu Z, Rhee J, Adelmant G,
Stafford J, Kahn CR, Granner DK, Newgard CB and Spiegelman BM
(2001) Control of hepatic gluconeogenesis through the transcriptional
coactivator PGC-1. *Nature* **413**:131-138.
- Yubero P, Hondares E, Carmona MC, Rossell M, Gonzalez FJ, Iglesias R, Giralt
M and Villarroya F (2004) The developmental regulation of peroxisome
proliferator-activated receptor-gamma coactivator-1alpha expression in
the liver is partially dissociated from the control of gluconeogenesis and
lipid catabolism. *Endocrinology* **145**:4268-4277.
- Zhou J, Febbraio M, Wada T, Zhai Y, Kuruba R, He J, Lee JH, Khadem S, Ren S,
Li S, Silverstein RL and Xie W (2008) Hepatic fatty acid transporter Cd36
is a common target of LXR, PXR, and PPARgamma in promoting
steatosis. *Gastroenterology* **134**:556-567.
- Zhou J, Zhai Y, Mu Y, Gong H, Uppal H, Toma D, Ren S, Evans RM and Xie W
(2006) A novel pregnane X receptor-mediated and sterol regulatory

- element-binding protein-independent lipogenic pathway. *J Biol Chem* **281**:15013-15020.
- Zhou X, Zhuo X, Xie F, Kluetzman K, Shu YZ, Humphreys WG and Ding X (2010) Role of CYP2A5 in the clearance of nicotine and cotinine: insights from studies on a Cyp2a5-null mouse model. *J Pharmacol Exp Ther* **332**:578-587.
- Zielinska E, Zubowska M and Bodalski J (2004) Polymorphism within the glutathione S-transferase P1 gene is associated with increased susceptibility to childhood malignant diseases. *Pediatr Blood Cancer* **43**:552-559.
- Zinchuk VS, Okada T, Akimaru K and Seguchi H (2002) Asynchronous expression and colocalization of Bsep and Mrp2 during development of rat liver. *Am J Physiol Gastrointest Liver Physiol* **282**:G540-548.
- Zollner G, Wagner M, Fickert P, Geier A, Fuchsbichler A, Silbert D, Gumhold J, Zatloukal K, Kaser A, Tilg H, Denk H and Trauner M (2005) Role of nuclear receptors and hepatocyte-enriched transcription factors for Ntcp repression in biliary obstruction in mouse liver. *Am J Physiol Gastrointest Liver Physiol* **289**:G798-805.
- Zollner G, Wagner M, Moustafa T, Fickert P, Silbert D, Gumhold J, Fuchsbichler A, Halilbasic E, Denk H, Marschall HU and Trauner M (2006) Coordinated induction of bile acid detoxification and alternative elimination in mice: role of FXR-regulated organic solute transporter-alpha/beta in the adaptive

response to bile acids. *Am J Physiol Gastrointest Liver Physiol* **290**:G923-932.

APPENDICES

Appendix I: Citations of Publication

1. Aleksunes, L. M., **Cui, Y.**, and Klaassen, C. D. (2008). Prominent expression of xenobiotic efflux transporters in mouse extraembryonic fetal membranes compared with placenta. *Drug Metab Disp* 36, 1960-70. PMID: 18566041
2. **Cui, Y. J.**, Cheng, X., Weaver, Y. M., and Klaassen, C. D. (2009). Tissue distribution, gender-divergent expression, ontogeny, and chemical induction of multidrug resistance transporter genes (Mdr1a, Mdr1b, Mdr2) in mice. *Drug Metab Disp* 37, 203-10. PMID: 18854377
3. Tanaka, Y., Aleksunes, L. M., **Cui, Y. J.**, and Klaassen, C. D. (2009). ANIT-induced intrahepatic cholestasis alters hepatobiliary transporter expression via Nrf2 dependent and independent signaling. *Toxicol Sci.* PMID: 19181614
4. Li, Y., **Cui, Y.**, Hart, S. N., Klaassen, C. D., and Zhong, X. (2009). Dynamic patterns of histone methylation are associated with ontogenic expression of the Cyp3a genes during mouse liver maturation. *Mol Pharm.* PMID:19188337
5. **Cui, Y.**, Aleksunes, L.M., Tanaka, Y., Goedken, M.J., and Klaassen, C.D. (2009). ANIT-treated FXR-null mouse livers exhibit more single cell degeneration due to impaired induction of efflux transporters *Toxicol Sci.* 110: 47 - 60. PMID: 19407337
6. Hart, S.N., **Cui, Y.**, Klaassen, C.D., and Zhong, X. (2009). Three patterns of Cytochrome P450 gene expression during liver maturation in mice. *Drug Metab Disp* 37: 116-121
7. **Cui, Y.J.**, Yeager, R.L., Zhong, X.B., and Klaassen, C.D. (2009) Ontogenic

expression of hepatic AhR mRNA correlates with histone H3K4 dimethylation during mouse liver development Toxicol Letters. 189, 1840190
PMID: 19481593

8. Staudinger, JL, Xu, CS, **Cui, Y.J.**, and Klaassen, C.D. (2010) Nuclear receptor mediated regulation of carboxylesterase expression and activity Expert Opinion on Drug Metabolism and Toxicology. 261-71 PMID: 20163318
9. Choudhuri, S., **Cui, Y.**, and Klaassen, C.D. (2010) Molecular Targets of Epigenetic Regulation and Effectors of Environmental Influences Toxicology and Applied Pharmacology. 245:378-93 PMID: 20381512
10. **Cui, J.Y.**, Choudhuri, S., House-Knight, T, and Klaassen, C.D. (2010) Genetic and Epigenetic Regulation and Expression Signatures of Glutathione S-Transferases in Developing Mouse Liver Toxicol Sci. 115: 32-43 PMID: 20395309
11. **Cui, J.Y.**, Gunewardena, S.S., and Klaassen, C.D. (2010) ChIPing the Cistrome of PXR in Mouse Liver Nucleic Acids Research (*accepted*)
12. **Cui, J.Y.**, Aleksunes, L.M., Tanaka Y., Fu, Z.D., Guo, Y.J., and Klaassen, C.D.. Bile acids via FXR initiate the expression of major transporters involved in the enterohepatic circulation of bile acids in newborn mice (*a draft finished*)
13. **Cui, J.Y.**, Badham, H.J., and Klaassen, C.D. The ontogeny of novel cytochrome P450 gene isoforms during postnatal liver maturation in mice (*a draft finished*)
14. **Cui, J.Y.**, Lu, H, Zhong, and Klaassen, C.D. Postnatal increase in

histone H3K4 di-methylation correlates with the up-regulation of hepatic PPAR α mRNA expression during mouse liver development (*a draft finished*)

15. Badham, H.J., **Cui, J.Y.**, Khan, M, and Klaassen, C.D., Tissue distribution of novel cytochrome P450 isoforms in mice (*a draft finished*)
16. **Cui, J.Y.** and Klaassen, C.D. (2010) Ontogenic expression of hepatic microRNAs correlates with histone H3K4 di-methylation during mouse liver development (*in preparation*)
17. Aleksunes, L.M., Yeager, R.L., **Cui, J.Y.**, and Klaassen, C.D. (2010) Regulation of Liver transporters during pregnancy and lactation in mice (*in preparation*)

Appendix II: Peer-reviewed Presentation / Poster Abstracts

1. **Cui, Y.**, Cheng, X.G., and Klaassen, C.D.: Tissue distribution, gender differences, ontogeny, and chemical induction of multidrug resistance genes (Mdr1a, Mdr1b, Mdr2) in mice 46th National Society of Toxicology Meeting, 2007 ID # 344
2. **Cui, Y.**, Aleksunes, L.M., Tanaka, Y., Goedken, M.J., and Klaassen, C.D.: ANIT-treated FXR-null mouse livers exhibit more single cell degeneration due to impaired induction of efflux transporters 47th National Society of Toxicology Meeting, 2008 ID # 415727
3. Aleksunes, L.M., **Cui, Y.**, Hunt, J., and Klaassen, C.D.: Preferential expression of xenobiotic efflux transporters in mouse fetal membranes compared to placenta 47th National Society of Toxicology Meeting, 2008 ID # 2020
4. **Cui, Y.**, Aleksunes, L.M., Tanaka, Y., and Kaassen, C.D.: Bile acids in newborns initiate the expression of major hepatic transporters involved in enterohepatic circulation 59th National AASLD Meeting, 2008 ID # 503760
5. **Cui, Y.**, Aleksunes, L.M., Tanaka, Y., Goedken, M.J., and Klaassen, C.D.: Compensatory induction of liver efflux transporters in response to ANIT-induced liver injury is impaired in FXR-Null mice Central State Society of Toxicology Meeting 2008
6. **Cui, Y.**, Zhong, X.B., and Klaassen, C.D.: Ontogenic expression of hepatic microRNAs correlates with histone H3K4 di-methylation during mouse liver

development 48th National Society of Toxicology Meeting, 2009 ID # 559714

7. Hart, S.N., Li, Y., **Cui, Y.**, Klaassen, C.D., and Zhong, X.B.: Dynamic DNA and histone methylation influences the ontogeny of xenobiotic metabolizing genes during postnatal mouse liver maturation National Experimental Biology Meeting, FASEB J, Apr 2009; 23: 752.4.
8. Li, Y., **Cui, Y.**, Hart, S.N., Klaassen, C.D., and Zhong, X.B.: Dynamic histone methylation is associated with ontogenic expression of Cyp3a genes during mouse liver maturation National Experimental Biology Meeting FASEB J, Apr 2009; 23: 752.5.
9. **Cui, Y.J.**, Gunwardena, S.S., and Klaassen C.D.: Global nuclear occupancy of PXR and co-existence of histone H3K4 di-methylation resulting in activation of drug-processing genes in mouse liver 16th North American Regional ISSX Meeting, 2009 ID: 17309
10. **Cui, Y.J.**, Gunwardena, S.S., and Klaassen C.D.: ChIPing the Cistrome of PXR in Mouse Liver 2009 Central States Society of Toxicology
11. **Cui, Y.J.**, Gunwardena, S.S., and Klaassen C.D.: Genome-wide profiling of PXR reveals unique DNA binding patterns and co-existence of distinct epigenetic signatures resulting in temporal activation of drug-processing genes and miRNAs in mouse liver 60th National AASLD Meeting, 2009 ID# 673

12. Cui, Y.J., Gunwardena, S.S., and Klaassen C.D.: Characterizing the global nuclear occupancy of hepatic PXR and target gene profiles in the mouse genome 4th Annual National Graduate Student Research Festival, 2009